Tesis doctoral

Dpto. de Química Inorgánica e Ingeniería Química

Dpto. de Ingeniería Rural

Escuela Politécnica Superior de Belmez

Universidad de Córdoba

Estudio de hormigones autocompactantes fabricados con residuos industriales como filler

Study of self-compacting concrete made with industrial waste as filler

Álvaro Romero Esquinas

Belmez (Córdoba), 2018

TITULO: *ESTUDIO DE HORMIGONES AUTOCOMPACTANTES FABRICADOS CON RESIDUOS INDUSTRIALES COMO FILLER*

AUTOR: *Álvaro Romero Esquinas*

Campus de Rabanales
Ctra. Nacional IV, Km. 396 A
14071 Córdoba

https://www.uco.es/ucopress/index.php/es/
ucopress@uco.es

Tesis Doctoral para aspirar al Grado de
Doctor por la Universidad de Córdoba

Estudio de hormigones autocompactantes fabricados con residuos industriales como filler

"Study of self-compacting concrete made with industrial waste as filler"

Autor:

D. Álvaro Romero Esquinas

Directores:

Dr. José María Fernández Rodríguez

Dr. José Ramón Jiménez Romero

Programa de Doctorado de Química Fina
Departamento de Química Inorgánica e Ingeniería Química
Departamento de Ingeniería Rural
Escuela Politécnica Superior de Belmez
Universidad de Córdoba

Belmez (Córdoba), 23 de octubre de 2018

TÍTULO DE LA TESIS:

Estudio de hormigones autocompactantes fabricados con residuos industriales como filler

DOCTORANDO: D. Álvaro Romero Esquinas

INFORME RAZONADO DE LOS DIRECTORES DE LA TESIS

(se hará mención a la evolución y desarrollo de la tesis, así como a trabajos y publicaciones derivados de la misma).

La presente Tesis Doctoral aborda la búsqueda de alternativas sostenibles en el campo del hormigón, que es el material más usado en el sector de la construcción. La industria del hormigón es la que más recursos naturales consume. El Hormigón Autocompactante necesita incorporar un alto contenido de finos y aditivos químicos en su dosificación. Esta particularidad en el diseño hace que este material pueda ser considerado como poco amigable con el medio ambiente. Una solución es la utilización de residuos o subproductos industriales de granulometría fina como sustitutivo de los finos convencionales necesarios en la fabricación de los HAC.

En este trabajo se ha evaluado el potencial de reutilización y reciclado de residuos tales como finos procedentes del proceso de secado y calentamiento del árido utilizado en la fabricación de mezclas bituminosas calientes, por una parte y por otra de cenizas volantes no conformes procedentes de centrales termoeléctricas de carbón, como filler en HAC, en sustitución del filler comercial empleado en las mezclas convencionales. Estos residuos en la mayoría de los casos tienen nula o escasa aplicabilidad y son depositados en vertederos.

En primer lugar, se llevó a cabo una profunda caracterización de las propiedades físico-químicas y microestructurales de todos los materiales comerciales y residuos empleados. A continuación,

se realizó un estudio comparativo de las propiedades de autocompactabilidad, comportamiento mecánico, mecanismos de endurecimiento, características microestructurales y comportamiento durable de las mezclas realizadas con residuos respecto a un HAC fabricado con filler comercial.

Se han obtenido diferentes tipos de hormigones autocompactantes empleando residuos de granulometría fina en sustitución total o parcial de un filler comercial, consiguiendo un comportamiento mecánico mayor que los niveles mínimos estipulados por el Código Español sobre Hormigón Estructural (EHE-08) y alcanzando alto rendimiento frente al ataque de agentes agresivos y de retracción.

Estos resultados han contribuido a la valorización y la optimización de los recursos naturales utilizados en la fabricación de HAC, así como a hacer al hormigón más compatible con la nueva realidad y necesidad medioambiental de nuestra sociedad.

El Ingeniero de Minas, D. Álvaro Romero Esquinas ha llevado a cabo con éxito el desarrollo de la Tesis Doctoral "Estudio de hormigones autocompactantes fabricados con residuos industriales como filler", que se presenta como un compendio de publicaciones, bajo la dirección de los doctores abajo firmantes, en las Áreas de Química Inorgánica y de Ingeniería de la Construcción de la Universidad de Córdoba. El doctorando ha experimentado una formación continua tanto en la práctica experimental como en la discusión de los resultados obtenidos. Los objetivos marcados en el Proyecto inicial de la Tesis Doctoral se han completado de manera sobresaliente, obteniendo resultados relevantes que han dado lugar a la publicación de cinco artículos científicos en revistas internacionales de prestigio JCR (Q1, primer cuartil):

1. A.R. Esquinas, C. Ramos, J.R. Jiménez, J.M. Fernández, J. de Brito, Mechanical behaviour of self-compacting concrete made with recovery filler from hot-mix asphalt plants, Construction and Building Materials, 131 (2017) 114–128. doi:10.1016/J.CONBUILDMAT.2016.11.063.
2. A.R. Esquinas, J.I. Álvarez, J.R. Jiménez, J.M. Fernández, J. de Brito, Durability of self-compacting concrete made with recovery filler from hot-mix asphalt plants, Construction and Building Materials, 161 (2018) 407–419. doi:10.1016/J.CONBUILDMAT.2017.11.142.
3. A.R. Esquinas, D. Motos-Pérez, M.E. Jiménez, C. Ramos, J.R. Jiménez, J.M. Fernández, Mechanical and durability behaviour of self-compacting concretes for application in the manufacture of hazardous waste containers, Construction and Building Materials, 168 (2018) 442–458.

doi:10.1016/J.CONBUILDMAT.2018.02.138.

4. A.R. Esquinas, E.F. Ledesma, R. Otero, J.R. Jiménez, J.M. Fernández, Mechanical behaviour of self-compacting concrete made with non-conforming fly ash from coal-fired power plants, Construction and Building Materials, 182 (2018) 385–398. doi:10.1016/J.CONBUILDMAT.2018.06.094.
5. A.R. Esquinas, J.I. Álvarez, J.R. Jiménez, J.M. Fernández, Durability of self-compacting concrete made from non-conforming fly ash from coal-fired power plants, Construction and Building Materials, 189 (2018) 993–1006. doi:10.1016/J.CONBUILDMAT.2018.09.056.

Por todo ello, se autoriza la presentación de la tesis doctoral.

Córdoba, a 23 de octubre de 2018

Firma de los directores

Fdo.: Dr. José María Fernández Rodríguez

Fdo.: Dr. José Ramón Jiménez Romero

A mi familia

Agradecimientos

La culminación de esta etapa académica no hubiera sido posible sin todas aquellas personas e instituciones que han formado parte de ella, A TODOS ELLOS, MUCHAS GRACIAS.

Agradecer al Ministerio de Educación, Cultura y Deporte del Gobierno de España la concesión de la Ayuda para la Formación de Profesorado Universitario (FPU13/04030) que ha permitido la realización de esta Tesis Doctoral.

Al Dr. José María Fernández Rodríguez, mi agradecimiento más sincero por todo su tiempo dedicado, paciencia, ayuda tanto en el ámbito personal como académico y conocimientos aportados en la realización de este trabajo. Al Dr. José Ramón Jiménez Romero, gracias por su ayuda, colaboración prestada y sus valiosas aportaciones. A ambos, gracias por vuestra guía, la cual ha sido fundamental.

Mi gratitud hacia el personal y alumnado de TFG de la Escuela Politécnica Superior de Belmez, al personal del Área de Química Inorgánica y del Área de Ingeniería de la Construcción de la Universidad de Córdoba, por la ayuda brindada, el apoyo recibo, los sabios consejos y, principalmente, por su amistad.

A los profesores Dr. Jorge de Brito, Dr. Pedro Raposeiro da Silva y Dr. Rui Vasco Silva por sus conocimientos, motivación y apoyo durante mis estancias en el Instituto Superior Técnico de la Universidad de Lisboa. A Tiago Barroqueiro por ayudarme desde el primer día, hiciste mi estancia más cómoda dentro y fuera del laboratorio. A todo el personal del Laboratorio de Construcción, gracias por todo lo que aprendí en vuestro centro.

Y, por último, agradecer a toda mi familia, todo lo que soy es gracias a vosotros.

A mi esposa, Ana Belén, por ser la ayuda adecuada en mi vida, tu amor, comprensión, paciencia y apoyo incondicional desde siempre hacen posible todo.

A mis padres, Jacinto y María Adelina, por su sacrificio permanente, por la educación recibida y ser un verdadero ejemplo de amor a hacia mí y mi hermana. A mi hermana, Lidia, por sentir su apoyo y confianza en todo momento.

Resumen

La presente Tesis Doctoral aborda la búsqueda de alternativas sostenibles en el campo del hormigón ya que es el material más usado en el sector de la construcción. Actualmente, podemos decir que el hormigón sostiene nuestra vida cotidiana. Sin embargo, no todo es bueno, ya que es la industria que más recursos naturales consume, por ello está considerado como un material poco respetuoso con el medio.

Por este motivo la industria del hormigón está en constante evolución, buscando técnicas más eficientes que permitan la optimización de los recursos naturales. Dentro de esta tendencia, en la década de los 80, nace el Hormigón Autocompactante como evolución de la tecnología existente y con el fin de aportar soluciones a los diferentes inconvenientes que presenta el hormigón convencional.

El HAC se caracteriza por fluir bajo su propio peso, por ello no requiere vibración durante su ejecución en obra. Lo cual se traduce en diversas ventajas (reducción de los plazos de ejecución, fabricación de estructuras complejas, mejores acabados superficiales, disminución de la mano de obra, disminución de ruido y vibraciones, entre otras). Para que estas ventajas se puedan dar, el HAC necesita incorporar un alto contenido de finos (cemento, filler y/o árido fino) y aditivos químicos en su dosificación. Esta particularidad en el diseño hace que este material pueda ser considerado como poco amigable con el medio ambiente.

Una solución es la utilización de residuos o subproductos industriales de granulometría fina como sustitutivo de los finos convencionales necesarios en la fabricación de los HAC.

En este trabajo se ha evaluado el potencial de reutilización y reciclado de los residuos de granulometría fina (finos o polvo) generados en la industria y/o minería, tales como finos procedentes del proceso de secado y calentamiento del árido utilizado en la fabricación de mezclas bituminosas calientes y cenizas volantes no conformes procedentes de centrales termoeléctricas de carbón, como filler en HAC en sustitución del filler comercial empleado en las mezclas convencionales. Estos residuos en la

mayoría de los casos tienen nula o escasa aplicabilidad y son depositados en vertederos.

En primer lugar, se llevó a cabo una profunda caracterización de las propiedades físico-químicas y microestructurales de todos los materiales comerciales y residuos empleados. Además, se realizó un análisis completo de las propiedades en estado fresco y en estado endurecido de diferentes dosificaciones que permitió definir con alto grado de certeza, la mezcla óptima para incorporar los residuos como filler.

A continuación, se realizó un estudio de viabilidad del residuo de granulometría fina generado en las plantas de mezclas bituminosas calientes como filler. Se realizó un estudio comparativo de las propiedades de autocompactabilidad, comportamiento mecánico, mecanismos de endurecimiento, características microestructurales y comportamiento durable de esta mezcla respecto a un HAC fabricado con filler comercial.

Posteriormente, se evaluó el uso de cenizas volantes de una central termoeléctrica de carbón que no cumple con los criterios de conformidad marcado por la normativa como filler en HAC. Se analizaron las propiedades en estado fresco (autocompactabilidad y propiedades físicas) y en estado endurecido (propiedades mecánicas, mecanismos de endurecimiento, características microestructurales y durabilidad) de dosificaciones que incorporan el residuo al 50% y al 100% de sustitución respecto al HAC con filler comercial.

Se han obtenido diferentes tipos de hormigones autocompactantes empleando estos residuos de granulometría fina en sustitución total o parcial de un filler comercial, consiguiendo un comportamiento mecánico mayor que los niveles mínimos estipulados por el Código Español sobre Hormigón Estructural (EHE-08) y alcanzando alto rendimiento frente al ataque de agentes agresivos y de retracción.

Se pretende que estos resultados contribuyan a eliminar la falta de confianza en la calidad de estos materiales, así como su valorización y la optimización de los recursos naturales utilizados en la fabricación de HAC. Consiguiendo que este material sea más compatible con la nueva realidad y necesidad medioambiental de nuestra sociedad.

Abstract

This Doctoral Thesis addresses the search for sustainable alternatives in the field of concrete since it is the most used material in the construction sector. Currently, we can say that concrete supports our daily life. However, not everything is good, since it is the industry that consumes the most natural resources, which is why it is considered as a material that does not respect the environment.

For this reason, the concrete industry is constantly evolving, seeking more efficient technologies with high optimization of natural resources. In the 1980s, Self-Compacting Concrete was born as an evolution of existing technology and with the aim to provide solutions to the different problems presented by ordinary concrete.

SCC is characterized by flowing under its own weight, thus not requiring vibration during its execution in work, which translates into benefits (reduced lead times, production of complex structures, better surface finishes, noise and vibration reduction, among others). For these advantages to occur, the SCC needs to incorporate a high content of fine material (cement, filler and/or fine aggregate) and chemical additives in its dosage. This particularity in the design means this material can be considered as not very environment-friendly.

One solution is the use of industrial fine waste or by-products as a substitute for the conventional fine materials required in the manufacture of SCC.

In this work, the potential for reuse and recycling of fine granulometry waste (fine materials or dust) generated in industry and/or mining has been evaluated, such as generated waste in the drying and heating process of aggregates in hot-mix asphalt manufacturing plants and non-conforming fly ash from coal-fired power plants. In most cases, this waste has no or little applicability and is deposited in landfills.

Firstly, a deep characterization of the physical-chemical and microstructural properties of all the commercial materials and waste used was carried out. In addition, a complete analysis of the properties in the fresh state and in the hardened state of

different dosages was carried out, which made it possible to define, with a high degree of certainty, the optimum mix to incorporate the wastes as filler.

Then, a feasibility study of the fine grain waste generated in hot-mix asphalt manufacturing plants such as filler was carried out, as well as comparative study of the properties of self-compactability, mechanical behaviour, hardening mechanisms, microstructural characteristics and durable behaviour of this mix with respect to a SCC manufactured with commercial filler.

Subsequently, the use of fly ash from a coal-fired power plant that does not meet the criteria of conformity marked by the regulations as a filler in SCC was evaluated. The properties in fresh state (self-compactability and physical properties) and hardened state (mechanical properties, hardening mechanisms, microstructural characteristics and durability) of dosages that incorporate the waste at 50% and 100% of substitution respect to the SCC with filler commercial were analysed.

Different types of self-compacting concretes have been obtained using these fine granulometry wastes in total or partial replacement of a commercial filler, achieving a mechanical performance higher than the minimum levels stipulated by the Spanish Code on Structural Concrete (EHE-08) and achieving high performance against the attack of aggressive agents and shrinkage.

It is intended that these results contribute to eliminate the lack of confidence in the quality of these materials, as well as their valorisation and optimization of the natural resources used in the manufacture of SCC, making this material more compatible with the new reality and environmental needs of our society.

Índice de Contenidos

Informe razonado de los directores de la tesis v
Agradecimientos xi
Resumen xiii
Abstract xv
Índice de Contenidos xvii
Índice de Figuras xxiii
Índice de Tablas xxvii
Abreviaturas xxix
Capítulo 1.Justificación, Objetivos y Plan de Investigación de la Tesis Doctoral 33
1.1 Justificación 33
1.2 Objetivos 35
1.3 Plan de investigación de la tesis doctoral 37
1.4 Estructura de la Memoria de Tesis Doctoral 40
Capítulo 2.Introducción 45
2.1 Origen y desarrollo del Hormigón Autocompactante 45
2.2 Propiedades del Hormigón Autocompactante 48
2.3 Consideraciones sobre los materiales empleados en la fabricación del HAC . 50
2.4 Comportamiento dinámico del HAC 55
2.5 Comportamiento del HAC en estado endurecido 58
2.6 Consideraciones medio ambientales del HAC 66
2.7 Referencias bibliográficas 70
Capítulo 3.Materiales y Métodos 75
3.1 Materiales 75
3.2 Dosificaciones y preparación de los HAC 82
3.3 Métodos 84
3.3.1 Distribución de tamaño de partícula 84
3.3.2 Difracción de rayos X 84
3.3.3 Análisis termogravimétrico 85
3.3.4 Isotermas de adsorción-desorción de nitrógeno 86
3.3.5 Espectroscopía de infrarrojos 89
3.3.6 Microscopía electrónica de barrido 89

3.3.7 Microscopía electrónica de transmisión 90
3.3.8 Porosimetría por intrusión de mercurio 90
3.4 Referencias bibliográficas 92
Capítulo 4.Mechanical and durability behaviour of self-compacting concretes for application in the manufacture of hazardous waste containers 95
Abstract 95
4.1 Introduction 97
4.2 Experimental methodology 99
4.2.1 Materials 99
4.2.2 Concrete mixes 102
4.2.3 Test methods 106
4.3 Results and discussion 109
4.3.1 Properties of SCC in fresh-state—Self-compactability 109
4.3.2 Physical properties of hardened SCCs 112
4.3.2.1 Bulk density and evolution during drying 112
4.3.2.2 Pore size distribution 115
4.3.3 Mechanical properties of SCCs 118
4.3.3.1 Compressive strength 118
4.3.3.2 Splitting tensile strength 121
4.3.3.3 Flexural strength 124
4.3.4 Water absorption properties of hardened SCCs 127
4.3.4.1 Water absorption by immersion 127
4.3.4.2 Water absorption by capillarity 128
4.3.5 Durability of hardened SCCs 130
4.3.5.1 Permeability and penetration of water under pressure 130
4.3.5.2 Chloride ion penetration 131
4.3.5.3 Sulphate ion penetration 133
4.3.5.4 Drying shrinkage 135
4.4 Conclusions 137
4.5 Acknowledgements 139
4.6 References 139
Capítulo 5.Mechanical behaviour of self-compacting concrete made with recovery filler from hot-mix asphalt plants 147
Abstract 147

5.1 Introduction 148
5.2 Experimental plan 151
5.2.1 Materials characterization 151
5.2.2 Concrete mixes and composition tests 159
4.2.3 Test methods 161
5.3 Results and discussion 163
5.3.1 Fresh-state properties of SCC 163
5.3.1.1 Self-compactability 163
5.3.1.2 Fresh density of SCC 166
5.3.2 Hardened-state properties of SSC 167
5.3.2.1 Physical-chemical characterization of hardened SCC 167
5.3.2.2 Wet and dry density 172
5.3.2.3 Compressive strength 173
5.3.2.4 Splitting tensile strength 175
5.3.2.5 Flexural strength 178
5.3.2.6 Static modulus of elasticity and Poisson ratio 180
5.3.2.7 UPV test 182
5.3.2.8 Shrinkage 183
5.4 Conclusions 184
5.5 Acknowledgements 186
5.6 References 186
Capítulo 6.Durability of self-compacting concrete made with recovery filler from hot-mix asphalt plants 193
Abstract 193
6.1 Introduction 194
6.2 Experimental methodology 197
6.2.1 Materials 197
6.2.2 Concrete mixes and composition tests 200
6.2.3 Test methods 201
6.3 Results and discussion 205
6.3.1 Properties of SCC in the fresh-state 205
6.3.1.1 Self-compactability 205
6.3.1.2 Density 208
6.3.2 Properties of SSC in the hardened-state 208

6.3.2.1 Physical properties 208
6.3.2.1.1 Apparent density, evolution during drying and dry density ... 208
6.3.2.1.2 Open porosity or accessible porosity for water 210
6.3.2.1.3 Pore size distribution 211
6.3.2.2 Water absorption properties 213
6.3.2.2.1 Water absorption by immersion and with vacuum 213
6.3.2.2.2 Water absorption by capillarity 215
6.3.2.3 Durability 217
6.3.2.3.1 Permeability and penetration of water under pressure 217
6.3.2.3.2 Chloride ion penetration 219
6.3.2.3.2.1 *Rapid chloride ion penetration test by electrical conductance* 219
6.3.2.3.2.2 *Penetration of chloride ion into concrete determined by ponding* 220
6.3.2.3.3 Carbonation depth 222
6.3.2.3.4 Sulphate ion penetration 224
6.3.2.3.5 Long-term shrinkage 227
6.4 Conclusions 230
6.5 Acknowledgements 232
6.6 References 232
Capítulo 7.Mechanical behaviour of self-compacting concrete made with non-conforming fly ash from coal-fired power plants 239
Abstract 239
7.1 Introduction 240
7.2 Experimental methodology 243
7.2.1 Materials 243
7.2.2 Concrete mixes and composition tests 250
7.2.3 Test methods 250
7.3 Results and discussion 253
7.3.1 Properties of SSC in fresh state 253
7.3.1.1 Self-compactability 253
7.3.1.2 Density of SCC in fresh state 256
7.3.2 Properties of SSC in hardened state 256
7.3.2.1 Physical-chemical characterization of hardened SCC 256

7.3.2.2 Density of SCC 262
7.3.2.3 Compressive strength 263
7.3.2.4 Splitting tensile strength 265
7.3.2.5 Flexural strength 269
7.3.2.6 Static elastic modulus 271
7.3.2.7 UPV test 273
7.3.2.8 Shrinkage 274
7.4 Conclusions 275
7.5 Acknowledgements 277
7.6 References 278
Capítulo 8.Durability of self-compacting concrete made from non-conforming fly ash from coal-fired power plants 283
Abstract 283
8.1 Introduction 284
8.2 Experimental methodology 287
8.2.1 Materials 287
8.2.2 Concrete mixes and composition tests 291
8.2.3 Test methods 291
8.3 Results and discussion 294
8.3.1 Properties of SCC in fresh state 294
8.3.1.1 Self-compactability 294
8.3.1.2 Density of SCC in fresh state 296
8.3.2 Properties of SSC in the hardened state 297
8.3.2.1 Physical properties of hardened SCCs 297
8.3.2.1.1 Bulk density and evolution during drying and skeletal density 297
8.3.2.1.2 Open porosity or accessible porosity for water 300
8.3.2.1.3 Pore size distribution 300
8.3.2.2 Water absorption properties of hardened SCCs. 303
6.3.2.2.1 Water absorption by immersion and with vacuum 303
8.3.2.2.2 Water absorption by capillarity 305
8.3.2.3 Durability 308
8.3.2.3.1 Permeability and penetration of water under pressure 308
8.3.2.3.2 Rapid chloride ion penetration test by electrical conductance 310

8.3.2.3.3 Penetration of chloride ion into concrete determined by ponding 312
8.3.2.3.4 Carbonation depth 313
8.3.2.3.5 Sulphate ion penetration 315
8.3.2.3.6 Long-term shrinkage 319
8.4 Conclusions 320
8.5 Acknowledgements 322
8.6 References 323
Capítulo 9.Conclusiones/conclusions. 329
Futuras líneas de investigación 329
9.1 Conclusiones 329
9.2 Conclusions 339
9.3 Futuras líneas de investigación 348
Anexo A.Producción científica derivada directamente de la Tesis Doctoral 351
Anexo B.Producción científica derivada directamente de la Tesis Doctoral, en fase de publicación 357
Anexo C.Otras aportaciones científicas 361

Índice de Figuras

Figura 1.1: Metodología del Plan de Investigación de la Tesis Doctoral. 38
Figura 1.2: Campaña experimental. 39
Figura 2.1: La necesidad del hormigón autocompactante. 45
Figura 2.2: Desarrollo del hormigón autocompactante desde su origen. 47
Figura 2.3: Proporciones volumétricas aproximadas de los componentes principales empleados para la fabricación de hormigón convencional y autocompactante. 50
Figura 2.4: Curva de flujo del HAC y del hormigón convencional. 56
Figura 2.5: Fases presentes en el cemento en función del tiempo (a) y en función del grado de hidratación (b). 58
Figura 2.6: Etapas del proceso de hidratación del cemento respecto al calor de hidratación. 59
Figura 2.7: Clasificación de la porosidad en función del diámetro de poro. 62
Figura 2.8: Resistencia a la compresión, respecto al tiempo de curado para las fases del cemento. 63
Figura 2.9: Principales agentes agresivos del hormigón y mecanismos de transporte. 66
Figura 2.10: Economía circular en el sector de la construcción. 68
Figura 3.1: Áridos empleados en este trabajo. 76
Figura 3.2: a) Áridos Gallardo S.L. y b) Charamuzca Movimiento de Tierras, Áridos y Hormigones S.L. 76
Figura 3.3: Filler comercial y finos residuales empleados en este trabajo. 77
Figura 3.4: Minas Carmina. 77
Figura 3.5: Planta de fabricación de Mezclas Bituminosas Calientes. 78
Figura 3.6: Central Térmica de Puente Nuevo. 78
Figura 3.7: Diagrama de flujo general C.T. de Puente Nuevo. 80
Figura 3.8: Fábrica de Cementos de Alcalá de Guadaíra de Cementos Portland Valderrivas S.A. 81
Figura 3.9: Secuencia del proceso de amasado. 83
Figura 3.10: Clasificación de isotermas de adsorción 87
Figure 4.1: Particle size distribution for gravel, coarse and fine sands, mixes SCC-A, SCC-B, SCC-C, and SCC-D and Bolomey ideal. 100

Figure 4.2: Grain-size distribution of SF filler and CEM I as measured by laser diffraction. 100
Figure 4.3: PXRD patterns of SF filler and cement. 101
Figure 4.4: Pore size distribution and TEM micrographs of the SF fillers. 102
Figure 4.5: Properties of SCCs in fresh-state and self-compactibility. 110
Figure 4.6: Workability boxes of several self-compacting mixes. 111
Figure 4.7: Evolution of the density relative to variation of mass. 114
Figure 4.8: Cumulative pore volume and log differential intrusion of the mixes. 115
Figure 4.9: Mechanical properties of hardened SCCs. 120
Figure 4.10: Compressive strength (f_c) versus splitting tensile strength (top) and compressive strength (f_{ck}) versus splitting tensile strength (bottom). 123
Figure 4.11: Compressive strength versus flexural strength. 126
Figure 4.12: Evolution of the mass loss by drying (100 ºC) and absorption by immersion. 127
Figure 4.13: Capillary water absorption of the mixes. 129
Figure 4.14: Ion Cl^- concentration profile of the mixes. 132
Figure 4.15: Ion SO_3 concentration profile of the mixes. 134
Figure 4.16: Drying shrinkage of the mixes. 135
Figure 5.1: Particle size distribution for gravel, coarse and fine sands, mixes SCC-SF and SCC-RF and Bolomey ideal. 151
Figure 5.2: PXRD patterns for gravel (G), coarse (S1) and fine (S2) sands. 153
Figure 5.3: Grain-size distribution of SF, RF and CEM I by laser diffraction. 154
Figure 5.4: PXRD patterns for SF, RF and cement. 155
Figure 5.5: TG (solid lines) and DTA (dotted line) curves for the SF and RF fillers. 156
Figure 5.6: Pore size distribution for the SF and RF fillers. 156
Figure 5.7: TEM micrographs for the SF and RF fillers. 157
Figure 5.8: FT-IR for the SF and RF fillers. 158
Figure 5.9: Workability boxes for several self-compacting mixes. 166
Figure 5.10: TGA (solid lines) and TDA (dotted lines) for several hardened SCCs. 169
Figure 5.11: PXRD patterns for hardened SCC-SF at different ages. 171
Figure 5.12: PXRD patterns for hardened SCC-RF at different ages. 172
Figure 5.13: Mechanical properties of hardened SCCs. 174
Figure 5.14: Compressive strength versus splitting tensile strength. 176

Figure 5.15: Compressive strength versus flexural strength. 179
Figure 5.16: Static Modulus of Elasticity of hardened SCCs. 180
Figure 5.17: Compressive strength versus modulus of elasticity. 181
Figure 5.18: Compressive strength versus ultrasonic pulse velocity. 183
Figure 6.1: PXRD patterns of the SF and RF fillers. 198
Figure 6.2: Pore size distribution and TEM micrographs of the SF and RF fillers. . 199
Figure 6.3: Grain-size distribution of the SF and RF fillers as measured by laser diffraction. 199
Figure 6.4: Workability boxes of several self-compacting mixes. 207
Figure 6.5: Evolution of the density relative to the variation of mass. 210
Figure 6.6: Cumulative pore volume and log differential intrusion of the mixes. .. 212
Figure 6.7: Evolution of the mass loss by drying (100 ºC) and absorption by immersion. 214
Figure 6.8: Capillary water absorption of the mixes. 216
Figure 6.9: Rapid chloride ion penetration test by electrical conductance of the mixes. 220
Figure 6.10: Ion Cl^- concentration profile of the mixes. 221
Figure 6.11: Depth of carbonation as a function of t of the mixes. 223
Figure 6.12: Ion SO_3 concentration profile of the mixes. 225
Figure 6.13: PXRD patterns of SCC-SF before and after exposure to SO_3. 226
Figure 6.14: PXRD patterns of SCC-RF before and after exposure to SO_3. 227
Figure 6.15: Total shrinkage and mass loss of the mixes. 228
Figure 7.1: Particle size distribution for gravel, coarse and fine sands, mixes SCC-1, SCC-12 and SCC-2. 243
Figure 7.2: PXRD patterns for gravel (G), coarse (S1) and fine (S2) sands. 245
Figure 7.3: Grain-size distribution of SF, NCFA and CEM I by laser diffraction. 245
Figure 7.4: PXRD patterns for SF, NCFA and cement. 248
Figure 7.5: TG (solid lines) and DTA (dotted line) curves for the SF and NCFA fillers. 248
Figure 7.6: Pore size distribution for the SF and NCFA fillers. 249
Figure 7.7: Workability boxes for several self-compacting mixes. 255
Figure 7.8: TGA (solid lines) and TDA (dotted lines) for several hardened SCCs. . 257
Figure 7.9: PXRD patterns for hardened SCC-1 and SCC-2 in the short term. 260
Figure 7.10: PXRD patterns for hardened SCC-1, SCC-12 and SCC-2 at 250 days. 261

Figure 7.11: Mechanical properties of hardened SCCs. 263
Figure 7.12: Compressive strength (f_c) versus splitting tensile strength (top) and compressive strength (f_{ck}) versus splitting tensile strength (bottom). 267
Figure 7.13: Compressive strength versus flexural strength. 270
Figure 7.14: Compressive strength versus modulus of elasticity. 272
Figure 7.15: Compressive strength versus ultrasonic pulse velocity. 274
Figure 8.1: PXRD patterns for SF and NCFA. 288
Figure 8.2: TG (solid lines) and DTA (dotted line) curves for the SF and NCFA fillers. 288
Figure 8.3: Grain-size distribution of SF, NCFA and CEM I as measured by laser diffraction. 289
Figure 8.4: Pore size distribution for the SF and NCFA fillers. 290
Figure 8.5: Workability boxes for several self-compacting mixes. 295
Figure 8.6: Evolution of the density relative to the variation of mass. 297
Figure 8.7: Cumulative pore volume and log differential intrusion of the mixes. (Dotted line) extrusion and (solid line) instrusion. 301
Figure 8.8: Evolution of the mass loss by drying (100 ºC) and absorption by immersion. 304
Figure 8.9: Capillary water absorption of the mixes. 306
Figure 8.10: Rapid chloride ion penetration test by electrical conductance of the mixes. 311
Figure 8.11: Ion Cl^- concentration profile of the mixes. 313
Figure 8.12: Depth of carbonation as a function of t of the mixes. 314
Figure 8.13: Ion SO_3 concentration profile of the mixes. 316
Figure 8.14: PXRD patterns of SCC-1 before and after exposure to SO_3 317
Figure 8.15: PXRD patterns of SCC-2 before and after exposure to SO_3. 318
Figure 8.16: Total shrinkage of the mixes. 319

Índice de Tablas

Tabla 3.1: Propiedades de los aditivos. 81
Table 4.1: Properties of additives. 102
Table 4.2: Self-compaction test. 104
Table 4.3: Concrete mix proportions and dosing tests. 105
Table 4.4: Results of the self-compactability tests for the two types of SCC. 109
Table 4.5: Physical, water absorption & durability properties hardened SCCs. 113
Table 4.6: Comparing the experimental results with estimated by EHE-08 and references. 119
Table 5.1: Characterisation of aggregates. 152
Table 5.2: Characterisation of filler and cement. 154
Table 5.3: Self-compactability tests. 160
Table 5.4: Concrete mix proportions and EFNARC composition parameters. 161
Table 5.5: Results of the self-compactability tests for the two types of SCC. 164
Table 5.6: Results obtained in the test of thermal analysis (TG/TD) for each SCC studied. 168
Table 5.7: Comparing the experimental results with those estimated using EHE-08 and other references. 177
Table 5.8: Total shrinkage. 184
Table 6.1: Concrete mix proportions and EFNARC composition parameters. 200
Table 6.2: Results of the self-compactability tests of the two types of SCC. 206
Table 6.3: Physical and water absorption properties of the hardened SCCs. 209
Table 6.4: Durability properties of the hardened SCCs. 218
Table 7.1: Characterisation of aggregates. 244
Table 7.2: Characterisation of filler and cement. 247
Table 7.3: Concrete mix proportions and dosing tests. 251
Table 7.4: Results of the self-compactability tests for the two types of SCC. 254
Table 7.5: Results obtained in the test of thermal analysis (TG/TD) for each SCC studied. 258
Table 7.6: Comparing the experimental results with those estimated using EHE-08 and other references. 268

Table 7.7: Total shrinkage. 275
Table 8.1: Characterisation of filler and cement. 289
Table 8.2: Concrete mix proportions and dosing tests. 292
Table 8.3: Results of the self-compactability tests for the two types of SCC. 294
Table 8.4: Physical and water absorption properties hardened SCCs. 299
Table 8.5: Durability properties hardened SCCs. 309

Abreviaturas

HAC	Hormigón Autocompactante
JCR	Journal Citation Report
CANMET & ACI	Canadian Centre for Mineral and Energy Technology and American Concrete Institute
RILEM	Réunion Internationale des Laboratoires et Experts des Matériaux, systèmes de construction et ouvrages
EFNARC	European Federation of National Associations Representing for Concrete
BIBM	European Precast Concrete Organisation
CEMUREAU	European Cement Association
ERMCO	European Ready-Mix Concrete Organisation
AENOR	Asociación Española de Normalización
EHE-08	Instrucción Española del Hormigón Estructural
CEN	Comité Europeo de Normalización
EN	Normas Europeas
UNE	Una Norma Española
ASTM	American Society for Testing and Materials
d_f	Diámetro de escurrimiento
d_{jf}	Diámetro de escurrimiento con Anilo J
T_{50}	Tiempo de flujo del ensayo de Escurrimiento
T_V	Tiempo de flujo del ensayo del Embudo V
C_{bl}	Tiempo de flujo del ensayo de la Caja L
IUPAC	Unión Internacional de Química Pura y Aplicada
UE	Unión Europea
PEMAR	Plan Estatal Marco de Gestión de Residuos
RCD	Residuos de construcción y demolición
SF	Filler silíceo
MBC	Mezclas Bituminosas Calientes
RF	Filler de recuperación
NCFA	Cenizas no conformes

XRD	Difracción de rayos X
DTA-TG	Análisis termogravimétrico
B.E.T.	Brunauer-Emmett-Teller
BJH	Barret-Joyner-Halenda
DFT	Density functional theory
FT-MIR	Espectroscopía de infrarrojos con transformada de Fourier
SEM	Microscopía electrónica de barrido
EDX	Energía dispersiva de rayos X
TEM	Microscopía electrónica de transmisión
MIP	Porosimetría por intrusión de mercurio
UPV	Ultrasonic Pulse Velocity
SCC	Self-compacting concrete
OC	Ordinary concrete

Capítulo 1

Justificación, Objetivos y Plan de Investigación de la Tesis Doctoral

1.1 Justificación

La presente memoria de Tesis Doctoral se ha desarrollado dentro de las líneas de investigación del grupo FQM-391, Materiales y Aplicaciones, de la Universidad de Córdoba, en una estrecha colaboración con el grupo TEP-227, Ingeniería de la Construcción, de la misma Universidad. Además, ha existido una colaboración internacional con el Departamento de Engenharia Civil, Arquitectura e Georrecursos del Instituto Superior Técnico de la Universidad de Lisboa, donde se han realizado varias estancias internacionales.

El tema sobre el que versa este trabajo es la búsqueda de alternativas sostenibles en el campo del hormigón ya que es el material más usado en el sector de la construcción, dos veces más que el resto de materiales (madera, acero, plástico o aluminio), debido a sus buenas propiedades estructurales, su sencilla fabricación y su bajo coste. Actualmente, podemos decir que el hormigón sostiene nuestra vida cotidiana. Desde las viviendas y los hospitales hasta los puentes y las aceras, así como cualquier infraestructura. Su omnipresencia es innegable. Mundialmente, su

producción se estima en 4 toneladas per cápita. Sin embargo, no todo es bueno, ya que es la industria que más recursos naturales consume, por ello está considerado como un material poco respetuoso con el medio.

Por este motivo la industria del hormigón está en constante evolución, buscando técnicas más eficientes que permitan la optimización de recursos naturales. Dentro de esta corriente, en la década de los 80, nace el Hormigón Autocompactante (en adelante, HAC), como evolución de la tecnología existente y con el fin de aportar soluciones a los diferentes inconvenientes que presenta el hormigón convencional (fundamentalmente el proceso de vibrado que da lugar a mayores tiempos de ejecución, a altos niveles de ruido, a una mayor y más cualificada mano de obra, y en algunos casos la durabilidad puede quedar comprometida si la operación de vibrado no se realiza correctamente). En los últimos años, la aplicación de este material se ha desarrollado en obra civil y edificación y se ha generalizado en la industria del prefabricado.

El HAC se caracteriza por no requerir vibración y compactación en la colocación, por fluir bajo su propio peso, rellenando completamente las zonas a hormigonar, por alcanzar una completa compactación en presencia de alto grado de armado y alta densidad y por la homogenización del hormigón endurecido. Lo cual se traduce en ventajas tales como reducción de los plazos de ejecución, fabricación de estructuras complejas, mejores acabados superficiales, disminución de la mano de obra, disminución de ruido y vibraciones. En consecuencia, mayor ahorro económico y mayor seguridad laboral.

Para que estas ventajas se puedan dar, el HAC necesita incorporar un alto contenido de finos (cemento, filler y/o árido fino) y aditivos químicos en su dosificación. Esta particularidad hace que este material pueda ser considerado como poco amigable con el medio ambiente. Hoy en día, una solución sería la utilización de residuos o subproductos industriales de granulometría fina como sustitutivo de los finos convencionales necesarios en la fabricación de los HAC. Ello permitiría la valorización de los residuos, el uso de los subproductos y una reducción de su emisión al medio ambiente, así como la optimización de los recursos naturales utilizados. Esto supone un viraje en la percepción ambiental del HAC.

La evaluación del potencial de reutilización y reciclado de los finos residuales generados en la industria y/o minería es un gran desafío, ya que el obstáculo principal es la falta de confianza en la calidad de estos materiales. La investigación es el único instrumento para que el HAC pueda responder a los requerimientos exigidos para cada uso específico y que permitirá alcanzar los compromisos globales y comunitarios en materia de cambio climático y de implementación de la economía circular, convergiendo en la gestión real e integral de los residuos generados y consiguiendo el final de la condición de residuo de estos materiales. Hay que tener en cuenta que la demora en la adopción de medidas proactivas, únicamente servirá para encarecer las medidas que nos veremos obligados a adoptar en el futuro.

Por lo tanto, un conocimiento detallado del comportamiento del HAC con finos residuales tanto en estado fresco como estado endurecido permitiría conocer con exactitud la viabilidad técnica de dichos materiales residuales como filler para HAC y las posibles aplicaciones de este material de construcción más sostenible.

1.2 Objetivos

El objetivo principal de este trabajo es el estudio de viabilidad técnica de aplicación de finos residuales de origen industrial, tales como, residuos de granulometría fina (finos o polvo) procedentes del proceso de secado y calentamiento del árido utilizado en la fabricación de mezclas bituminosas calientes (en adelante, RF), así como, cenizas volantes no conformes, es decir, sin marcado CE, procedentes de centrales termoeléctricas de carbón (en adelante, NCFA), como filler en HAC en sustitución del filler comercial (en adelante, SF) empleado en las mezclas convencionales, con el fin de obtener un material de construcción más sostenible con el medio ambiente. El HAC seleccionado para incorporar estos finos residuales proviene de los resultados parciales de un trabajo llevado a cabo por los grupos de investigación FQM-391 y TEP-227 de la Universidad de Córdoba en colaboración con la Empresa Nacional de Residuos Radiactivos (ENRESA), la cual investiga el uso de HAC, como sustitutivo del hormigón convencional utilizado en las estructuras de las instalaciones de almacenamiento de residuos radiactivos de baja y media actividad localizada en El Cabril (Córdoba).

Para la consecución del objetivo principal, en la investigación se han desarrollado los siguientes objetivos parciales:

- Caracterizar todos los materiales convencionales utilizados en la fabricación del HAC. Se realizó un estudio completo de las propiedades físico-químicas y microestructurales, lo cual permitió evaluar la influencia de estos en el comportamiento del HAC.

- Caracterizar los finos residuales utilizados como filler en la fabricación del HAC. Se llevó a cabo un completo estudio de las propiedades físico-quimicas y microestructurales de los residuos, lo cual permitió evaluar, por un lado, la influencia de estos subproductos en el comportamiento del HAC respecto a un filler comercial y por otro, su potencial como filler para HAC.

- Diseñar y evaluar las propiedades en estado fresco de las dosificaciones de HAC con materiales convencionales. Se realizó el diseño de varias dosificaciones de HAC y se llevó a cabo un estudio de la influencia de diferentes factores, tales como la cantidad de árido grueso, de árido fino y de filler en las propiedades de autocompactabilidad. Dicho objetivo se realizó en colaboración con la Empresa Nacional de Residuos Radiactivos (ENRESA).

- Analizar el comportamiento mecánico y durable a lo largo del tiempo de las dosificaciones de HAC con materiales convencionales. Se abordó el estudio de la estructura porosa y el comportamiento mecánico de las dosificaciones. Además, como parte importante para alcanzar este objetivo, se realizó un estudio comparativo de la durabilidad ante las acciones de agentes agresivos de las diferentes mezclas. Todas las propiedades analizadas fueron correlacionadas con las características microestructurales de las dosificaciones. Finalmente, el trabajo se completó con el estudio de la retracción. El análisis conjunto de todos los parámetros analizados permitió definir, con alto grado de certeza, la dosificación óptima.

- Diseñar las dosificaciones de HAC con los finos residuales de origen industrial como filler. Se llevó a cabo el diseño de varias dosificaciones de HAC con residuos en sustitución del filler comercial.

- Evaluar y comparar las propiedades en estado fresco de las dosificaciones de HAC con finos residuales respecto a la dosificación con filler convencional. Se realizó un estudio de la influencia de los finos residuales como filler en las propiedades de autocompactabilidad de los HAC, evaluándose su comportamiento en estado fresco respecto a la mezcla fabricada con materiales comerciales.

- Analizar y comparar el comportamiento mecánico y durable a lo largo del tiempo de las dosificaciones de HAC con finos residuales como filler respecto a la dosificación con filler convencional. Se llevó a cabo un análisis profundo, evaluando el comportamiento mecánico a larga edad y su correlación con las diferentes reacciones químicas que se producen durante el endurecimiento del HAC. Posteriormente se analizaron las propiedades microestructurales y propiedades físicas de absorción de los HAC. Y, por último, se realizó un estudio de la durabilidad ante las acciones de agentes agresivos que se completó con el análisis de la retracción a larga edad.

La consecución de estos objetivos ha permitido un análisis de la viabilidad técnica de los residuos anteriormente comentados como filler en HAC. Hay que tener en cuenta que a medida que el conocimiento acumulado sobre el comportamiento de estos nuevos materiales se vaya incrementando, será posible alcanzar una fiabilidad similar, sino superior, a la de los materiales convencionales. Este aspecto es fundamental para resolver las incertidumbres en relación a su estabilidad a lo largo del tiempo que permitirá la puesta en valor de subproductos industriales y en consecuencia la minimización del impacto ambiental, lo que contribuirá sin duda a convertir al hormigón en un material más amigable con el medio ambiente.

1.3 Plan de investigación de la tesis doctoral

La metodología seguida para la consecución de los objetivos establecidos en esta investigación se resume en las etapas que se muestran en la Figura 1.1.

Figura 1.1: Metodología del Plan de Investigación de la Tesis Doctoral.

La campaña experimental, se llevó a cabo en los laboratorios del Área de Química Inorgánica y del Área de Ingeniería de la Construcción de la Escuela Politécnica Superior de Belmez (Universidad de Córdoba), principalmente. Aunque, otras instalaciones fueron usadas de refuerzo para completar la fase experimental, tales como los laboratorios del Área de Química Inorgánica y del Área de Ingeniería de la Construcción del Campus de Rabanales (Universidad de Córdoba), el Servicio Central de apoyo a la Investigación (SCAI) de la Universidad de Córdoba, el Instituto de Química Fina de la Universidad de Córdoba, el Laboratorio del Departamento de Química de la Universidad de Navarra y el Laboratório de Construção del Departamento de Engenharia Civil, Arquitectura e Georrecursos del Instituto Superior

Técnico de la Universidad de Lisboa. Un resumen de las tareas llevadas a cabo en la fase experimental se muestra en la Figura 1.2.

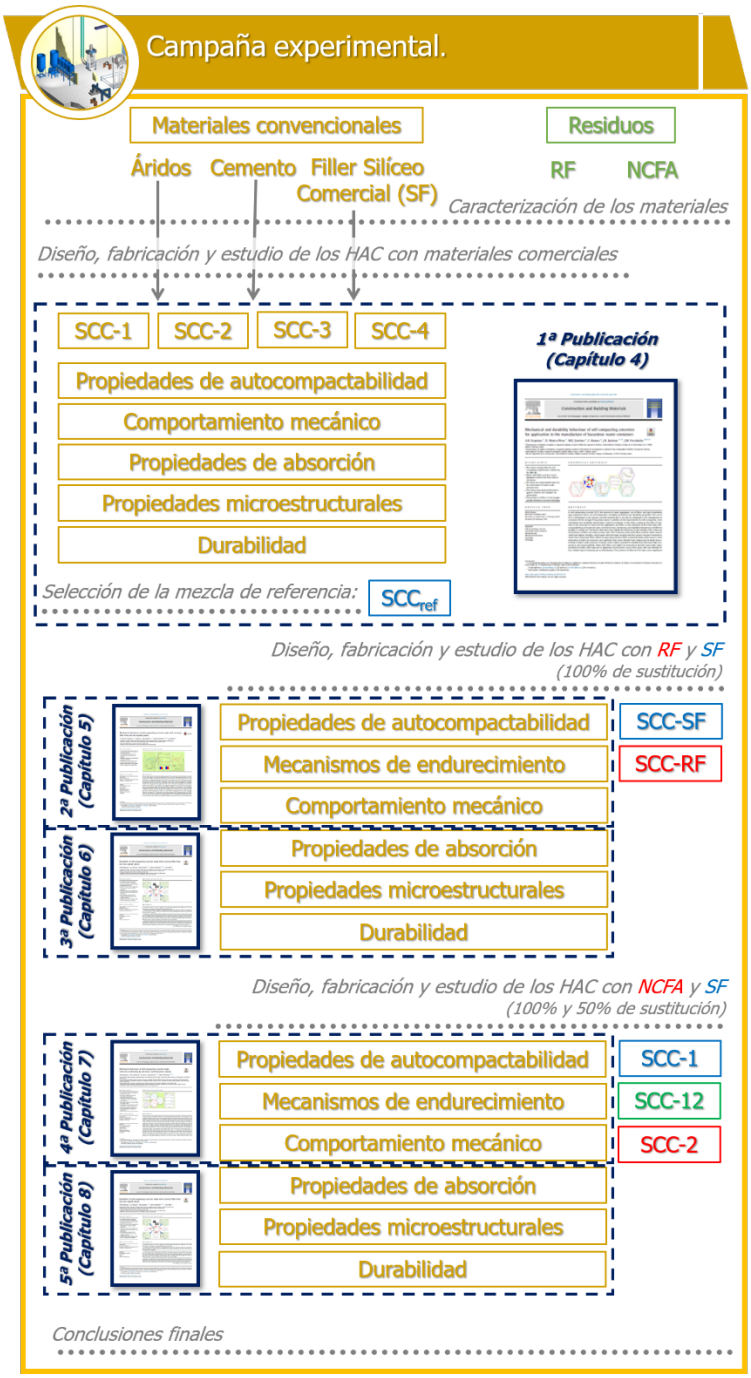

Figura 1.2: Campaña experimental.

1.4 Estructura de la Memoria de Tesis Doctoral

Con el objetivo de facilitar la lectura de la memoria y situar al lector, en las siguientes líneas se resume el contenido de la presente Tesis. Esta Memoria de Tesis Doctoral se presenta como compendio de publicaciones y se ha estructurado en nueve capítulos.

En primer lugar, el Capítulo 1, *Justificación, Objetivos y Plan de Investigación de la Tesis Doctoral*, justifica el tema sobre el que versa la Tesis Doctoral, explica las hipótesis y los objetivos a alcanzar, así como el plan de investigación.

En el Capítulo 2, *Introducción*, se realiza una inmersión en la unidad temática a estudiar y analizar en esta Tesis Doctoral.

El Capítulo 3, *Materiales y Métodos*, se introducen los materiales y métodos utilizados en el desarrollo de la investigación.

Los Capítulos 4, 5, 6, 7 y 8 corresponden a los cinco artículos publicados en revistas internacionales indexadas (el requisito establecido para presentar la Tesis Doctoral en la modalidad como compendio de publicaciones, son tres artículos publicados en los tres primeros cuartiles de la relación de revistas del ámbito de la especialidad y referenciadas en la última relación publicada por el Journal Citation Reports), donde se exponen y analizan los resultados obtenidos en cada uno de los apartados (Figura 1.2).

- Capítulo 4: "*Mechanical and durability behaviour of self-compacting concretes for application in the manufacture of hazardous waste containers*".

En este capítulo se ha llevado a cabo un estudio del efecto de la variación de la cantidad de árido grueso, fino y filler en las propiedades en estado fresco (autocompactabilidad) y en estado endurecido (microestructurales, comportamiento mecánico y durable) de diferentes dosificaciones de HAC. El análisis conjunto de todos los parámetros analizados, permitió definir con alto grado de certeza, la dosificación óptima.

A.R. Esquinas, D. Motos-Pérez, M.E. Jiménez, C. Ramos, J.R. Jiménez, J.M. Fernández, Mechanical and durability behaviour of self-compacting concretes for application in the manufacture of hazardous waste containers, Construction and Building Materials, 168 (2018) 442–458. doi:10.1016/J.CONBUILDMAT.2018.02.138.

- Capítulo 5: "*Mechanical behaviour of self-compacting concrete made with recovery filler from hot-mix asphalt plants*".

En este capítulo se estudia la viabilidad de aplicación de un residuo de granulometría fina (RF) generado en las plantas de mezclas bituminosas calientes, procedente del secado y calentamiento del árido utilizado en la fabricación de las mezclas bituminosas, como filler para HAC. Se realizó un estudio comparativo de dos tipos de HAC. El primer tipo (SCC-RF) se realizó incorporando RF de naturaleza dolomítica como filler y el segundo (SCC-SF) se realizó con filler silíceo comercial, este último utilizado como referencia. La cantidad de filler utilizada fue similar en ambos casos. Para determinar el comportamiento de estos dos tipos de HAC, se realizó en primer lugar un estudio del HAC en fresco, donde se midieron las propiedades de autocompatibilidad, tales como fluidez, resistencia al bloqueo y resistencia a la segregación. Y a continuación se llevó a cabo una amplia investigación del HAC en estado endurecido donde se abordó su comportamiento mecánico a larga edad y su correlación con los mecanismos de endurecimiento. Por último, también se estudió la retracción a corta edad. Lo que permitió conocer de manera más exhaustiva el comportamiento de HAC con este residuo.

A.R. Esquinas, C. Ramos, J.R. Jiménez, J.M. Fernández, J. de Brito, Mechanical behaviour of self-compacting concrete made with recovery filler from hot-mix asphalt plants, Construction and Building Materials, 131 (2017) 114–128. doi:10.1016/J.CONBUILDMAT.2016.11.063.

- Capítulo 6: "*Durability of self-compacting concrete made with recovery filler from hot-mix asphalt plants*".

En este capítulo se ha llevado a cabo un análisis de la viabilidad del RF como filler en SCC desde el punto de vista de su comportamiento durable. Se realizó un estudio comparativo en dos tipos de SCC; uno empleando RF y otro empleando un filler silíceo comercial como referencia. En primer lugar, se corroboraron las propiedades

autocompactabilidad. A continuación, se analizaron las propiedades físicas de los HAC (densidad aparente, densidad en seco y porosidad abierta) y las propiedades de absorción de agua (por inmersión y por capilaridad). Se definieron las propiedades microestructurales (estructura porosa) y su influencia en la durabilidad, para lo cual se estudió la permeabilidad de agua a presión, la penetración del ion cloruro, la profundidad de carbonatación y la penetración del ion sulfato en las diferentes mezclas. El trabajo se completó con el estudio de la retracción a larga edad. Estos aspectos son fundamentales para resolver las incertidumbres en relación a la estabilidad a largo plazo del HAC fabricado con RF y permitir su puesta en valor, y en consecuencia la minimización del impacto ambiental, lo que contribuirá a convertir al HAC en un material más amigable con el medio ambiente.

A.R. Esquinas, J.I. Álvarez, J.R. Jiménez, J.M. Fernández, J. de Brito, Durability of self-compacting concrete made with recovery filler from hot-mix asphalt plants, Construction and Building Materials, 161 (2018) 407–419. doi:10.1016/J.CONBUILDMAT.2017.11.142.

- Capítulo 7: "*Mechanical behaviour of self-compacting concrete made with non-conforming fly ash from coal-fired power plants*".

En este capítulo se evalúa el uso de cenizas volantes de una central termoeléctrica de carbón que no cumple con los criterios de conformidad marcado por la normativa (NCFA) como filler en HAC. Se realizó un estudio comparativo de tres mezclas de HAC; en la primera se empleó un filler silíceo comercial (SF) como referencia, en la segunda una mezcla, 1:1 en volumen, de SF y NCFA y en la tercera se empleó únicamente NCFA. La cantidad de filler utilizada en volumen es similar en todos los casos. Para determinar el comportamiento de los tres HAC, se realizó en primer lugar un estudio en estado fresco, donde se estudiaron las propiedades de autocompatibilidad, tales como fluidez, resistencia al bloqueo y resistencia a la segregación. Posteriormente se llevó a cabo un profundo análisis de los HAC en estado endurecido donde se abordó su comportamiento mecánico a larga edad y su correlación con las diferentes reacciones químicas que se producen durante el endurecimiento del hormigón. Por último, también se incluye el estudio de retracción a corta edad. Lo que permitirá responder a los requerimientos mecánicos exigidos para el uso de este residuo.

A.R. Esquinas, E.F. Ledesma, R. Otero, J.R. Jiménez, J.M. Fernández, Mechanical behaviour of self-compacting concrete made with non-conforming fly ash from coal-fired power plants, Construction and Building Materials, 182 (2018) 385–398. doi:10.1016/J.CONBUILDMAT.2018.06.094.

- Capítulo 8: "*Durability of self-compacting concrete made non-conforming fly ash from coal-fired power plants*".

Este capítulo tiene como objeto llevar a cabo una evaluación del uso NCFA como filler en HAC desde el punto de vista de la durabilidad. Se ha realizado un análisis comparativo de tres mezclas; en la primera se ha empleado un filler silíceo comercial (SF) como referencia, en la segunda una mezcla, 1:1 en volumen, de SF y NCFA y en la tercera se empleó únicamente NCFA. Para determinar el comportamiento de los tres HAC, se realizó en primer lugar un estudio en estado fresco, donde se corroboraron las propiedades de autocompatibilidad. Posteriormente se analizaron las propiedades físicas y de absorción, así como las propiedades microestructurales de los HAC. Y, por último, se realizó un estudio de la durabilidad de estos materiales que se completó con el análisis de la retracción a larga edad.

A.R. Esquinas, J.I. Álvarez, J.R. Jiménez, J.M. Fernández, Durability of self-compacting concrete made from non-conforming fly ash from coal-fired power plants, Construction and Building Materials, 189 (2018) 993–1006. doi:10.1016/J.CONBUILDMAT.2018.09.056.

En el Capítulo 9, "*Conclusiones/Conclusions. Futuras líneas de investigación*", se presentan las conclusiones alcanzadas, así como se exponen las futuras líneas de investigación.

Y, por último, este documento finaliza con tres Anexos. En el Anexo A, se recogen la producción científica derivada directamente de la Tesis Doctoral. En el Anexo B, se introduce el resto de la producción científica llevada a cabo durante el periodo de la Tesis Doctoral, en fase de publicación. Y, finalmente, en el Anexo C, se presentan otras aportaciones científicas vinculadas con el autor, realizadas durante el periodo de Tesis Doctoral.

Capítulo 2

Introducción

2.1 Origen y desarrollo del Hormigón Autocompactante

El HAC nace como una evolución del hormigón convencional. La idea de un hormigón de calidad, compacto y durable que pudiera ser empleado en estructuras fuertemente armadas donde el proceso de vibración era complicado y cuyo rendimiento y calidad no dependiese de la mano de obra de los operarios, era perseguida por el Dr. Hajime Okamura. En la década de los 80s, este profesor de la Universidad de Tokio ideó y desarrolló un hormigón que podía ser colocado sin utilizar ningún medio de compactación y conseguía rellenar el encofrado de las estructuras por gravedad sin sufrir ningún tipo de segregación ni otros defectos en el hormigonado [1]. El desarrollo del HAC y el estudio de la trabajabilidad del hormigón fueron llevados a cabo por Ozawa y col. en la Universidad de Tokio [2].

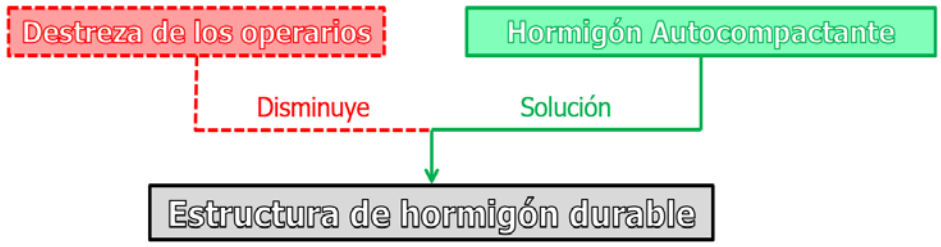

Figura 2.1: La necesidad del hormigón autocompactante.
Fuente: Adaptado de [2].

En su origen, este hormigón fue denominado "High Performance Concrete" (Hormigón de Alto Rendimiento), aunque esta designación fue modificada por "Self-Compacting High Performance Concrete" (Hormigón Autocompactante de Alto Rendimiento), ya que el término "high performance concrete" había sido usado ya internacionalmente para referirse a un hormigón con altas prestaciones de durabilidad [3].

En 1992, Ozawa y col. presentaron en el 4º Internacional Conference on Fly Ash, Silica Fume, Slag and Natural Pozzolans in Concrete del CANMET & ACI (Canadian Centre for Mineral and Energy Technology and American Concrete Institute) celebrado en Estambul, el trabajo titulado "Role of Powder Material on the Filling Capacity of Fresh Concrete" [4], el cual aceleró la difusión mundial del concepto HAC. A partir de entonces se comenzaron a desarrollar trabajos de investigación sobre este novedoso material por todo el mundo.

En 1997, el RILEM (Réunion Internationale des laboratoires et experts des matériaux, systèmes de construction et ouvrages) crea un comité de trabajo para abordar los aspectos técnicos sobre el HAC (RILEM TC 174-SCC). Un año más tarde, en 1998 se organiza en Kochi (Japón) el primer workshop sobre el HAC (International Workshop on Self-Compacting Concrete) y se estableció la base de una red de intercambio de información sobre este material. En 1999, se organiza el primer congreso internacional (1st International RILEM Symposium on Self-Compacting Concrete) en Estocolmo, con el objetivo de ofrecer una amplia plataforma de información y debate sobre esta tecnología. Ya que el interés por el HAC había crecido rápidamente en todo el mundo tras el trabajo realizado por el profesor Okamura.

En 2002, European Federation of National Associations Representing for Concrete (EFNARC), federación europea dedicada a sistemas específicos de hormigón y productos químicos especializados para la construcción, publica un informe técnico sobre las "Especificaciones y directrices para el Hormigón Autocompactante - HAC" [5] donde recogen la experiencia práctica, así como los descubrimientos en la investigación de los miembros de la EFNARC para obtener un marco de referencia en el diseño y la utilización del HAC de alta calidad.

En 2005, EFNARC junto a otras federaciones europeas dedicadas a la promoción de materiales avanzados y el suministro de hormigón; European Precast Concrete Organisation (BIBM), European Cement Association (CEMUREAU) y European Ready-Mix Concrete Organisation (ERMCO), publicaron una revisión del anterior informe técnico, denominado "The European Guidelines for Self-Compacting Concrete. Specification, Production and Use" [6]. Este documento revisaba las prácticas existentes y aspectos pre-normativos del HAC, abordando los problemas generados por la ausencia de especificaciones, normas o métodos de ensayo sobre el HAC en Europa y proporcionando un enfoque técnico para su aceptación y uso.

En España, en 2007 la Asociación Española de Normalización (AENOR) publica las primeras normas para la caracterización del HAC en estado fresco (fluidez, fluidez en presencia de barras y determinación del tiempo de flujo).

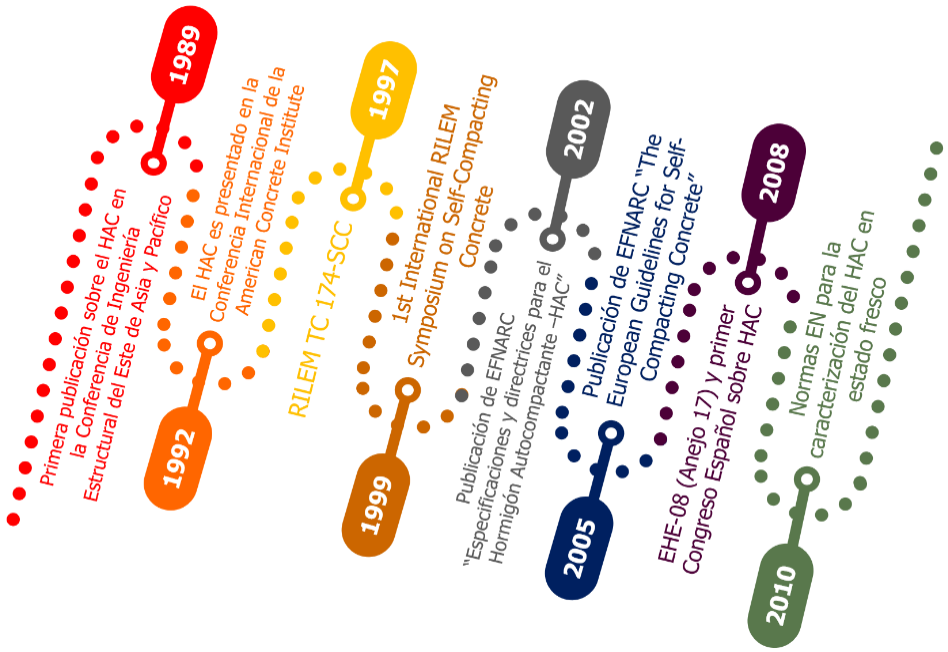

Figura 2.2: Desarrollo del hormigón autocompactante desde su origen.
Fuente: Elaboración propia.

En 2008, se publica una revisión de la Reglamentación Técnica relativa al proyecto y ejecución de las estructuras de hormigón, Instrucción Española del Hormigón Estructural (EHE-08), la cual incluye un apartado específico (Anejo 17) titulado "Recomendaciones para la utilización del hormigón autocompactante" [7], donde se

recogen las especificaciones para el empleo adecuado de estos hormigones que, por su autocompactabilidad, poseen propiedades en estado fresco que le confieren una docilidad y consistencia que no puede ser evaluada por medio del ensayo de asentamiento según la UNE-EN 12350-2.

En este mismo año, se celebra en Valencia, el 1er Congreso Español sobre el Hormigón Autocompactante, organizado por la Universidad Politécnica de Madrid, la Universidad Politécnica de Cataluña y la Universidad Politécnica de Valencia.

En 2010, el Comité Europeo de Normalización (CEN) publica un conjunto de normas europeas (EN) para caracterizar el HAC en estado fresco, donde especifican los métodos de ensayo para definir al hormigón como autocompactante. De acuerdo con estas normativas europeas, las normas UNE publicadas por AENOR en 2007 son revisadas y actualizadas.

A partir de entonces la aplicación de este novedoso hormigón podía ser llevada a cabo de acuerdo a unos documentos técnicos unificados, elaborados por comités de expertos a partir del desarrollo tecnológico, de trabajos experimentales y del consenso, que garantizan unos niveles de calidad y seguridad en su empleo.

2.2 Propiedades del Hormigón Autocompactante

Las características más significativas del HAC respecto al hormigón convencional residen en su estado fresco. De acuerdo con el Anejo 17 de la EHE-08 el HAC se puede definir como *"a aquel hormigón que, como consecuencia de una dosificación estudiada y del empleo de aditivos superplastificantes específicos, se compacta por la acción de su propio peso, sin necesidad de energía de vibración ni de cualquier otro método de compactación, no presentando segregación, bloqueo de árido grueso, sangrado, ni exudación de la lechada. El hormigón autocompactante añade a las propiedades del hormigón convencional, en cualquiera de las clases resistentes, la propiedad de autocompactabilidad, descrita anteriormente*" [7].

Por lo que se pueden enumerar las siguientes características:

- Capacidad de fluir y rellenar el encofrado sin ayuda externa, bajo la acción de su propio peso.
- Resistencia al bloqueo y capacidad de flujo entre el armado y huecos estrechos.
- Resistencia a la segregación y homogénea distribución de los áridos dentro de la mezcla.

Estas propiedades le confieren al HAC las siguientes ventajas [6]:

- Compactación adecuada del hormigón, eliminando los problemas de una vibración inadecuada por la falta de destreza de los operarios.
- Facilidad de hormigonado de estructuras complejas y/o densamente armadas.
- Ejecución de elementos arquitectónicos y estructurales más complejos.
- Mejores acabados superficiales.
- Reducción de la mano de obra y equipos auxiliares necesarios. Aumento de la vida útil de los moldes o encofrados. Elementos de encofrado más ligeros y menor mantenimiento de los mismos.
- Eliminación de la vibración y disminución del ruido ambiental.
- Disminución de los riesgos laborales mejorando la salud laboral y el ambiente de trabajo.
- Disminución del plazo de ejecución.
- Aumento de la rentabilidad en el coste total de la obra.

Estas propiedades dan lugar a un hormigón, que se diferencia del resto de los hormigones, por sus propiedades en estado fresco. Esto se logrará gracias al empleo de un alto contenido de finos, disminuyendo el contenido de áridos gruesos y a la acción de aditivos superplastificantes que van a proporcionar una alta fluidez. Hay que tener en cuenta, que este comportamiento diferencial en estado fresco va a influir en las propiedades en estado endurecido del hormigón tales como la microestructura del material, la interfase árido-pasta y en un aumento de la sensibilidad en las condiciones de curado [8].

2.3 Consideraciones sobre los materiales empleados en la fabricación del HAC

Los materiales empleados en la fabricación del HAC no difieren de los del hormigón convencional. Aunque las proporciones de ellos varían, ya que es necesario una mayor cantidad de finos (partículas que pasan por el tamiz 0.125 mm) y la incorporación de aditivos para obtener las propiedades requeridas [9], como se ha comentado anteriormente.

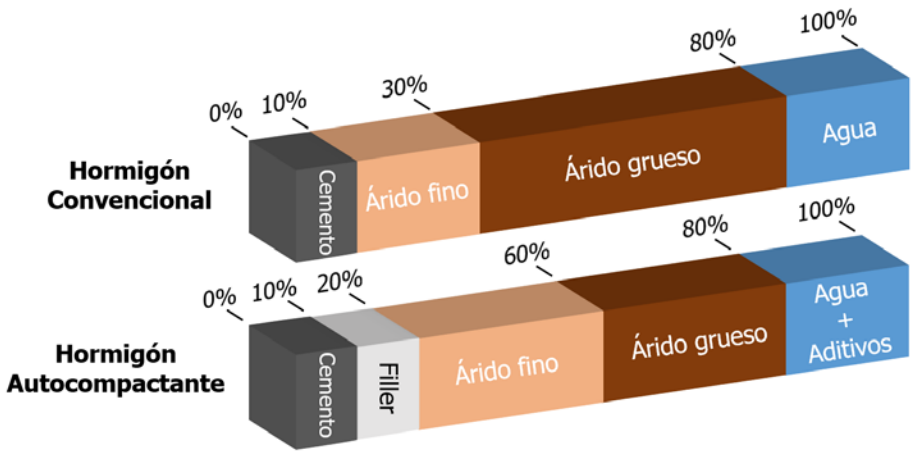

Figura 2.3: Proporciones volumétricas aproximadas de los componentes principales empleados para la fabricación de hormigón convencional y autocompactante.
Fuente: Adaptado de [9].

Respecto al Cemento, no existen unos requisitos específicos para su uso en el HAC. Estos deberán cumplir con la Instrucción para la Recepción de Cementos (RC-16, Real Decreto 256/2016), al igual que ocurre en los hormigones convencionales. Cualquier tipo de cemento puede ser utilizado, no obstante, se deberán tener en cuenta sus propiedades particulares. El CEM I es el tipo de cemento más común. También se podrán utilizar cementos para uso específico en HAC, que incluyan en su composición una cantidad de adiciones complementarias destinadas a dotar a la mezcla de la cantidad de finos necesaria. La cantidad de cemento recomendable oscila entre los 250-500 kg/m^3, cantidades de cemento superiores serían perjudiciales respecto a la retracción y el calor de hidratación [10,11].

El Filler o las adiciones son materiales que tienen la finalidad de aportar finos a la mezcla. Por definición, es deseable que presenten más del 70% de las partículas inferiores a 0.063 mm. Pueden clasificarse como inertes (filler mineral y pigmentos), puzolanas (cenizas volantes y humo de sílice) e hidráulicamente activas (escorias granulada de alto horno). Este componente es indispensable para la fabricación del HAC ya que además de generar una granulometría más continua, da lugar a una mayor cohesión, evitando la segregación del árido grueso y la exudación, proporcionando un mayor control de la demanda de agua y de la densidad de la matriz del hormigón. El filler tendrá un efecto químico ya tiene un papel activo en las reacciones de hidratación, un efecto físico debido a que puede actuar como centro de nucleación de los productos hidratados y un efecto de relleno, como anteriormente ha sido comentado. Además, permite reducir la cantidad de cemento para conseguir los finos necesarios y por consiguiente reduciendo los efectos negativos tanto de carácter técnico como medioambiental. Por otro lado, la EHE-08 aconseja que el contenido máximo de partículas inferiores a 0.063 mm sea de 250 kg/m^3. También podrían ser empleados como filler otros materiales o subproductos de granulometría fina. Es necesario tener en cuenta el efecto de estos materiales secundarios sobre las propiedades del HAC, por lo que sus características deberán ser evaluadas previamente mediante ensayos. En consecuencia, las características física-químicas del filler y su interacción con la mezcla serán variables, afectando tanto a las propiedades en estado fresco como endurecido del HAC [12–19].

En cuanto a los áridos empleados en la fabricación del HAC, al igual que en el hormigón convencional, deben cumplir con las especificaciones que marca la EHE-08. Este material puede proceder de plantas de machaqueo (árido machacado) y de origen natural (árido rodado), estos últimos favorecerán la fluidez del hormigón debido a la menor relación superficie/volumen respecto a los primeros, los cuales presentan una mayor fricción entre las partículas.

El Árido Fino se caracteriza por influir significativamente en la viscosidad de la mezcla y por tanto en las características de autocompactabilidad del hormigón. De acuerdo con la EFNARC el contenido de árido fino debería estar entre el 48 y 55% del peso total de los áridos. El contenido de partículas inferiores a 0.125 mm tendrá una importancia significativa, ya que proporciones elevadas de esta fracción en el árido

fino disminuirá la cantidad de filler necesaria para conseguir los finos exigidos. Por esta razón, la proporción de árido fino empleado en el HAC es superior al hormigón convencional (Figura 2.3). De acuerdo con la EFNARC la cantidad de finos totales (teniendo en cuenta el cemento, filler y árido fino) debería estar entre los 380 – 600 kg/m^3.

La EHE-08 expresa que el Árido Grueso empleado en la fabricación del HAC tiene que tener un tamaño máximo de 25 mm, aunque se aconseja que no supere los 20 mm, para evitar el posible bloqueo ante estrangulamientos. Los tamaños máximos habituales son 12 y 16 mm, ya que cuanto menor sea el tamaño máximo, mayor será la distancia entre las partículas gruesas, disminuyendo la probabilidad de que se den bloqueos [1]. Por esta razón, el contenido de árido grueso en HAC es menor que en los hormigones convencionales (Figura 2.3). De acuerdo con la EFNARC el contenido de árido grueso debería estar entre el 750 y 1000 kg/m^3, no debiendo superar el 50% del total de los áridos.

Por lo que una disminución del contenido de árido grueso y un aumento del árido fino proporcionará al hormigón mayor fluidez, facilidad para atravesar zonas fuertemente armadas, resistencia a la segregación y al bloqueo ante la presencia de obstáculos debido al efecto lubricante de las partículas finas respecto a las gruesas [20]. La relación árido fino/árido grueso tiene una importancia característica para el rendimiento del HAC y la densidad de empaquetamiento [21,22].

El último componente necesario para formar la mezcla es el Agua. Al igual que el resto de componentes debe cumplir los requisitos marcados por la EHE-08.

Para poder conseguir las propiedades de autocompactabilidad se tienen que incorporar los Aditivos, sin los cuales no es posible la obtención del HAC, ya que es la única manera de compensar la demanda de agua del filler y del árido fino sin aumentar la relación A/C. El desarrollo de los aditivos superfluidificantes de policarboxilato, que proporcionan una elevada capacidad reductora de agua en comparación con los superplastificantes tradicionales basados en naftaleno-sulfonado o melamina-sulfonada, permitió el desarrollo del HAC. Existen varios tipos de aditivos: superplastificantes/reductores de agua de alta actividad, moduladores de viscosidad

o cohesionantes y otros aditivos químicos (retenedores de agua, inclusores de aire, aceleradores, retardantes, hidrófugos o reductores de retracción).

El aditivo superplastificante se caracteriza por proporcionar una elevada trabajabilidad con una relación A/C baja, garantizando el desarrollo de las propiedades mecánicas y durables. Las moléculas de este aditivo se adsorben en la superficie de los granos del cemento generando una repulsión entre ellos (efecto estérico), provocando su dispersión en la fase acuosa y liberando el agua contenida en las partículas aglomeradas de cemento, lo cual proporciona un aumento de la fluidez a la mezcla [23]. Este aditivo permite un mayor control de la viscosidad de la mezcla, en comparación con el empleo de agua únicamente [24], sin el efecto negativo sobre el rendimiento mecánico y de durabilidad.

Los aditivos moduladores de viscosidad mejoran sustancialmente la cohesión del hormigón manteniendo la fluidez. Su composición varía dependiendo del tipo (orgánicos e inorgánicos), los más usuales están compuestos por polisacáridos microbianos (goma Welan), derivados de celulosa (metil-celulosa) y polímeros acrílicos [25,26]. Los mecanismos de acción en cada caso son diferentes. Los polímeros (naturales, semisintéticos y sintéticos) actúan fijando el agua libre del hormigón mediante la creación de puentes de hidrógeno impidiendo la exudación y proporcionando una mayor viscosidad. Existen otros tipos, como los basados en fluidos con partículas de nanosílice coloidales, las cuales se adsorben en los granos de cemento aumentando la viscosidad y proporcionando una elevada estabilidad del hormigón. Su uso es necesario cuando no existe una cantidad de finos suficiente, o no es necesario un rendimiento mecánico elevado, o para minimizar la variación en la calidad de las materias primas o sus proporciones.

Es recomendable comprobar la compatibilidad del aditivo con el cemento y el filler. Ya que pueden originarse problemas, como una inadecuada y prematura pérdida de autocompactabilidad, segregación o exudación, excesivo retraso del fraguado, pérdida de aire ocluido o aumento del mismo, etc. El fabricante deberá proporcionar las indicaciones adecuadas en cuanto a su dosificación.

Existen otros elementos que pueden ser adicionados al HAC para dotarle de ciertas propiedades, como es el caso de las Fibras o Pigmentos.

La mezcla de todos los componentes formará el hormigón. Si se considera la mezcla de finos junto con el agua (y el aire) se hablará de pasta, cuya misión no es solamente la de rellenar los huecos entre los áridos sino también la de proporcionar fluidez, lubricar el sistema y arrastrar al árido sin que se produzca un alto rozamiento entre ellos que pueda dar lugar a bloqueos en estructuras densamente armadas. De acuerdo con la EFNARC [6] el contenido de pasta debería estar entre el 300 y 380 L/m^3. Si a los anteriores componentes se le suman los tamaños inferiores a 4 mm, se denominará mortero.

Existen numerosos métodos de dosificación para fijar las cantidades y proporciones de estos elementos, generalmente de base empírica. Su fundamento se basa en conseguir una cantidad de pasta mayor y un contenido de árido grueso menor que en los hormigones convencionales, para reducir la fricción entre partículas y así alcanzar una alta fluidez. Una de las posibilidades para conseguir el mayor volumen de pasta sería aumentar el contenido de cemento, lo cual podría evitarse si se utilizan filler y aditivos que permitan obtener mezclas con cantidades de cemento del mismo orden que en los hormigones convencionales, pero con el contenido de finos necesario y eliminando los efectos negativos de utilizar un alto contenido de cemento.

La relación A/C, las adiciones, los aditivos y la cantidad de arena presentes en el mortero influirán en la autocompactabilidad de la mezcla. Por otro lado, el volumen del árido grueso afecta a la autocompactabilidad y juega un papel importante en la resistencia al bloqueo de la mezcla. Es recomendable tender a granulometrías de máxima compacidad, con el objetivo de aumentar la estabilidad del sistema frente a la segregación y conseguir mezclas con un menor contenido de pasta.

El diseño de la mezcla se puede dividir en dos fases, una relativa a la pasta y otra al esqueleto granular (árido fino y grueso). Existen también modelos teóricos, basados en sistemas iterativos hasta obtener la dosificación final. No obstante, no existe un consenso en la obtención de HAC, por lo que las empresas productoras tendrán que

utilizar su propio conocimiento, derivado de la experiencia y de la destreza técnica de su personal [27].

2.4 Comportamiento dinámico del HAC

Como se ha comentado anteriormente, las propiedades que caracterizan al HAC dependerán del comportamiento en estado fresco y por tanto de la reología del material, es decir, del comportamiento respecto a la deformación y movimiento que se produce ante una tensión a lo largo del tiempo. El hormigón se comporta como un fluido de Bingham (fluido no newtoniano) [28,29], donde su comportamiento dinámico se caracterizará por la relación lineal entre la velocidad de deformación (γ) y a la tensión de corte (τ), Ecuación 2.1:

$$\tau = \tau_0 + \mu \cdot \gamma \qquad \text{(Ec. 2.1)}$$

donde τ_0 es la tensión umbral que será necesaria vencer para poner en movimiento el fluido debido al rozamiento entre las partículas y γ es la viscosidad plástica. La reología del hormigón será definida a partir de estos dos parámetros y dependerá de los áridos utilizados, del volumen de pasta y de la propia reología de la pasta.

La tensión umbral está asociada a la fluidez, disminuirá cuanto más fluido sea el hormigón, y la viscosidad plástica está relacionada con la resistencia a la segregación y con la estabilidad del hormigón. Tanto una baja como una alta viscosidad provocarán la segregación de la mezcla. La representación gráfica de la Ecuación 2.1, denominada Curva de flujo, se muestra en la Figura 2.4.

A mayor viscosidad, el hormigón tiende a fluir de manera más lenta, mientras que a mayor tensión umbral, el movimiento de la masa es más limitado. La diferencia entre hormigones convencionales y hormigones autocompactantes radica en la diferencia de estos parámetros. El HAC presenta una menor tensión umbral y una mayor viscosidad respecto al hormigón convencional debido al mayor contenido de finos y aditivos que contiene. La reducción de la tensión umbral hasta valores apropiados para el HAC es posible gracias al empleo de aditivos superplastificantes.

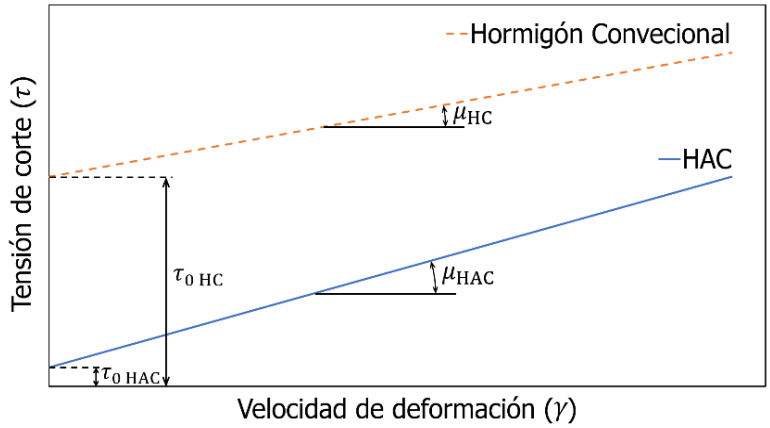

Figura 2.4: Curva de flujo del HAC y del hormigón convencional.
Fuente: Adaptado de [30].

Dependiendo de la dosificación y de la naturaleza de los materiales, el HAC puede comportarse como un fluido tixotrópico, es decir, en reposo el material presenta una red estructural tridimensional, la cual se rompe cuando se aplica una tensión que provoca la reorientación o deformación de las partículas y la viscosidad se minimiza. Cuando dicho esfuerzo cesa, la red estructural tridimensional se reestablece, así como la viscosidad original.

El comportamiento dinámico del HAC deberá garantizar la "Capacidad de Relleno", es decir, la capacidad de fluir y rellenar un encofrado bajo la acción de su propio peso, garantizando el recubrimiento de las armaduras y sin originarse coqueras. Por otro lado, deberá tener la "Capacidad de Paso o Resistencia al Bloqueo", es decir la habilidad de pasar entre las armaduras, obstáculos o estrechamientos de los encofrados, lo cual es sensible tanto a la distribución de las armaduras como al tamaño máximo de árido. Además, deberá presentar "Resistencia a la Segregación", es decir, no se producirá separación entre los áridos o exudación del agua. Estando relacionado con la estabilidad y viscosidad de la mezcla, como anteriormente se ha comentado. Esta tendrá que tener "Robustez", es decir, la capacidad de mantener las características en estado fresco incluso si se producen pequeñas variaciones en las propiedades de los materiales o en la temperatura de fabricación y mantener sus características durante el lapso de tiempo desde la fabricación hasta su puesta en obra, "Tiempo abierto".

Los ensayos normalizados que definen el comportamiento dinámico del HAC son:

- Ensayo de escurrimiento (UNE-EN 12350-8) [31], permite evaluar la capacidad de relleno y de forma cualitativa la existencia de segregación.
- Ensayo del embudo V (UNE-EN 12350-9) [31], permite evaluar la capacidad de relleno y de paso por aberturas estrechas.
- Ensayo de la caja en L (UNE-EN 12350-10) [31], permite evaluar la capacidad de paso a través de barras de armadura.
- Ensayo de escurrimiento con el anillo J (UNE-EN 12350-12) [31], permite evaluar la capacidad de paso a través de barras de armadura y de forma cualitativa la existencia de segregación.

La tensión umbral y la viscosidad presentan una relación bastante estrecha con el diámetro de escurrimiento (d_f) y el tiempo de flujo del ensayo de escurrimiento (T_{50}) y del embudo V (T_V), respectivamente [32,33]. Además de los ensayos normalizados comentados anteriormente, existen otros métodos de ensayo que permiten definir las características del HAC de forma complementaria:

- Ensayo Orimet [34], que permite evaluar la capacidad de relleno y de paso bajo la acción de su propio peso.
- Caja en U [6], que permite evaluar la capacidad de paso a través de barras de armadura en condiciones de flujo confinado y en contra de la fuerza de la gravedad.
- Caja de relleno [35], que permite evaluar la capacidad de relleno y de paso a través de barras de armadura.
- Tubo-U [30], que permite evaluar la robustez y la resistencia a la segregación estática o dinámica de forma cuantitativa.
- Ensayo de la columna (ASTM C1610/C1610M–17) [36], que permite evaluar la resistencia a la segregación estática de forma cuantitativa.
- Ensayo de segregación por tamiz (UNE-EN 12350-11) [31], que permite evaluar la resistencia a la segregación de forma cuantitativa.
- Ensayo de control de recepción del HAC [30], que permite evaluar la autocompactabilidad en obra, antes de ser colocado.

2.5 Comportamiento del HAC en estado endurecido

Las singularidades que presenta el HAC, influirán significativamente en los mecanismos de hidratación y fraguado y, por consiguiente, afectarán al rendimiento del HAC en estado endurecido, tanto desde el punto de vista mecánico como durable.

Las reacciones químicas que se producen durante el fraguado y el endurecimiento del hormigón ocurren de forma acoplada, a una velocidad determinada y de forma irreversible. Estas dependerán de los materiales que intervienen en el sistema. El elemento que tendrá una mayor influencia en este proceso es el cemento debido a las reacciones de hidratación de sus fases, cuando se mezcla con agua, que dará como resultado el endurecimiento del hormigón. La cinética y la estequiometría de las reacciones son complejas. Los cambios temporales en las fases presentes durante la solidificación del cemento se muestran en la Figura 2.5.

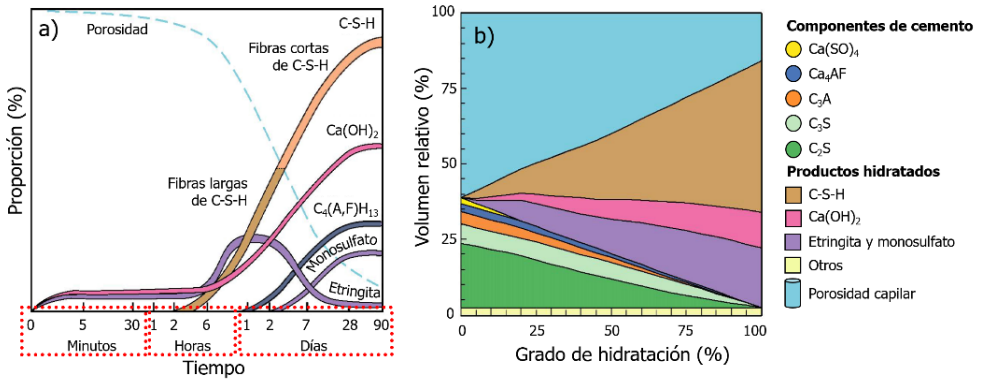

Figura 2.5: Fases presentes en el cemento en función del tiempo (a) [37] y en función del grado de hidratación (b) [38].

La velocidad de reacción de las diferentes fases es diferente: el aluminato (C_3A) y la alita (C_3S) se hidratan más rápidamente que la ferrita (C_4AF) y la belita (C_2S) [39,40]. El desarrollo del proceso de hidratación respecto al calor de hidratación que se genera se muestra en la Figura 2.6 y se puede dividir en cinco etapas: Disolución o Hidrólisis Inicial, Periodo de Reposo o Latente, Fraguado y Aceleración, Endurecimiento y el Estado Estable o de Desaceleración [41].

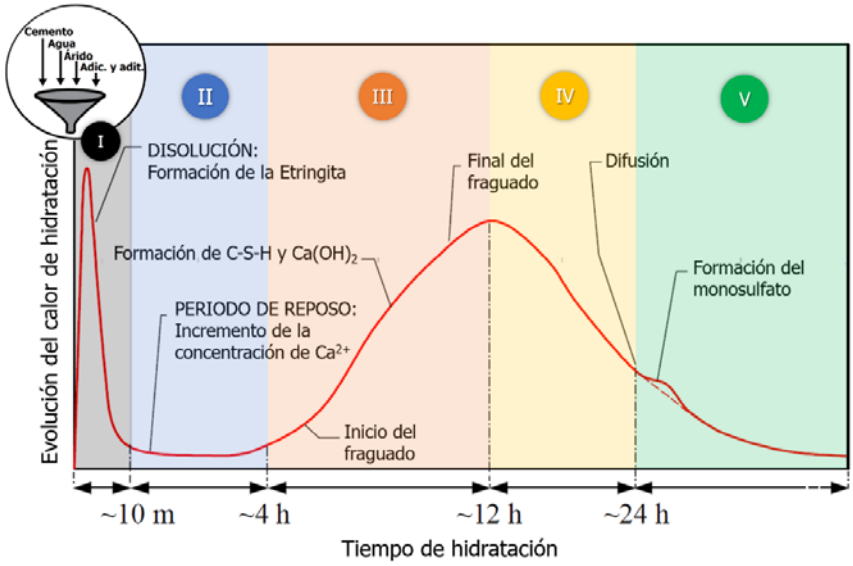

Figura 2.6: Etapas del proceso de hidratación del cemento respecto al calor de hidratación. Fuente: Adaptado de [42].

La Primera Etapa (Disolución o Hidrólisis inicial) comienza cuando el cemento entra en contacto con el agua (Figura 2.6). En este momento, los iones de Ca^{2+} se disuelven rápidamente y el pH de la disolución aumenta por encima de 12 a los pocos minutos. Se produce la inmediata formación de la etringita (sulfoaluminato tricálcico hidratado formado a partir de la reacción del C_3A, yeso y agua). El C_3A es la fase más reactiva del cemento, la cual reacciona rápidamente con el agua disolviéndose y provocando un endurecimiento de la pasta debido a la formación del aluminato de calcio hidratado. El C_3A será el responsable del desarrollo de una pobre resistencia inicial, denominada "fraguado rápido" [43–46]. Para evitar este rápido endurecimiento y regular el fraguado, se añade yeso ($Ca(SO)_4$) al cemento, dando lugar a la formación de etringita, como se ha comentado previamente. El $CaSO_4$ aporta iones Ca^{2+} que frenan el desplazamiento del equilibrio de la hidrólisis de los compuestos cálcicos por efecto del ion común. Además, se produce una inmediata precipitación de los iones Al^{3+} en forma de etringita, antes de que estos iones actúen como coagulantes del sistema coloidal. Asimismo, la precipitación de la etringita actúa físicamente, bloqueando por su insolubilidad el acceso del agua al interior de las partículas de C_3A y retardando su hidrólisis. La duración de esta etapa es aproximadamente de media hora tras el amasado.

En esta Etapa, hay que tener en cuenta que adiciones con un alto contenido de calcio (principalmente en forma de aluminato cálcico) podrían incrementar el riesgo de "fraguado rápido" en caso de que no exista suficiente sulfato en la mezcla. Por otro lado, cuando la adición proceda de algún proceso de combustión, el exceso de inquemados podría absorber los aditivos químicos [47].

La hidrólisis se ralentiza, aunque continúa lentamente en la siguiente etapa, Etapa 2: Período de Reposo o Latente (Figura 2.6), el cemento continúa disolviéndose, formándose la etringita y comienzan a formarse paulatinamente los silicatos cálcicos hidratados (C-S-H) en la superficie de las partículas de cemento en forma de haces de fibras que unen unas partículas con otras. La composición del C-S-H variará en función de factores como la relación A/C, la relación CaO/SiO_2, la temperatura o la presencia de iones (Al^{3+}, Fe^{2+}, SO_4^{2-}, etc.). Por otro lado, el empleo de filler puede provocar la disminución del periodo latente. Durante esta etapa el hormigón es un material plástico y no se aprecia calor de hidratación durante el fraguado. Esta etapa se da entre 1 y 2 horas después del amasado. La solución acuosa se satura de iones Ca^{2+} y OH^-, incrementándose la conductividad de la disolución.

La Tercera Etapa se corresponde con el Fraguado y Aceleración de la hidratación. En la misma, se produce una sobresaturación en la solución acuosa de iones Ca^{2+}. Se produce a las 5 horas aproximadamente después del amasado. Y comienzan a formarse y a precipitar cristales de Portlandita ($Ca(OH)_2$), aumentando la formación de productos hidratados. La mezcla comienza a endurecerse (inicio del fraguado) y aumenta el calor de hidratación (Figura 2.6). La hidratación del C_3S y del C_2S da lugar a un sólido poroso y poco cristalino, denominado también gel de C-S-H [40,44], estos compuestos se entrelazan y se juntan alrededor de los áridos, lo que provoca que el hormigón se vuelva más rígido y solidifique. Durante la hidratación del C_3S y C_2S se genera una cantidad importante de $Ca(OH)_2$, aproximadamente un 39% y 18% en peso, respectivamente. Por ello, cuando en la dosificación se incluyan adiciones con carácter puzolánico se deben utilizar cementos ricos en C_3S (es decir, CEM I), debido a que la sílice o los silicatos que forman parte de estos materiales van a reaccionar con el $Ca(OH)_2$, lo cual va a permitir el incremento en el rendimiento del HAC. El $Ca(OH)_2$ contribuye relativamente poco a la resistencia del hormigón, mientras que el C-S-H es el principal contribuyente a la resistencia e impermeabilidad del hormigón.

Estas reacciones son lentas y comienzan en esta etapa, aunque continúa en las siguientes, donde son observadas. Los cristales de $Ca(OH)_2$ suelen representar entre el 20 y el 25% del volumen total de sólidos de la pasta de cemento totalmente hidratada. Se trata de una especie cristalina relativamente grande respecto al C-S-H y, por ello, su capacidad cementante es mucho menor. La mayor parte suele localizarse en el espacio ocupado inicialmente por el agua, como por ejemplo la zona interfacial de transición árido-pasta.

Durante la Etapa de Endurecimiento (Etapa 4), continúa la hidratación y se produce una disminución del calor de hidratación debido al aumento del espesor de la capa que forman las especies hidratadas (C-S-H y $Ca(OH)_2$), que genera una barrera que el agua deberá a travesar para alcanzar a las especies sin hidratar. Por otro lado, cuando se agota la fuente de sulfatos, la etringita se vuelve inestable y comienza a descomponerse, liberando iones sulfatos, los cuales reaccionan con el C_3A y el $Ca(OH)_2$ para formar cristales de monosulfalto de calcio hidratado, que es más estable, y aluminato de calcio hidratado. Esta reacción, se produce en torno a las 9 horas, es rápida y genera un pico exotérmico (Figura 2.6). El calor que se libera acelera a su vez la velocidad de hidratación de los silicatos. Por lo que respecta al C_4AF, su hidratación es similar a la de los aluminatos, aunque la reactividad es algo más lenta [44].

Y, por último, se produce la Estabilización o Densificación (Etapa 5) (Figura 2.6), donde se desarrolla la completa hidratación de todas las especies lentamente. La hidratación del C_3A no reaccionado contribuirá a la deshidratación de los geles C-S-H. Esta etapa dura un tiempo indeterminado (semanas, meses o años) dependiendo de los factores internos y externos que interfieran y es clave para el desarrollo de las resistencias y la reducción de la permeabilidad del hormigón.

Durante el fraguado del hormigón, el agua va a ser una parte fundamental de las reacciones de hidratación. Una parte del agua de la mezcla no llegará a intervenir en las reacciones, por lo que permanecerá en la microestructura del material formando parte de la fase acuosa o evaporándose, lo que dará lugar a la estructura porosa. El volumen de la porosidad disminuirá con el tiempo de reacción y con el grado de hidratación (Figura 2.5) e influirá significativamente en la resistencia y durabilidad del

hormigón, ya que puede provocar zonas de debilidad y vías de acceso para los agentes agresivos desde el exterior. Para minimizar estos efectos y aumentar la compacidad de la microestructura, los productos de hidratación deberían rellenar la red porosa. Para que esto ocurra, es necesario una cantidad de cemento óptima, una relación agua cemento baja y unas buenas condiciones de curado.

Por ello, la porosidad va a ser la principal característica de la microestructura del hormigón, la cual va a quedar caracterizada a partir del tamaño, forma y distribución de los poros. La mayor cantidad finos, el menor volumen de áridos grueso, el uso de filler y de aditivos en el HAC, dará lugar a una microestructura menos porosa, aunque estará supeditada a las características de físico-químicas de estos elementos [48]. La porosidad se puede clasificar en función del diámetro de poro en espacios interlaminares (<0.5 nm), microporos gel (0.5 – 2.5 nm), poros gel pequeños (2.5 – 10 nm), poros capilares medianos (10 – 50 nm), poros capilares grandes (50 nm – 10 µm) y aire ocluido (>10 µm) (Figura 2.7).

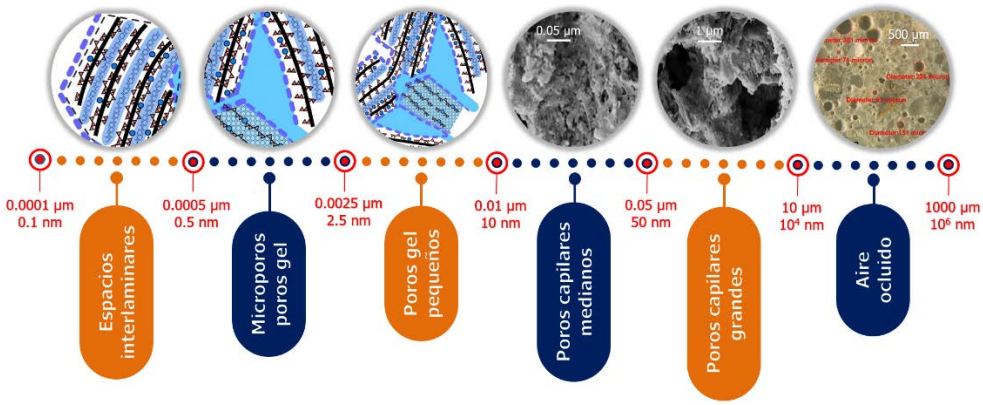

Figura 2.7: Clasificación de la porosidad en función del diámetro de poro [49].
Fuente: Elaboración propia. Imágenes [50–52].

Los espacios interlaminares, los microporos gel y los poros gel pequeños pueden afectar a la estabilidad volumétrica, es decir, a la retracción del material. Los poros capilares medianos y los poros capilares grandes influirán en las propiedades mecánicas y en la permeabilidad. Por último, el aire ocluido influirá en el comportamiento mecánico del hormigón [44,49]. Otra clasificación puede ser la propuesta por la Unión Internacional de Química Pura y Aplicada (IUPAC), que

clasifica la porosidad en microporos (< 2 nm), capilares o mesoporos (2 – 50 nm) y macroporos (> 50 nm).

En resumen, en la hidratación del cemento se van a formar tres especies principalmente, C-S-H, $Ca(OH)_2$ y etringita (Figura 2.5). El C-S-H es el componente cementante principal y más importante de los productos hidratados debido a su alta resistencia y representa entre el 50 y el 60% del volumen de las fases solidas de la pasta de cemento endurecido, si se logra su total hidratación [40]. Como se ha comentado anteriormente, este producto procede del C_3S, que se hidrata rápidamente y desarrolla una alta resistencia a edades tempranas y del C_2S, que se endurece lentamente y va a ser el responsable de la resistencia a largo plazo (Figura 2.8). Los productos de hidratación generados a partir del C_3A y C_4AF tienen poca repercusión en la resistencia final en el hormigón, aunque tienen un papel importante respecto a la durabilidad en medios sulfatados, desde un punto de vista negativo ya que pueden formarse especies expansivas. Estas fases constituyen entre el 15 y 20% del volumen total de las fases sólidas de la pasta de cemento endurecido, si se logra su total hidratación.

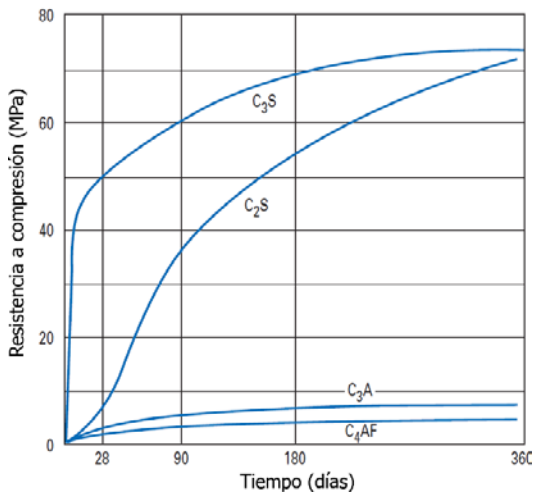

Figura 2.8: Resistencia a la compresión, respecto al tiempo de curado para las fases del cemento.
Fuente: Adaptado de [53].

A medida que se vayan formando los productos de hidratación, el hormigón autocompactante irá aumentando progresivamente su rigidez hasta llegar al

endurecimiento total. A lo largo de todo este proceso se producirá la evolución y el desarrollo de las propiedades mecánicas del material.

El HAC se caracteriza por un alto rendimiento mecánico. La capacidad de absorber los esfuerzos a compresión vendrá influenciada por diferentes factores como la cantidad de cemento, la relación A/C, el tamaño y cantidad de árido, las características físico-químicas de las adiciones, la relación agua/fino, los aditivos, la estructura porosa, factores externos, etc. [44]. Al igual que ocurre con la resistencia a compresión, el hormigón presenta una rotura sin apenas ductilidad al superar su resistencia a tracción. Además de los anteriores factores, la microestructura, la microfisuración y la zona de transición árido-pasta del hormigón tendrán una importancia significativa en la resistencia a tracción [54]. La resistencia a tracción será inferior a la resistencia a compresión, aunque estas propiedades están relacionadas entre sí ya que una alta resistencia a compresión supone una alta resistencia a tracción. La EHE-08 establece una correlación entre ambos. La deformación que el HAC soporta cuando se somete a un esfuerzo de compresión uniaxial será definida a través de su módulo de elasticidad. Los factores que afectan a esta propiedad son el volumen, la naturaleza y tamaño del árido, el volumen de pasta, la cantidad y características de los finos utilizados y la zona de transición árido-pasta. También, la EHE-08 establece una correspondencia entre resistencia a compresión y esta propiedad.

Otra propiedad mecánica del hormigón es la resistencia a flexotracción (módulo de rotura), la cual puede considerarse secundaria para los hormigones estructurales, aunque para aplicaciones de pavimentos de hormigón es fundamental. Principalmente depende del tipo, tamaño y cantidad de árido grueso utilizado en la dosificación y de la adherencia entre el árido y la pasta. El valor de la flexotracción del hormigón se puede estimar entre el 10 y el 20% de la resistencia a compresión, aproximadamente, y al igual que en el caso de la resistencia a tracción, la resistencia a flexotracción se incrementa con el aumento de la resistencia a compresión, pero en menor proporción. Para este caso, la EHE-08 establece una correlación entre resistencia a tracción y esta propiedad.

Además de la capacidad de soportar esfuerzos y tensiones, otro aspecto fundamental en el comportamiento del HAC en estado endurecido, es el rendimiento frente a las acciones de agentes físicos o químicos agresivos y la protección de las armaduras y demás elementos metálicos embebidos en el hormigón durante su vida de servicio [7]. Como ya se ha comentado, la motivación inicial para el desarrollo del HAC fue obtener un hormigón con un alto potencial frente al ataque de agentes agresivos respecto a hormigones convencionales que presentaban una compactación inadecuada.

La durabilidad dependerá de las condiciones ambientales y de la estructura porosa del material ya que es la vía de entrada de sustancias agresivas (líquidos, gaseosos o iones en disolución) desde el exterior hasta el interior del HAC. Por ello, es fundamental definir la estructura porosa (tipos, tamaño y distribución de los poros) para comprender el comportamiento ante la penetración de estos agentes. Además, dependerá de los mecanismos de transporte que actúen: permeabilidad (diferencia de presión), capilaridad (tensión superficial en las paredes de los capilares), difusión (gradiente de concentración), migración (diferencia de potencial electrostático), convección (gradiente de densidad o temperatura) y de los agentes químicos (cloruros, sulfatos, CO_2, disoluciones, etc.), los cuales interactuarán con los componentes del hormigón y provocarán el deterioro del material [8].

Uno de los factores que influirá significativamente en la durabilidad de las mezclas es la presencia de agua o humedad dentro de la estructura porosa del material [55] ya que es el medio de transporte para los elementos agresivos y el principal agente lixiviante. La EHE-08 tiene en cuenta estos factores y en función del tipo de ambiente de exposición y de la agresividad ambiental, exige determinadas características a los materiales y especificaciones en las dosificaciones y en su ejecución (relación A/C máxima, contenido de cemento mínimo, tipo de cemento, etc.) [7].

Generalmente, el HAC se va a caracterizar por presentar una permeabilidad baja y por ello, las sales como el NaCl, Na_2SO_4 y $MgSO_4$ no van a penetrar fácilmente, ofreciendo una buena durabilidad y una alta resistencia al deterioro ambiental por intercambio iónico. Para asegurar que el hormigón desarrolle una baja permeabilidad,

es importante proporcionar unas condiciones adecuadas de curado para que la hidratación sea total y se evite la evaporación del agua que forma parte del HAC.

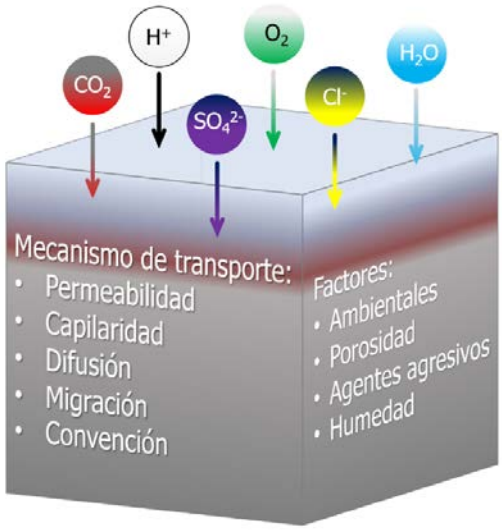

Figura 2.9: Principales agentes agresivos del hormigón y mecanismos de transporte.
Fuente: Elaboración propia.

Al igual que en las propiedades mecánicas, la durabilidad de HAC que incorporen adiciones minerales o fillers deberá ser analizada experimentalmente para estimar y garantizar el comportamiento deseado del hormigón con estos materiales y verificar la dosificación, así como detectar cualquier efecto negativo. Adiciones con carácter puzolánico reaccionarán con el hidróxido de calcio ($Ca(OH)_2$) para formar silicatos cálcicos hidratados (C-S-H), con el correspondiente efecto positivo en el comportamiento mecánico y durable. Hay que tener en cuenta que el empleo de combinaciones de estos materiales puede ser incompatible, incluso cumpliendo con las especificaciones de calidad, pudiendo comprometer el comportamiento del HAC en estado endurecido debido a las interacciones que se produzcan entre ellos.

2.6 Consideraciones medioambientales del HAC

Por un lado, como se ha comentado anteriormente, el HAC permite reducir la afección al medio durante las etapas de ejecución y puesta en obra al eliminar la vibración y disminuir el ruido ambiental generado en dichas labores. Aunque, por otro lado, hay que tener en cuenta que debido a las particularidades necesarias en la dosificación

(un mayor contenido de finos y el empleo de aditivos químicos, principalmente), para conseguir las propiedades que lo caracterizan, puede ser considerado como un material de construcción poco amigable con el medio ambiente. La incorporación de finos en forma de adiciones o filler comerciales, procedentes de procesos de trituración y molienda de áridos naturales, van a tener un importante impacto ambiental, derivado del consumo de recursos naturales no renovables, las elevadas emisiones de CO_2 y el consumo energético de los propios procesos productivos, dando lugar a un mayor coste ambiental del HAC y favoreciendo la degradación del medio.

Lo cual puede considerarse incompatible con la nueva realidad de nuestra sociedad, donde existe una gran necesidad mundial de promover la productividad integral de todos los sectores económicos con el fin de conseguir la optimización de los recursos naturales, así como la minimización y valorización de residuos, dando respuesta a los retos medioambientales que se nos plantean. Este es el fundamento en el que se basa la economía circular. Dicho concepto comenzó a surgir en 1981, cuando Stahel & Reday [56] idearon un sistema económico-productivo circular donde la eficiencia integral de los procesos productivos era la estrategia para un crecimiento industrial sostenible. Esta idea se ha empezado a implantar en la política mundial.

En la Unión Europea (en adelante, UE) se está empezando a implantar la Economía Circular en la industria de la construcción por la elevada cantidad de residuos generados a través del Plan de Acción para la Implementación de la Economía Circular de la Comisión del Parlamento Europeo (COM(2017)33) [57] donde se exponen las acciones y compromisos globales, y los sectores prioritarios. En España, el plan actual que establece las líneas estratégicas y las medidas necesarias para avanzar hacia la denominada economía circular e impulsar la reutilización y el reciclado, es el Plan Estatal Marco de Gestión de Residuos (PEMAR) 2016-2022, aprobado por el Acuerdo del Consejo de Ministros de 6 de noviembre de 2015, a propuesta de la Ministra de Agricultura, Alimentación y Medio Ambiente (actual Ministerio para la Transición Ecológica).

El objetivo final del PEMAR, en paralelo a la política comunitaria de la UE, es convertir a España en una sociedad eficiente en el uso de los recursos. Se trata de transformar la economía lineal basada en producir, consumir y tirar, en una economía circular en

la que se reincorporen al proceso productivo una y otra vez los materiales (residuos o subproductos) para la producción de nuevos productos o materias primas de cualquier industria o sector (Figura 2.10).

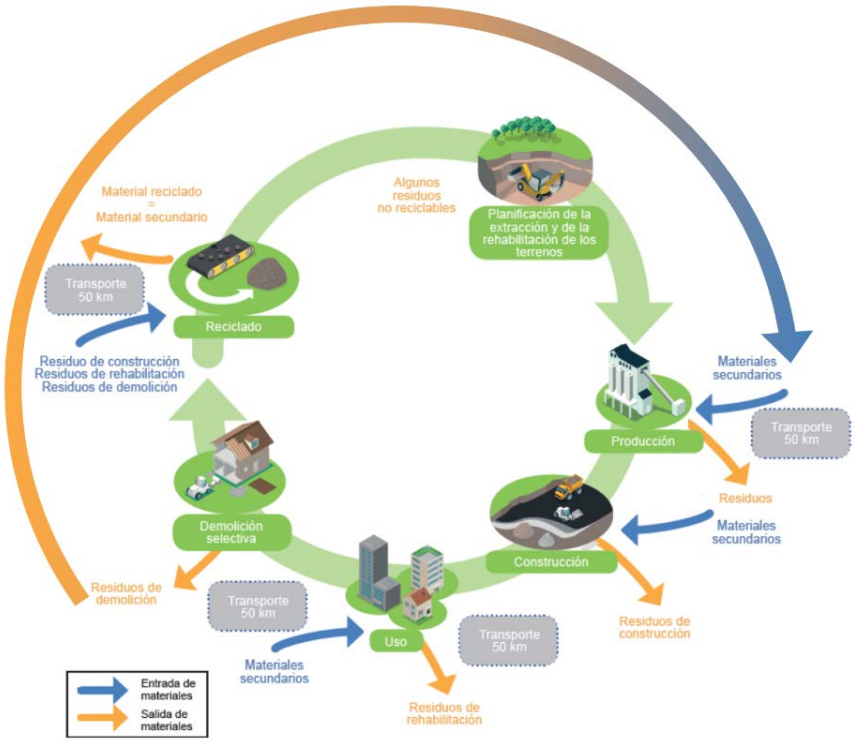

Figura 2.10: Economía circular en el sector de la construcción.
Fuente: Adaptado de Asociación Nacional de Empresarios del Árido (ANEFA).

Dentro del sector de la construcción, el hormigón desempeña un papel muy importante, ya que es el material de construcción más consumido mundialmente (4 toneladas por persona y año) y el que más recursos naturales consume [58,59]. Por lo que el futuro del sector pasa por el desarrollo de tecnologías más eficientes, la optimización del consumo de recursos naturales y el fomento del empleo de materiales reciclados (Figura 2.10). Por ello, en el caso concreto del HAC, una oportunidad para disminuir o eliminar el alto contenido de finos convencionales (filler comerciales) necesarios en la fabricación del HAC, su principal desventaja desde el punto de vista medioambiental frente al hormigón convencional, sería sustituirlos total o parcialmente por materiales de granulometría fina reciclados. Lo que permitiría la minimización y valorización de dichos residuos, así como la optimización de los

recursos naturales utilizados en la fabricación del HAC. Esto supone un viraje en la percepción ambiental del HAC.

Estos materiales de naturaleza residual pueden proceder de diferentes actividades productivas. Los residuos de fracción fina procedentes del sector de la construcción, residuos de construcción y demolición (RCD), tienen una alta reutilización o/y reciclabilidad en aplicaciones propias al ámbito del que proceden debido a la naturaleza de los mismos. Lo cual tiene una gran importancia por el alto volumen de RCD que se originan en la UE, de acuerdo con los datos oficiales de Eurostat 2017 [60]. En 2014 se generaron 62 millones de toneladas, un 35% del total de residuos generados en la EU-28. También pueden ser considerados todos los finos residuales no peligrosos que proceden de los procesos industriales de la fabricación de los materiales de construcción (los cuales no están catalogados como RCD), así como finos residuales procedentes de otros procesos de fabricación, de transformación, de utilización, de consumo, de limpieza o de mantenimiento que son generados por otros sectores industriales o mineros. Estas partículas de polvo suelen ser recolectadas por los sistemas de purificación de aire antes de ser evacuados a la atmósfera, los cuales pueden ser considerados, muchas veces químicamente activos por lo que afectan negativamente al entorno cercano, con su vertido incontrolado. Su reutilización como filler puede ser una solución para el polvo generado en los diferentes procesos industriales y mineros, consiguiendo reciclar los residuos, y conseguir la catalogación de subproducto en lugar de la de residuo.

No obstante, una de las mayores dificultades a la hora de reciclar y reutilizar residuos es la falta de confianza en la calidad de los materiales reciclados. Esta desconfianza restringe y reduce la demanda de los mismos, lo cual inhibe el desarrollo de la gestión de residuos y de las infraestructuras de reciclaje, y por tanto preservar y optimizar los recursos naturales.

En este sentido, la comunidad científica viene alertando que el consumo actual de recursos naturales es insostenible. Un ejemplo claro de esta problemática es el consumo de arena ya que el ritmo de extracción es dos veces superior al ritmo al que se depositan nuevos sedimentos, siendo el reciclado de materiales una medida necesaria para mitigar esta situación [61].

Herramientas como la innovación y la investigación son la clave para adaptarnos a la nueva realidad, implantando la economía circular en el sector de la construcción, lo cual es fundamental para la sostenibilidad del mundo actual. La demora en la adopción de medidas proactivas, únicamente servirá para encarecer las medidas que nos veremos obligados a adoptar en el futuro. Por otro lado, el ámbito de la gestión de los residuos constituye la segunda contribución más importante al crecimiento del empleo en la economía medioambiental, tal y como muestra la contabilidad relativa a los bienes y servicios medioambientales [60].

2.7 Referencias bibliográficas

[1] H. Okamura, M. Ouchi, Self-compacting concrete. J Adv Concrete Technol (2003),1(1):5–15.

[2] K. Ozawa, K. Maekawa, H. Kunishima, H. Okamura, Performance of concrete based on thedurability design of concrete structures. Proc Second East Asia-Pacific Conf Struct Eng Const (1989)1:445–56

[3] P.C. Aitcin, High-performance concrete. E & FN Spon; 1998. p. 591.

[4] K. Ozawa, S. Tangtermsirikul, K. Maekawa, Role of powder materials on the filling capacity of fresh concrete. In: The 4th CANMET/ACI international conference on fly ash, silica fume, slag and natural pozzolans in concrete, Supplementary Papers. (1992) p. 121–30.

[5] European Federation of National Associations Representing producers and applicators of specialist building products for Concrete (EFNARC). Specification and guidelines for self-compacting concrete, Hampshire, UK; (2002), www.efnarc.org.

[6] European Federation of National Associations Representing producers and applicators of specialist building products for Concrete (EFNARC). The European guidelines for self-compacting concrete specification. Production and Use. Hampshire, UK; (2005), www.efnarc.org.

[7] EHE-08. Instrucción de Hormigón Estructural EHE-08. R.D. 1247/2008, Spain, 2008.

[8] A. Skarendahl, O. Petersson, editors. Self-compacting concrete: state of the art report of RILEM TC 174-SCC, Report 23, RILEM Publishers, Cachan, France; 2000.

[9] K. Holschemacher, Y. Klug, A database for the evaluation of hardened properties of SCC. LACER (2002)7:124–34

[10] K.H. Khayat, C. Hu, H. Monty, Stability of SCC, advantages and Potential applications. In: RILEM international conference on self-compacting concrete. Rilem Publications SARL; (1999). p. 143–52.

[11] P. Gomes, R. Gettu, L. Agulló, C. Bernardet, Diseño de Hormigones Autocompactables de alta resistencia. Procedimiento para su dosificación y métodos de caracterización. Cemento – Hormigón, España, 2002;832:30–42.

[12] M. Uysal, K. Yilmaz, M. Ipek, The effect of mineral admixtures on mechanical properties, chloride ion permeability and impermeability of self-compacting concrete, Constr. Build. Mater. 27 (2012) 263–270.

[13] A. Beycioğlu, H.Y. Aruntaş, Workability and mechanical properties of self-compacting concretes containing LLFA, GBFS and MC, Constr. Build. Mater. 73 (2014) 626–635.

[14] V. Kannan, K. Ganesan, Mechanical properties of self-compacting concrete with binary and ternary cementitious blends of metakaolin and fly ash, J. South African Inst. Civ. Eng. 56 (2014) 97–105.

[15] A.R. Esquinas, E.F. Ledesma, R. Otero, J.R. Jiménez, J.M. Fernández, Mechanical behaviour of self-compacting concrete made with non-conforming fly ash from coal-fired power plants, Constr. Build. Mater. 131 (2018) 114–128.

[16] A.R.R. Esquinas, J.I.I. Álvarez, J.R.R. Jiménez, J.M.M. Fernández, J. de Brito, Durability of self-compacting concrete made with recovery filler from hot-mix asphalt plants, Constr. Build. Mater. 161 (2018) 407–419.

[17] A.R. Esquinas, C. Ramos, J.R. Jiménez, J.M. Fernández, J. De Brito, Mechanical behaviour of self-compacting concrete made with recovery filler from hot-mix asphalt plants, Constr. Build. Mater. 131 (2017) 114–128.

[18] K. Celik, M.D. Jackson, M. Mancio, C. Meral, A.-H. Emwas, P.K. Mehta, P.J.M. Monteiro, High-volume natural volcanic pozzolan and limestone powder as partial replacements for portland cement in self-compacting and sustainable concrete, Cem. Concr. Compos. 45 (2014) 136–147.

[19] P.R. Da Silva, J. de Brito, Durability performance of self-compacting concrete (SCC) with binary and ternary mixes of fly ash and limestone filler, Mater. Struct. 49 (2016) 2749–2766.

[20] W.W.S. Fung, A.K.H. Kwan, Effect of particle interlock on flow of aggregate

through opening, Powder Technol. 253 (2014) 198–206.

[21] A.C.P. Santos, J.A. Ortiz-Lozano, N. Villegas, A. Aguado, Experimental study about the effects of granular skeleton distribution on the mechanical properties of self-compacting concrete (SCC), Constr. Build. Mater. 78 (2015) 40–49.

[22] J.K. Su, S.W. Cho, C.C. Yang, R. Huang, Effect of sand ration on the elastic modulus of self-compacting concrete, J. Mar. Sci. Technol. 10 (2002) 8–13.

[23] E. Sakai, M. Daimon, Mechanisms of superplastification, in: J. Skalny, S. Mindess (Eds.), Materials Science of Concrete IV, American Ceramic Society, Westerville, OH, (1995), pp. 91 – 111.

[24] H. Okamura, Self-compacting high-performance concrete. Concrete Int (1997),19(7):50–4

[25] S. Rols, J. Ambroise, J. Pera, Effects of different viscosity agents on the properties of self-leveling concrete, Cem. Concr. Res. 29 (1999) 261–266.

[26] A. Leemann, F. Winnefeld, The effect of viscosity modifying agents on mortar and concrete, Cem. Concr. Compos. 29 (2007) 341–349.

[27] M. Collepardi, Self-compacting concrete: What is new, Proceedings of the 7th CANMET/ACI Conference on superplasticizer and other chemical admixtures in concrete, (2003), pp. 1-16.

[28] C. Ferraris, F. De Larrard, N. Martys, Fresh concrete rheology: recent developments, Mater. Sci. Concr. VI, Amer. Cer. Soc. Ed. S. Mindess, J. Skaln. (2001) 215–241.

[29] P.F.G. Banfill, Rheology of fresh cement and concrete, Rheol. Rev. (2006) 61–131.

[30] Asociación Cientifico Técnica del Hormigón Estructural (ACHE). M-13: Hormigón Autocompactante. Diseño y Aplicación; 2008.

[31] Asociación Española de Normalización y Certificación, AENOR, Madrid, España, 2018.

[32] J.E. Wallevik, Relationship between the Bingham parameters and slump, Cem. Concr. Res. 36 (2006) 1214–1221.

[33] R. Zerbino, B. Barragan, L. Agullo, R. Gettu, Reología de Hormigones Autocompactables. Rev Cienc Tecnol Hormig (2006)13:51–64

[34] P.J.M. Bartos, Assessment of properties of underwater concrete by the Orimet test, Spec. Concr. Mix. (1993) 191–200.

[35] M. Yurugi, G. Sakai, A proven QA system for flowable concrete, Concr. Int. 20

(1998), 10:44–48.

[36] American Society of Testing Materials, ASTM International, West Conshohocken, USA, 2018.

[37] F.W. Locher, W. Richartz, S. Sprung, Erstarren von zement, Zement Kalk Gips. 29 (1976) 435–442.

[38] P.D. Tennis, H.M. Jennings, A model for two types of calcium silicate hydrate in the microstructure of Portland cement pastes, Cem. Concr. Res. 30 (2000) 855–863.

[39] P.C. Hewlett, Lea's Chemistry of Cement and Concrete, fourth ed., Butterworth Heinemann, London, 2003.

[40] H.F.W. Taylor, Cement Chemistry, 2nd ed., Thomas Telford, London, 1997.

[41] P.C. Aïtcin, Binders for Durable and Sustainable Concrete, Taylor and Francis, New York, (2008), pp. 347–348.

[42] O. Esping, I. Löfgren, Investigation of early age deformation in self-compacting concrete, Conf. Advanced Cement-based Materials, DTU, Copenhagen, (2005).

[43] W.C. Hansen, Fraguado rápido y falso fraguado en los cementos portland, Mater. Construcción. 12 (1962) 29–42.

[44] P.K. Mehta, P.J.M. Monteiro. Concrete structure, properties and materials. New Jersey: Prentice Hall, 1993.

[45] J.W. Bullard, H.M. Jennings, R.A. Livingston, A. Nonat, G.W. Scherer, J.S. Schweitzer, K.L. Scrivener, J.J. Thomas, Mechanisms of cement hydration, Cem. Concr. Res. 41 (2011) 1208–1223.

[46] S. Donatello, A. Fernández-Jimenez, A. Palomo, Very high volume fly ash cements. Early age hydration study using Na 2 SO 4 as an activator, J. Am. Ceram. Soc. 96 (2013) 900–906.

[47] P.C. Taylor, S.H. Kosmatka, G.F. Voigt, M.E. Ayers, A. Davis, G.J. Fick, J. Gajda, J. Grove, D. Harrington, B. Kerkhoff, Integrated materials and construction practices for concrete pavement, Fed. Highw. Adm. Off. Pavement Technol. 2007.

[48] M. Valcuende, C. Parra, E. Marco, A. Garrido, E. Martínez, J. Cánoves, Influence of limestone filler and viscosity-modifying admixture on the porous structure of self-compacting concrete, Constr. Build. Mater. 28 (2012) 122–128.

[49] S. Mindess, J. F. Young, D. Darwin, Concrete, Prentice Hall, Pearson Education, Inc., Upper Saddle River, NJ 07458, U.S.A., 2003.

[50] H.M. Jennings, A. Kumar, G. Sant, Quantitative discrimination of the nano-pore-structure of cement paste during drying: New insights from water sorption isotherms, Cem. Concr. Res. 76 (2015) 27–36.

[51] Z. Liu, W. Hansen, A geometrical model for void saturation in air-entrained concrete under continuous water exposure, Constr. Build. Mater. 124 (2016) 475–484.

[52] R. Walker, S. Pavia, R. Mitchell, Mechanical properties and durability of hemp-lime concretes, Constr. Build. Mater. 61 (2014) 340–348.

[53] Z. Taschenbuch, Verein Deutscher Zementwerke, Verlag Bau+ Technik, 50, 2002.

[54] G. Agranati Landsberger, Estudio sobre la aplicabilidad de los modelos de cálculo de la fluencia y retracción al hormigón autocompactable, Tesis, Universidad Politécnica de Madrid, 2008.

[55] M.A. Shazali, M.H. Baluch, A.H. Al-Gadhib, Predicting residual strength in unsaturated concrete exposed to sulfate attack, J. Mater. Civ. Eng. 18 (2006) 343–354.

[56] W.R. Stahel, G. Reday-Mulvey, Jobs for tomorrow: the potential for substituting manpower for energy, Vantage Press, New York 1981.

[57] European Commission, Report from the commission to the European parliament, the council, the European Economic and Social Committee and the Committee of the Regions on the Implementation of the Circular Economy Action Plan, 2017.

[58] K. Celik, C. Meral, A. Petek Gursel, P.K. Mehta, A. Horvath, P.J.M. Monteiro, Mechanical properties, durability, and life-cycle assessment of self-consolidating concrete mixtures made with blended portland cements containing fly ash and limestone powder, Cem. Concr. Compos. 56 (2015) 59–72.

[59] A.M. J. Moya, N. Pardo, Energy efficiency and CO_2 emissions: Prospective scenarios for the Cement industry, Publ. Off. 2010.

[60] Agencia Europea de Estadística (Eurostat), 2015. Generación de tratamiento de residuos en la Unión Europea. Disponible en: http://ec.europa.eu/eurostat/statisticsexplained/index.php/Waste_statistics.

[61] A. Torres, J. Brandt, K. Lear, J. Liu, A looming tragedy of the sand commons, Science, 357 (2017) 970–971.

Capítulo 3

Materiales y Métodos

3.1 Materiales

A continuación, se exponen todos los materiales utilizados en la presente Tesis Doctoral. En los capítulos 4, 5, 6, 7 y 8 se realiza una descripción detallada y completa de sus propiedades, fruto de la profunda caracterización físico-química a los que fueron sometidos de acuerdo a la normativa existente.

Los áridos utilizados (Figura 3.1) fueron grava 4/16, arena gruesa 0/4 y arena fina 0/2 de naturaleza silícea. Estos materiales fueron suministrados por dos canteras:

a) Áridos Gallardo S.L. (Figura 3.2a), cuya explotación minera y planta de tratamiento de áridos está localizada en el municipio de Campanario (Badajoz). Dichos áridos fueron utilizados en los capítulos 4 (1ª publicación), 5 (2ª publicación) y 6 (3ª publicación).

b) Charamuzca Movimiento de Tierras, Áridos y Hormigones S.L. (Figura 3.2b) cuya explotación minera y planta de tratamiento de áridos está localizada en el municipio de Palma del Río (Córdoba). Estos materiales fueron utilizados en los capítulos 7 (4ª publicación) y 8 (5ª publicación).

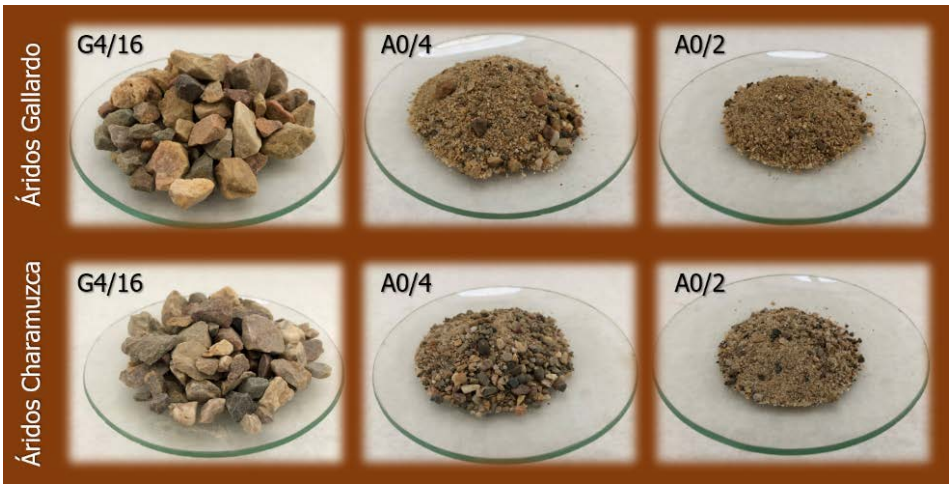

Figura 3.1: Áridos empleados en este trabajo.

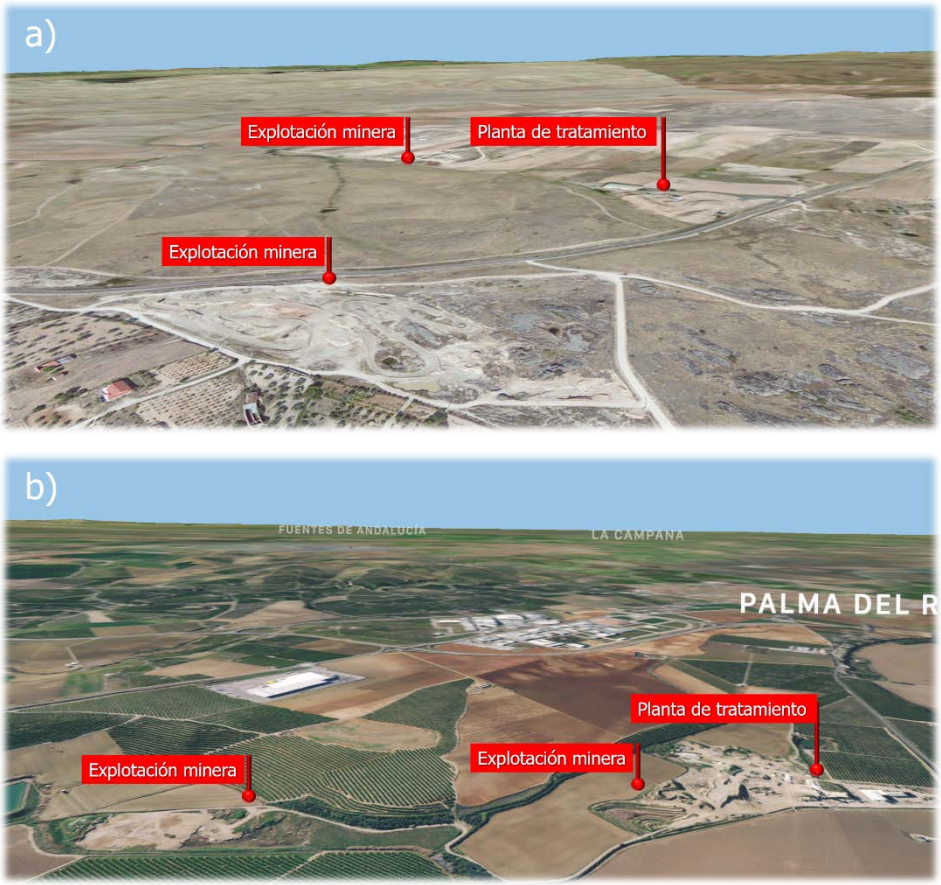

Figura 3.2: a) Áridos Gallardo S.L. y b) Charamuzca Movimiento de Tierras, Áridos y Hormigones S.L.

Por otro lado, el filler comercial (SF) utilizado (Figura 3.3) es de naturaleza silícea y fue suministrado por la empresa Lorda y Roig S.A. y procede de la explotación minera Minas Carmina (Figura 3.4) localizada en el municipio de Llansá (Gerona).

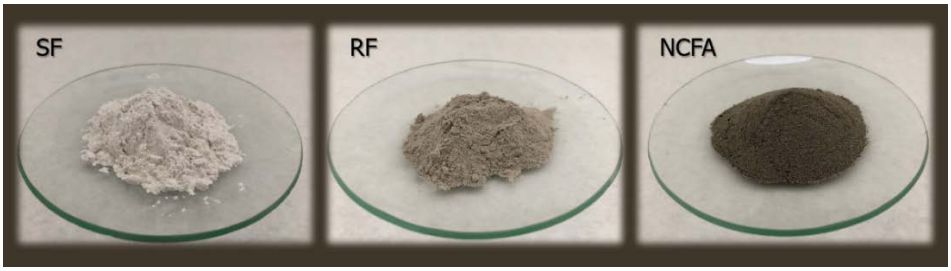

Figura 3.3: Filler comercial y finos residuales empleados en este trabajo.

Figura 3.4: Minas Carmina.

Uno de los finos residuales usados en esta Tesis Doctoral procede de la Planta de Fabricación de Mezclas Bituminosas Calientes (en adelante, MBC) propiedad de la empresa Pavimentos Asfálticos Málaga S.A. (PAMASA) (Figura 3.5) localizada en el término municipal Churriana (Málaga).

Dicho residuo (RF) (Figura 3.3) se genera en el proceso de secado y calentamiento de los áridos empleados en la fabricación de MBC. Este polvo sale del tambor rotatorio junto con los gases de combustión y el vapor de agua y es retenido por los filtros de mangas para evitar su dispersión a la atmósfera.

Este material residual es parcialmente almacenado en silos para su aprovechamiento como filler de recuperación en la fabricación de MBC, empleado en la capa base de firmes de carreteras, aunque su uso está limitado (3-4%). El resto es destinado a escombreras, a vertederos o a la propia cantera como material de relleno, con el consiguiente problema medioambiental y riesgos para la salud.

Figura 3.5: Planta de fabricación de Mezclas Bituminosas Calientes.

El otro fino residual utilizado en este trabajo fueron las cenizas no conformes (Figura 3.3) procedentes de la Central Térmica de Puente Nuevo (Figura 3.6) propiedad de la empresa Viesgo localizada en el término municipal de Espiel (Córdoba). Esta central termoeléctrica utiliza carbón como combustible, por lo que se considera una central termoeléctrica convencional y su objetivo es generar electricidad a partir de un ciclo termodinámico de agua/vapor.

Figura 3.6: Central Térmica de Puente Nuevo.

El proceso de combustión se produce en la caldera y fruto del mismo se genera el humo de combustión, que va a estar compuesto por los gases de combustión, cenizas e inquemados. Este flujo heterogéneo pasa por diferentes partes del proceso antes de ser evacuado limpio a la atmosfera a través de la chimenea (Figura 3.7).

En primer lugar, las cenizas e inquemados se separan de los gases de combustión en los puntos de captación existentes, desde donde se transportan hasta dos silos de almacenamiento mediante el sistema neumático de extracción de cenizas.

En el recorrido que realiza el humo de combustión desde la salida de la caldera hasta la chimenea existen 5 puntos de captación de cenizas volantes (Figura 3.7):

- C-1: Economizador.
- C-2: Calentador de aire secundario (aire de combustión, comburente).
- C-3: Calentadores de aire primario (aire para secar el carbón en los molinos).
- C-4: Precalentadores de aire PAC (aire que aumenta la temperatura de los humos en chimenea y permite que asciendan).
- Precipitador Electrostático.

La captación de cenizas en el economizador (C-1), en los calentadores de aire (C- 2/3) y en los precalentadores (C-4) se realiza mediante su depósito por gravedad en las tolvas instaladas en la parte inferior de cada elemento o sistema.

Desde las tolvas de recogida, las cenizas pasan al sistema de transporte y son conducidas hacia el silo 1 de almacenamiento. Estas cenizas no cumplen con la finura exigida por la normativa (UNE-EN 450-1), es decir que la masa retenida sobre el tamiz 0.045 mm es superior del 40%, por lo que no cumplen con los requisitos del marcado CE, considerándose como cenizas no conformes (NCFA).

De acuerdo con los datos de la Central, este subproducto representa entre el 30% y 40% de la producción total de cenizas volantes y debido a su nula o escasa aplicabilidad, son destinadas a vertedero con el importante impacto medioambiental que conlleva (Figura 3.6), a diferencia de las cenizas volantes con marcado CE, es decir, las cenizas volantes retenidas en el precipitador electrostático (el último punto de captación del sistema de depuración de partículas) que son comercializadas como adición para la fabricación del cemento o hormigón.

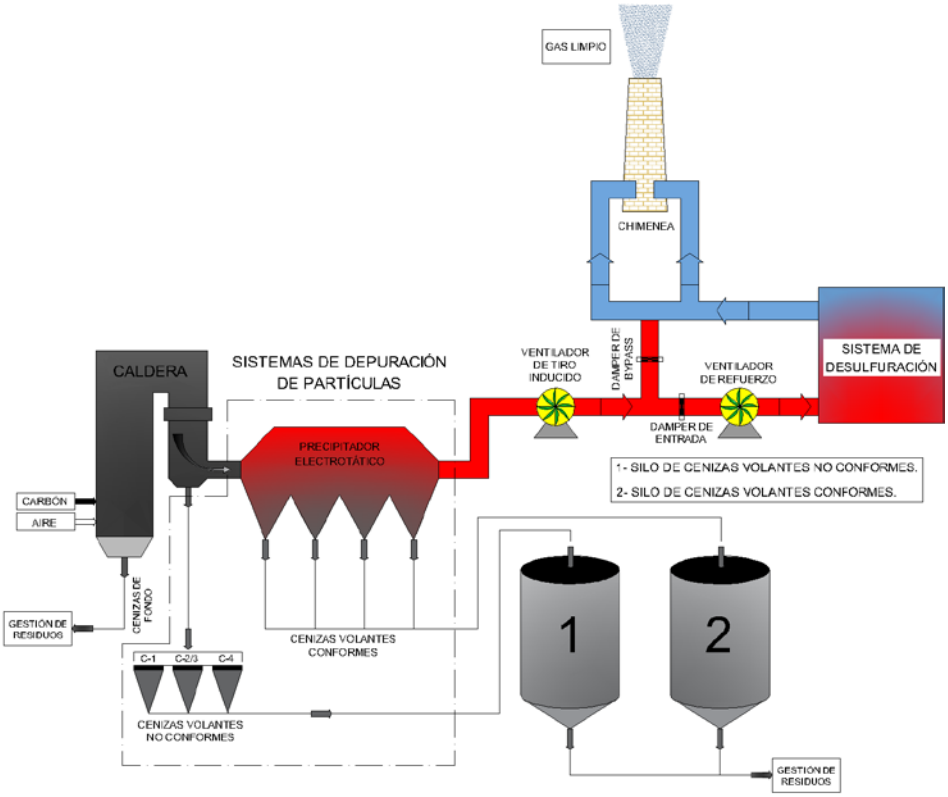

Figura 3.7: Diagrama de flujo general C.T. de Puente Nuevo.

Respecto al cemento utilizado, CEM I 42,5 R/SR, fue suministrado por la empresa Cementos Portland Valderrivas S.A. y procede de la Fábrica de Cementos de Alcalá de Guadaíra (Sevilla) (Figura 3.8).

Figura 3.8: Fábrica de Cementos de Alcalá de Guadaíra de Cementos Portland Valderrivas S.A.

Como aditivos, para la obtención de los HAC con una adecuada relación agua/cemento, se utilizaron superplastificantes/reductores de agua de altas prestaciones y específicos para HAC, tales como Glenium 303 SCC de Basf Chemical Company [1] y Adva® flow 400 de Grace Construction Products [2]. Las propiedades definidas por el fabricante se recogen en la Tabla 3.1.

Tabla 3.1: Propiedades de los aditivos.

Propiedades	**Glenium 303SCC**	**Adva® flow 400**
Función principal:	Reductor de agua de alta actividad/Superplastificante	Reductor de agua de alta actividad/Superplastificante
Función secundaria:	Retenedor de agua	Retenedor de agua
Efecto secundario:	Riesgo de disgregación a dosis elevadas	Riesgo de disgregación a dosis elevadas
Aspecto físico:	Líquido verdoso	Líquido marrón claro
Densidad, 20° C:	1.035 ± 0.02 g/cm^3	1.05 ± 0.02 g/cm^3
pH, 20º C:	6.5 ± 1	5.8 ± 1
Contenido en cloruros:	≤ 0.1 %	Exento
Viscosidad 20ºC (Brookfield Sp00/100rpm)	< 60cps	-

Y, por último, el agua utilizada procede de la red de abastecimiento de agua potable de la localidad de Belmez (Córdoba).

3.2 Dosificaciones y preparación de los HAC

Las dosificaciones utilizadas en la campaña experimental (Figura 1.2) quedan definidas en los capítulos 4, 5, 6, 7 y 8 de esta memoria, donde se detallan las premisas y los requisitos técnicos fijados, tales como tipo de cemento, cantidad mínima de cemento, relación agua/cemento máxima, tamaño máximo de árido y ambiente de exposición de acuerdo con la EHE-08, así como la composición de cada dosificación (porcentajes de los materiales de partida utilizados y su cantidad en masa y en volumen).

Previamente, debido a las diferentes características físico-químicas de los materiales, fue necesario llevar a cabo los ajustes experimentales en las mezclas para lograr el diseño de las dosificaciones definitivas, es decir que el hormigón cumpla con los requisitos de autocompactabilidad que marca la EHE-08 (capacidad de relleno, capacidad de paso o resistencia al bloqueo, resistencia a la segregación y robustez).

Tras la fase preliminar se realizaron diversas amasadas de cada dosificación diseñada con el fin de obtener la cantidad suficiente de muestra que permita determinar y evaluar las propiedades de los HAC, tanto en estado fresco como en estado endurecido, de acuerdo a la normativa existente.

La dosificación se realizó en volumen (1025 L) [3]. Aunque para el procedimiento de amasado se utilizó una fracción (1/24) del volumen de diseño, con el objetivo de trabajar con cantidades de materiales más manipulables en el entorno del laboratorio.

El procedimiento de amasado se estandarizó, de acuerdo con la bibliografía existente y con la experiencia de trabajo del grupo de investigación. La secuencia del proceso de amasado se muestra en la Figura 3.9.

El proceso de amasado se llevó a cabo en una hormigonera basculante de la marca Miral, modelo 300.

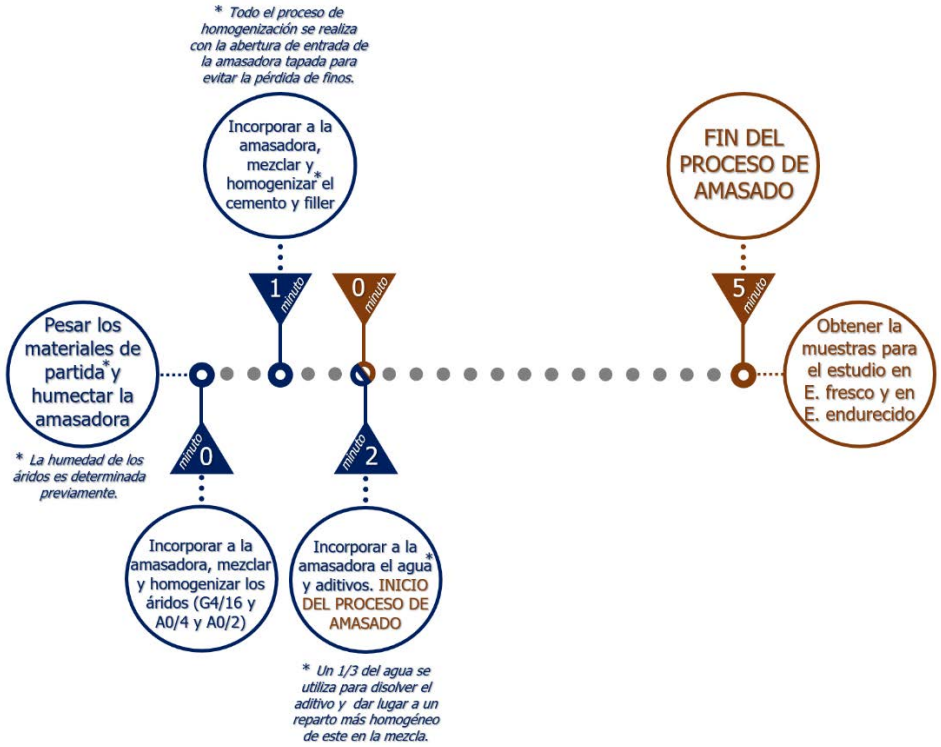

Figura 3.9: Secuencia del proceso de amasado.

Tras el amasado se procedió a la caracterización de los HAC en estado fresco donde se determinaron las propiedades de autocompactabilidad de las mezclas. A continuación, se rellenaron los moldes para fabricar los lotes de probetas que servirían para llevar a cabo la caracterización de los HAC en estado endurecido. Las dimensiones de las probetas dependerán del tipo de ensayo a realizar, de acuerdo con las normas y procedimientos de ensayo.

Las probetas se extrajeron de los moldes a las 24 horas del ser fabricadas. Durante este periodo de tiempo, fueron protegidas de posibles agentes externos o pérdidas de humedad. Finalmente, todas las probetas fueron curadas en agua hasta la fecha de ensayo programada, diferenciando los baños de curado en función de los tipos HAC diseñados.

3.3 Métodos

En los capítulos 4, 5, 6, 7 y 8 se realiza una descripción detallada y completa de la metodología seguida en las diferentes técnicas analíticas usadas tanto para la caracterización de los materiales de partida como para la caracterización de los HAC en estado fresco y estado endurecido. No obstante, en este apartado se realiza una descripción breve de las técnicas analíticas llevadas a cabo en la caracterización de los materiales de partida y HAC, que han permitido conocer su composición y sus principales características estructurales.

3.3.1 Distribución de tamaño de partícula

La técnica usada para determinar la distribución granulométrica de los granos de los finos empleados en este trabajo ha sido la distribución de tamaño de partícula por difracción de láser. Este procedimiento consiste en medir la intensidad de la luz dispersada cuando un haz láser pasa a través de una dispersión de partículas [4,5]. Una serie de detectores miden con precisión la intensidad de la luz dispersada por los granos en un amplio rango de ángulos.

El equipo empleado fue un Mastersizer S de la marca Malvern Instrument. Previamente al análisis, las muestras fueron tratadas en ultrasonidos durante al menos 10 minutos para dispersar los finos en etanol, el cual fue empleado como dispersante. Finalmente, mediante el programa informático del equipo se analizan los resultados de dispersión que permiten el cálculo de la distribución del tamaño de partícula de estos materiales de granulometría fina.

3.3.2 Difracción de rayos X

Esta técnica fue utilizada tanto para identificar las fases químicas que componen los materiales de partida como para definir las fases formadas en el proceso de hidratación de los HAC. Además, ha sido una técnica complementaria en la evaluación de la durabilidad de los HAC, desde el punto de vista de su comportamiento ante el ataque por sulfatos. Es una técnica básica que permite realizar tanto un análisis cualitativo como cuantitativo de las fases cristalinas de cualquier tipo de material,

tanto natural como sintético. La difracción de rayos X (XRD) se basa en la dispersión coherente de un haz monocromático de rayos X por parte de la materia y en la interferencia constructiva de las ondas que están en fase y que se dispersan en determinadas direcciones del espacio [6,7].

Este fenómeno se puede explicar mediante la ley de Bragg que predice la dirección en la que se da la interferencia constructiva de las ondas que están en fase y que se dispersan en determinadas direcciones del espacio [8].

$$n \cdot \lambda = 2 \cdot d \cdot \ sen\theta \qquad \text{(Ec. 3.1)}$$

Esta ecuación nos indica la relación que existe entre el espaciado entre dos planos de átomos (d), la longitud de onda de la radiación de rayos X utilizada (λ) y el ángulo de incidencia de los rayos X (θ), siendo n un número entero.

Los resultados se representan en difractogramas, donde el eje horizontal muestra el espaciado de la red cristalina o el ángulo de difracción, y el eje vertical reproduce la intensidad del rayo difractado (altura del pico). Cuando una muestra está formada por varias fases, las intensidades de los picos característicos de las misma son proporcionales a su cantidad [9], aunque una misma señal puede tener componentes de diferentes fases cristalinas.

Los estudios de difracción de rayos X fueron realizados sobre muestras en polvo en un difractómetro D8 Discover A25 de la marca Bruker, provisto de un monocromador de germanio para el haz difractado y detector de tipo multirango Lynxeye. La radiación utilizada fue CuKα (1.54059 Å) y las condiciones de operación fueron 40 kV y 40 mA. El proceso de análisis es controlado por el paquete informático DIFFRAC.SUITE.

3.3.3 Análisis termogravimétrico

Esta técnica (DTA-TG) fue utilizada tanto en la caracterización del filler comercial y de los finos residuales como de los HAC fraguados, permitiendo definir los mecanismos de endurecimiento y cuantificando los productos hidratados del

hormigón. Es una técnica que mide simultáneamente la variación de masa y de temperatura de un compuesto en el proceso de calcinación respecto a un crisol de referencia [10]. Las variaciones de temperatura no siempre implican un cambio en la masa de la muestra, aunque pueden asociarse, en algunos casos, a cambios de fase. Sin embargo, existen cambios térmicos que sí se acompañan de un cambio de masa, como la descomposición, la sublimación, la reducción-oxidación, la desorción-absorción o la deshidratación. Estos cambios son medidos con un analizador termogravimétrico.

Con esta técnica es posible cuantificar determinadas fases del hormigón endurecido, el cual es el resultado de la mezcla de áridos, cemento y adiciones con una determinada cantidad de agua. Como se ha comentado previamente en el Capítulo 2, el agua puede combinarse químicamente o ser adsorbida en la superficie del sólido o quedarse alojada en los poros capilares. Estos tipos de agua y algunas fases como la portlandita, el carbonato cálcico o la etringita pueden ser cuantificados con el análisis termogravimétrico [11].

El análisis de las muestras se realizó mediante un equipo Setsys Evolution 16/18 de la marca SETARAM con flujo de aire y una rampa de calentamiento de 5 °C/min, en un rango de temperatura entre 30-1000 °C y utilizando crisoles de alúmina.

3.3.4 Isotermas de adsorción-desorción de nitrógeno

La adsorción física o fisisorción de gases es una técnica que ha permitido analizar las propiedades texturales (superficie específica, volumen y tamaño de poros) del filler comercial y de los finos residuales. Esta técnica se basa en la interacción que tiene lugar entre un gas (adsorbato) y el sólido que se quiere caracterizar (adsorbente). La interpretación de estas isotermas mediante diferentes modelos matemáticos permite obtener las propiedades que caracterizan texturalmente a un sólido. Las más empleadas suelen ser:

- Superficie específica (m^2/g): Para la medida de esta propiedad se emplean modelos matemáticos como Langmuir o Brunauer-Emmett-Teller (B.E.T), siendo este último el más empleado.

- Volumen total de poros (cm^3/g): Hace referencia al volumen ocupado por el adsorbato, dentro del adsorbente a una presión determinada, normalmente $P/P_0=1$. En este caso, se trata de una medida directa y expresa el volumen que ocupan los poros en una unidad másica de sólido.

- Distribución de tamaño de poro: consiste en expresar el volumen de poro frente al tamaño de poro al que se adscribe. No es una medida directa, sino la consecuencia de aplicar modelos matemáticos más o menos complejos. El modelo más utilizado para el rango de los mesoporos es el de Barret-Joyner-Halenda (BJH) y para mesoporos de pequeño tamaños y microporos el metodo Density functional theory (DFT)

La isoterma de adsorción es el resultado de la representación gráfica de la cantidad adsorbida, a temperatura constante, en función de la presión (o concentración) del adsorbato. Los autores del método BET propusieron una clasificación de las isotermas (Figura 3.10), conocida como BDDT [12].

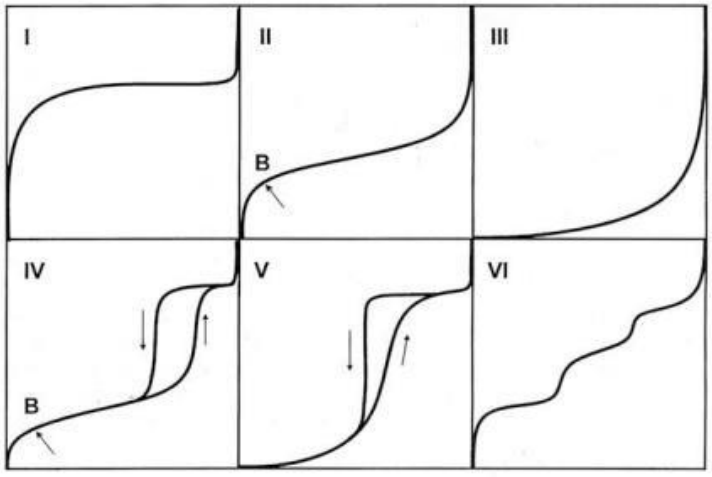

Figura 3.10: Clasificación de isotermas de adsorción

- Tipo I: la isoterma es cóncava respecto al eje de la presión relativa (P/P_0), aumenta rápidamente a baja presión ($P/P0 < 1 \cdot 10^{-3}$) y posteriormente alcanza una meseta de saturación horizontal. Este tipo de isotermas la muestran los sólidos microporosos.

- Tipo II: esta clase de isoterma es característica de sólidos no porosos o de adsorbentes macroporosos. La total reversibilidad de la isoterma de adsorción-desorción, es decir, la ausencia de histéresis, es una condición que se cumple en este tipo de sistemas.

- -Tipo III: es característico de procesos de adsorción en sólidos no porosos en los que la interacción adsorbente-adsorbato es débil. En la práctica no es común este tipo de isotermas.

- -Tipo IV: a bajas presiones se comporta como la isoterma de Tipo II. Es característica de los sólidos mesoporosos. El ciclo de histéresis está asociado con la condensación capilar que tiene lugar en los mesoporos. Esta presenta un incremento de la cantidad adsorbida importante a presiones relativas intermedias y ocurre mediante un mecanismo de llenado en multicapas.

- -Tipo V: del mismo modo que las de Tipo III, esta clase de isotermas se obtiene cuando las interacciones entre el adsorbato y el adsorbente son débiles. La presencia de histéresis está asociada con el mecanismo de llenado y vaciado de los poros. En la práctica es poco usual encontrase con este tipo de isotermas.

- Tipo VI: Es muy poco frecuente. Es característico de la adsorción en multicapa de gases nobles sobre superficies altamente uniformes. Este tipo de adsorción en escalones ocurre sólo para sólidos con una superficie no porosa muy uniforme.

Esta técnica se ha llevado a cabo en dos equipos de adsorción-desorción de gases. El primer equipo fue un porosímetro de la marca Micromeritics modelo ASAP 2020 y el segundo fue un porosímetro Autosorb iQ de la marca Quantachrome Instruments. Las isotermas se realizaron a la temperatura de N_2 líquido (-196 ºC). Se usó N_2 gaseoso como adsorbato y antes del análisis, las muestras fueron desgasificadas a 100 ºC bajo vacío durante 2 h. Para el cálculo del área superficial se utilizó el método BET [13].

3.3.5 Espectroscopía de infrarrojos

La espectroscopía de infrarrojos con transformada de Fourier (FT-MIR) se ha empleado para identificar moléculas del filler comercial y del fino residual de las plantas de MBC a través del análisis de sus enlaces químicos. Cada enlace químico en una molécula vibra a una frecuencia característica y, generalmente, esta frecuencia se encuentra dentro del intervalo de la radiación infrarroja. Cuando una molécula absorbe un fotón, salta de un estado fundamental a un estado excitado, y da lugar a una vibración [14].

Los espectros de absorción de infrarrojo de las distintas muestras se registraron con un espectrofotómetro Tensor 27 FT-MIR de la marca Bruker. Las mediciones se realizaron en muestras molidas en un mortero de ágata. Se usó bromuro de potasio molido y previamente secado como referencia para las mediciones de FT-MIR. El programa OPUS v. 6.5 se utilizó para recopilar los espectros de transmisión.

3.3.6 Microscopía electrónica de barrido

La microscopía electrónica de barrido (SEM) nos ha permitido realizar una caracterización morfológica y microestructural del filler comercial y de los finos residuales utilizados [15–17]. Esta técnica utiliza un haz de electrones secundarios para generar una imagen. Los requerimientos previos de análisis más importantes son; la deshidratación de la muestra y que sea eléctricamente conductora. Estos equipos suelen estar equipados de un analizador de energías dispersivas de rayos X (EDX) [18].

El equipamiento consta de un detector de electrones secundarios que proporciona imágenes topográficas de la superficie de la muestra y un detector de energías dispersivas de rayos X que permite el análisis cualitativo y semicuantitativo de los elementos constituyentes de la muestra, lo cual ha permitido determinar la composición química elemental de todos los materiales de partida.

Se han utilizado dos microscopios electrónicos de barrido. En primer lugar, un microscopio de la marca Jeol modelo JMS 6300 que utiliza un voltaje de aceleración

del haz de electrones de 20 kV para analizar la morfología superficial de las muestras. El sistema de microanálisis es de la marca Oxford Instruments modelo ATW2-6699, utilizando un voltaje de aceleración del haz de electrones de 20 kV y una distancia de trabajo de 15 mm. Y, en segundo lugar, un microscopio de la marca Jeol modelo JSM-7800F utiliza un voltaje de aceleración del haz de electrones de 5 kV para analizar la morfología superficial de las muestras. El sistema de microanálisis es de la marca Oxford Instruments modelo X-Max 150, utilizando un voltaje de aceleración del haz de electrones de 15 kV y una distancia de trabajo de 10 mm. En ambos casos, las muestras son colocadas sobre cinta adhesiva de cobre que se une a un portamuestras también de cobre de 15 mm de diámetro. Después se recubren, solo los sistemas no conductores, con una capa fina de oro.

3.3.7 Microscopía electrónica de transmisión

La microscopía electrónica de transmisión (TEM) ha permitido visualizar las partículas del filler comercial y finos residuales utilizados con una mayor magnificación. Esta técnica se basa en aprovechar los fenómenos físico-atómicos que se producen cuando un haz de electrones suficientemente acelerado colisiona y atraviesa una muestra delgada convenientemente preparada [19].

El microscopio electrónico de transmisión utilizado fue de la marca JEOL modelo JEM 2010 de alta resolución (resolución de 0.194 nm entre puntos) y un voltaje de aceleración de 200Kv. Previo a su análisis, las muestras se dispersaron en tetracloruro de carbono sometidas a ultrasonidos durante 15 minutos para evitar la aglomeración de las partículas. A continuación, una microgota de suspensión fue depositada sobre una rejilla de cobre recubierta de carbón suministrado por la empresa ANAME.

3.3.8 Porosimetría por intrusión de mercurio

La porosimetría por intrusión de mercurio (MIP) ha permitido llevar a cabo la caracterización de la microestructura, distribución y tamaño de poros de los HAC. Esta técnica es la más utilizada para caracterizar la porosidad de rocas naturales o de materiales base cemento [20]. Se basa en las leyes capilares que gobiernan la intrusión de un líquido, que no moja el material, la penetración del líquido será

directamente proporcional al diámetro del poro y la presión, es decir, que solo los poros pequeños serán accesibles por el líquido cuando se le aplique una presión suficiente. Para este caso, el líquido que se utiliza es el mercurio, dado que posee una alta tensión superficial y se considera un líquido que no moja. Por lo que, al tener un material sumergido en mercurio, a la presión atmosférica, este fluido no lo penetraría y solo lo haría al someterlo a un aumento de presión, penetrando primeramente en poros de mayor tamaño a bajas presiones y al aumentar la presión penetraría en poros cada vez más pequeños. Dichas leyes pueden expresarse a partir de la ecuación de Washburn:

$$D = -\left(\frac{1}{P}\right) \cdot 4 \cdot \gamma \cdot \cos\varphi \qquad \text{(Ec. 3.2)}$$

donde D es el diámetro de poro (nm), P es la presión absoluta aplicada (N/nm^2), γ la tensión superficial del mercurio (485 N/mm) y φ el ángulo de contacto entre el mercurio y la muestra (130°) [21]. El método consiste en forzar la entrada de mercurio en los poros del material mediante un incremento gradual de la presión. Para cada incremento discreto de presión se registra el volumen de mercurio introducido en los poros y posteriormente, con esta información y a partir de la ecuación de Washburn, se obtiene el volumen de poros y la distribución de tamaño de poro.

Los inconvenientes de utilizar la ecuación de Washburn resultan del hecho de asumir que todos los poros son circulares y que son igualmente accesibles a la superficie exterior de la muestra (poros abiertos), lo cual no se ajusta a la morfología real de los poros. Este problema puede originar errores en las curvas de distribución de poros, en las que se puede observar erróneamente grandes volúmenes de poros muy pequeños o bien pequeños volúmenes de poros grandes. No obstante, la técnica MIP es muy útil en estudios comparativos.

El equipo utilizado en este trabajo ha sido un porosímetro de la marca Micromeritics, modelo Autopore IV 9500, con un rango de presión de entre 0,0015 y 207 MPa y cubriendo un rango de tamaño de poros entre 5 nm y 180 µm. El volumen de muestra usado fue de un centímetro cúbico aproximadamente.

3.4 Referencias bibliográficas

[1] http://www.master-builders-solutions-basf.es.

[2] https://gcpat.com/construction/es-es.

[3] M. Fernández Cánovas, Hormigón, Ed. Colegio de Ingenieros de Caminos, Canales y Puertos, 2007.

[4] A. Rawle, Basic of principles of particle-size analysis, Surf. Coatings Int. Part A, Coatings J. 86 (2003) 58–65.

[5] T. Allen, Particle Size Measurement, fifth ed., Chapman and Hall, New York, 1997.

[6] L. V. Azaroff, M.J. Buerger, The powder method in X-ray crystallography, McGrow-Hill B. Company, New York, 1958.

[7] B.D. Cullity, S.R. Stock, Elements of X-Ray Diffraction, Prentice Hall, Upper Saddle River, 2001.

[8] M.F. Ladd, R.A. Palmer, Structure Determination by X-Ray Crystallography, Kluwer, Dordrecht, 1994.

[9] P.K. Mehta, P.J.M. Monteiro. Concrete structure, properties and materials. New Jersey, Prentice Hall, 1993.

[10] M.E. Brown, Introduction to Thermal Analysis: Techniques and application, Chapman and Hall New York, 2012.

[11] H.F.W. Taylor, K. Mohan, G.K. Moir, Analytical study of pure and extended Portland cement pastes fly ash and slag cement pastes, J. Am. Ceram. Soc. 68 (1985) 685–690.

[12] K.S.W. Sing, Reporting physisorption data for gas/solid systems with special reference to the determination of surface area and porosity (Recommendations 1984), Pure Appl. Chem. 57 (1985) 603–619.

[13] S. Brunauer, P.H. Emmett, E. Teller, Adsorption of gases in multimolecular layers, J. Am. Chem. Soc. 60 (1938) 309–319.

[14] N.B. Colthup, L.H. Daly, S.E. Wiberly, Introduction to Infrared and Raman Spectroscopy, third ed., Academic Press, Boston, 1990.

[15] C.R. Brundle, C.A. Evans, S. Wilson, Encyclopedia of materials characterization: surfaces, interfaces, thin films, Gulf Professional Publishing, 1992.

[16] J. Humphreys, R. Beanland, P.J. Goodhew, Electron Microscopy and Analysis, CRC Press, 2014.

[17] S. Zhang, L. Li, A. Kumar, Materials characterization techniques, CRC Press, 2009.

[18] A.J. Garratt-Reed, D.C. Bell, Energy-dispersive X-ray Analysis in the Electron Microscope, 1 ed., BIOS Scientific Publishers Ltd, United Kingdom, 2003.

[19] L. Reimer , Transmission Electron Microscopy: Physics of Image Formation and Microanalysis, in: Springer Series in Optical Sciences, 3rd edition, Springer-Verlag, Berlin, 1993.

[20] S. Diamond, Mercury porosimetry: an inappropriate method for the measurement of pore size distributions in cement-based materials, Cem. Concr. Res. 30 (2000) 1517–1525.

[21] R.A. Cook, K.C. Hover, Mercury porosimetry of hardened cement pastes, Cem. Concr. Res. 29 (1999) 933–943.

Capítulo 4

Mechanical and durability behaviour of self-compacting concretes for application in the manufacture of hazardous waste containers

"A.R. Esquinas, D. Motos-Pérez, M.E. Jiménez, C. Ramos, J.R. Jiménez, J.M. Fernández, Mechanical and durability behaviour of self-compacting concretes for application in the manufacture of hazardous waste containers, Construction and Building Materials, 168 (2018) 442–458. doi:10.1016/J.CONBUILDMAT.2018.02.138."

Abstract

In self-compacting concrete (SCC), the amount of coarse aggregates, use of fillers, and type of additives play important roles in its self-compaction, including mechanical and durability properties. The use of SCC is widespread in the precast concrete industry and it can also be employed in the manufacture of containers for the storage of hazardous waste. In addition to the requirements for self-compaction, strict mechanical and durability requirements must be considered. In this work, a study on the effect of variation in the amounts of coarse and fine aggregates, and fillers on

the properties of the fresh state (self-compactability) and hardened state (microstructural, mechanical, and durability behaviours) of different dosages is carried out. The factors that have more significant influences on the density of the mixes are the presence of fillers and water-cement ratio. This is because mixes with fillers and low water-cement ratios have higher densities, which agree with the lower porosity and finer porous structure observed in mixes that incorporate fillers. Mixes incorporating siliceous fillers presented better performances in the absorption of water by immersion and capillarity than mixes without them. Measuring the depth of penetration of water under pressure in various mixes makes it possible to identify those that have high compactness and impermeability. Mixes with fillers and higher microstructural densities have lower water penetration depths. After exposure to aggressive environments, none of the mixes, with and without fillers, showed signs of wearing out or deterioration. The presence of fillers in SCCs had a more significant influence on its shrinkage than the amount of coarse aggregates. Thus, it is possible to obtain high performance SCC in relation to its mechanical and durability properties by reducing the coarse aggregate content and incorporating siliceous fillers in the dosage. Moreover, for applications where high mechanical requirements are not necessary, it is possible to produce an SCC with high performance against the attack of aggressive agents such Cl− and SO3 without using siliceous fillers.

Key words: Self-compacting concrete; hazardous waste container; microstructure; mechanical behaviour; durability; shrinkage.

Highlights:

- The mixes comply with the self-compacting requirements marked by the EHE-08.
- Mixes with fillers and low coarse aggregate content had finer porous structures.
- All mixes are impermeable based on the penetration of water under pressure test.
- The mixes have good performances against chloride and sulphate ion penetration.
- The presence of fillers in the dosages greatly influences concrete shrinkage.

4.1 Introduction

Self-compacting concrete (SCC) was developed in Japan in the mid-1980s under the direction of Professor Okamura of the University of Tokyo [1]. Previously, it was named High Performance Concrete, but was later renamed Self-Compacting Concrete. The objective was to create a type of concrete whose performance did not depend on manpower during the implementation process. In 1988, the first prototype of self-compacting concrete that worked satisfactorily in terms of shrinkage, heat of hydration, density, and other properties was successfully completed [2].

The SCC can be defined as a type of concrete whose main characteristic is its ability to flow and correctly fill the volume to be concreted by the action of its own weight, i.e., without any method of compaction [3]. The main characteristics of SCC compared to conventional concrete (OC) are its fresh state, superior fluidity, cohesiveness, homogeneity, resistance to segregation, and good finishes. These characteristics allow the concreting of more complex and/or tall reinforced concrete buildings, including the design of more complex architectural and structural elements [4, 5]. In SCCs, the amount of coarse aggregates, use of fillers, and type of additive play important roles both in its mechanical and durability properties [6].

Currently, there is a strong line of research related to the use of materials with fine granulometry (powder), both natural and residual, from industry and/or mining, as substitutes for cement or fine aggregates in SCC [7-13]. Another line of research on SCCs—although less frequent but very important—deals with the study on the influence of the amounts of aggregates and paste on the properties of SCC. Along this concept, Fung and Kwan [14] carried out an analysis of the blocking effect in SCCs having different aggregate contents. They found that the fluidity of the mixture was greater with the increase in fine aggregate content, which is attributed to the ball bearing and filling effects of the finer particles. These reduced the blocking action of coarse aggregates and increased the packing density of aggregates. Kwan and Ling [15] analysed the performance of SCC by varying the amounts of aggregates in the dosage. Fly ash was used in all mixtures and the water-binder ratio was kept constant. These authors concluded that the effect of reducing coarse aggregate content and increasing the amount of fine aggregates did not present negative effects

on the mechanical behaviour and nor on the depth of water penetration. On the other hand, Santos et al. [16] observed that the performance of SCC is influenced by the particle size distribution of the aggregate mix because it is related to the packing density and volume of voids to be filled. Likewise, Nikbin et al. [17] carried out a study on the effects of coarse aggregate size and volume on the mechanical resistance of SCCs, where it was observed that increasing the volume of coarse aggregates from 30 to 60% caused a non-constant mechanical behaviour. This conclusion was reached because when the volume of coarse aggregates was increased to 40%, there was a decrease in compressive and splitting tensile strengths, whereas for larger volumes (50 and 60%) these strengths increased. Jawahar et al. [18] analysed the short-term mechanical behaviour of SCCs with varying mixes of coarse aggregates. These authors concluded that the compressive strength was not affected by the variation of the proportions of coarse aggregates although other mechanical properties—unit weight, modulus of elasticity, and splitting tensile strength—were affected.

Currently, there is no consensus in obtaining SCC with a specific performance to suit the particular needs of each project using available materials. Consequently, production companies will have to rely on their own knowledge derived from experience and technical skills of their staff [19]. In this regard, research on SCC is the only instrument that can be used to respond to quality requirements for every specific use. Therefore, companies must use published results as guide in implementing their own dosages to satisfy the required performance in each of their particular applications.

Today, SCCs are widely used in the construction and building sector, particularly in the precast concrete industry. One specific use of this type of concrete is the manufacture of containers for the storage of hazardous waste. For that purpose, strict mechanical and durability requirements must be satisfied in addition to self-compactability.

Several research groups are studying cement-based materials for the immobilisation and containment of hazardous waste [20-24] with the objective that companies dealing with waste management can apply the results to their activities. In this

context, SCC can be used as immobilizer and waste container in place of the commonly used OC but one with better performances both in concrete placement, and mechanical strength and durability. Simply put, SCC is concrete that is easier and safer to use.

In the present study, an analysis of the self-compacting, mechanical, and durability properties of SCCs with different dosages is carried out. Moreover, the effect of variations in the amounts of coarse and fine aggregates, and fillers in the properties of the concrete material is examined. This study has been carried out in collaboration with the National Company for Radioactive Waste (ENRESA) [25], which investigates the use of SCC as substitute for OC in structures used for storing wastes of low and medium radioactive levels located at El Cabril (Córdoba). To determine the behaviour of SCCs, a fresh-state study was first conducted by measuring self-compactability properties such as flowability, blocking resistance, and segregation resistance. Subsequently, an extensive investigation of hardened SCCs was carried out by focusing on the porous structure and its mechanical behaviour. In addition, as an important part of the research, a comparative study of the durability of the different mixes was carried out. All the properties analysed were correlated with the microstructural characteristics of the dosages. Finally, the work was completed with the study of shrinkage. The analysis of all the parameters considered made it possible to define the optimum dosage with a high degree of certainty.

4.2 Experimental methodology

4.2.1 Materials

The aggregates were gravel 4/16, coarse sand 0/4, and fine sand 0/2 (henceforth referred to as G, S1, and S2, respectively) of siliceous nature. The particle size distributions of these aggregates are shown in Figure 4.1. These materials were obtained from a crushing plant located in southwestern Spain (Áridos Gallardo S.L.). In addition to silica, the fine aggregates contain orthoclase and albite. The physical-chemical characterisation of the aggregates was studied by Esquinas et al. [26]. The aggregates were found suitable for the manufacture of concrete according to EHE-08 [26].

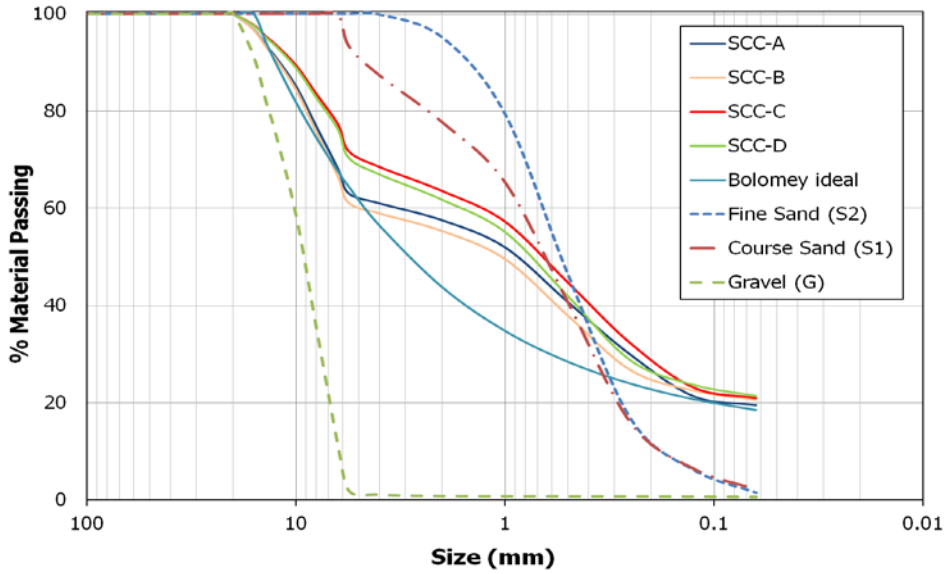

Figure 4.1: Particle size distribution for gravel, coarse and fine sands, mixes SCC-A, SCC-B, SCC-C, and SCC-D and Bolomey ideal.

The cement used was CEM I 42.5 R/SR (UNE 80303-1 and UNE-EN 197-1) [27], and its physical-chemical characterisation was determined through research [26]. The particle size distribution of the cement (Figure 4.2) showed that 61.28% are major particles and are 3–32 μm in size, which are important for the hydration process [28-30].

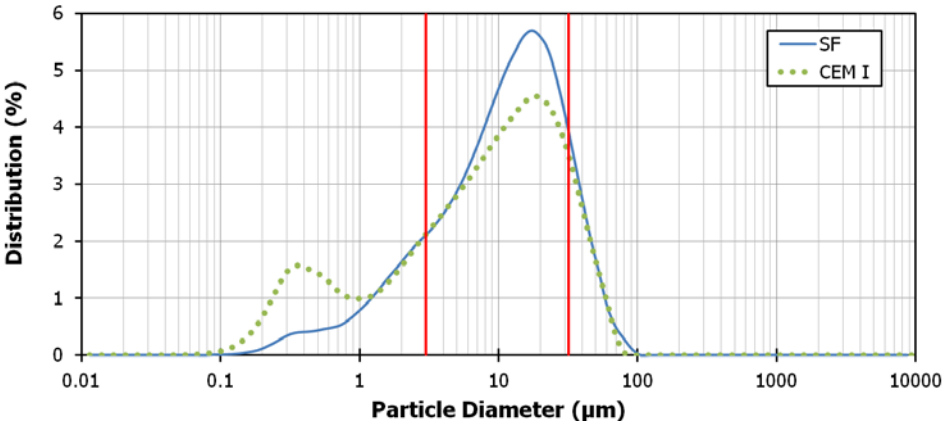

Figure 4.2: Grain-size distribution of SF filler and CEM I as measured by laser diffraction.

A filler of siliceous nature (Figure 4.3), henceforth referred to as SF—obtained by grinding fine sands and supplied by Lorda and Roig, SA (Gerona, Spain)—was used

as mineral additive. The pore size distribution in Figure 4.4 showed a reduced volume of pores, which are 5–70 nm and calculated from the desorption branch according to the BJH method. The SF particles had a BET (Brunauer-Emmett-Teller) surface of 0.25 m2/g. Both these aforementioned properties agree with the microphotography of the transmission electron microscopy, as shown in Figure 4.4. The granulometry obtained using the Standard UNE-EN 933-1 [27] showed that SF complies with the requirements marked by EHE-08 because 100% pass through 2, 0.25, and 0.125 mm sieves, and 74.33% pass through the 0.063 mm sieve [31]. These conform with the grain size distribution obtained by laser diffraction (Figure 4.2)—using ethanol as dispersant—in which a distribution of 0.1–100 μm was observed. The majority of the sizes is approximately 20 μm and 71.3% of the particles are 3–32 μm, optimal for the hydration process [28-30].

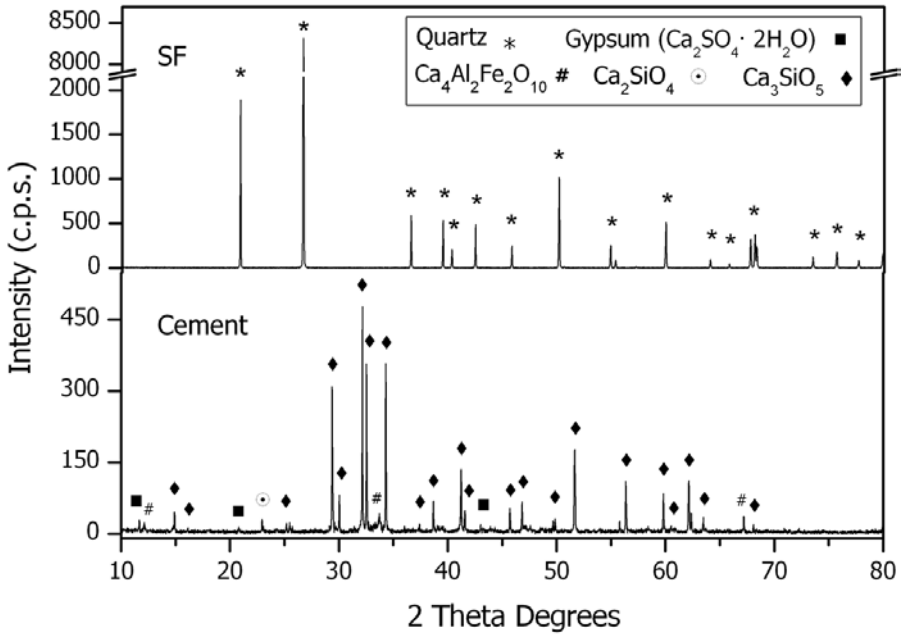

Figure 4.3: PXRD patterns of SF filler and cement.

For the preparation of self-compacting concretes with low water-cement ratios (w/c), Glenium 303 SCC from Basf Chemical Company [32] and Adva® flow 400 from Grace Construction Products [33] (Table 4.1) were used as additives.

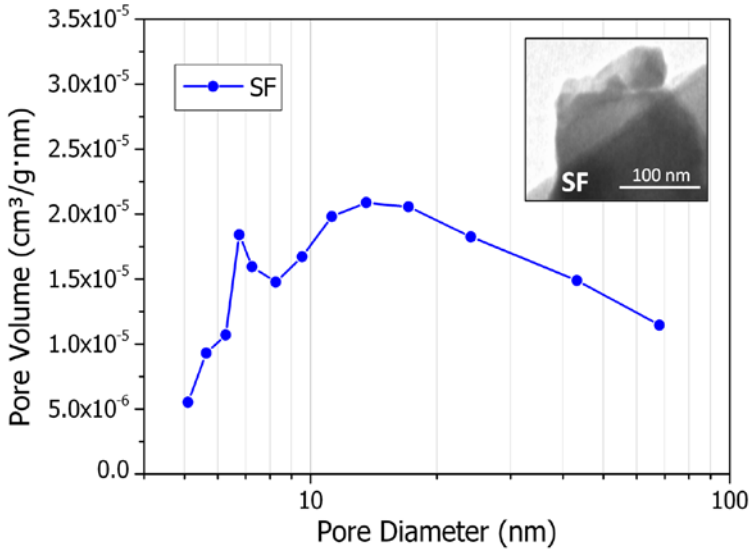

Figure 4.4: Pore size distribution and TEM micrographs of the SF fillers.

Table 4.1
Properties of additive.

	Glenium 303SCC	**Adva® flow 400**
Main function:	High water-reducing power/superplasticizers	High water-reducing power/superplasticizers
Secondary function:	Retainer water.	Retainer water.
Side effect:	Risk of disintegration at high doses.	Risk of segregation at high doses.
Form:	Greenish liquid.	Light brown liquid
Density, 20° C:	1.035 ± 0.02 g/cm^3	1.05 ± 0.02 g/cm^3
pH, 20º C:	6.5 ± 1	5.8 ± 1
Chloride content:	≤ 0.1 %	Exempt

4.2.2 Concrete mixes

Two dosing lines were developed to study the effect of the amount of coarse and fine aggregates on the properties of the SCCs in terms of self-compactability, mechanical resistance, and durability. In the first line, the SCC-A mix consisted of fine aggregates (sand 0/2 and 0/4), coarse aggregates (approximately 800 kg/m^3), SF (approximately 100 kg/m^3), cement (approximately 400 kg/m^3), Glenium 303 SCC additive, and water with a water-fines ratio less than 1. In the second line, the SCC-C mix was defined with the following variations with respect to the previous mixture: Fine aggregates used were only sand 0/4 at a higher percentage, the amount of coarse aggregate

was approximately 600 kg/m^3, and the additive was Adva® flow 400. Moreover, the absence of fillers was analysed for the two dosing lines. For this purpose, two other mixes were defined. First, the SCC-B is similar to the SCC-A mixture except in the use of fillers and in keeping the coarse-fine aggregate ratio constant. Second, the SCC-D mix was developed similar to SCC-C except in the use of fillers and in keeping the coarse-fine aggregate ratio constant.

In all mixtures, self-compaction was studied according to the requirements of EHE-08 [31] as listed in Table 4.2. The following analyses were conducted: the unobstructed filling capacity and resistance to segregation through the parameters d_f and T_{50}, respectively; the ability to pass through spaces between reinforcing bars and resistance to segregation by means of the parameter d_{Jf}; the capacity to pass through narrow openings and the capacity of filling through the parameter Tv; the ability to pass through spaces between reinforcing bars and the resistance to segregation by means of the parameter C_{bl}.

To obtain the dosages of SCC, doses provided by the National Company for Radioactive Waste (ENRESA) [25] were used. This company investigates the use of SCC in structures utilised to store wastes of low and medium radioactive levels in El Cabril (Cordoba). The company requires the cement content maintained at approximately 400 kg/m^3, water-cement ratio not to exceed 0.45, and resistance higher than 48.6 MPa in 28 days considering class IIIc exposure. According to EHE-08, the concrete is classified as HA-40/AC/16/IIIc. The dosage adjustment was performed by volume (1025 L).

As listed in Table 4.3, in the SCC-A dosage, the components of the mix are within the recommended values of the EFNARC (European Federation of National Associations Representing producers and applicators of special building products for Concrete) [4, 5]. Although the SCC-B, SCC-C, and SCC-D mixes comply with most of the specifications recommended by EFNARC, the modifications made in the content of gravel, fine sand, and/or fillers alter some parameters and are outside the guidelines, though very close to the limits marked by the EFNARC. The influence of these modifications on the self-compactability of the mixes is analysed. For as long as they

are within the self-compactability requirements accepted by EHE-08 [31], the mixes are defined as SCC.

Table 4.2
Self-compaction test.

Test	**Characteristics evaluated**	**Standard**	**Parameters**	**Admissible values** [31]
Slump flow test	Filling ability unobstructed	UNE-EN 12350-8 [27]	d_f = final flow diameter	550 mm ≤ d_f ≤ 850 mm
	Resistance to segregation [a]		T_{50} = time spent to reach the 500 mm	T_{50} ≤ 8s
J-Ring test	Passing ability	UNE-EN 12350-12 [27]	d_{jf} = final flow diameter	≥ d_f - 50 mm
	Resistance to segregation [a]			
V-funnel test	Filling ability	UNE-EN 12350-9 [27]	Tv = funnel flow time	4 s ≤ Tv ≤ 20 s
	Passing ability			
L-box test	Passing ability	UNE-EN 12350-10 [27]	C_{bl} = blocking coefficient	0.75 ≤ C_{bl} ≤ 1
	Resistance to segregation [a]			

[a] No standardized

Table 4.3
Concrete mix proportions and dosing tests.

Mixes	**SCC-A**				**SCC-B**				**SCC-C**				**SCC-D**			
	Dry weight		*Volume*		Dry weight		*Volume*		Dry weight		*Volume*		Dry weight		*Volume*	
Constituent	Kg/m^3	%	*Liters*	*%*	Kg/m^3	%	*Liters*	*%*	Kg/m^3	%	*Liters*	*%*	Kg/m^3	%	*Liters*	*%*
Gravel 4/16 (G)	794.75	32.80	*305.67*	*29.96*	827.58	34.35	*318.30*	*31.20*	564.54	23.26	*217.13*	*21.20*	582.58	24.20	*224.07*	*21.88*
Sand 0/4 (S1)	646.79	26.70	*246. 87*	*24.20*	677.46	28.12	*258.57*	*25.34*	1130.5	46.57	*431.49*	*42.14*	1174.7	48.79	*448.36*	*43.79*
Sand 0/2 (S2)	276.33	11.41	*106.28*	*10.42*	268.47	11.14	*106.23*	*10.12*	0.00	0.00	*0.00*	*0.00*	0.00	0.00	*0.00*	*0.00*
Filler	100.12	4.13	*38.51*	*3.77*	0.00	0.00	*0.00*	*0.00*	96.00	3.95	*36.92*	*3.61*	0.00	0.0	*0.00*	*0.00*
Cement	410.00	16.92	*132.26*	*12.96*	430.00	17.85	*138.71*	*13.60*	438.92	18.08	*141.59*	*13.83*	440.00	18.28	*141.94*	*13.86*
Superplasticizer	9.18	0.38	*8.87*	*0.87*	9.52	0.39	*9.20*	*0.90*	12.30	0.51	*11.71*	*1.14*	11.00	0.46	*10.48*	*1.02*
Water	185.54	7.66	*185.54*	*18.19*	195.96	8.09	*195.96*	*19.21*	185.16	7.63	*185.16*	*18.08*	199.16	8.27	*199.16*	*19.45*
Superplasticizer	**Glenium 303SCC**				**Glenium 303SCC**				**Adva® flow 400**				**Adva® flow 400**			
(W/C)	0.453				0.456				0.422				0.453			
(W/C) $_{ef}$ ratio	0.438				0.442				0.413				0.441			

	Typical range[a]	SCC-A	SCC-B	SCC-C	SCC-D
Coarse aggregate (kg/m^3)	750-1000	794.75	827.58	564.54	582.58
Fine aggregate (sand) (%)	48-55[b]	53.6	53.2	66.5	66.7
Fines (kg/m^3) / [L/m^3]	380-600	569.80 / [193.6]	490.92 / [162.0]	599.98 / [203.3]	507.59 / [167.7]
Water (litres/m^3)	150-210	185.54	195.96	185.16	199.16
Paste (litres/m^3)	300-380	379.15	357.99	388.51	366.90
Water/fines [c]	0.85-1.10	0.96	1.21	0.91	1.19

[a] EFNARC dosage parameters [2]

[b] Volume total weight of aggregate in balanced quintiles. % of sand S1and S2 relative to the whole of the aggregates.

[c] by volume.

4.2.3 Test methods

The characterisation of the materials was carried out through different techniques. Particle sizes were measured in a Mastersizer S analyser (Malvern Instruments) using ethanol as dispersant. The samples were analysed by X-ray diffraction patterns (XRD) using a Bruker D8 Discover A25 instrument with CuKα radiation. All diffraction patterns were obtained by scanning the goniometer 10–80° (2θ) at a rate of 0.05°s^{-1}. Using a Micromeritics ASAP 2010 analyser, N_2 isotherms were determined in the samples having been previously degassed at 100 °C in a vacuum for 2 h. The surface was calculated using the BET method in the range of equilibrium relative pressure $0.05 \leq P/Po \leq 0.20$ [34]. Microstructural characterisation of the materials was carried out using JEOL 1400 TEM and JEOL 2010 TEM equipment.

The wet and dry bulk densities (UNE-EN 12390-7 and UNE 83980) [27] were measured for specimens of 150×150×150 mm cured in water for 28 days, with volume determined by measuring the actual sizes of the specimens. The values of mercury intrusion porosimetry were obtained using a Micromeritics AutoPore IV 9500 in a pressure range of 0.0015–207 MPa. This test was done on representative samples of 1 cm^3 extracted from the central area of cylindrical specimens 150 mm in diameter and 300 mm in height cured in water at 91 days.

The compressive strength (UNE-EN 12390-3) [27] and splitting tensile strength (UNE-EN 12390-6) [27] in cylindrical specimens of 300×150 mm, and flexural strength (UNE-EN 12390-5) [27] in prismatic specimens of 100×100×40 mm were evaluated after 7, 28, and 91 days of curing in water according to UNE-EN 12390-2 [27]. For this batch of tests, a Proeti SA press model ETI0225 with a maximum capacity of 2000 kN was used.

The water absorption capacity of hardened concrete was measured by means of two procedures. In the first procedure, water absorption in the 100-mm cubic specimens cured beforehand in water for 28 days was determined by immersion (UNE 83980) [27]. In the second procedure, water absorption in the specimens of 100×100×200 mm cured in water for 28 days was determined by capillarity (UNE 83982) [27]. Prior to the test, the specimens were oven-dried at a temperature of 60 ºC until constant

mass was reached. The latter test enables determination of the resistance to penetration, absorption coefficient, and effective porosity of the samples. Effective porosity herein means interconnected porosity and connected to the exterior.

Permeability was assessed by measuring the depth of water penetration under pressure (UNE-EN 12390-8) [27] in cylindrical specimens 150 mm in diameter and 300 mm in height, and cured in water for 28 days. The determination of concrete permeability is necessary, but not sufficient, to make an adequate evaluation of concrete exposed to aggressive agent attacks.

The total chloride is the sum of chloride plus the free chloride content in the pore liquid, combined chemically and physically with the cement matrix. The penetration of chloride ions through the cement pores results in a chemical attack because of the reaction between the ions dissolved in water and concrete, thereby producing an expansive compound called Friedel's salt ($Ca_2Al(OH)_6(Cl, OH)\cdot 2H_2O$). When the threshold value of ion chlorides is reached, the corrosion of reinforced concrete occurs. To determine the penetration of chloride ions, the test procedure called "Determining the Penetration of Chloride Ion into Concrete by Ponding" (ASTM C 1543) [35], was used. It provided the study with a very precise measurement of the resistance of concrete against chloride ion penetration in quasi-real conditions. First, the chloride ion concentration curve is constructed to obtain its penetration depths in the 100-mm-diameter and 200-mm-high cylindrical specimens, all previously cured in water for 91 days and subsequently submerged for another 91 days in a dissolution of NaCl to 3%. Afterwards, samples are extracted from the specimens at a depth of every 5 ± 1 mm until 30 ± 5 mm is reached, as based on ASTM C1543 [35] and UNE 112010 [27]. Finally, according to ASTM C1556 [35], using Eq. 4.1, which corresponds to the solution of Fick's second law, the coefficient of transport and theoretical superficial concentration can be determined:

$$C(x,t) = Cs - (Cs - Ci)\cdot \operatorname{erf}\left(\frac{x}{\sqrt{4\cdot De\cdot t}}\right) \qquad (4.2)$$

where C(x,t) is the percentage of chloride concentration at a depth of x meters in concrete at time t in seconds, Cs is the percentage of superficial chloride content, erf is the error function, and De is the effective coefficient of chloride transport in m^2/s.

To analyse the penetration of sulphates, a procedure was carried out based on the standards of chemical analysis of cement (UNE-EN 196-2) [27] and of chloride attack in concrete—ASTM C1543-02 [35] and UNE 112010 [27]. The first step was the preparation of 100-mm cubic specimens cured for 91 days in water and covered by a 1-mm-thick layer of waterproof epoxy resin, Sikaguard-62, except for one of the faces. In the second step, once the resin was dry, two 10-mm-thick slices were wet-cut from each face without resin. The outside part was discarded and the other part was kept under curing conditions as an SCC reference (i.e., not exposed to aggressive environment). In the third step, the rest of the specimens were submerged with the sides without epoxy facing up for 91 days in a solution of Na_2SO_4 in distilled water at a concentration of 8.26 g/L (65% higher than the maximum concentration used in EHE-08 for aggressive environments) kept constant throughout this period. In the fourth step, after the exposure time, the specimens were dried and dry samples were taken from them using a column drill. Six samples were extracted, each 5 ± 1 mm apart until a depth of 30 ± 5 mm was reached. The fifth and final step was the determination of sulphate ion concentrations (UNE-EN 196-2) [27] to determine the profile of the sulphate ion penetration in the designed SCCs.

The long-term study of drying shrinkage (ASTM C157/C157M-08 (2014) e1.) [35] was carried out in specimens of 100×100×500 mm cured for 28 days in water. Then, they were introduced into a curing chamber under constant ambient conditions (temperature of 20 °C and 50% relative humidity).

All tests were triplicated in specimens made from the same concrete mix to obtain average values and standard deviations.

4.3 Results and discussion

4.3.1 Properties of SCC in fresh-state—Self-compactability

The values of the self-compactability parameters obtained in the four mixes are listed in Table 4.4 and shown in Figure 4.5. These results comply with the requirements of EHE-08 (Figure 4.5 and Table 4.2) [31].

Table 4.4
Results of the self-compactability tests for the two types of SCC.

Mixtures	Retakes	Slump flow test		J-Ring test		V-funnel test	L-box test
		T_{50} (s)	d_f (mm)	T_{J50} (s)	$d_f - d_{jf}$	T_v (s)	C_{bL}
SSC-A	Average (SD) [a]	3.75 (0.06)	657.50 (3.19)	6.81 (0.16)	30.00 (1.63)	15.31 (0.78)	0.80 (0.01)
Class [31]	*AC-V1*	*AC-E2*	*AC-RB2*		*AC-V1*	*AC-RB2*	
SSC-B	Average (SD) [a]	4.00 (0.11)	620.00 (7.48)	5.00 (0.25)	10.00 (2.16)	6.81 (0.42)	0.80 (0.01)
Class [31]	*AC-V2*	*AC-E1*	*AC-RB2*		*AC-V2*	*AC-RB2*	
SSC-C	Average (SD) [a]	6.00 (0.19)	712.50 (6.10)	9.00 (0.22)	12.50 (0.51)	11.00 (0.36)	0.92 (0.02)
Class [31]	*AC-V1*	*AC-E2*	*AC-RB2*		*AC-V1*	*AC-RB2*	
SSC-D	Average (SD) [a]	1.66 (0.12)	677.50 (3.08)	5.00 (0.15)	22.50 (0.96)	6.75 (0.2)	0.81 (0.01)
Class [31]	*AC-V3*	*AC-E2*	*AC-RB2*		*AC-V2*	*AC-RB2*	

[a] Standard deviation

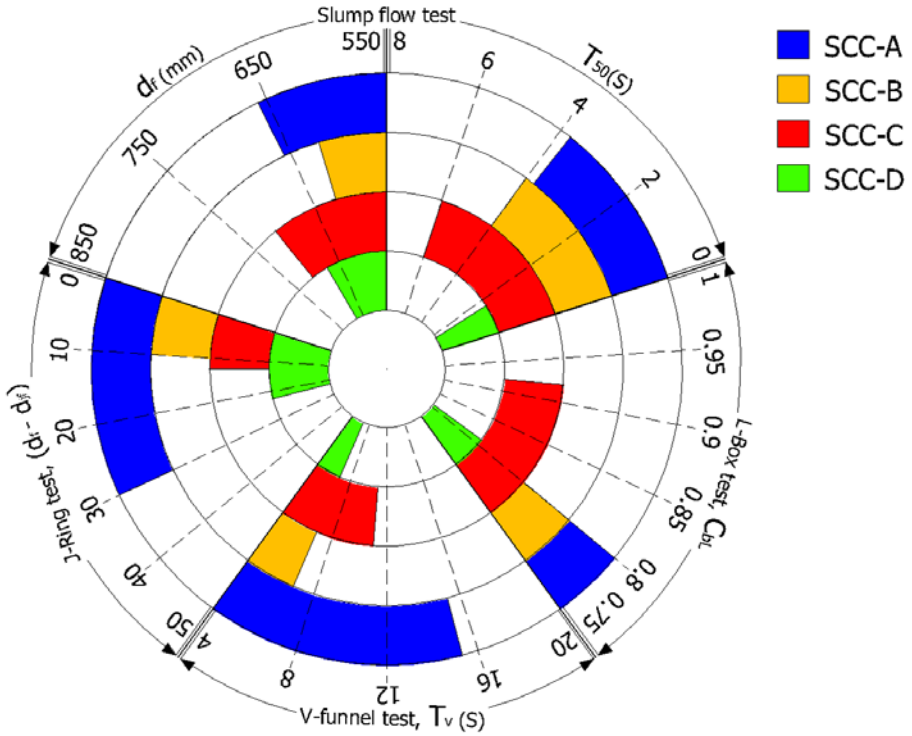

Figure 4.5: Properties of SCCs in fresh-state and self-compactibility.

The self-compactability of the mixtures was corroborated by the workability box (Figure 4.6), where mixtures within the area marked as acceptable SCC [9], and differences between mixes with silica filler (SCC-A and SCC-C) and without silica filler (SCC-B and SCC-D) can be observed. The first ones inside the box in the section called "Proper SCC area," are regarded as suitable and acceptable SCCs, whereas the second ones are immersed in the "Marginal SCC area" in the box, where a slight segregation could occur according to the author. This aspect was not observed in any of the mixes of the present work. Such a diverse behaviour can be explained as effects of the filler and higher content of fines, which fluidise the mixes and make them more cohesive, resulting in more viscous mixes. This result conforms with the lower water content required to achieve self-compactability in mixes with fillers (185 vs. 196–199 L/m^3), fine materials, and paste, as these parameters favour cohesion.

The coarse aggregate content affected the slump flow test more than the funnel test in V [26, 36], because in both systems, with or without fillers, the increase in coarse

aggregate content (from ~600 to ~800 kg/m^3) caused a reduction in slump flow (d_f). This agrees with the study of Okamura and Ouchi [37], affirming that the increase in the contents of coarse aggregates caused the decrease in the capacity of passage. On the other hand, the effect of coarse aggregate variation differs between mixes with fillers (SCC-A and SCC-C) and mixes without fillers (SCC-B and SCC-D) in terms of the Tv value. In other words, the increase in coarse aggregates (from ≈600 kg/m^3 to ≈800 kg/m^3) only affected the V-funnel test in dosages that incorporated fillers, as shown in Figures 4.5 and 4.6. In general, this behaviour conforms with the observations of Emborg et al. [38], who concluded that from a reference dosage, the increase in water and coarse aggregates, or the decrease in cement, reduces the fluidity of mixes. However, a reduction in the amount of filler would cause a more drastic reduction in self-compactability.

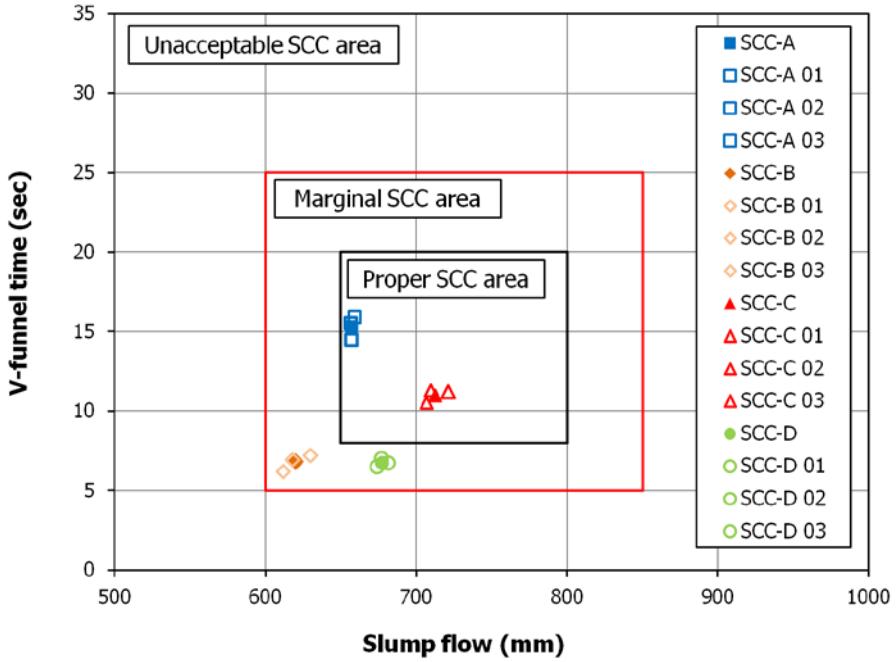

Figure 4.6: Workability boxes of several self-compacting mixes.

These results show that the mixtures are within the range accepted as SCC [31], that is, it is possible to obtain SCCs with dosages where parameters such as the amount of coarse aggregates, paste, and water-fines ratio are not within the values proposed by EFNARC.

The self-compacting parameters of the mixes agree with results obtained by Topçu et al. [39], who carried out a study of the fresh properties of SCC with different filler amounts incorporated in the dosage. For specific cases of mixes with 100 kg/m^3 of fillers, the results are of the same order as those obtained in the SCC-A mixture in this present paper. On the other hand, Felekoglu et al. [9] and Valdez et al. [40] obtained similar fluidity and blocking results in mixes with low contents of coarse aggregates and without fine sand, similar in composition to SCC-C. However, the times T_{50} and Tv obtained by Valdez et al. [40] are lower because the amount of paste in the SCC-C mix was higher, giving it more cohesion. The self-compacting results of SCC-B and SCC-D conform with those obtained by Alyamac and Ince [7] in mixes manufactured without filler.

These results indicate that it is possible to obtain SCCs for dosages with coarse aggregate contents of more than 300 L/m^3 and fine material contents of less than 190 L/m^3, as in the SCC-B mix (Table 4.3), in contrast with those commented by Silva et al. [41].

4.3.2 Physical properties of hardened SCCs

4.3.2.1 Bulk density and evolution during drying

Bulk densities during the wet state of the four mixes (SCC-A, SCC-B, SCC-C, and SCC-D) showed slight differences—2.367, 2.340, 2.376, and 2.363 T/m^3 respectively (Table 4.5). It is noteworthy that mixes with fillers (SCC-A and SCC-C) have higher density values, corresponding with lower water-cement ratios (Table 4.3). The dry bulk densities were 2.238, 2.206, 2.267, and 2.224 T/m^3 for SCC-A, SCC-B, SCC-C and SCC-D, respectively (Table 4.5), conforming with the water-cement ratios presented by the different mixes (Table 4.3). It is observed that the wet and dry densities differ by approximately 5%, which may be mainly because of the loss of free water after the drying process. The lowest losses of water occurred in mixes with fillers, SCC-C (4.6%) and SCC-A (5.4%) compared to mixes without fillers, SCC-D (5.9%) and SCC-B (5.7%).

Table 4.5
Physical, water absorption & durability properties hardened SCCs.

	Unit	Standard/Test	SCC-A (SD)	SCC-B (SD)	SCC-C (SD)	SCC-D (SD)
Wet apparent density	(T/m^3)	UNE 83980	2.367 (0.003)	2.340 (0.009)	2.376 (0.02)	2.363 (0)
Dry bulk density (ρ_{ap})	(T/m^3)	UNE 83980	2.238 (0.001)	2.206 (0.01)	2.267 (0.002)	2.224 (0)
Threshold diameter	(μm)	MIP	0.18	0.22	0.16	0.43
Median Pore Diameter	(nm)	MIP	57	134	48	117
Porosity (MIP)	(%)	MIP	10.2	12.3	9.3	17.1
Abs. by immersion at 24h	(%)	UNE 83980	4.05 (0.01)	4.13 (0.01)	3.67 (0)	4.61 (0.01)
Capillary Absorption at 24 h	(g/cm^2)	UNE 83982	0.42 (0.01)	0.49 (0.01)	0.35 (0.01)	0.47 (0.02)
Capillary Abs. Coef. (K)	($g/cm^2 \cdot min^{1/2}$)	UNE 83982	0.0098 (0)	0.0112 (0)	0.0084 (0)	0.0106 (0)
Resistance to penetration (m)	(min/cm^2)	UNE 83982	9.0 (0.1)	12.3 (0.1)	7.6 (0.01)	13.3 (0.02)
Effective Porosity (ξ)	(%)	UNE 83982	2.92 (0)	3.90 (0)	2.30 (0)	3.87 (0)
Sorptivity (S)	($cm / min^{1/2}$)	UNE 83982	0.0102	0.0121	0.086	0.0115
Permeability	(mm)	UNE-EN 12390	1.90	6.13	1.57	5.73
Permeability coefficient	(10^{-14} m/s)	Valenta Ec. [65]	0.10	0.89	0.09	0.65
Effect. Cl^- Transp. Coeff. (D_e)	(10^{-12} m^2/s)	ASTM C 1556	9.06	9.85	9.84	8.50
Effect. SO_3 Transp. Coeff. (D_e)	(10^{-12} m^2/s)	ASTM C 1556	6.79	7.51	6.38	7.11

It can be concluded that the factors that have the most influence in the density of the mixes are the presence of fillers and water-cement ratio. The use of fillers together with low water-cement ratios allows obtaining SCCs with high densities, that is, with a granular skeleton that contains the minimum number of empty voids because most of them would have been filled by paste.

A linear behaviour was observed in the evolution of the bulk density (ρ_{bulk}) to dry bulk density of SCC-A (Eq. 4.2), SCC-B (Eq. 4.3), SCC-C (Eq.4. 4), and SCC-D (Eq. 4.5) with respect to the loss of mass (m) during the drying process (Figure 4.7):

$$\rho_{bulk} = 0.023\ m + 0.08 \quad (4.2)$$

$$\rho_{bulk} = 0.024\ m - 0.06 \quad (4.3)$$

$$\rho_{bulk} = 0.020\ m + 0.41 \quad (4.4)$$

$$\rho_{bulk} = 0.023\ m + 0.03 \quad (4.5)$$

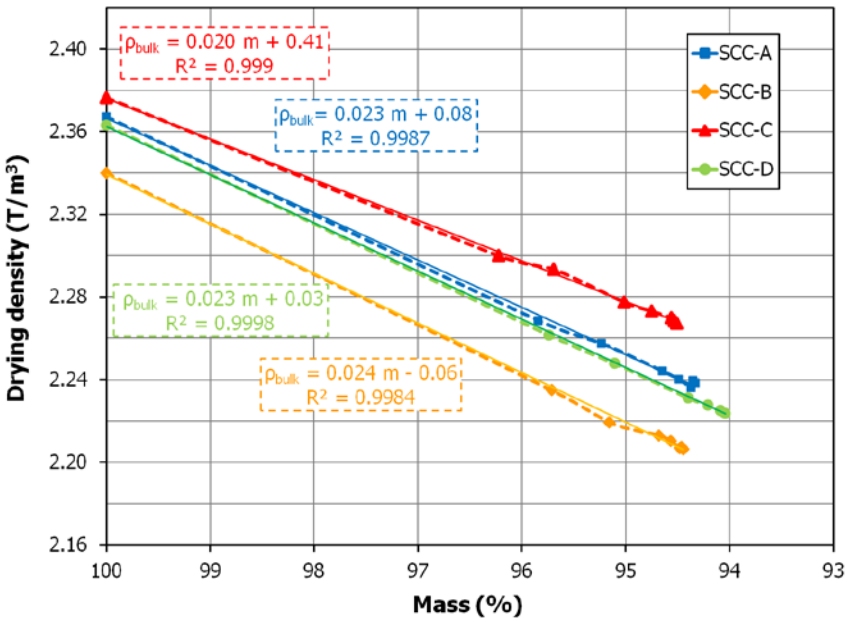

Figure 4.7: Evolution of the density relative to variation of mass.

The mixes experienced similar mass loss during drying, with a slightly greater loss in the SCC-D mix, which has the highest water content. The volumetric stability of the four dosages was similar because the straight lines present gradients of the same order. The slightly lower gradient for sample SCC-C in relation to density loss may be

related to the lower water-cement ratio, implying that a small amount of water is susceptible to elimination during the drying process.

4.3.2.2 Pore size distribution

The cumulative values of Hg volume in the intrusion and extrusion cycles with respect to pore diameter are shown on the top portion of Figure 4.8. These volumes can be correlated with the total porosity of the different mixes. Accordingly, the SCC-C mix has the lowest porosity (9.3%), followed by SCC-A (10.2%), SCC-B (12.3%), and SCC-D (17.1%) (Table 4.5), respectively.

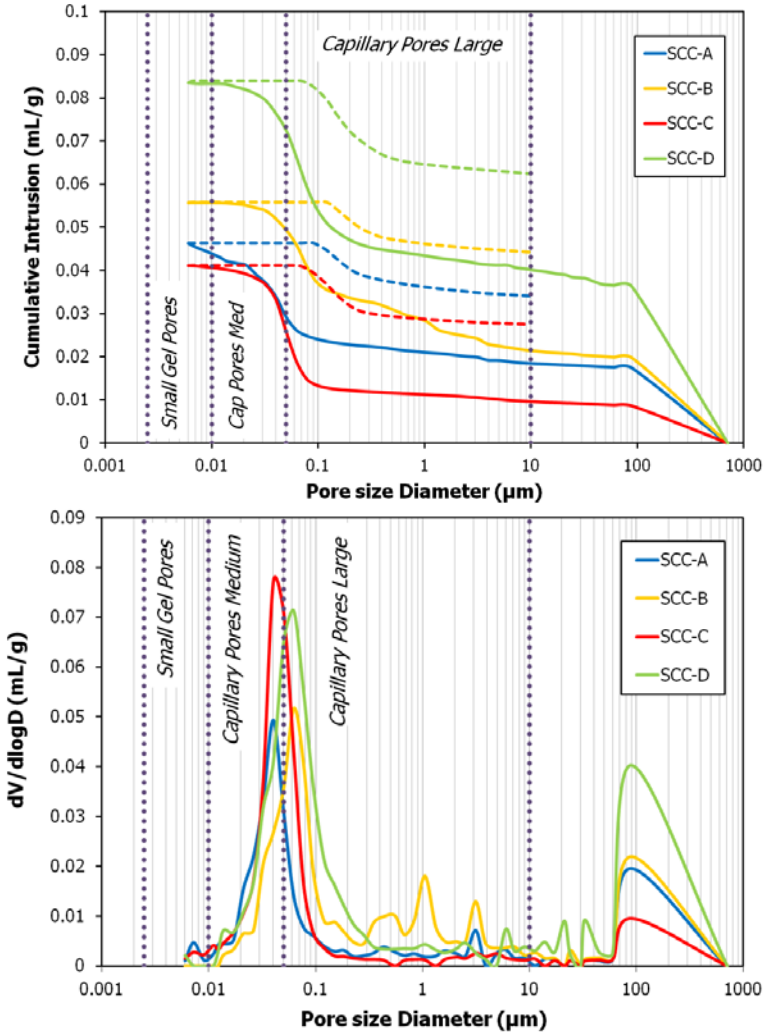

Figure 4.8: Cumulative pore volume and log differential intrusion of the mixes.

The bottom portion of Figure 4.8 right shows the intrusion differential volume for each pore diameter. It was observed that the four mixes present two maximums of mercury intrusion. One is found to be ~90 μm—which may be because of air occluded in the mix (pores larger than 100 μm) [42]—and the other is 20–90 nm, i.e., in the area of capillary pores. In the area of large capillarity pores (50 nm–10 μm), the volumes of samples SCC-A, SCC-B, SCC-C, and SCC-D were 0.011, 0.028, 0.016, and 0.032 mL/g, respectively. In the medium capillarity pores zone (10–50 nm) the volumes for SCC-A, SCC-B, SCC-C, and SCC-D were 0.014, 0.006, 0.015, and 0.011 mL/g, respectively. And finally, in the small gel pores zone (2.5–10 nm) the volumes for SCC-A, SCC-B, SCC-C, and SCC-D were 0.0028, 0.00003, 0.0006, and 0.0002 mL/g, respectively.

For diameters greater than 70 μm and for large capillary pores (50.0 nm–10.0 μm), higher volumes of mercury intrusion were observed in mixes that do not contain fillers (SCC-B and SCC-D). These pores influence the permeability of the material [43]. In the pore ranges of 10–50 nm (medium capillary pores) and 2.5–10.0 nm diameters (small gel pores) it is observed that the highest volumes of mercury occur in mixes with fillers (SCC-A and SCC-C), which conforms with the incorporation of mineral additions to the mixes [44]. These additions cause reduction in the large capillary pores as these are filled with powder, resulting in a finer porous distribution and higher structural density. The particle size distribution of SF (Figure 4.2) is optimal for its reaction with portlandite ($Ca(OH)_2$) to form hydrated products such as CSH, which fills the porous structure, giving rise to smaller pore sizes. The water-cement ratio also influences the porous structure because at a lower ratio structural density is higher.

In the four mixes studied, the highest pore content is located at the separation limit of large and medium capillary pores (50.0 nm). Mixes without fillers (SCC-B and SCC-D) have their maximum concentration shifted to the right with respect to mixtures with fillers (SCC-A and SCC-C). This means that in mixes without fillers, the highest concentration of pores is in the range of large capillary pores (60 nm) versus mixes with fillers having their maximum concentration within the medium capillary pores zone (40 nm) [43, 45]. Therefore, the addition of fillers to dosages may cause the majority of pores to be smaller.

Another difference also observed is in the threshold diameter or maximum pore diameter, where there is a continuous increase in mercury intrusion. The values are 0.18, 0.22, 0.16, and 0.43 μm for SCC-A, SCC-B, SCC-C, and SCC-D, respectively (Table 4.5). These values give information regarding the minimum diameter and present continuous geometry throughout the hardened SCC [46]. The average pore diameter (Table 4.5) is lower than the threshold diameter in all cases. This could indicate that the designed mixes have high density microstructure, because after attaining pressure relative to the threshold diameter, few pores filled with Hg remain [47].

On the other hand, mixes with lower contents of coarse aggregates (SCC-C and SCC-D) present greater mercury intrusion volumes in the zones between medium and large capillary pores, compared to mixes with higher coarse aggregate percentages (SCC-A and SCC-B). These may be because of the greater compactness of SCC-C and SCC-D mixes caused by the higher percentage of fine aggregates in them. This explanation conforms with the higher density observed in the SCC-C and SCC-D mixes relative to SCC-A and SCC-B, respectively.

The results obtained in this paper agree with those of Pipilikaki and Beazi-Katsioti [48] who carried out an analysis of the porous structure of cement paste, incorporating different amounts of limestone fillers. They concluded that the mineral addition led to better packing of particles because of the filling effect on the pores, which would make the entry of chemical agents through the hardened paste difficult. Similarly, Parra et al. [49] concluded that the addition of limestone fillers produced better packing of the particles, resulting in SCC with finer porous structures. Moreover, it is also observed that as the fine aggregate content decreases, the maximum concentration of pores is displaced towards larger pore diameters, that is, large capillary pores are the majority in the porous structure.

Therefore, it can be concluded that mixes incorporating fillers in their dosages (SCC-A and SCC-C) result to SCC with finer porous structures than mixes with dosages that do not contain fillers (SCC-B and SCC-C).

4.3.3 Mechanical properties of SCCs

4.3.3.1 Compressive strength

The values of the compressive strengths of the SCCs produced are listed in Table 4.6 and shown in Figure 4.9. At 7, 28, and 91 days, respectively, compressive strengths are as follows: in the SCC-A mix, values are 41.50, 47.23, and 52.32 MPa, respectively; in the SCC-B sample, strengths are 33.20, 37.09, and 37.90 MPa, respectively; the SCC-C presented strengths of 43.82, 51.17, and 56.79 MPa, respectively; finally, in the SCC-D mix, strengths are 33.98, 37.48, and 38.50 MPa, respectively.

As can be seen, for mixtures analysed under all ages, the SCC-C mix has the highest compressive strength, which conforms with it having the lowest water-cement ratio (Table 4.3). The SCC-A mix presents a 7.7% reduction in strength with respect to the previous mix at 28 days of curing, which conforms with its higher water-cement ratio. This seems to indicate that in dosages with fillers, the influence exerted by the water-cement ratio on compressive strength is more determinant than the amount of coarse aggregates. This conforms with the similar compressive strengths of the SCC-B and SCC-D mixes, containing different amounts of coarse aggregates but having water-cement ratios of the same order (0.442 vs. 0.441).

Among samples with coarse aggregate contents of approximately 800 kg/m^3, the mix containing SF (SCC-A) presents a 20% higher compressive strength than the mix without fillers (SCC-B), although in the latter, the amounts of gravel and cement are slightly higher. In both samples, water-cement ratios are practically identical (0.438 vs. 0.442). This differentiated behaviour may be justified by the presence of SF in SCC-A, because the physicochemical characteristics of SF give rise to pozzolanic reactions [26]. In addition, an increase in the difference between the strengths of both mixes can be observed with curing time, being maximum at 91 days (~28%). Similar behaviour is observed in the other dosage line with a low coarse aggregate content of 600 kg/m^3, where the mix without filler (SCC-D) has lower compressive strengths (22.5% at 7 days) at its analogue with the SF (SCC-C). As with the previous dosing series (800 kg/m^3), the fundamental difference between the SCC-C and SCC-

D mixes was the use of SF. Thus, the higher mechanical strengths of the SCC-C may be because of the filler reactions with $Ca(OH)_2$. Moreover, the water-cement ratio is lower in the SCC-C compared to that of SCC-D, leading to greater observed differences in the compressive strengths with curing time (~32% in 91 days) than those between the SCC-A and SCC-B mixes.

Table 4.6
Comparing the experimental results with estimated by EHE-08 and references.

Mixtures	Age (Days)	Experimental			Estimated by EHE-08		Parra[a]	Correlation coefficient		
		f_{cm} (MPa)	f_{ci} (MPa)	$f_{ct,fl}$ (MPa)	f_{ci} (MPa)	$f_{ct,fl}$ (MPa)	$f_{ci(SCC)}$ (MPa)	$f_{ci(EHE)}$	$f_{ct,fl(EHE)}$	$f_{ci\,(SCC)}$
SCC-A	7	41.50	3.67	5.85	3.46	5.51	2.91	1.06	1.06	1.09
	28	47.23	4.30	7.98	3.85	6.45	3.23	1.10	1.19	1.15
	91	52.32	4.36	8.32	4.17	6.54	3.51	1.04	1.21	1.10
SCC-B	7	33.20	3.00	4.40	2.87	4.50	2.41	1.04	1.00	1.04
	28	37.09	3.29	5.95	3.15	4.94	2.65	1.04	1.17	1.05
	91	37.90	3.35	6.15	3.21	5.03	2.70	1.04	1.18	1.06
SCC-C	7	43.82	3.92	6.28	3.62	5.88	3.04	1.08	1.06	1.11
	28	51.17	4.46	8.24	4.10	6.69	3.45	1.08	1.19	1.13
	91	56.79	4.52	8.66	4.45	6.78	3.74	1.01	1.22	1.08
SCC-D	7	33.98	3.01	4.71	2.92	4.52	2.46	1.03	1.04	1.02
	28	37.48	3.36	6.08	3.18	5.04	2.67	1.05	1.17	1.07
	91	38.50	3.40	6.35	3.25	5.10	2.73	1.04	1.20	1.06

[a] (Eq. 9)

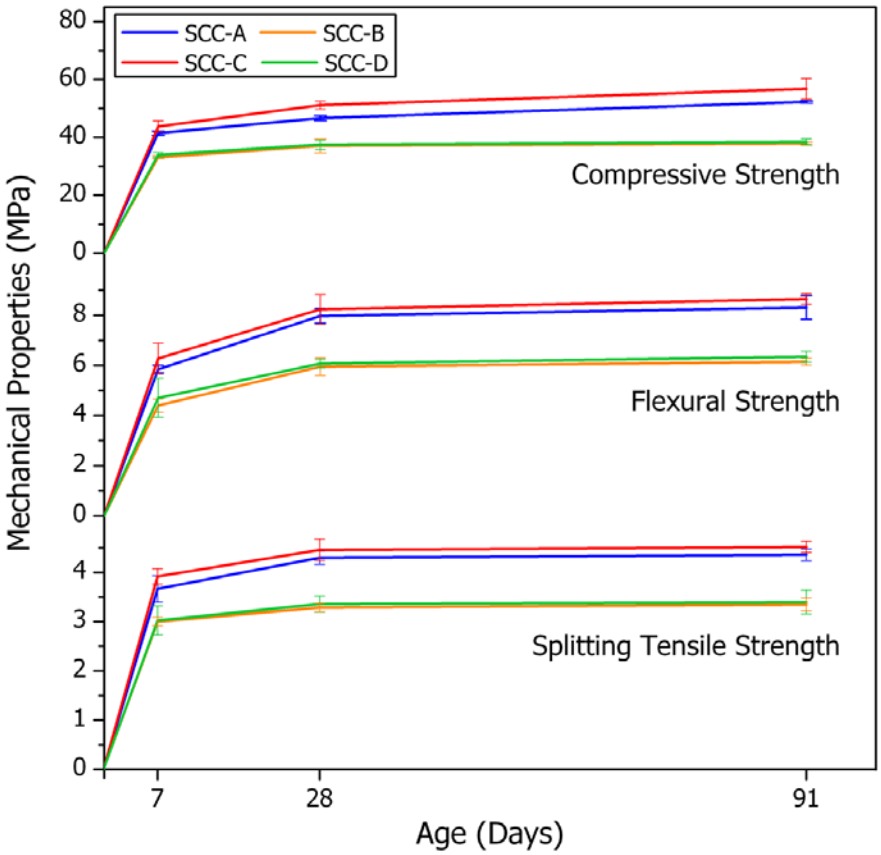

Figure 4.9: Mechanical properties of hardened SCCs.

Finally, if the behaviour of the mixes without fillers (SCC-B and SCC-D) is analysed, it can be observed that the compressive strength in the mix with less coarse aggregate content is slightly higher. This agrees with the lower compactness of the SCC-B dosage as evidenced by the results of the study on bulk density (Figure 4.7). In both mixes, water-cement ratios are practically identical (0.442 vs. 0.441).

The behaviour observed in both series (800 kg/m^3 and 600 kg/m^3) corresponds with the work done by Moini et al. [50], whose experimental results showed that mixes with higher contents in fine aggregates had higher compressive strengths than concretes with low sand contents. Furthermore, Steopoe [51] analysed the influence of aggregates on the strength of concrete and noted that concrete resistance can be reduced because of structural defects caused by coarse aggregates.

On the other hand, the analysis of the porous structure of the mixes (Figure 4.8) also conforms with compressive strengths because mixes with lower porosities (dosages with fillers) have greater strengths (SCC-C and SCC-A).

The range of compressive strengths obtained in the mixes conforms with other works, such as that carried out by Hoo et al. [52], where obtained compressive strengths are of the same order as SCC-A. Quarry dust of granitic nature and with similar geometric characteristics were used in the mixes. Furthermore, the strength obtained by Valdez et al. [40] of 50 MPa at 28 days, conforms with that obtained for SCC-C mix. On the other hand, Silva et al. [41] commented strengths of approximately 40 MPa at 28 days in mixes with high contents in coarse aggregates and without fillers, agreeing with the results for SCC-B. Alyamac and Ince [7] obtained strengths higher than 40 MPa at 28 and 91 days in mixes containing low coarse aggregate contents and without fillers, but with amounts of cement higher than that used in the SCC-D mix in this article.

The results presented in this paper pertaining to SCCs without SF and with varying coarse aggregate contents, showed that it is possible to obtain compressive strengths greater than the minimum levels stipulated by the Spanish Structural Concrete Code [31] for a HAC-30. On the other hand, it is possible to obtain resistances of approximately 50 MPa at 28 days for mixes that incorporate SF even with low coarse aggregate contents (Table 4.6).

4.3.3.2 Splitting tensile strength

Figure 4.9 shows the results of the splitting tensile strength test obtained from the four mixes for the three test ages (7, 28, and 91 days). The value of this parameter is related to compressive strength, although it also depends on other factors such as paste volume and fines. Thus, splitting tensile strength is significantly influenced by dosage.

The values of the splitting tensile strength obtained (Table 4.6 and Figure 4.9) in the three test ages of 7, 28, and 91 days, respectively, are as follows: 3.67, 4.30, and 4.36 MPa, respectively, in the SCC-A mix; 3, 3.29, and 3.35 MPa, respectively, in the

SCC-B mix; 3.92, 4.46, and 4.52 MPa, respectively, in the SCC-C; finally for the SCC-D mix, 3.01, 3.36, and 3.40 MPa, respectively.

The evolution of the splitting tensile strength has a tendency similar to that observed in compressive strength, reaching maximum values in the SCC-C mix. The SCC-A shows values of the same order as the previous mix, although slightly lower—approximately 6% at 7 days and 4% for the rest of the curing ages. This difference may be because of the lower water-cement ratio of the mix and less amount of coarse aggregates (SSC-C). For the mixes without SF (SCC-B and SCC-D), the splitting tensile strength has similar values between them, although approximately 25% lower than mixes with SF (SCC-A and SCC-C). This may be justified by reactions of pozzolanic nature because of the presence of SF in a way similar to that mentioned above in the section on compressive strength.

The splitting tensile strengths obtained at different dosages conform with results presented by Domone [53]. The results obtained in the SCC-B and SCC-D mixes are of the same order as the values reported by Alyamac and Ince [7] because the splitting tensile strengths of the dosages without fillers were in the range of 2.5–4.8 MPa. On the other hand, the dosages with high coarse aggregate contents and with filler agree with the values obtained by Zhu and Gibbs [13] at 28 days (3.3–6 MPa), which depended on the type of filler and water-cement ratio.

Splitting tensile strength can be defined as a function of the compressive strength. Figure 4.10 shows the splitting tensile strengths of all mixes and for all ages with respect to compressive strength. All values are within the limits estimated by the CEB-FIB Code (Comité Euro-Internacional du Béton (International Federation for Structural Concrete)). The correlation between the two parameters is represented and is expressed mathematically by Eq. 4.6 with R^2 equal to 0.98.

$$f_{ci} = 0.072 \cdot f_c + 0.64 \qquad (4.6)$$

where f_{ci} is the splitting tensile strength and f_c is the compressive strength.

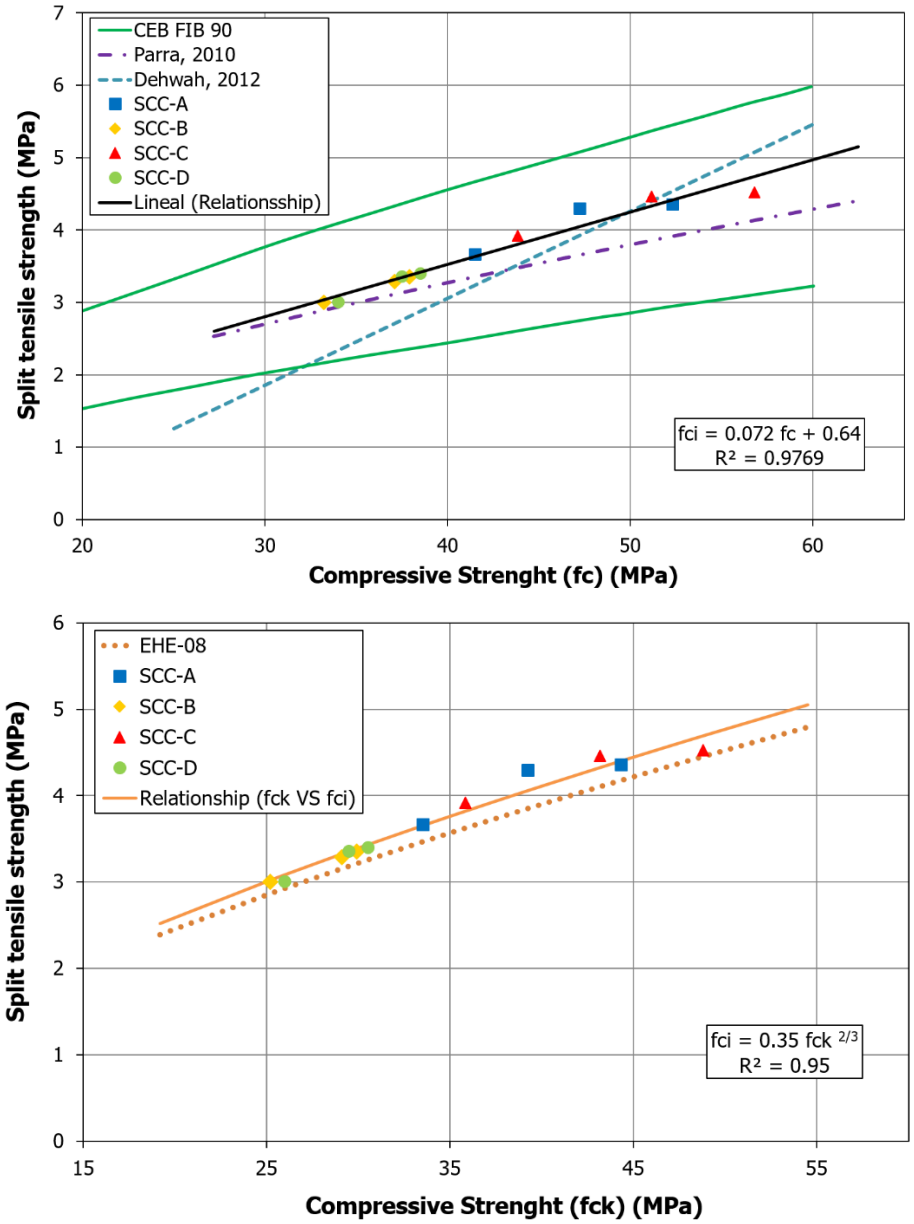

Figure 4.10: Compressive strength (f_c) versus splitting tensile strength (top) and compressive strength (f_{ck}) versus splitting tensile strength (bottom).

The tensile strength, f_{ct}, can be found from the characteristic compressive strength, f_{ck} (Eq. 4.7), according to EHE-08 [31]:

$$f_{ct} = 0.3 f_{ck}^{2/3} \qquad (4.7)$$

The splitting tensile strength, f_{ci}, can be calculated from the tensile strength (Eq. 4.8).

$$f_{ci\ (EHE\text{-}08)} = f_{ct}\ /0.9 \qquad (4.8)$$

Parra et al. [49] proposed a modification of Eq. 4.8, so that it could be applied to the SCC because the splitting tensile strength in SCC is lower than in OC.

$$f_{ci\ (SCC)} = 0.28 f_{ck}^{2/3} \qquad (4.9)$$

The correlation found in this paper (Figure 4.10 and Eq. 4.6) is quite close to the correlation values proposed by EHE-08 and Parra et al. To the contrary, the values differ quite a bit from the correlation proposed by Dehwah [54].

Table 4.6 lists the experimental and estimated f_{ci} values according to EHE-08 (Eq. 4.8) and the expression proposed by Parra et al. (Eq. 4.9). The calculated values are slightly lower than those obtained experimentally. Also included are the correlation coefficients between the experimental values and those estimated by the two equations above. The average of the correlation coefficients for EHE-08 is 1.06, equivalent to that of the equation that correlates f_{ci} with f_{ck} in the following.

$$f_{ci} = 1.06\ f_{ci\ (EHE\text{-}08)} = 0.35\ f_{ck}^{2/3} \qquad (4.10)$$

The correlation coefficient, with the modification proposed by Parra et al. (Eq. 4.9), presents a value of 1.1. Therefore, for dosages of this work, the use of equation Eq. 4.10 would work with a margin of safety higher than those provided by the expression of EHE-08 (Eq. 4.8).

4.3.3.3 Flexural strength

The results obtained in the flexural strength test at 7, 28, and 91 days (Table 4.6), respectively, are as follows: 5.85, 7.89, and 8.32 MPa, respectively, for the SCC-A mix; 4.4, 5.95, and 6.15 MPa, respectively, for the SCC-B mix; 6.28, 8.24, and 8.66 MPa, respectively, for the SCC-C mix; 4.71, 6.08, and 6.35 MPa, respectively, for the

SCC-D mix. As can be observed, the SCC-C mix has the highest flexural strength for all test ages (Figure 4.9).

These values conform with the results of the compressive and splitting tensile strengths tests, where the SCC-C mix had the best mechanical performance—in the same way that the differentiated behaviour was observed between the mixes with and without SF. Among mixes with fillers (SCC-A and SCC-C), the difference at a short age of 7 days is approximately 6% and reducing to approximately 4% with curing age (without variation in the differences between the results at 28 and 91 days). Regarding mixes without fillers in their dosages (SCC-B and SCC-D) with respect to its analogues with fillers (SCC-A and SCC-C, respectively), the difference is approximately of 25%. This difference undergoes a slight increase with curing age, leading to the conclusion that this behaviour can be justified by the pozzolanic reactions of SF during the hardening process.

The results obtained in the present work conform with those of other researchers, such as Dehwah [54], who obtained values of flexural strength in the order of 7 MPa in 28 days in mixes with greater amounts of mineral additions (quarry dust powder and silica fume). Fathi et al. [55] conducted a study of the influence of mineral additives (fly ash, silica fume, and incinerated rice husk ash) on the mechanical strength of SCC made with 750 kg/m^3 of coarse aggregates, obtaining values of 6.8–8.4 MPa. Jamaluddin et al. [11] performed a flexural strength study in SCC with ~700 kg/m^3 of coarse aggregates, where the fine aggregate was replaced by coal bottom ash and without mineral additions, subsequently obtaining values of flexural strength of ~6 MPa at 28 days.

Figure 4.11 shows the relationship between flexural and the compressive strengths expressed by Eq. 4.11, with $R^2 = 0.90$.

$$f_{fl} = 0.174 \cdot f_c - 0.81 \qquad (4.11)$$

where f_{fl} is the flexural strength and f_c is the compressive strength. The relationship proposed here differs appreciably from that of Dehwah [54].

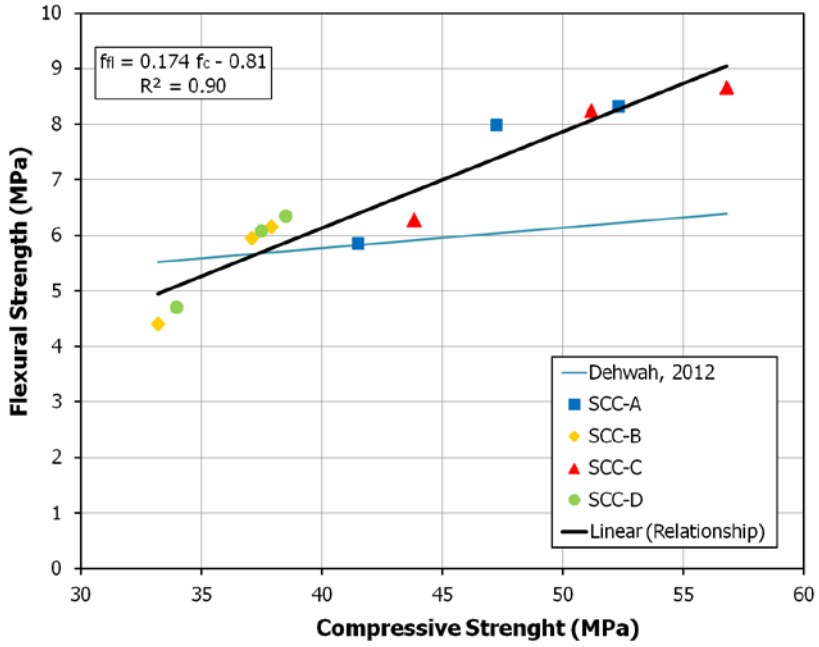

Figure 4.11: Compressive strength versus flexural strength.

The EHE-08 [31] code establishes that the values of flexural strength, $f_{ct,fl}$, can be calculated from those of splitting tensile strength using Eq. 4.12:

$$f_{ct,fl} = f_{ct} \frac{1+1.5\left(\frac{h}{100}\right)^{0.7}}{1.5\left(\frac{h}{100}\right)^{0.7}} \qquad (4.12)$$

where f_{ct} is the tensile strength obtained from the resistance to fracture from splitting tensile strength (Eq. 4.7) and h is the height of the element in mm.

The results obtained using Eq. 4.12 are listed in Table 4.6, where the results are lower than experimental values. Consequently, the correlation coefficient values are higher than 1, which means that the experimental results support the validity of the application of EHE-08 to SCC. It can therefore be concluded that if it works with the model proposed by the EHE-08, the calculation of flexural strength from the characteristic resistance values proceeds with a greater margin of safety.

4.3.4 Water absorption properties of hardened SCCs

4.3.4.1 Water absorption by immersion

Porosity significantly influences the absorption capacity of concrete. Figure 4.12 shows, on the one hand, the loss of mass suffered by the mixes during the drying process, and on the other hand, the absorption capacity during immersion in water with respect to time.

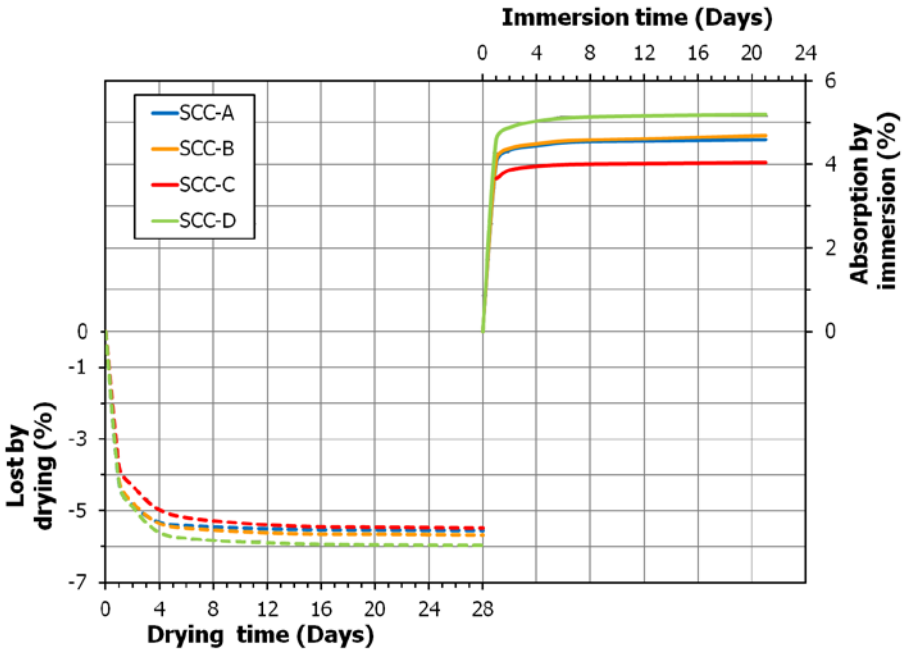

Figure 4.12: Evolution of the mass loss by drying (100 ºC) and absorption by immersion.

The amounts of water absorption by immersion at 24 h and 48 h, respectively, are as follows: 4.05 and 4.34%, respectively, for SCC-A; 4.13 and 4.38%, respectively, for SCC-B; 3.67 and 3.87%, respectively, for SCC-C; 4.61 and 4.88 %, respectively, for SCC-D (Table 4.5).

The values of loss of mass reached until constant weight were −5.55% for SCC-A, −5.67% for SCC-B, −5.49% for SCC-C, and −5.96% for SCC-D. The maximum water absorption values recorded were 4.59% for SCC-A, 4.69% for SCC-B, 4.04% for SCC-C, and 5.19% for SCC-D. It is observed that the samples do not absorb the entire

mass loss during drying. This amount of water that is not recovered depends on the porous structure of the material. For all mixes, the percentages were 17.41% for SCC-A, 17.18% for SCC-B, 26.39% for SCC-C, and 12.86% for SCC-D.

The reason for this behaviour is the incomplete rehydration of the medium capillary pores and small gel pores [43], which are inaccessible to water in the process of absorption under atmospheric pressure. The results conform with the porosity of the mixes observed in the mercury intrusion porosimetry test, as well as the porous structure. As mentioned above, this is explained by the higher percentage of medium capillarity pores and small gel pores in the SCC-A and SCC-C mixes, whereas in the SCC-D and SCC-B mixes there is a greater number of large capillarity pores including those with sizes larger than 10 μm. Hence, mixes that incorporate SF present better behaviour than mixes without SF in terms of water absorption by immersion because of the finer porous structure of the former.

Such behaviour was similar to that observed by Jalal et al. [56] who obtained an improvement with respect to resistance to absorption in SCCs with microsilica. The values presented in this paper agree with those obtained by Schutter et al. [57], who observed that mixes with lower amounts of coarse aggregates had lower absorption percentages.

4.3.4.2 Water absorption by capillarity

The interconnection of the pores in the concrete structure critically influences exchange of moisture with the environment and transport mechanisms as well. The absorption of an aqueous solution by capillarity has two stages—the first corresponds to the filling of capillary pores and the second relates to the saturation of the material because of the diffusion and dissolution of air present within the porous structure.

Figure 4.13 shows the capillary absorption values obtained in samples SCC-A, SCC-B, SCC-C and SCC-D. The results have been adjusted according to the model proposed by Hall [58], defining capillary absorption (W) by Eq. 4.13:

$$W = A + S\sqrt{t} - C\,t \quad (4.13)$$

where t is the time, S is the sorptivity or capillary absorption rate, and A and C are constants. Equations 4.14–4.17 show good fit because R^2 is greater than 0.99 in all cases for test times of up to 15 days.

$$W = -0.000026\,t^2 + 0.0102\sqrt{t} + 0.0461 \quad \text{(SCC-A)} \quad (4.14)$$

$$W = -0.000030\,t^2 + 0.0121\sqrt{t} + 0.0604 \quad \text{(SCC-B)} \quad (4.15)$$

$$W = -0.000022\,t^2 + 0.0086\sqrt{t} + 0.0384 \quad \text{(SCC-C)} \quad (4.16)$$

$$W = -0.000030\,t^2 + 0.0115\sqrt{t} + 0.0571 \quad \text{(SCC-D)} \quad (4.17)$$

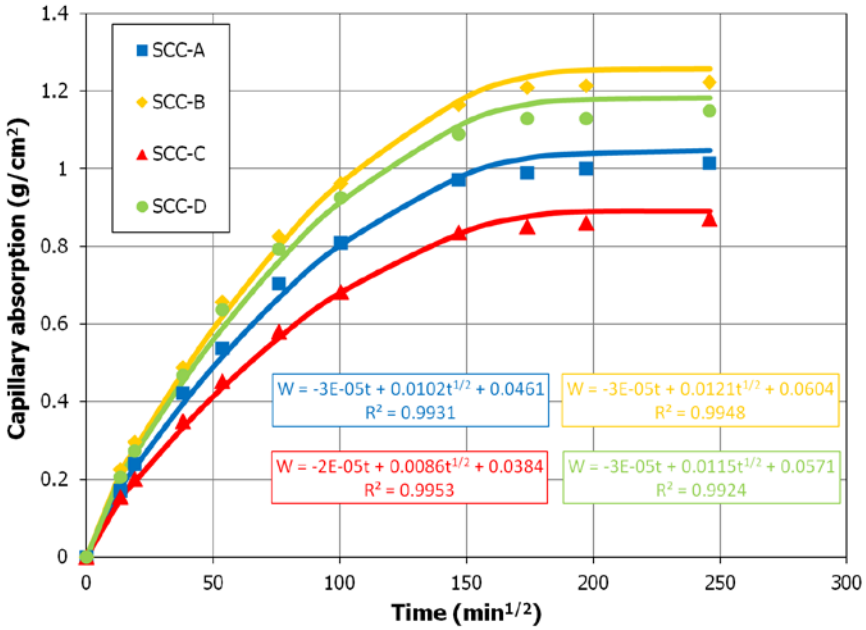

Figure 4.13: Capillary water absorption of the mixes.

The absorption values in the capillarity and sorptivity of both mixes are listed in Table 4.5, in which a differentiated behaviour is observed between the two dosing lines. The mixes with fillers, SCC-C and SCC-A, exhibited the lowest absorption by capillarity and sorptivity, followed by SCC-D and SCC-B (mixes without fillers), respectively. Likewise, mixes having higher contents of coarse aggregates, SCC-A and SCC-B, have higher absorption values than SCC-C and SCC-D mixes (with ~600 kg/m^3 of coarse aggregates), respectively. This difference may be because of the different structural

densities of each dosage (Figure 4.7) that influence the absorption of water by capillarity. As for porosity interconnected and connected to the exterior (effective porosity), the same behaviour as above is observed (Table 4.5).

These results conform with those of Torres et al. [59], who observed a decrease in the absorption by capillarity in mortars with metakaolin with respect to mixes without this mineral addition because of the refinement of the porous structure. This refinement led to greater structural density values in the mixes. Likewise, Jalal et al. [56] observed greater packing and refinement in the porous structure of SCC when incorporating micro-silica, resulting in lower water absorption by capillarity. Valcuende et al. [60] observed that in SCCs with higher volumes of paste and less amounts of coarse aggregates, the cement matrices are denser, has greater tortuosity, and greater distances between aggregates, which translates into greater restriction in water circulation through the capillary pores. Using fly ash or silica fume as mineral addition, Turk et al. [61] obtained values of sorptivity comparable to those observed in this research.

The SCC mixes designed in the present study could be used in aggressive environments with adequate durability. This is because the values of sorptivity and effective porosity are less than the limits of sorptivity (0.039 cm/min$^{1/2}$) and effective porosity (10%) established by Trocónis-Rincon et al. [62] for structures exposed to high environmental aggressiveness.

4.3.5 Durability of hardened SCCs

4.3.5.1 Permeability and penetration of water under pressure

The resistance to attacks of aggressive agents in concrete depends on the permeability of the material. Concrete presents high durability if the penetration of any gaseous or aqueous solution is minimised. Thus, the penetration of water under pressure provides an analysis of the ease with which fluid under constant pressure moves through the material matrix.

The maximum penetration values observed in different SCCs are listed in Table 4.5. All mixes can be considered impermeable because they do not exceed 30 mm, which is marked as maximum limit by Neville [63]. As can be seen in the table, mixes with fillers (SCC-A and SCC-C) have lower penetration values than those of mixes without fillers (SCC-B and SCC-D). These results corroborate the observation that SF increases the compactness of the matrix, in part because of pozzolanic reactions [26], making it more difficult for water to penetrate. These conform with the results of mercury intrusion porosimetry and water absorption results (Figures 4.8, 4.12, and 4.13), where the differences between the porous structures of the four mixes were observed. These results also agree with the water-cement ratio. If this ratio is low, then permeability is also low because the cementitious matrix becomes less porous. Additionally, the values of the permeability coefficient [64] are lower than 10^{-14} m/s for all mixtures (Table 4.5), indicating high impermeability of the samples.

The results of the present study conform with those observed by Uysal et al. [65], showing reductions in the depths of penetration of water under pressure in SCC when mineral additives of pozzolanic character (fly ash or granulated blast furnace slag) are incorporated in contrast with mixes that did not use any type of filler. Likewise, Vejmelkavá el al. [66] observed that at 28 days of curing, the penetration depth in SCC with metakaolin as a mineral additive was 40% lower than that of SCC that did not incorporate this filler. This reduction is attributed by the authors to the more even distribution of pores and low quantity of capillary pores. Along the same line, Ahari et al. [67] observed lower depths of penetration using silica fume, metakaolin, fly ash, and blast furnace slag as supplementary cementitious material in contrast with the mix without any mineral addition, thus attributing this effect to the porous structure of the finer matrix. With fillers of non-pozzolanic nature in SCC, Ghafoori et al. [68] observed a considerable reduction in the depths of penetration (more than 30%) when using limestone powder because of the filling effect of the mineral additive on the porous structure of SCC.

4.3.5.2 Chloride ion penetration

The durability of the SCC depends on the depth of penetration of the chloride ion into the material. Hence, this test on chloride ion penetration provides an estimate of the

protection of reinforcements against the attack of aggressive agents. The most important factors to take into account in this attack are the porous structure of the concrete and the concentration of Cl^- in the solution.

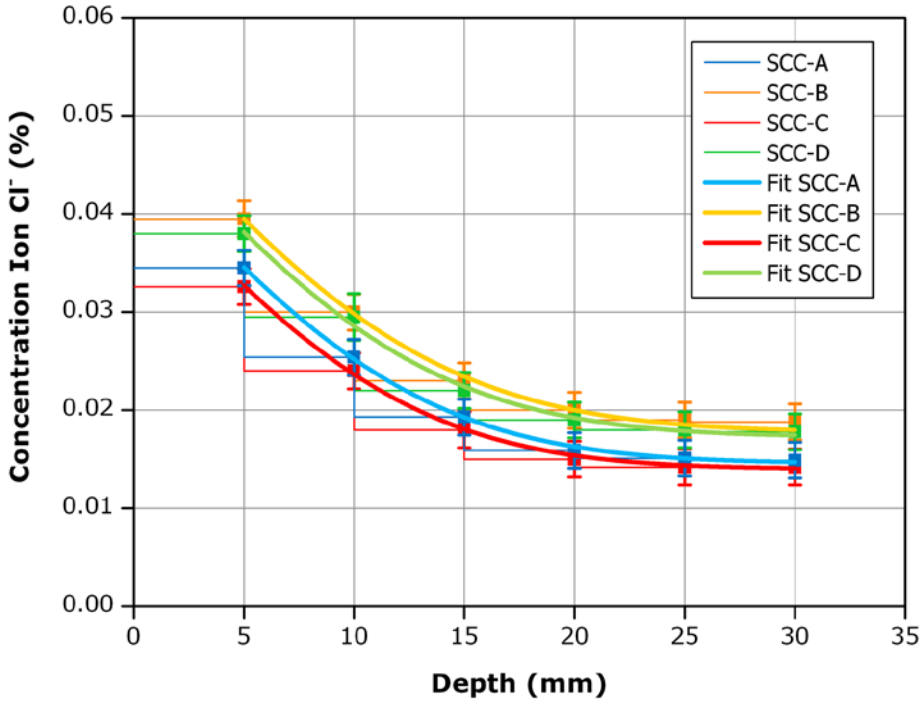

Figure 4.14: Ion Cl^- concentration profile of the mixes.

Figure 4.14 shows the concentration profile of the chloride ion with respect to the depth of penetration in the mixes. A similar evolution was observed in all mixes. The SCC-C mix had the lowest penetration followed by SCC-A, SCC-D, and SCC-B, respectively. These results were adjusted by the least squares to Eq. 4.1 as proposed in ASTM C 1556 [35] and obtaining Eqns. 4.18–4.21, which have R^2 higher than 0.99.

$$C(t,x) = 0.046 - (0.046 - 0.015) \cdot \operatorname{erf}\left(\frac{x}{\sqrt{4 \cdot 6.79 \cdot 10^{-12} \cdot 7.86 \cdot 10^{6}}}\right) \text{ SCC-A} \quad (4.18)$$

$$C(t,x) = 0.051 - (0.051 - 0.019) \cdot \operatorname{erf}\left(\frac{x}{\sqrt{4 \cdot 7.51 \cdot 10^{-12} \cdot 7.86 \cdot 10^{6}}}\right) \text{ SCC-B} \quad (4.19)$$

$$C(t,x) = 0.044 - (0.044 - 0.014) \cdot \operatorname{erf}\left(\frac{x}{\sqrt{4 \cdot 6.38 \cdot 10^{-12} \cdot 7.86 \cdot 10^{6}}}\right) \text{ SCC-C} \quad (4.20)$$

$$C(t,x) = 0.050 - (0.050 - 0.018) \cdot \operatorname{erf}\left(\frac{x}{\sqrt{4 \cdot 7.11 \cdot 10^{-12} \cdot 7.86 \cdot 10^{6}}}\right) \text{ SCC-D} \quad (4.21)$$

The least squares adjustment allowed the calculation of the effective coefficients of the transport of chloride ions of the mixtures (Table 4.5), which were 6.38×10^{-12}, 6.79×10^{-12}, 7.11×10^{-12}, and 7.51×10^{-12} m^2/s for SCC-C, SCC-A, SCC-D, and SCC-B mixes, respectively, after 91 days of exposure. Also, the theoretical surface concentration that conform with the diffusion profiles collected in Figure 4.14 have values of 0.044, 0.046, 0.050, and 0.051% for the SCC-C, SCC-A, SCC-D, and SCC-B, respectively. These agree with the evolution of the pore size distribution, microstructural density, and permeability discussed previously. The presence of fillers and the lower coarse aggregate content provide positive influence on SCC durability in relation to chloride ion penetration.

In addition, it can be observed in Figure 4.14 that the concentration values of the mixes are lower than those of the typical threshold level of chloride concentration (0.05%) beyond which steel corrosion in concrete results according to Glass and Buenfeld [69]. Thus, reinforcements would not be affected by the presence of Cl^- ion. If it is also taken into account that in terms of durability under aggressive environments [31] the minimum cover required by the EHE-08 for each defined SCC type (HA-40/AC/16/ IIIc) [31] is 45 mm, then the safety margin is very high. On the other hand, using a salt fog chamber, Ryan and O'Connor [70] obtained effective transport coefficients of the same order (10^{-12} m^2/s), although lower than those obtained in this paper. The higher coefficients obtained in these mixes may be because of the constant action of Cl^- ion in the immersion process with respect to chloride interaction in wetting-drying cycles used by these authors.

4.3.5.3 Sulphate ion penetration

Expansive compounds (calcium sulphates and hydrated sulfoaluminates) formed from the reaction of the sulphate ion with the hydrated products generated during the concrete hardening process can cause disintegration of cementitious material. Humidity, microstructure, cement type, dosage, speed of ion penetration, as well as chemical nature, are the most important factors in this attack.

Figure 4.15 shows the different behaviours of mixes with respect to the penetration of SO_3. The SCC-C mix had the lowest penetration followed by SCC-A, SCC-D and

SCC-B, respectively. The experimental penetration profiles were adjusted by least squares to the solution equation of the Law of Fick (Eq. 4.1), obtaining R^2 greater than 0.99 in all the adjustments (Eqs. 4.22–4.25).

$$C(t,x) = 0.85 - (0.85 - 0.50) \cdot \operatorname{erf}\left(\frac{x}{\sqrt{4 \cdot 9.06 \cdot 10^{-12} \cdot 7.86 \cdot 10^{6}}}\right) \quad \text{SCC-A} \quad (4.22)$$

$$C(t,x) = 0.90 - (0.90 - 0.54) \cdot \operatorname{erf}\left(\frac{x}{\sqrt{4 \cdot 9.85 \cdot 10^{-12} \cdot 7.86 \cdot 10^{6}}}\right) \quad \text{SCC-B} \quad (4.23)$$

$$C(t,x) = 0.79 - (0.80 - 0.49) \cdot \operatorname{erf}\left(\frac{x}{\sqrt{4 \cdot 8.50 \cdot 10^{-12} \cdot 7.86 \cdot 10^{6}}}\right) \quad \text{SCC-C} \quad (4.24)$$

$$C(t,x) = 0.89 - (0.89 - 0.52) \cdot \operatorname{erf}\left(\frac{x}{\sqrt{4 \cdot 9.84 \cdot 10^{-12} \cdot 7.86 \cdot 10^{6}}}\right) \quad \text{SCC-D} \quad (4.25)$$

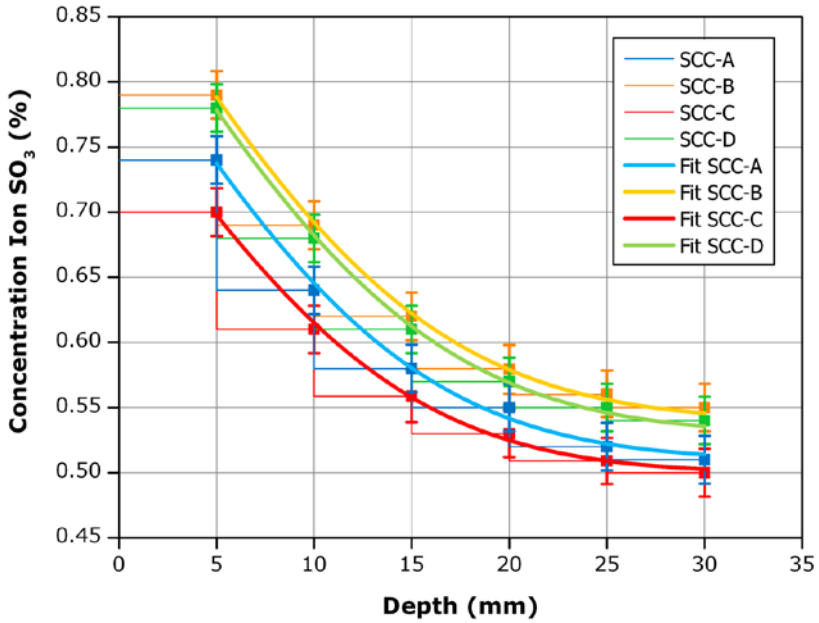

Figure 4.15: Ion SO_3 concentration profile of the mixes.

The effective transport diffusion coefficients of SO_3 were 8.50×10^{-12} m^2/s for the SCC-C mix, 9.06×10^{-12} m^2/s for the SCC-A mix, 9.84×10^{-12} m^2/s for the SCC-D mix, and 9.85×10^{-12} m^2/s for the SCC-B mix. These conform with the low permeability of mixes with fillers (SCC-C and SCC-A) with respect to mixes without fillers (SCC-B and SCC-D), which are related to the smaller pore sizes of the former and in turn resulting to less diffusion of the SO_3 ion. The lower depths of penetration of SO_3 in samples SCC-C and SCC-A are related to the higher microstructural densities of these samples.

The surface concentrations obtained from Fick's second law were 0.79, 0.85, 0.89, and 0.90% for SCC-C, SCC-A, SCC-D, and SCC-B respectively.

These results agree with those obtained by Schutter and Audenaert [71] who concluded that mixes incorporating silica fume or fly ash as filler would result to denser porous structures with smaller capillaries that minimise SO_3 ion penetration.

4.3.5.4 Drying shrinkage

The dimensional variation of concrete due to factors such as temperature, humidity, weather, and physical-chemical characteristics of materials have significant impact on the durability of the material. The drying shrinkage test enables the determination of the resulting volume reduction because of the loss of water in the concrete.

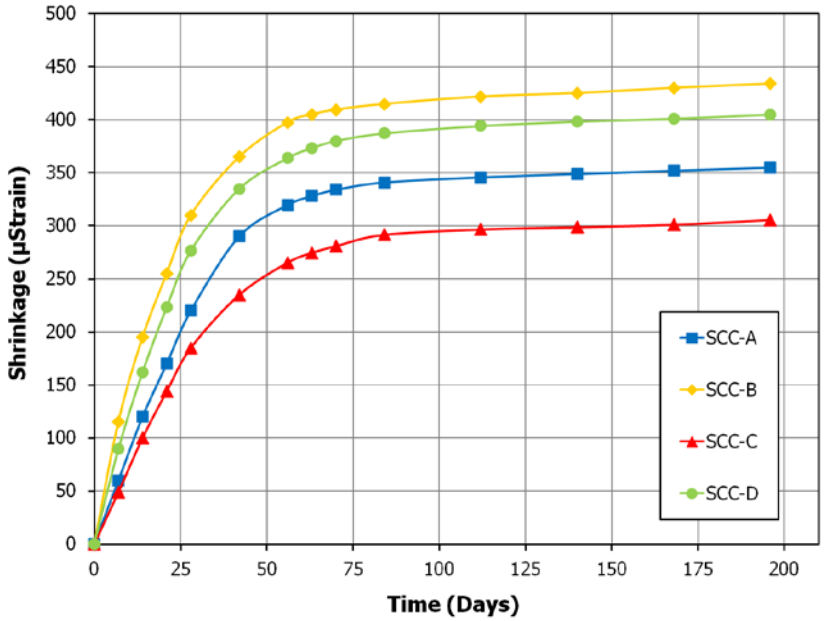

Figure 4.16: Drying shrinkage of the mixes.

For the four mixes, the recorded drying shrinkage results with respect to the test time of 196 days, are shown in Figure 4.16. It is observed that deformation is stabilised at approximately 100 days under curing conditions defined in the materials and methods section. The SCC-C mix has the lowest amount of shrinkage followed by the SCC-A,

SCC-D, and SCC-B mixes, respectively. Ninety percent of shrinkage was achieved in 56 days for SCC-A, SCC-B and SCC-D mixes, and 63 days for the SCC-C mix.

These results conform with the water-cement ratio and permeability of the mixes because these parameters play important roles in drying shrinkage. The SCC-C mix presents the lowest water-cement ratio and permeability (Tables 4.3 and 4.5). This means that almost all the water is used for the cement hydration process and the loss of water through exchange with the environment is low and slow, resulting in reduced shrinkage (Figure 4.16). Along this line, the higher values of water-cement ratio and permeability of the SCC-B and SCC-D mixes (Tables 4.3 and 4.5) cause increase in shrinkage (Figure 4.16).

Mixes with fillers (SCC-A and SCC-C) have lower shrinkage values than mixes without fillers (SCC-B and SCC-D). This may be related to the finer porous structure of mixes with fillers (SCC-A and SCC-C) (Figure 4.8), because most pores are located in the area of medium capillary pores, which would make it difficult for water to move through the narrow and fine pores to the outside. The lowest shrinkage of the SCC-C mix (600 kg/m^3 of coarse aggregates) with respect to SCC-A (800 kg/m^3) and SCC-D mix (600 kg/m^3) with respect to SCC-B (800 kg/m^3) may be related to the larger pores in the large capillary zone—shown in the pore size distribution—which has greater accessibility to moisture exchange. In addition, this differential behaviour conforms with the different densities of the SCC (Figure 4.7), because denser mixes offer greater resistance to shrinkage, as evidenced by the SCC-C mix presenting lower shrinkage and maximum density.

Therefore, it can be concluded that the presence of fillers has a more significant influence on shrinkage rather than on the variation of coarse aggregate content in the dosage.

The results of this paper agree with those obtained by Alrifai et al. [72] who observed that drying shrinkage was more significant when water-cement ratio and porosity values were higher. This is because when the porous structure is finer, the moisture exchange with the outside environment decreases, which translates into less drying shrinkage. Along this line, Aslani and Nejadi [73] observed an increase in drying

shrinkage when the water-cement ratio of SCC increased. On the other hand, Güneyisi et al. [10] and Ranjbar et al. [74] observed reductions in drying shrinkage when the mineral additions (fly ash, ground granulated blast furnace slag or metakaolin) or palm oil fuel ash were respectively incorporated in mixes.

4.4 Conclusions

A comparative study of four types of SCCs was carried out, in which the effects of the amounts of coarse and fine aggregates, and fillers in fresh-state (self-compacting) and hardened-state (porous structure, mechanical behaviour and durability) were analysed.

The mixes comply with the self-compacting requirements of EHE-08, showing that it is possible to obtain SCC dosages where parameters such as the amounts of coarse aggregate, paste, and water-fines ratio are not within the values proposed by EFNARC. The self-compactability tests show high reproducibility.

Slight differences are presented by the densities of the mixes. The factors that have more significant influences on the density of the mixes are the presence of fillers and water-cement ratio, because the mixes with fillers and smaller water-cement ratios (SCC-C and SCC-A) exhibited higher densities.

These results conform with the lower porosity observed in the pore size distribution of mixes incorporating fillers (SCC-A and SCC-C). The volume of mercury intrusion in pores having diameters greater than 70 μm and 50.0 nm–10.0 μm (large capillary pores) is higher in SCC-B and SCC-D. By contrast, in the ranges of 10–50 nm (medium capillary pores) and 2.5–10.0 nm (small gel pores), the volume of mercury intrusion is higher in SCC-A and SCC-C samples. All these reveal that the structures of mixes with fillers are more fine and porous. On the other hand, the greater compactness of the mixes SCC-C and SCC-D relative to SCC-A and SCC-B agrees with the greater mercury intrusion volume in the zones between medium and large capillary pores.

The mechanical behaviour of SCCs without SF and with different amounts of coarse aggregates (SCC-B and SCC-D), shows that it is possible to obtain compressive

strengths above the minimum levels stipulated by the Spanish Code of Structural Concrete for a HAC-30. Furthermore, it is possible to obtain strengths of approximately 50 MPa for SCC mixes in 28 days by incorporating SF (SCC-A and SCC-C) even with low coarse aggregate contents.

The values of splitting tensile and flexural strengths calculated by applying EHE-08 (calculated from the compressive strength) are lower than the values obtained experimentally. This means that the experimental results are congruent with the validity of EHE- 08—originally proposed for OC—when applied to SCC.

The mixes incorporating SF (SCC-A and SCC-C) presented better performance in absorption of water by immersion than mixes that do not (SCC-B and SCC-D). For the absorption of water by capillarity, mixes with fillers presented lower absorption by capillarity and sorptivity than mixes without fillers. Moreover, mixes with higher contents of coarse aggregates, SCC-A and SCC-B, presented higher absorption values than SCC-C and SCC-D mixes, respectively. All mixes had values lower than established limits in terms of effective porosity and sorptivity. Hence, these mixes could be used in aggressive environments along with adequate durability.

The results of penetration of water under pressure lead to the conclusion that all mixes have high compactness and are impermeable, because there were no penetrations higher than 30 mm, which is marked in literature as the maximum penetration for cementitious material to be considered impermeable.

As to the penetration of Cl^- and SO_3 ions, the SCC-C mix showed lower attacks, followed by the SCC-A, SCC-D and SCC-B mixes, respectively. The higher microstructural densities of the mixes with fillers led to lower penetration depths in those materials. After the exposure to aggressive environments, not one of the mixes showed signs of wearing out or deterioration.

Under the curing conditions used in this research, the drying shrinkage of the mixes are stabilised at an age of approximately 100 days. The SCC-C mix presented the lowest shrinkage, followed by the SCC-A, SCC-D, and SCC-B mixes, respectively. The

presence of fillers had a more significant influence on shrinkage than the amount of coarse aggregates.

It can be concluded that it is possible to obtain high performance SCC in relation to mechanical and durability properties, by reducing the content of coarse aggregates, and incorporating SF in the dosage. Moreover, for applications where high mechanical requirements are not necessary, it is possible to obtain SCCs with high performances against attacks of aggressive agents such Cl^- and SO_3 without using SF.

4.5 Acknowledgements

This work was partly supported by the Andalusian Regional Government (Research Groups FQM-391 and TEP-227). A. Romero Esquinas also acknowledges funding from MECD-Spain (http://www.mecd.gob.es/educacion-mecd/) FPU-13/04030. The authors wish to thank the Research Plan of the University of Cordoba (2016), the staff at the Electron Microscopy and Elemental Analysis units of the Central Research Support Service (SCAI) of University of Cordoba for their technical assistance, the Fine Chemistry Institute of the University of Córdoba for their technical support, BASF Chemical Company and GRACE for supplying the admixtures, and Portland Valderrivas (Alcalá de Guadaira, Seville) for the supplied cement. The authors also wish to thank the National Radioactive Waste Company (ENRESA) for Contract of Research 079000146.

4.6 References

[1] H. Okamura, Self-compacting high-performance concrete, Concrete international 19(7) (1997) 50-54.

[2] H. Okamura, K. Ozawa, Self-compactable high-performance concrete in Japan, Special publication 159 (1996) 31-44.

[3] Asociación Cientifico Técnica del Hormigón Estructural (ACHE). M-13: Hormigón Autocompactante. Diseño y Aplicación; 2008.

[4] European Federation of National Associations Representing producers and applicators of specialist building products for Concrete (EFNARC). The European

guidelines for self-compacting concrete specification. Production and Use. Hampshire, UK; (2005), www.efnarc.org.

[5] European Federation of National Associations Representing producers and applicators of specialist building products for Concrete (EFNARC). Specification and guidelines for self-compacting concrete, Hampshire, UK; 2002, www.efnarc.org.

[6] N. Su, K.-C. Hsu, H.-W. Chai, A simple mix design method for self-compacting concrete, Cement and concrete research 31(12) (2001) 1799-1807.

[7] K.E. Alyamaç, R. Ince, A preliminary concrete mix design for SCC with marble powders, Construction and Building Materials 23(3) (2009) 1201-1210.

[8] P. Dinakar, M.K. Reddy, M. Sharma, Behaviour of self compacting concrete using Portland pozzolana cement with different levels of fly ash, Materials & Design 46 (2013) 609-616.

[9] B. Felekoglu, Utilisation of high volumes of limestone quarry wastes in concrete industry (self-compacting concrete case), Resources, Conservation and Recycling 51(4) (2007) 770-791.

[10] E. Güneyisi, M. Gesoğlu, E. Özbay, Strength and drying shrinkage properties of self-compacting concretes incorporating multi-system blended mineral admixtures, Construction and Building Materials 24(10) (2010) 1878-1887.

[11] N. Jamaluddin, A.F. Hamzah, M.H.W. Ibrahim, R.P. Jaya, M.F. Arshad, N.E.Z. Abidin, N.H. Dahalan, Fresh properties and flexural strength of self-compacting concrete integrating coal bottom ash, MATEC Web of Conferences, EDP Sciences, 2016.

[12] L. Pereira-de-oliveira, J. Castro Gomes, C. Gonilho Pereira, Influence of mineral additions in the capillary absorption of self-compacting concrete, in 8th International Conference Modern Building Materials, Structures and Techniques, Vilnius, Lithuania 2004. 73–74.

[13] W. Zhu, J.C. Gibbs, Use of different limestone and chalk powders in self-compacting concrete, Cement and Concrete Research 35(8) (2005) 1457-1462.

[14] W. Fung, A. Kwan, Effect of particle interlock on flow of aggregate through opening, Powder Technology 253 (2014) 198-206.

[15] A. Kwan, S. Ling, Lowering paste volume of SCC through aggregate proportioning to reduce carbon footprint, Construction and Building Materials 93 (2015) 584-594.

[16] A.C. Santos, J.A. Ortiz-Lozano, N. Villegas, A. Aguado, Experimental study about the effects of granular skeleton distribution on the mechanical properties of self-compacting concrete (SCC), Construction and Building Materials 78 (2015) 40-49.

[17] I. Nikbin, M. Beygi, M. Kazemi, J.V. Amiri, E. Rahmani, S. Rabbanifar, M. Eslami, A comprehensive investigation into the effect of aging and coarse aggregate size and volume on mechanical properties of self-compacting concrete, Materials & Design 59 (2014) 199-210.

[18] J.G. Jawahar, C. Sashidhar, I.R. Reddy, J.A. Peter, Effect of coarse aggregate blending on short-term mechanical properties of self compacting concrete, Materials & Design 43 (2013) 185-194.

[19] M. Collepardi, Self-compacting concrete: What is new, Proceedings of the 7th CANMET/ACI Conference on superplasticizer and other chemical admixtures in concrete, 2003, pp. 1-16.

[20] F. Cartuxo, J. de Brito, L. Evangelista, J.R. Jiménez, E.F. Ledesma, Increased durability of concrete made with fine recycled concrete aggregates using superplasticizers, Materials 9(2) (2016) 98.

[21] M.L. Hart, A.C. Londoño, A.A. Silvius, Semipermeability of concrete for hazardous waste containment, Environmental Geotechnics 3(6) (2016) 408-419.

[22] E. Ledesma, J. Jiménez, J. Ayuso, J. Fernández, J. de Brito, Experimental study of the mechanical stabilization of electric arc furnace dust using fluid cement mortars, Journal of hazardous materials 326 (2017) 26-35.

[23] A. Taglioni, A. Castellani, P. De Stefanis, Hazardous-waste containers in cementitious materials: leakage test on small-scale specimens and on full-scale prototypes, WIT Transactions on Ecology and the Environment 109 (2008) 321-329.

[24] F.-J. Ulm, F.H. Heukamp, J.T. Germaine, Residual design strength of cement-based materials for nuclear waste storage systems, Nuclear Engineering and Design 211(1) (2002) 51-60.

[25] Contract of Research 079000146, Development of self-compacting concretes for use in the facilities of El Cabril, Empresa Nacional de Residuos Radiactivos (ENRESA). 2012-2014

[26] A.R. Esquinas, C. Ramos, J. Jiménez, J. Fernández, J. de Brito, Mechanical behaviour of self-compacting concrete made with recovery filler from hot-mix asphalt plants, Construction and Building Materials 131 (2017) 114-128.

[27] Asociación Española de Normalización y Certificación, AENOR, Madrid, Spain, (2017).

[28] D.P. Bentz, C.J. Haecker, An argument for using coarse cements in high-performance concretes, Cement and Concrete Research 29(4) (1999) 615-618.

[29] J.M. Pommersheim, Effect of particle size distribution on hydration kinetics, MRS Proceedings, Cambridge Univ Press, 1986, p. 301.

[30] S. Tsivilis, S. Tsimas, A. Benetatou, E. Haniotakis, Study on the contribution of the fineness on cement strength, Zem-Kalk-Gips 43 (1) (1990) 26–29.

[31] EHE-08. Spanish Structural Concrete Code EHE-08 [Instrucción de Hormigón Estructural EHE-08]. R.D. 1247/2008, Spain (2008).

[32] http://www.master-builders-solutions-basf.es.

[33] https://gcpat.com/construction/es-es.

[34] S. Brunauer, P.H. Emmett, E. Teller, Adsorption of gases in multimolecular layers, Journal of the American chemical society 60(2) (1938) 309-319.

[35] American Society of Testing Materials, ASTM International, West Conshohocken, USA, (2017).

[36] N. Nagamoto, K. Ozawa, Mixture properties of self-compacting, high-performance concrete, Special Publication 172 (1999) 623-636.

[37] H. Okamura, M. Ouchi, Self-compacting concrete, Journal of advanced concrete technology 1(1) (2003) 5-15.

[38] M. Emborg, Rheology Tests for Self-Compacting Concrete-How Useful are they for the Design of Concrete Mix for Full Scale Production, Self-Compacting Concrete: Proceedings of the First International RILEM Symposium held in Stockholm, Sweden 13-14 September 1999, 1999, pp. 95-105.

[39] I.B. Topcu, T. Bilir, T. Uygunoğlu, Effect of waste marble dust content as filler on properties of self-compacting concrete, Construction and Building Materials 23(5) (2009) 1947-1953.

[40] P. Valdez, B. Barragán, I. Girbes, N. Shuttleworth, A. Cockburn, Use of waste from the marble industry as filler for the production of self-compacting concretes, Materiales de Construcción 61(301) (2011) 61-76.

[41] P.M. Silva, J. de Brito, J.M. Costa, Viability of two new mix design methodologies for SCC, ACI Mater. J. 108 (6) (2011) 579–588. ISSN: 0889-325X.

[42] D. Silva, V. John, J. Ribeiro, H. Roman, Pore size distribution of hydrated cement pastes modified with polymers, Cement and Concrete Research 31(8) (2001) 1177-1184.

[43] Mehta PK, Monteiro PJM. Concrete structure, properties and materials. New Jersey: Prentice Hall, 1993:548.

[44] P. Brown, Porosity/permeability relationships, Materials science of concrete II (1991) 83-109.

[45] L. Cui, J.H. Cahyadi, Permeability and pore structure of OPC paste, Cement and Concrete Research 31(2) (2001) 277-282.

[46] Winslow D, Diamond SA. Mercury porosimetry study of the evolution of porosity in Portland cement: technical publication. Joint Trans Res Program 1969. http://dx.doi.org/10.5703/1288284314510

[47] P. Da Silva, J. De Brito, Experimental study of the porosity and microstructure of self-compacting concrete (SCC) with binary and ternary mixes of fly ash and limestone filler, Construction and Building Materials 86 (2015) 101-112.

[48] P. Pipilikaki, M. Beazi-Katsioti, The assessment of porosity and pore size distribution of limestone Portland cement pastes, Construction and Building Materials 23(5) (2009) 1966-1970.

[49] C. Parra, M. Valcuende, F. Gomez, Splitting tensile strength and modulus of elasticity of self-compacting concrete, Construction and Building materials 25(1) (2011) 201-207.

[50] M. Moini, I. Flores-Vivian, A. Amirjanov, K. Sobolev, The optimization of aggregate blends for sustainable low cement concrete, Construction and Building Materials 93 (2015) 627-634.

[51] A. Steopoe, Influence of aggregates on the strength of concrete, Materiales de Construcción 18(132) (1968) 67-73.

[52] D. Ho, A. Sheinn, C. Ng, C. Tam, The use of quarry dust for SCC applications, Cement and Concrete Research 32(4) (2002) 505-511.

[53] P. Domone, A review of the hardened mechanical properties of self-compacting concrete, Cement and Concrete Composites 29(1) (2007) 1-12.

[54] H. Dehwah, Mechanical properties of self-compacting concrete incorporating quarry dust powder, silica fume or fly ash, Construction and building materials 26(1) (2012) 547-551.

[55] A. Fathi, N. Shafiq, M. Nuruddin, A. Elheber, Study the effectiveness of the different pozzolanic material on self-compacting concrete, ARPN Journal of Engineering and Applied Sciences 8 (2013) 299-305.

[56] M. Jalal, E. Mansouri, M. Sharifipour, A.R. Pouladkhan, Mechanical, rheological, durability and microstructural properties of high performance self-compacting concrete containing SiO 2 micro and nanoparticles, Materials & Design 34 (2012) 389-400.

[57] G. De Schutter, K. Audenaert, Evaluation of water absorption of concrete as a measure for resistance against carbonation and chloride migration, Materials and Structures 37(9) (2004) 591-596.

[58] C. Hall, Water sorptivity of mortars and concretes: a review, Magazine of concrete research 41(147) (1989) 51-61.

[59] J. Torres, R. Mejía de Gutiérrez, F. Puertas, Efecto de la temperatura de tratamiento de un caolín en la permeabilidad a cloruros en morteros, Materiales de Construcción 57(285) (2007) 61-69.

[60] M. Valcuende, C. Parra, E. Marco, A. Garrido, E. Martínez, J. Cánoves, Influence of limestone filler and viscosity-modifying admixture on the porous structure of self-compacting concrete, Construction and Building Materials 28(1) (2012) 122-128.

[61] K. Turk, S. Caliskan, S. Yazicioglu, Capillary water absorption of selfcompacting concrete under different curing conditions, Indian J. Eng. Mater. Sci. 14 (5) (2007) 365–372.

[62] O. Trocónis-Rincón, A. Romero-Carruyo, C. Andrade, P. Helene, I. Díaz, Manual for inspection, evaluation and diagnosis of corrosion in reinforced concrete structures (in Spanish), DURAR Report, CyTED, Maracaibo, Venezuela, (1997), 208 p.

[63] A.M. Neville, Properties of concrete. 4th ed. Harlow, London: Longman Group Limited; 1995.

[64] O. Valenta, The permeability and durability of concrete in aggressive conditions, Proceedings of Tenth International Congress on Large Dams. Montreal, 1970.

[65] M. Uysal, K. Yilmaz, M. Ipek, The effect of mineral admixtures on mechanical properties, chloride ion permeability and impermeability of self-compacting concrete, Construction and Building Materials 27(1) (2012) 263-270.

[66] E. Vejmelková, M. Keppert, S. Grzeszczyk, B. Skaliński, R. Černý, Properties of self-compacting concrete mixtures containing metakaolin and blast furnace slag, Construction and Building Materials 25(3) (2011) 1325-1331.

[67] R.S. Ahari, T.K. Erdem, K. Ramyar, Permeability properties of self-consolidating concrete containing various supplementary cementitious materials, Construction and Building Materials 79 (2015) 326-336.

[68] N. Ghafoori, R. Spitek, M. Najimi, Influence of limestone size and content on transport properties of self-consolidating concrete, Construction and Building Materials 127 (2016) 588-595.

[69] G. Glass, N. Buenfeld, The presentation of the chloride threshold level for corrosion of steel in concrete, Corrosion science 39(5) (1997) 1001-1013.

[70] P.C. Ryan, A. O'Connor, Comparing the durability of self-compacting concretes and conventionally vibrated concretes in chloride rich environments, Construction and Building Materials 120 (2016) 504-513.

[71] G. De Schutter, K. Audenaert, Report 38: Durability of self-compacting concrete - State-of-the-art report, Technical Committee 205-DSC, RILEM publications 2007.

[72] A. Alrifai, S. Aggoun, E.-H. Kadri, G. De Schutter, A. Noumowe, Influence of aggregate skeleton on shrinkage properties: validation of the model developed by Le Roy for the case of self-compacting concrete, Materials and structures 44(9) (2011) 1593.

[73] F. Aslani, S. Nejadi, Shrinkage behavior of self-compacting concrete, Journal of Zhejiang University SCIENCE A 13(6) (2012) 407-419.

[74] N. Ranjbar, A. Behnia, B. Alsubari, P.M. Birgani, M.Z. Jumaat, Durability and mechanical properties of self-compacting concrete incorporating palm oil fuel ash, Journal of Cleaner Production 112 (2016) 723-730.

Capítulo 5

Mechanical behaviour of self-compacting concrete made with recovery filler from hot-mix asphalt plants

"A.R. Esquinas, C. Ramos, J.R. Jiménez, J.M. Fernández, J. de Brito, Mechanical behaviour of self-compacting concrete made with recovery filler from hot-mix asphalt plants, Construction and Building Materials, 131 (2017) 114–128. doi:10.1016/J.CONBUILDMAT.2016.11.063."

Abstract

The aim of this paper is to assess the feasibility of the use of a fine grain waste generated in hot-mix asphalt plants (HMA), namely recovery filler (RF), as filler materials in self-compacting concrete (SCC) production. A comparative study of two types of SCC was performed. The first concrete type was made incorporating recovery filler (SCC-RF) of a dolomitic nature and the second was made with commercial siliceous filler (SCC-SF), the latter used as reference. Good results of self-compatibility were obtained using RF. The thermogravimetric study showed that in SCC-SF the higher loss weight occurs in the dehydration zone (0-400 ºC) and in SCC-RF it occurs in the decarbonation area (550-735 ºC). The aging mechanism of both concrete types

(SCC-SF and SCC-RF) was different. In the SCC-SF mixes, portlandite undergoes carbonation processes and pozzolanic reactions and in the SCC-RF mixes it only undergoes carbonation processes. The experimental results (splitting tensile strength, flexural strength and static modulus of elasticity) show the validity of using EHE-08, initially proposed for OC (Ordinary Concrete), in SCC. The ultrasonic pulse velocity values for SCC-SF was greater than for SCC-RF, which can be attributed to compacity and compressive strength. The shrinkage behaviour was better in SCC-RF than SCC-SF, mainly due to the greater particle size of recovery filler (RF), although the SCC-RF mixes showed lower density and mechanical strength than SCC-SF. In short, the SCC manufactured with recovery filler from plants manufacturing hot-mix asphalt (HMA) - SCC-RF - is expected to have better features than SCC-SF in relation to shrinkage and early appearance of cracks.

Key words: Self-compacting concrete, recovery filler, siliceous filler, carbonation processes, pozzolanic reactions, ultrasonic pulse velocity, shrinkage.

Highlights:

- A comparative study of two types of SCC was carried out.
- The aging mechanism of the SCC mixes (SCC-SF and SCC-RF) was different.
- Pozzolanic reactions occurred during curing of the SCC-SF.
- Shrinkage in the SCC-RF was lower because of the larger particle size.
- Recovery filler from hot mix asphalt plants is adequate to produce SCC.

5.1 Introduction

Concrete is the building material most commonly used, twice more than other materials (wood, steel, plastic or aluminum). Its worldwide production is estimated at 4 tons per person and year [1]. Since it is the material that consumes more natural resources [2], it is not considered environmentally-friendly. For this reason, the concrete industry is constantly evolving, seeking more efficient technologies with high optimization of natural resources. In the 1980s, Self-Compacting Concrete was born (SCC), as an evolution of existing technology, and its use has been widespread in recent years in civil engineering, especially in the precasting industry, providing solutions to the different problems presented by ordinary concrete (OC). SCC is

characterized by not requiring vibration and compaction, flowing under its own weight, completely filling the mould to be cast, achieving full compaction in the presence of high-density reinforcement and homogenizing hardened concrete, all of which translates into benefits such as reduced lead times, production of complex structures, better surface finishes, reduced labour cost, improved job security, and noise and vibration reduction [3].

Nowadays there is a strong line of research related to global resource optimization and waste minimization in the construction field. The application of several wastes as replacement of the different materials involved in manufacture of SCCs has been studied. Some of this research has dealt with the use of mining waste as fine aggregate and/or filler with good results of self-compactability, excellent surface finish and high mechanical strength [4-6]. Granata [7] investigated SCC with pumice powder instead commercial filler, this research confirmed that pumice powder can be effectively used as filler in SCC. Da Silva & de Brito [8] carried out binary and ternary mixtures SCC with fly ash and limestone filler, concluding the replacement did not significatively affect the behaviour of the SCC studied by comparison with the control SCC with cement only. Ibrahim et al. [9] analysed the potential use of bottom ash as fine aggregate in SCC and observed that, due to the characteristics of this waste, to achieve optimal results regarding self-compactability and mechanical behaviour, three aspects must be taken into account: water/cement ratio, incorporation ratio of bottom ash and curing period. Glass is an indispensable material to man but it generates a lot of waste, creating serious problems for the environment; to contribute to solve this issue Ali et al. [10] proposed its use as fine aggregate because it can successfully be used to produce SCC. Blast furnace slag was investigated by Zhao et al. [11] as mineral admixture for the production of SCC. The differences between the mechanical properties of SCC with and without waste, fresh and at 90 days, were insignificant. Blast furnace slag was investigated by Valcuende et al. [12] as replacement of sand for the production of SCC, at early ages, SCC show similar compressive strength to the reference SCC. But, the greater the age, the concrete's compressive strength tends to be higher, due to slag reactivity. Other researchers have used other waste, such as Mishra et al. [13], who replaced the coarse aggregate with rubber chips at a percentage 0-20% and concluded that the resulting SCC is adequate for applications where strength is not needed but durability is important. Hesami et al. [14] replaced

the sand with tire rubber crumb at a percentage 5-15% and it can be stated that it has no considerable negative effect on some of the properties as abrasion resistance index. Ghernouti et al. [15] made SCC with plastic bag waste as fibres, obtaining a positive effect on mechanical behaviour, being more important in spilt tensile strength. Oerkan et al. [16] made SCC with plastic waste from municipal waste as fibres, obtaining a correct mechanical behaviour and less shrinkage. Mohammadhosseini et al. [17] studied the influence of palm oil fuel ash on SCC; the results revealed an acceptable range in terms the workability and an excellent compressive strength for 30% replacement of ash by cement. Ranjbar et al. [18] also studied the influence of palm oil fuel ash on SCC; the results revealed great potential to be used as a replacement of Portland cement in self-compacting concrete preserving fresh, mechanical and durability properties in an acceptable range.

The aim of this paper is the assessment of the feasibility of the fine grain waste, generated in the drying and heating process of aggregates in hot-mix asphalt (HMA) manufacturing plants, as a construction material. This powder named "recovery filler" (RF) drops from the rotating drum together with the combustion gases and water vapour and is retained by baghouse filters to prevent its dispersal into the atmosphere. Sometimes it is partially stored in silos for use as recovery filler in the manufacturing of new HMA used as base layer in road pavements. This use represents around 3-4%. The greater part of RF is sent to dumping grounds or, if the plants have their own quarry, is deposited as illegal filling, resulting in environmental problems and health risks. This type of waste is in direct contact with fuel oil burners and often cannot be classified as inert in accordance with the European Council Decision 2003/33/EC. The amount of RF generated is estimated at 4% by weight of HMA produced, which depends on the nature of the aggregate and the amount of HMA. World production exceeds 700 million tons of asphalt mixtures (2014), of which 14.5 million tons were produced in Spain [19]. This waste can be recycled and reduce the consumption of natural resources, save energy, reduce materials costs and waste dumping. The use of this waste as construction material has not been discussed in depth [20] and, given the high volume of fine materials required in SCCs, it would be useful to analyse its behaviour in the manufacture of SCCs.

In this paper a comparative study of two types of SCC was carried out. In the first one, a recovery filler (RF) of dolomitic nature was used and, in the second, a commercial siliceous filler (SF) was used as reference. The amount of filler used in both cases was the same. To determine the behaviour of these two types of SCC, fresh properties such as flowability, blocking resistance and resistance to segregation were analysed to know the properties of self-compatibility. An extensive research of hardened SCC was conducted to correlate the microstructural properties with the long-term mechanical behaviour. Finally, the early-age shrinkage was determined.

5.2 Experimental plan

5.2.1 Materials characterization

The crushed rock aggregates were supplied by Aggregates Gallardo S.L, "Campanario" (Badajoz, Spain): gravel 4/16 (G), coarse sand 0/4 (S1) and fine sand 0/2 (S2). The particle size distribution of the aggregates is shown in Figure 5.1. According to the results of the geometric-physical-chemical characterization (Table 5.1), the aggregates are suitable for concrete production according to the Spanish Instruction of Structural Concrete (EHE-08) [21]. XRD patterns (Figure 5.2) showed that the main phase was quartz (33-1161) [22]. In the sands (S1 and S2) the presence of orthoclase (31-0966) [22] and albite (41-1480) [22] was also observed.

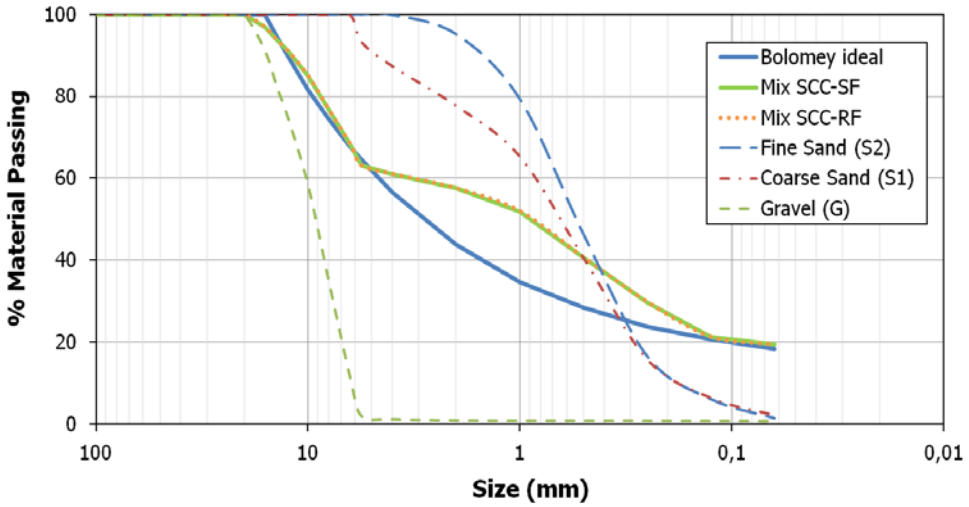

Figure 5.1: Particle size distribution for gravel, coarse and fine sands, mixes SCC-SF and SCC-RF and Bolomey ideal.

Table 5.1
Characterisation of aggregates.

Characteristic	Standard	G	S1	S2	Limit set by EHE-08
Size (mm)	UNE-EN 933-1	4/16	0/4	0/2	<25 mm
Index slabs (%)	UNE-EN 933-3	10.6	-	-	< 35
Crushed and broken surfaces (%)	UNE-EN 933-5	94	-	-	Not limited
Los Angeles coefficient	UNE-EN 1097-2	21	-	-	≤ 40
Dry sample density ρ_{rd} (g/cm^3)	UNE-EN 1097-6	2.60	2.60	2.60	Not limited
Water absorption (%)	UNE-EN 1097-6	0.96	0.67	0.62	≤ 5
Friability coefficient (%)	UNE 83115	-	14	14	< 40 [(a)]
Surface cleaning (%)	UNE 146130	0.45	0.49	-	Not limited
Water soluble chlorides (% Cl)	UNE-EN 1744-1	6×10^{-4}	6×10^{-4}	$2 \times 10^{-3} \leq 0.03$	
Acid soluble sulphates (% SO_3)	UNE-EN 1744-1	2×10^{-3}	2×10^{-3}	$4 \times 10^{-3} \leq 0.8$	
Water soluble sulphates (% SO_3)	UNE-EN 1744-1	0.06	0.03	0.05	≤ 0.8
Sulphur content (%)	UNE-EN 1744-1	ND [(b)]	ND	ND	≤ 1
Organic matter content (%)	UNE-EN 1744-1	0.08	0.11	0.11	≤ 1[(c)] - ≤ 0.5 [(d)]

[(a)] Recommendation; [(b)] ND: No Detected [(c)] Coarse aggregates; [(d)] Fine aggregates

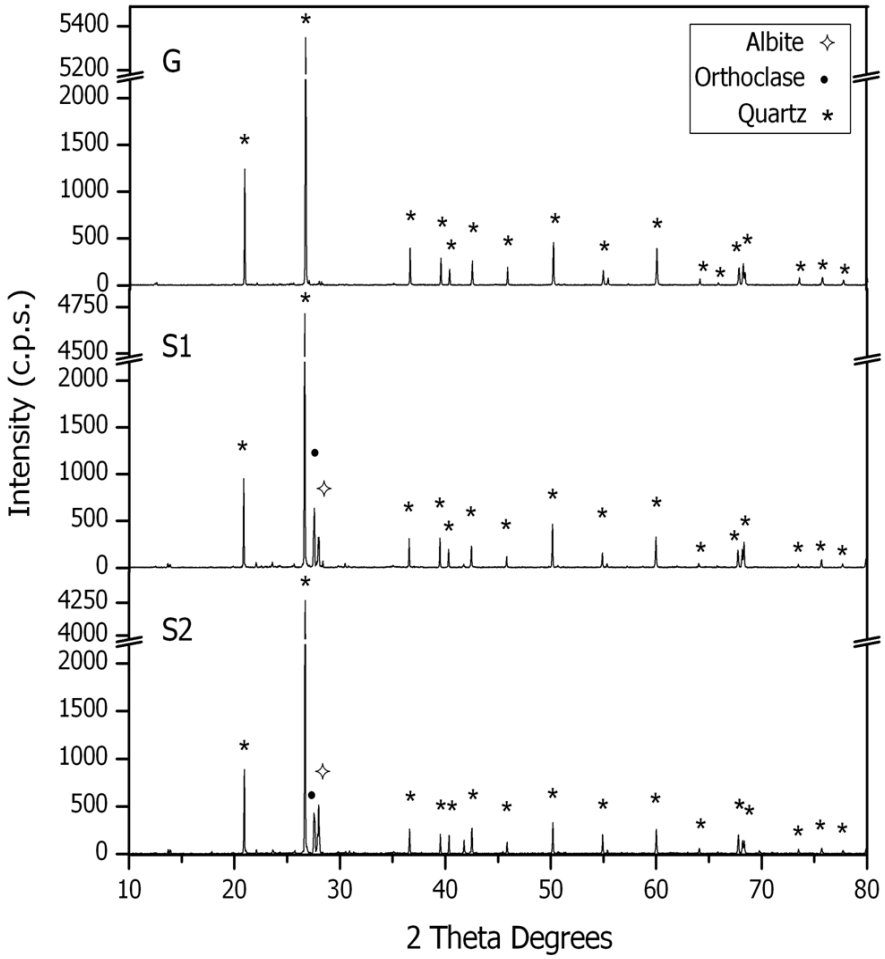

Figure 5.2: PXRD patterns for gravel (G), coarse (S1) and fine (S2) sands.

The commercial siliceous filler (SF) was supplied by Minas Carmina Llansá (Gerona, Spain) and comes from crushing siliceous quarry sands. The residual filler (RF) was supplied by hot-mix asphalt company PAMASA (Malaga, Spain). The particle size of the fillers used in this article was analysed by two methods. The results of the first one, using UNE-EN 933-1 [23], showed that 100% of both fillers passed through the 2 mm and 0.25 mm sieves, 100% of SF and 99.94% of RF passed through the 0.125 mm sieve and finally 74.33% of the commercial filler and 70.35% of the residual filler passed through the 0.063 mm sieve. This is in accordance with the requirements of EHE-08, as more than 70% passed through the 0.063 mm sieve, more than 85% passed through the 0.125 mm sieve and 100% passed through the 2 mm sieve [21].

The second procedure used was to study the distribution of grain size by laser diffraction. Figure 5.3 shows that the particle size distribution of RF was wider than that of SF (0.1 - 200 µm vs. 0.2 - 100 µm). SF had the highest content of particles around 20 µm, while for RF it was 40 µm. Both fillers had the highest percentage of particles between 3 µm and 32 µm (Table 5.2), 71.28% for SF and 49.85% for RF. These results are important since, above 32 µm, the particles are too large for full hydration and, below 3 µm, they have a smaller contribution to the strength while at the same time the water requirement is higher [24-26].

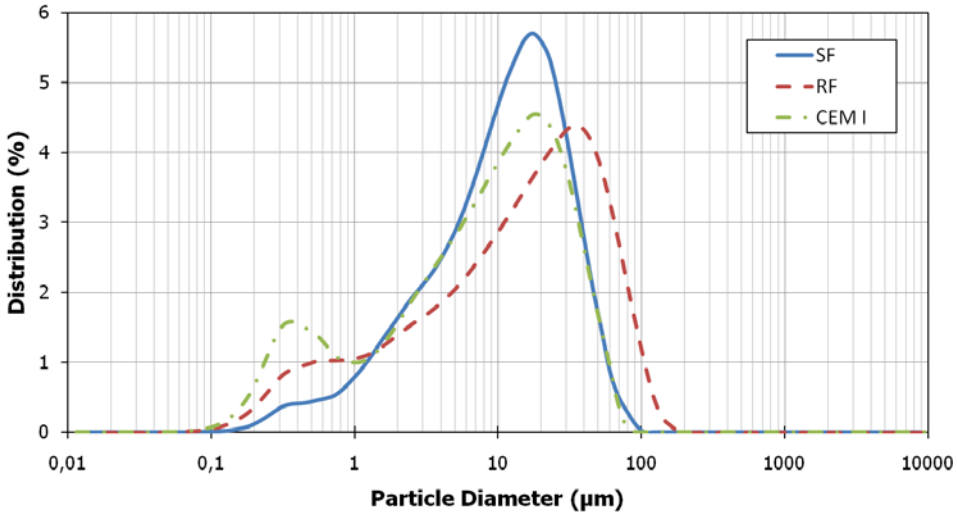

Figure 5.3: Grain-size distribution of SF, RF and CEM I by laser diffraction.

Table 5.2
Characterisation of filler and cement.

Characteristic	Standard	SF	RF	Cement
SiO_2 %	-	100	-	11.20
Al_2O_3 %	-	-	-	4.96
Fe_2O_3 %	-	-	-	16.53
SO_3 %	-	-	-	3.02
CaO %	-	-	55.85	61.79
MgO %	-	-	44.15	-
Other	-	-	-	2.00
Particle size > 32 µm (%)	-	17.13	28.23	27.99
Particle size 3 - 32 µm (%)	-	71.28	49.85	61.28
Particle size < 3 µm (%)	-	11.59	21.92	10.73
BET surface area (m^2/g)	-	0.25	76.04	0.67
Filler density (g/cm^3)	UNE-EN 1097-6	2.60	2.88	3.10
Densidad aparente (g/cm^3)	NLT 176 / 1992	0.689	1,01	-

XRD patterns (Figure 5.4) reveal that silica was the only phase present (33-1161) [22] in SF. The residual filler (RF) was only of dolomitic nature (Figure 5.4) (36-0426) [22]. A thermogravimetric analysis of the fillers (Figure 5.5) showed the purity of SF filler since no weight loss was observed. In the case of filler RF an endothermic peak and one weight loss between 600 ºC and 800 °C was observed, corresponding to the release of CO_2, due to the transformation from dolomite into oxides.

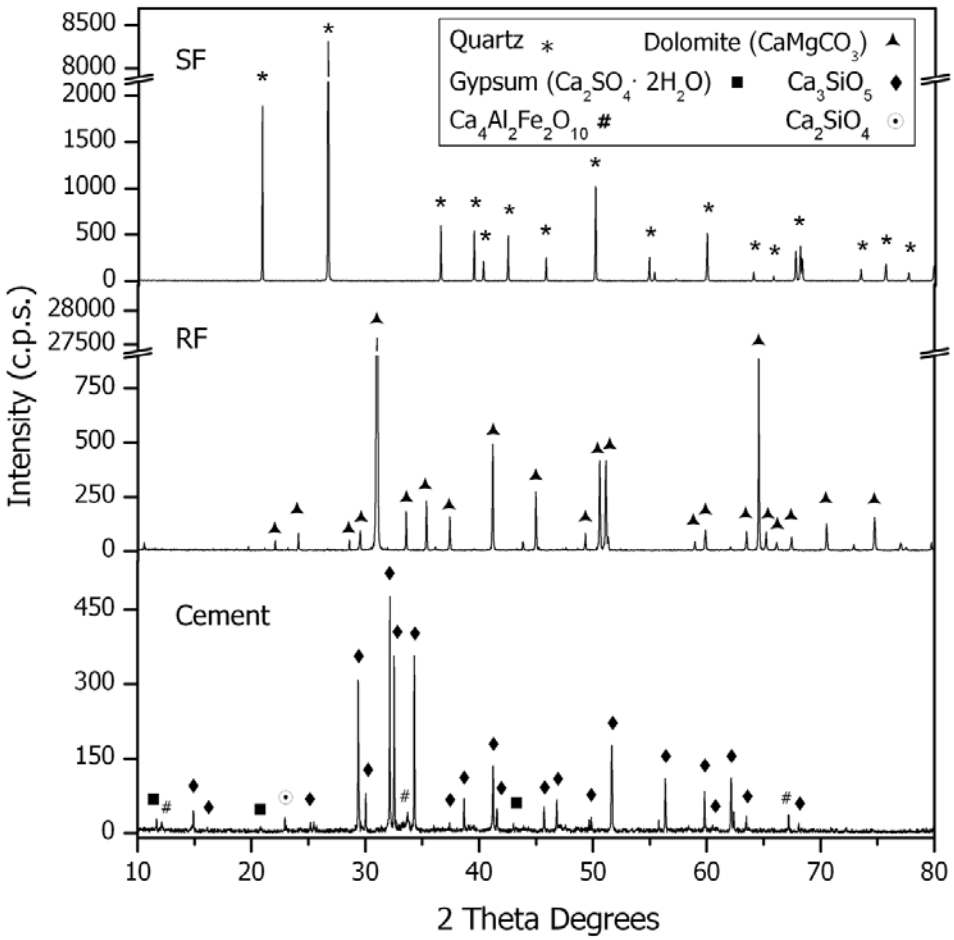

Figure 5.4: PXRD patterns for SF, RF and cement.

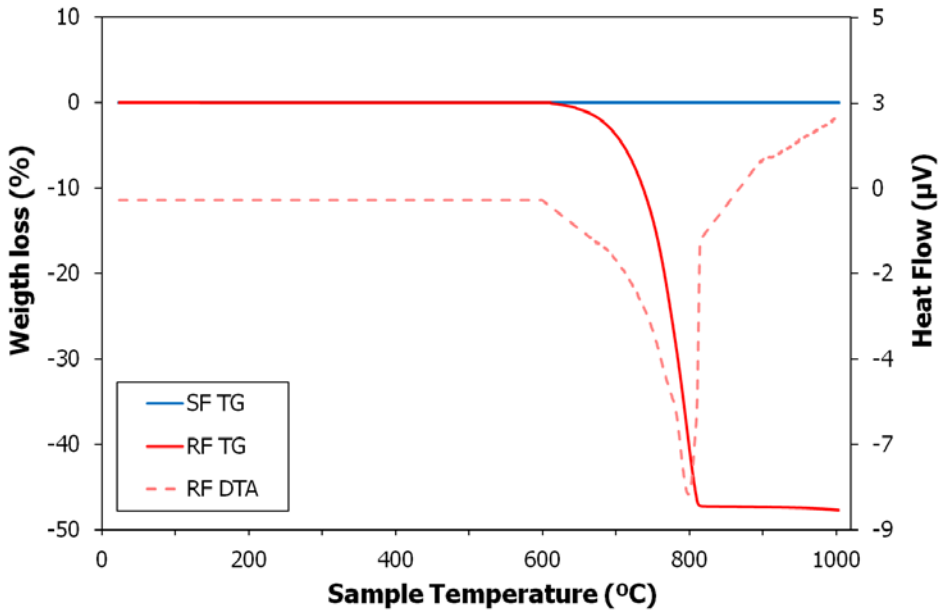

Figure 5.5: TG (solid lines) and DTA (dotted line) curves for the SF and RF fillers.

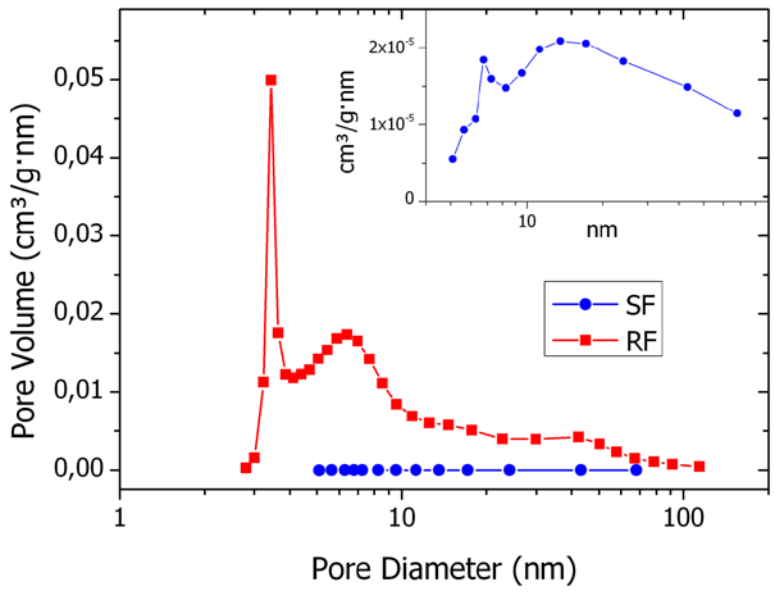

Figure 5.6: Pore size distribution for the SF and RF fillers.

In addition, adsorption-desorption isotherms of nitrogen were determined to study the texture properties. Table 5.2 shows that particles of RF had a BET surface 300 times greater than the surface of SF (76.04 m^2/g vs. 0.25 m^2/g). Figure 5.6 shows

the pore size distribution for both fillers, which was in the 3-110 nm range. The SF had a negligible pore volume compared to RF. The highest content of pore RF was between 3.5 nm and 7 nm. These data were consistent with the images of transmission electron microscopy (Figure 5.7), which showed a large number of pores in RF and total absence of pores in SF.

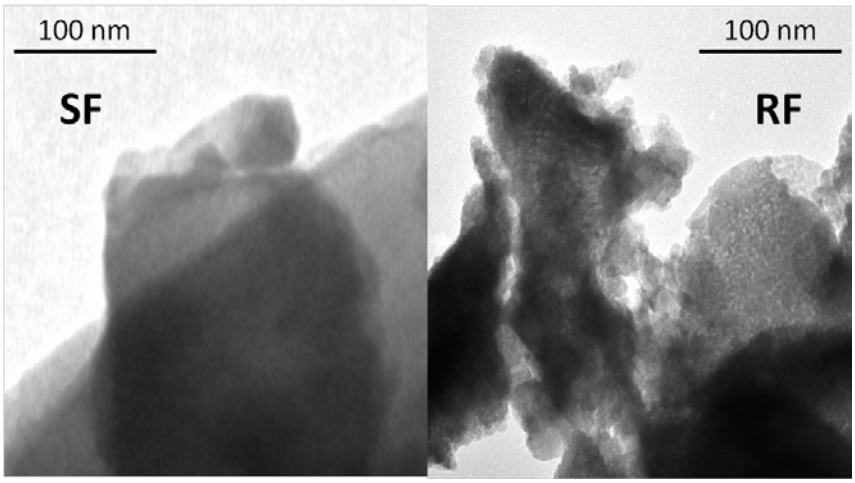

Figure 5.7: TEM micrographs for the SF and RF fillers.

The Fourier Transform Infrared Spectra (FT-IR) of SF and RF are shown in Figure 5.8. The shape of the spectra of silica and dolomite agrees with the literature [27, 28]. Regarding the SF spectrum, the bands appearing around 1170 cm^{-1} and 1028 cm^{-1} correspond to asymmetric stretching vibrations of Si–O–Si, and the characteristic doublet of quartz at 796 and 777 cm^{-1} corresponds to symmetric stretching vibrations of Si–O–Si bonds. The band appearing at 459 cm^{-1} is associated with O-Si-O bond bending vibration [29]. Regarding dolomite, the band observed at 3460 cm^{-1} is a characteristic stretch band of groups OH^-. The carbonates in the sample were demonstrated by bands around 3014 cm^{-1}, 2893 cm^{-1}, 2628 cm^{-1}, 2522 cm^{-1}, 1820 cm^{-1}, 1446 cm^{-1}, 879 cm^{-1}, 727 cm^{-1} and 667 cm^{-1}. The bands at 3014 cm^{-1}, 2628 cm^{-1} and 727 cm^{-1} confirm the presence of dolomite [27]. The FTIR bands detected at 3014 cm^{-1} and 2628 cm^{-1} are combination frequencies [30], and the band at 729 cm^{-1} is assigned to the in-plane bending mode of CO_3^{2-} in the dolomite structure [31].

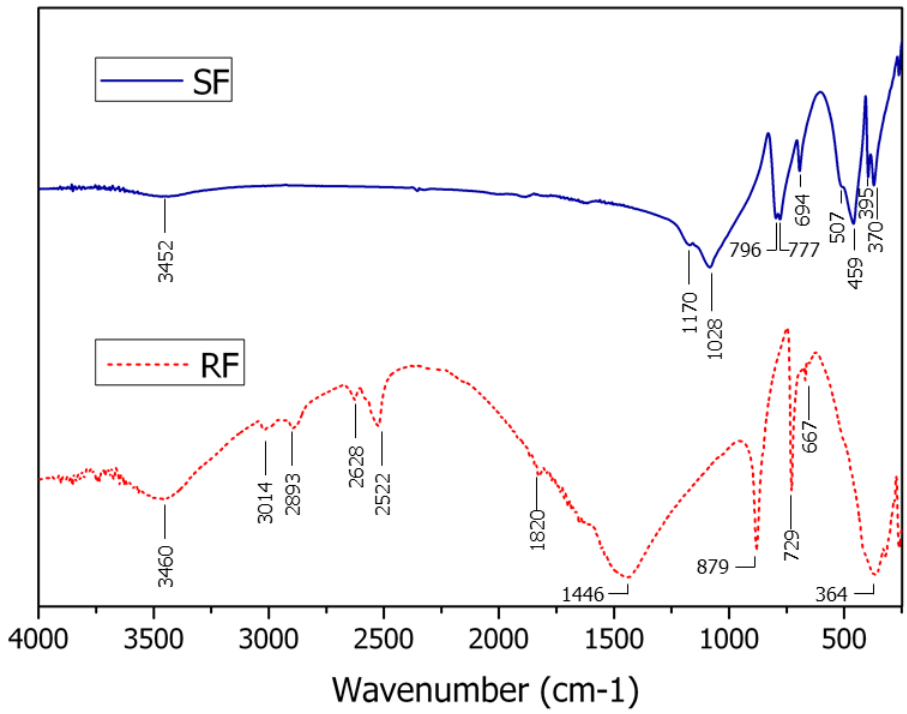

Figure 5.8: FT-IR for the SF and RF fillers.

The cement used was type CEM I 42.5 R/SR (UNE 80303-1 and UNE-EN 197-1) [23]. Figure 5.3 shows the particle size distribution. The major percentage of particles was between 3 µm and 32 µm (61.28%) (Table 5.2), which is important for the hydration process, as discussed above. Moreover, the chemical composition, expressed as oxides, which was determined by analysis of dispersive energy of X-ray (EDAX), is shown. The predominant oxide was calcium oxide (CaO) and the content of aluminum oxide (Al_2O_3) was very low. The analysis by X-ray diffraction patterns (PXRD) (Figure 5.4) showed that the main mineral phase was tricalcium silicate, Ca_3SiO_5 (42-0551) [22] and the presence of small proportion of dicalcium silicate, Ca_2SiO_4 (24-0034) [22], gypsum, $CaSO_4 \cdot H_2O$ (33-0311) [22] and tetracalcium aluminoferrite, $Ca_4Al_2Fe_2O_{10}$, (11-0124) [22] was detected.

A high-performance superplasticizer/water reducer specific for SCC, Glenium 303 SCC, supplied by BASF Chemical Company, was used. The aim was to produce a SCC with low effective water/cement ratio (w/c) [32].

5.2.2 Concrete mixes and composition tests

In order to study the effect of RF as filler, referring to its mechanical properties in SCC, two types of mixes were used. The first one incorporated SF (SSC-SF) and the second RF (SC-RF). In both cases their self-compactability was studied according to the requirements of EHE-08. The devices [33-35] and the properties associated are shown in Table 5.3. First the unobstructed filling capacity and segregation resistance given by parameters d_f and T_{50} were studied using the Abrams cone, (UNE-EN 12350-8) [23]. Then the passing capacity past bars and the segregation resistance given by parameter d_{jf} were determined with the J-Ring, (UNE-EN 12350-12) [23]. Also studied were its ability to go through narrow openings and filling capacity using parameter Tv, obtained with V-funnel, (UNE-EN 12350-9) [23] and finally its passing capacity past bars and segregation resistance using parameter C_{bl} obtained with L-box device, (UNE-EN 12350-10) [23].

To obtain the composition of the SCC (SCC-RF and SCC-SF) an initial composition provided by ENRESA (the national company for radioactive waste) was provided [36], with gravel content of around 800 kg/m^3 and cement content of 400 kg/m^3. This company studies the use of SCC in structures utilized to store waste of low and medium radioactive levels at El Cabril (Cordoba).

The specified requirements of this study for both mixes SCC-RF and SCC-SF were: type of exposition IIIc, strength characteristic of 40 MPa, cement content 400 kg/m^3, maximum ratio w/c 0.44 and 1.8% of admixture relative to total sum of cement plus filler. According to EHE-08 it was classified as HA-40/AC/16/IIIc. The contents adjustment was made in volume (1025 L).

The SCC-SF mix, whose composition expressed in dry weight and in volume is shown in Table 5.4, is taken as a standard concrete reference. These contents complied with the European Federation of National Associations Representing producers and appliers of specialized building products for Concrete (EFNARC) [3, 37].

Taking into account the different physical-chemical characteristics of RF with respect to SF, as previously mentioned, to achieve a SCC with RF small adjustments in cement

content and added water were made. Both mixes (SCC-RF and SCC-SF) show similar percentages of components as shown in Table 5.4, which demonstrates that the components comply with EFNARC's recommended values.

Table 5.3
Self-compactability tests.

Test	Characteristics evaluated	Standard	Parameters	Admissible values [21]
Slump flow test	Unobstructed filling ability	UNE-EN 12350-8 [23]	d_f = final flow diameter	550 mm ≤ d_f ≤ 850 mm
	Resistance to segregation [a]		T_{50} = time spent to reach the 500 mm	T_{50} ≤ 8s
J-Ring test	Passing ability	UNE-EN 12350-12 [23]	d_{jf} = final flow diameter	≥ d_f - 50 mm
	Resistance to segregation [a]			
V-funnel test	Filling ability	UNE-EN 12350-9 [23]	Tv = funnel flow time	4 s ≤ Tv ≤ 20 s
	Passing ability			
L-box test	Passing ability	UNE-EN 12350-10 [23]	C_{bL} = blocking coefficient	0.75 ≤ C_{bl} ≤ 1
	Resistance to segregation [a]			

[a] No standardized

Table 5.4
Concrete mix proportions and EFNARC composition parameters.

Mixes	**SCC-SF**				**SCC-RF**			
	Dry weight		*Volume*		Dry weight		*Volume*	
Constituent	kg/m³	%	L/m³	*%*	kg/m³	%	L/m³	*%*
Gravel 4/16 (G)	793.88	32.78	*305.34*	*29.82*	793.88	32.71	*305.34*	*29.82*
Sand 0/4 (S1)	646.08	26.68	*246.59*	*24.08*	646.08	26.62	*246.59*	*24.08*
Sand 0/2 (S2)	276.03	11.40	*106.17*	*10.37*	276.03	11.37	*106.17*	*10.37*
Filler	100.01	4.13	*38.47*	*3.76*	100.01	4.12	*34.76*	*3.39*
Cement	410.00	16.93	*132.26*	*12.92*	412.28	16.99	*132.99*	*12.99*
Superplasticizer	9.18	0.38	*8.87*	*0.87*	9.22	0.38	*8.91*	*0.87*
Water$_{ef}$	180.41	7.45	*180.41*	*17.58*	183.38	7.56	*183.38*	*17.91*
(W/C) $_{total}$	0.472				0.477			
(W/C) $_{ef}$	0.440				0.445			

	Typical range [a]	SCC-SF	SCC-RF
Coarse aggregate (kg/m³)	750-1000	793.88	793.88
Fine aggregate (sand) (%)	48-55[b]	50.78	50.78
Fines (kg/m³)	380-600	569.61	571.88
Water (litres/m³)	150-210	186.30	189.24
Paste (litres/m³)	300-380	314.18	317.88
Water/fines [c]	0.85-1.10	0.962	0.993

[a] EFNARC composition parameters [3]
[b] Volume total weight of aggregate in balanced quantiles. % of sand S1 and S2 relative to the whole of the aggregates.
[c] By volume.

4.2.3 Test methods

The constituents, as well as the composite materials, were characterized by different techniques. Particle sizes were measured in a Mastersizer S analyser (Malvern Instruments) using ethanol as dispersant. The samples were analysed by X-ray diffraction patterns (XRD) using a Bruker D8 Discover A25 instrument with Cu-Kα radiation. All diffraction patterns were obtained by scanning the goniometer from 10°

to 80° (2θ) at a rate of 0.05° min^{-1}. Thermogravimetric analysis was performed in a Setaram Setsys Evolution 16/18 apparatus at a heating rate of 5 °C/min. Specimens (150 x 150 x 150 mm) were kept in oven at 105 °C. Then, a little portion (a cube of 10x10x10mm) was taken from the centre of the specimen to do the thermic analysis (DTA-TGA). N_2 isotherms were determined in a Micromeritics ASAP 2010 analyser, samples having been previously degassed at 100 °C under vacuum for 2 h. The surface was calculated using the BET method in the range of equilibrium relative pressure $0.05 \leq P/Po \leq 0.20$ [38]. Microstructural characterization of the materials was carried out using JEOL 1400 TEM and JEOL 2010 TEM equipment. The electron microprobe technique was conducted using an electron microscope JEOL JSM-6300 with an acceleration voltage of 20 kV and a working distance of 15 mm. The X-ray detector was a model Oxford Instruments ATW2-6699. MIR spectra were obtained by transmission mode in a FT-MIR Bruker Tensor 27 (Bruker Optik GmbH; Rudolf-Plank-Str. 27; 76275 Ettlingen; GERMANY) spectrophotometer with CsI beam splitters and a DTGS detector. OPUS v. 6.5 software (Bruker Optik GmbH; Rudolf-Plank-Str. 27; 76275 Ettlingen; GERMANY) was used to collect the transmission spectra.

The compressive strength, (UNE-EN 12390-3) [23] and splitting tensile strength, (UNE-EN 12390-6) [23], in cylindrical specimens of 300 x 150 mm and flexural strength, (UNE-EN 12390-5) [23], in prismatic specimens of 100 x 100 x 40 mm, were evaluated after 7, 28, 91 and 250 days, cured in water according to UNE 12390-2 [23]. The secant modulus of elasticity in compression (modulus of elasticity), (UNE-EN 12390-13) [23], and the Poisson coefficient, (ASTMC469/C469M-14) [39], was determined at 28 and 91 days in cylindrical specimens of 300 x 150 mm. For this batch of tests an IBERTEST press was used, model MEH-3000, with a maximum capacity of 3000 kN.

The ultrasonic pulse velocity (UPV), (UNE-EN 12504-4) [23], was studied at 7, 28, 91and 250 days, using an ultrasound meter for concrete, a Matest, model C369N. This test was undertaken with two electro-acoustic transducers that acted as transmitter and receptor for ultrasound waves with given path lengths. Related to this parameter, the density values were determined (dry, wet and fresh), (UNE-EN 12390-7 & UNE-EN12350-6) [23], in 150 x 150 x 150 mm specimens cured in water. Total shrinkage, (ASTMC157/C157M-08e1) [39], over a short period (91 days) was

determined in 150 x 150 x 500 mm specimens. These samples were kept in a curing chamber at a constant environmental temperature of 20 ºC with a relative humidity of 50%.

5.3 Results and discussion

5.3.1 Fresh-state properties of SCC

5.3.1.1 Self-compactability

With the aim of testing the reproducibility of the mixes SSC-SF and SSC-RF relative to their self-compactability, the mixes were repeated four times and slump-flow was measured with the J-ring test, V-funnel test and L-Box test. Both mixes, SSC-SF (T_{50} = 2.5 s, d_f = 758.13 mm, d_f-d_{jf} = 20, C_{bL} = 0.81 and Tv = 6.73 s) and SCC-RF (T_{50} = 2.89 s, d_f = 695.63 mm, d_f-d_{jf} = 8.5, C_{bL} = 0.82 and Tv = 10.9 s) (Table 5.5), comply with the self-compactability criteria as they are within the reference values shown in Table 5.3.

In terms of slump-flow, the final diameter for SSC-RF was 8.24% less than for SCC-SF, and 15% more time was needed for SCC-RF to reach the 500 mm mark. As for the slump-flow test with the J-ring, the time to reach 500 mm diameter was 12% longer in SCC-RF than in SCC-SF. This behaviour is due to the particles being larger (Figure 5.3) in RF than in SF and to their greater porosity (Figures 5.6 and 5.7), which results in less free water to lubricate the particles and therefore an increase in the viscosity of the mix. Visually both mixes had a good distribution of coarse aggregate at the edges of the slump flow test specimen and absence of segregation and bleeding. This result is in compliance with the content of fine material and paste in both mixes, as these parameters favour a cohesive mix. SCC-RF had a lower (57%) d_f–d_{jf} compared to SCC-SF, so the presence of bars affected less the SCC-RF mix.

The results obtained from the V-funnel tests are higher for SCC-RF (61.9%) than for SCC-SF, which can be associated to the higher viscosity of SCC-RF. This effect cannot be attributed to the coarse material [40] because its content was identical in SCC-SF.

Despite these differences, a good filling capacity and a good ability to pass through narrow spaces were demonstrated.

Table 5.5
Results of the self-compactability tests for the two types of SCC.

Mixtures	**Retakes**	**Slump flow test**		**J-Ring test**		**V-funnel test**	**L-box test**
		T_{50} (s)	d_f (mm)	T_{J50} (s)	$d_f - d_{jf}$	T_v (s)	C_{bL}
SSC-SF	Average (SD) [a]	2.50 (0.1)	758.13 (5.54)	2.85 (0.20)	20.00 (5.20)	6.73 (0.53)	0.81 (0.04)
Class [21]		*AC-V2*	*AC-E3*		*AC-RB2*	*AC-V2*	*AC-RB2*
SSC-RF	Average (SD) [a]	2.89 (0.04)	695.63 (10.68)	3.21 (0.25)	8.50 (1.44)	10.90 (0.81)	0.82 (0.02)
Class [21]		*AC-V1*	*AC-E2*		*AC-RB2*	*AC-V1*	*AC-RB2*

[a] Standard deviation

The L-box test, for SCC-SF and SCC-RF, gave similar values of C_{bL}. This indicates a good passing and filling ability past reinforcement bars in both types of concrete, as well as resistance to segregation. There were no visual signs of bleeding or segregation, although the equipment shape, according to Khayat [41], makes it difficult to detect segregation unless it is very obvious. The results demonstrate that both mixes are within the ranges accepted by EHE-08 as SCC.

The collective analysis of these tests demonstrate that concrete produced as a residual filler gave values of self-compactability closer to the limits given by EHE-08, though without losing the ability of self-compacting and filling every empty space as observed in the results of the L-Box. This behaviour may be attributed to the difference in particle fineness, shape characteristics of fillers and surface porosity.

The results obtained for slump-flow tests, slump-flow tests with J-ring and V-funnel tests resembled those obtained by Martin et al. [20]. The Tv values of SCC-RF in our article were greater and the values for C_{bL} less than those obtained by these authors, which is in line with the lower superplasticizer content and greater coarse aggregates content used in our work.

The results show, in accordance with the conditions set out by Ferreira [42], that it is possible to obtain an SCC similar to those obtained by Martin et. al. [20] with greater gravel content and lower superplasticizer content. Similar results for fresh-state, using similar contents of superplasticizer, cement and residual filler were obtained by Ho et.al. [43], using as filler natural granite from quarry dust and a commercial limestone filler, and by Topçu et al. [6] incorporating marble dust as filler.

Figure 5.9 shows, in accordance with the investigation of Felekoglu [44], who applied the concept of workability boxes to evaluate self-compactability by using the workability, slump flow and V-funnel tests [45], that the SCC-SF mix was graded in the “Marginal SCC area” at the bottom right hand corner. This, according to the author, should show a mild segregation, but in our case there were no signs of segregation. Moreover, the SCC-RF mix is within the category “Proper SCC area”, i.e. they were considered adequate and acceptable SCCs. The diagram also clearly

demonstrates the reproducibility that occurs with repetitions of different contents in reference to self-compactability.

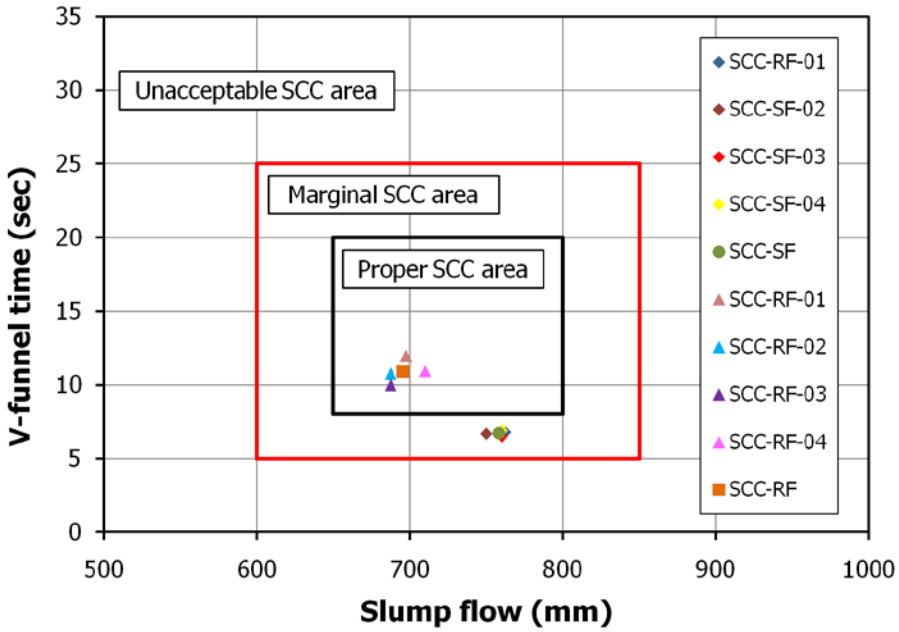

Figure 5.9: Workability boxes for several self-compacting mixes.

It is therefore possible to conclude that a SCC can be obtained using given coarse aggregates, cement content and water/cement ratio set by replacing natural siliceous filler (SF) with residual dolomite residual filler (RF) in mass, with minor adjustments in cement (0.5%) and water (1%) so as to maintain the volume of the mix (1025 L) constant.

5.3.1.2 Fresh density of SCC

The fresh density of SCC-RF (2.365 T/m^3) is slightly lower than that of SCC-SF (2.392 T/m^3), which is due to the lower content of filler RF in volume and the greater water content in SCC-RF. In addition, the filler RF displays more gaps as a consequence of the greater content of small mesopores (< 10 nm) (Figures 5.6 and 5.7), which is relevant to lower the density in fresh concrete. These results are in accordance with those results by other authors [6, 20] who noticed that mixes with residual filler resulted in less dense SCC.

5.3.2 Hardened-state properties of SSC

5.3.2.1 Physical-chemical characterization of hardened SCC

The thermal analysis by means of TGA and DTA of hardened SCCs (Table 5.6 and Figure 5.10) can be split into three areas. The first of these, from environmental temperature up to 400 ºC, takes into account the loss of "free water" physically absorbed, the water present in the pores, the loss of interlayer water and the loss of mass due to dehydration processes of the silicates and aluminates calcium (structural water). In our case the "free water" (loss between environmental temperature and 100 ºC) is negligible as the samples were kept in ovens at 105 ± 5 ºC at constant weight. The second area is set between 400 ºC and 550 ºC, which applies to dihydroxylation, between 425 ºC and 455 ºC occurs the decomposition of portlandite. The DTA analysis did not show any effect attributed to the presence of $Mg(OH)_2$ (Brucite) [46]. The third area is between 550 ºC and 735 ºC, which relates to the decomposition of initial carbonates or those formed in the hardening process [47]. Broad peaks between 600 ºC and 700 ºC for samples SCC-SF and between 650 ºC and 735 ºC for samples SCC-RF are observed. The loss of weight after 735 ºC is similar in any case and corresponds to the removal of OH^- residuals.

SCC-SF tends to a higher level of hydration as it hardens. Of special interest was the grade of hydration upon reaching 250 days, 7.15% for SCC-SF and 4.88% for SCC-RF (Table 5.6). In the column "H_2OTotal" (Table 5.6) there is an increase in water content that is related to hardening. A higher water content in the SSC-SF sample relative to the SCC-RF sample, both cured for 250 days, is noticeable. This can be attributed to the pozzolanic reaction of $Ca(OH)_2$ with SF to form CSH, which agrees with the greater decrease in $Ca(OH)_2$ content in the SCC-SF sample relative to the decrease produced in the SSC-RF sample at the same curing time. This reaction does not occur in SSC-RF because there is no SF.

Table 5.6
Results obtained in the test of thermal analysis (TG/TD) for each SCC studied.

Mixtures	Age (days)	Δ mass (%)				Chemical species (kg/m³)				
		0-400ºC	400-550ºC	550-750ºC	750-800ºC	$Ca(OH)_2$	$CaCO_3$	$MgCa(CO_3)_2$	$Ca(OH)_{2\ Total}$	H_2O_{Total}
SCC-SF	28	-2.3188	-0.7066	-1.3452	-0.0551	65.9	69.4	-	117.2	52.6
	91	-4.0178	-1.2556	-1.3403	-0.0657	117.1	69.1	-	168.2	91.1
	250	-7.1453	-1.1015	-1.4291	-0.0556	102.7	73.7	-	157.2	162.0
SCC-RF	28	-1.8308	-0.8336	-2.7547	-0.0542	76.8	40.3	100.00	106.6	41.0
	91	-4.3884	-1.2709	-3.6960	-0.0638	117.0	88.2	100.00	182.3	98.3
	250	-4.8801	-1.1998	-4.3415	-0.1115	110.5	121.1	100.00	200.1	109.3

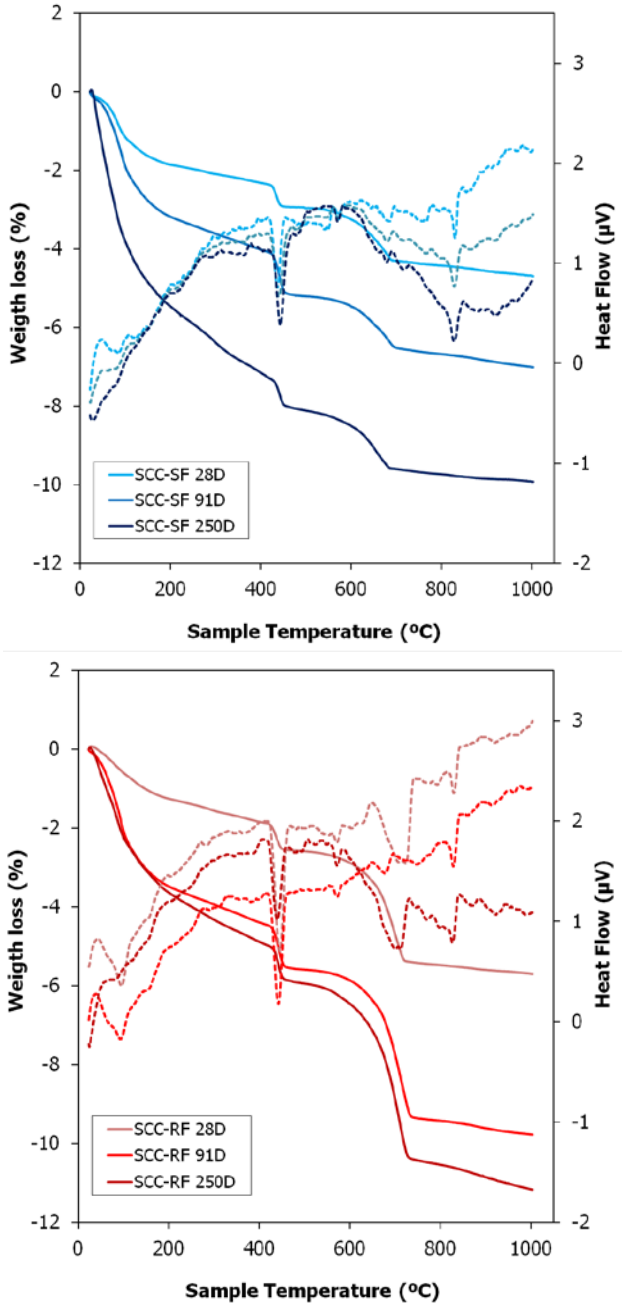

Figure 5.10: TGA (solid lines) and TDA (dotted lines) for several hardened SCCs.

The amount of $Ca(OH)_2$ calculated with a weight loss between 400-550 ºC, which corresponded to the formation of portlandite during the process of hydration of calcium silicates, showed a similar evolution in both mixes, which is congruent with

their cement content. The amount of portlandite formed increases with hardening at the initial stage and thereafter decreases due to the carbonation process. The carbonate content is much higher in SCC-RF, as seen in a weight loss between 550 ºC and 735 ºC (Figure 5.10), due to the dolomite content in the mix. Column "$CaCO_3$" shows the content of $CaCO_3$, which was calculated from the loss of weight between 550 ºC and 735 ºC. In the case of SCC-RF the amount of CO_2 corresponding to the quantity of 100 kg/m^3 of dolomite present in the mix had been previously subtracted. In both mixes increasing the hardening time increased the $CaCO_3$ content although in SCC-SF after 250 days this increase was much lower, because part of the $Ca(OH)_2$ took part in pozzolanic reactions. The correlation between the "$Ca(OH)_2$" and "H_2OTotal" columns in Table 5.6 has been calculated (without taking into account the value of "SCC-SF 250 days"). The equation ($y = 1.1128 \cdot x - 30.007$) obtained allows to calculate the theoretical amount of $Ca(OH)_2$ for "SCC-SF 250 days" in "$Ca(OH)_2$" column. The obtained value was 172.5. The difference between this value and the actual listed in Table 5.6 would be the amount of $Ca(OH)_2$ which has participated in pozzolanic reactions. Consequently, the total amount of $Ca(OH)_2$ present in the sample "SCC-SF 250 days" is significantly lower than would exist if there were not pozzolanic reactions. This is clearly shown in the column "$Ca(OH)_2$ Total", corresponding to the sum of the $Ca(OH)_2$ carbonated and non-carbonated, which has been calculated as the sum of columns "$Ca(OH)_2$" and "$CaCO_3$" previously transformed into $Ca(OH)_2$. In summary, in the case of SSC-RF an increase occurred in the curing time, although in the case of SCC-SF, at the first stage of hardening, the amount of portlandite formed increased and then decreased (250 days). This process may be due to reaction processes with the SF to form CSH (pozzolanic reaction).

The results coincide with the given data for the X-ray diffraction (DRX) technique (Figures 5.11 and 5.12). The main phases of SSC-SF are quartz (33-1161) [22] and portlandite (04-0733) [22], and to a lesser degree ettringite (41-1451) and albite (09-0466) [22], present in the four ages process, except for ettringite that disappears after 91 days of hardening. In SCC-RF, besides the previous phases, there is dolomite (36-0426) [22] and caminite ($M_{g3}(SO_4)_2(OH)_2$) (39-0359) [22]. Ettringite and portlandite behaved in the same way in both mixes but in advanced hardening stages the amount in portlandite is greater in SCC-RF than in SCC-SF, due to the pozzolanic

reaction which occurs between portlandite and SF. This agrees with the fact that in SCC-SF the greater weight loss, in the thermogravimetric study, is produced in the dehydration area (0-400 ºC), and in SCC-RF this weight loss occurs in the decarbonation area (460-750 ºC). It is concluded that the ageing mechanism of these mixes (SCC-SF and SCC-RF) is different. Finally, in the SSC-SF mix, portlandite undergoes processes of carbonation and pozzolanic reactions, and in the SCC-RF mix it only undergoes carbonation processes.

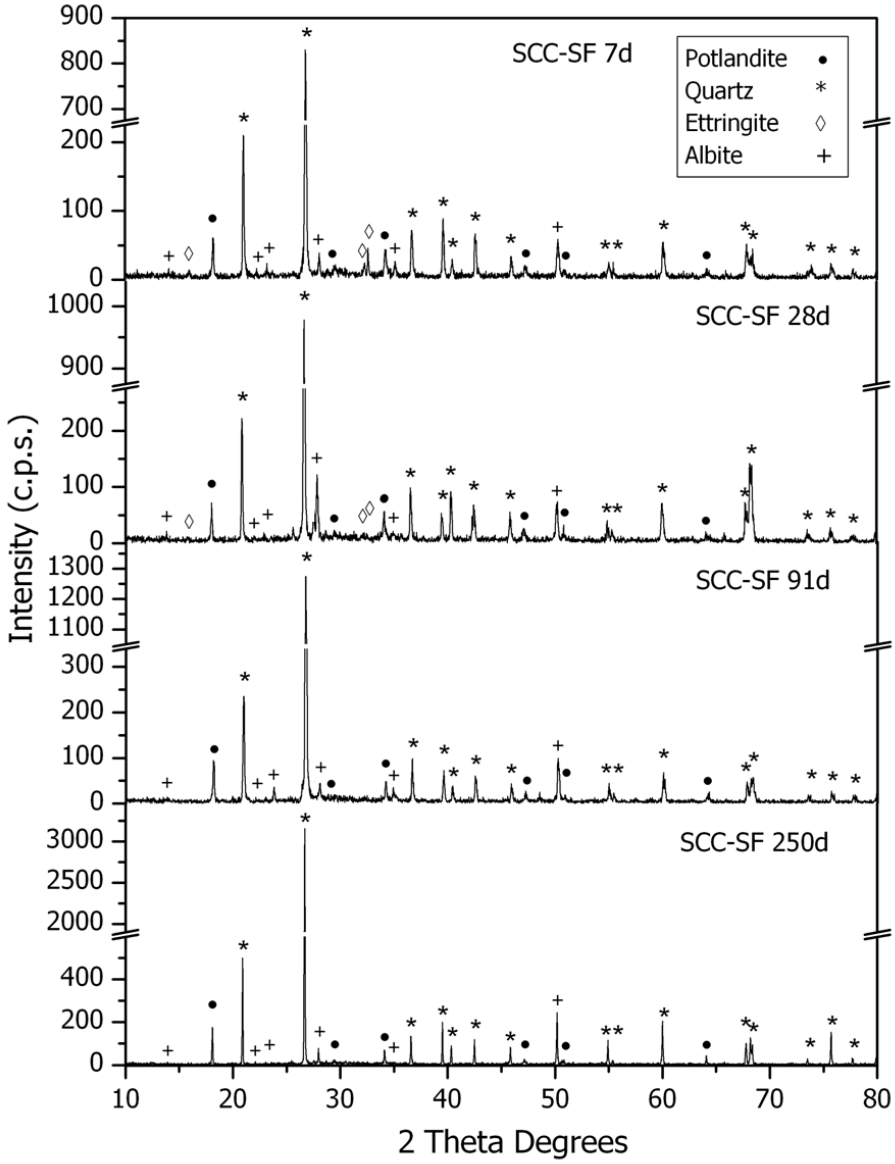

Figure 5.11: PXRD patterns for hardened SCC-SF at different ages.

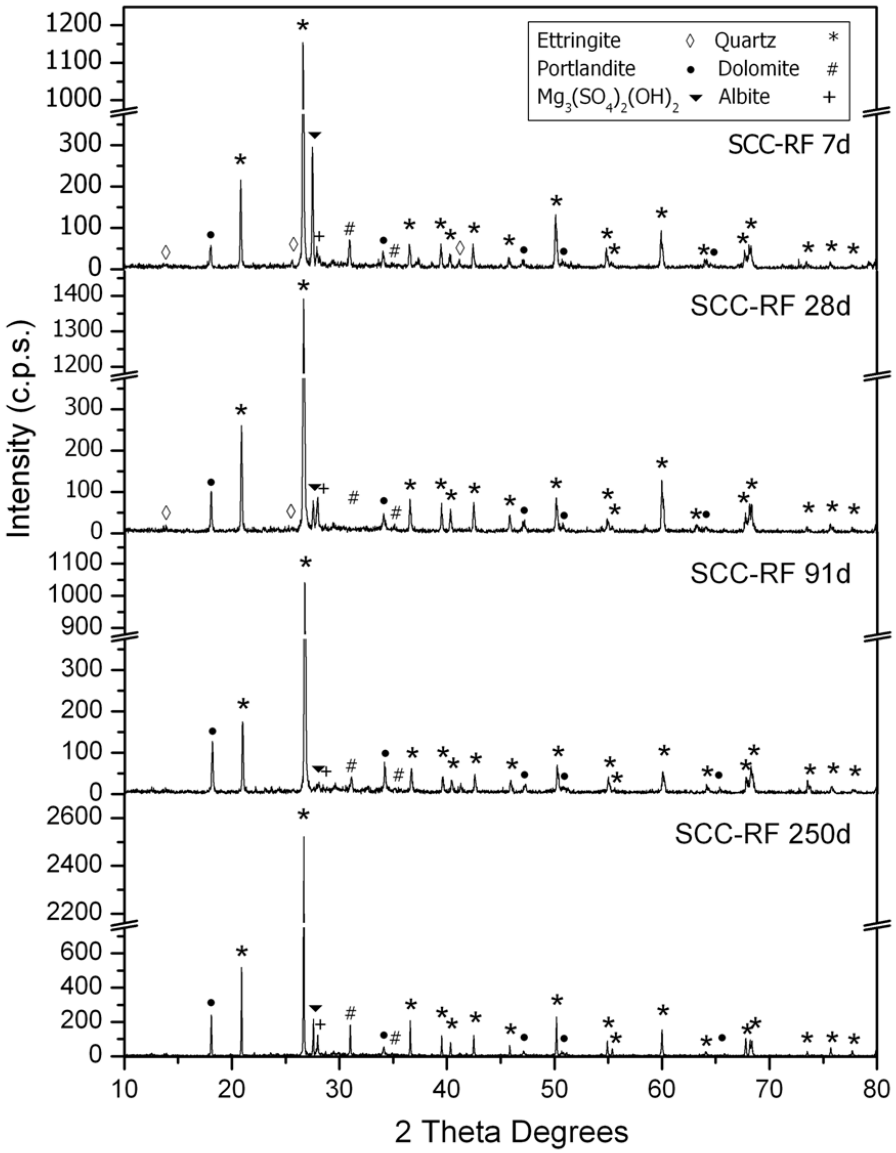

Figure 5.12: PXRD patterns for hardened SCC-RF at different ages.

5.3.2.2 Wet and dry density

The wet density of hardened concrete (measured after 28 days) gave similar values for SCC-SF (2.405 T/m^3) and SCC-RF (2.368 T/m^3), which is in accordance with the mix design aforementioned, consisting of replacing (in mass) a siliceous filler (SF) with a dolomitic one (RF) denser, resulting in less volume corrected with extra water

(Table 5.4). Ho et al. [43] obtained similar results for SCC samples with a similar composition as in our study. These values are very close to the fresh densities previously mentioned.

The difference between the dry density of both samples (oven dried at 105 ± 5 ºC up to constant mass) was similar to the differences for wet density, i.e. 2.267 T/m^3 and 2.239 T/m^3 for SCC-SF and SCC-RF, respectively. Comparing the wet and dry densities, both SCC-SF and SSC-RF lose 5% due to drying and corresponding to loss of free water. Bearing in mind that the SSC-RF mix has 17.91% of effective water and SSC-SF 17.58%, the water content for the mix with RF is slightly higher than that of the mix with SF. Consequently, the extra water incorporated in the mix will influence the mechanical strength. These results are in accordance with those obtained by Barbhuiya [48], who managed to reach higher densities for an SCC using dolomite powder as a filler that had a lower specific surface than the one utilized in our experiment.

5.3.2.3 Compressive strength

The compressive strength of SCC-RF is lower than that of SCC-SF for all curing ages (Figure 5.13).

The compressive strength at 7, 28, 91 and 250 days was: 42.28, 47.72, 54.49, and 63.41 MPa for SCC-SF and 27.19, 36.81, 42.05 and 49.28 MPa for SCC-RF. The highest difference in compressive strength between the mixes, approximately 35%, was observed at an early curing age (7 days). A similar behaviour was observed by Barbhuiya [48] in SCCs manufactured with fly ash or dolomite powder as filler. This delay in the hydration of SCC-RF can be attributed to the particles size of the RF filler (maximum at 35 µm) (Figure 5.3), which is quite larger than that of SF (maximum at 18 µm). Other authors attributed this to existing impurities in residual fillers, derived from combustion that feed the burners, causing its contamination in the drying process [20].

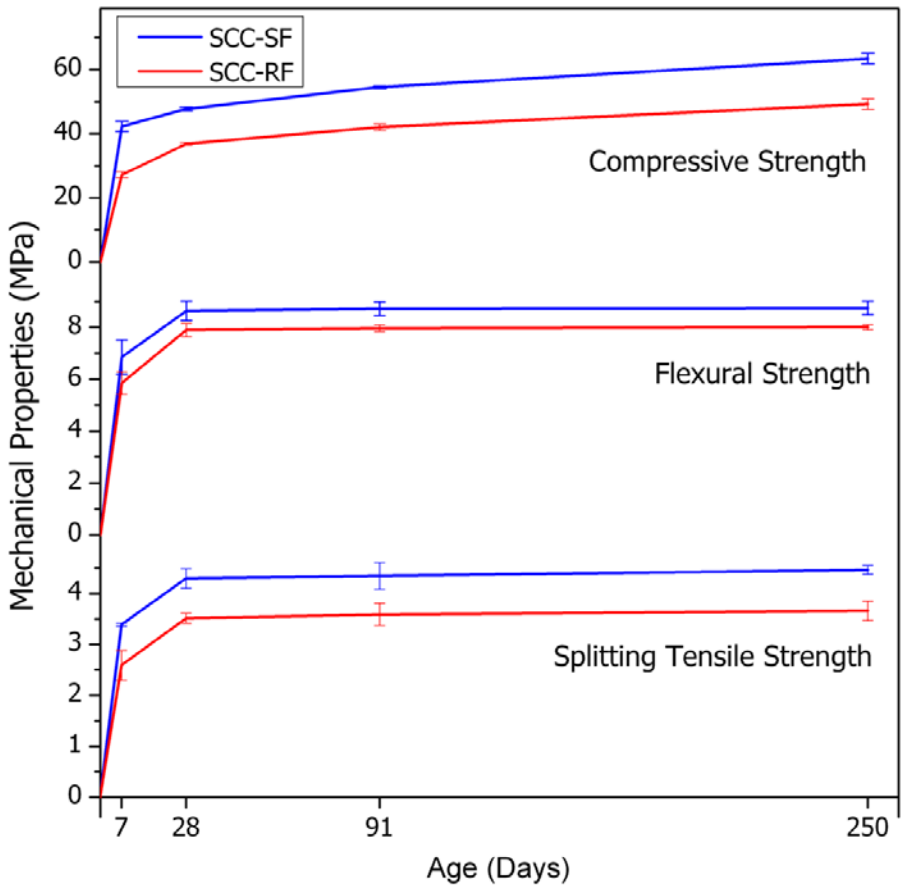

Figure 5.13: Mechanical properties of hardened SCCs.

After 28 days, for the SCC-RF mix, the increasing trend line for compressive strength shows a slope of 5.6%, whilst for SSC-SF it is 7.1%. The only difference between the two samples is the type of filler employed, so that the greater increase in mechanical strength of SSC-SF compared to SSC-RF is attributed to pozzolanic reactions [49-51] (70% of the SF particles showed a size between 3 µm 32 µm (Figures 5.2 and 5.3), which is appropriate for chemical interaction and is coherent with the greater decrease in $Ca(OH)_2$ in SCC-SF compared to SCC-RF, as seen in the TGA tests (Table 5.6). This behaviour is backed by the variation of intensity of the peaks corresponding to portlandite and quartz in the DRX patterns (Figures 5.11 and 5.12). Up to 91 days one notices a slight increase in this relation, which decreases in both samples after curing for 250 days. These results are supported by those obtained by Ho et al. [43] in SSCs using granite and limestone quarry dust of similar geometrical

and physicochemical characteristics. Felekoglu [44] obtained strengths of 30-40 MPa at 28 days in SCCs with similar characteristics to the SSC-RF mix, using high volumes of quarry limestone wastes and claiming that to achieve greater strength (45-50 MPa) the cement content should be increased. Moreover, Topçu et al. [6] designed a SCC with high strength after 28 days (> 50 MPa), using a similar cement content and a mixture of marble waste as filler and fly-ash as binder.

These results show that it is possible to use a residual filler derived from HMA and obtain compressive strength greater than the minimum levels required by the Spanish Instruction of Structural Concrete [21] for an HAC-30, by simply replacing siliceous filler with dolomite waste, according to the aforementioned material contents and methods (Table 5.4).

5.3.2.4 Splitting tensile strength

The determination of this parameter is useful as it can help in making decisions to reduce cracking problems, better assess shear strength and minimize cracking of concrete under tension [52].

The results of the splitting tensile strength test (Figure 5.13) show that the strength of SCC-SF is greater than that of SCC-RF at all testing ages. The strength at 7, 28, 90 and 250 days were 3.39, 4.30, 4.35 and 4.47 MPa for SCC-SF and 2.59, 3.53, 3.59 and 3.66 MPa for SCC-RF, respectively. Dehwah [53] obtained slightly higher results, adding a filler of limestone and fly ash and a lower water/cement ratio. By contrast, Parra et al. [54] and Felekoglu et al. [44] obtained similar values to those presented here for SCC-SF and SCC-RF using a limestone filler. At 7 days SCC-SF had a value 23% higher than SCC-RF, and for the remaining ages it decreased to 17%. This behaviour can be accounted for, as in compressive strength, by the difference in natural chemicals in the filler [55] and/or the distribution of the particles size, greater in RF, which hinders it acting as a centre for nucleation of the hydrated calcium silicates.

Figure 5.14 represents the relationship between splitting tensile strength and compressive strength and can be expressed by Eq. 5.1, with a value of $R^2 = 0.8293$.

$$f_{ci} = 0.0514\, f_c + 1.4011 \qquad \text{(Eq. 5.1)}$$

where f_{ci} is the splitting tensile strength and f_c is the compressive strength. This relationship is within the estimated limits in the CEB-FIB (Comité Euro-Internacional du Béton - International Federation for Structural Concrete) code.

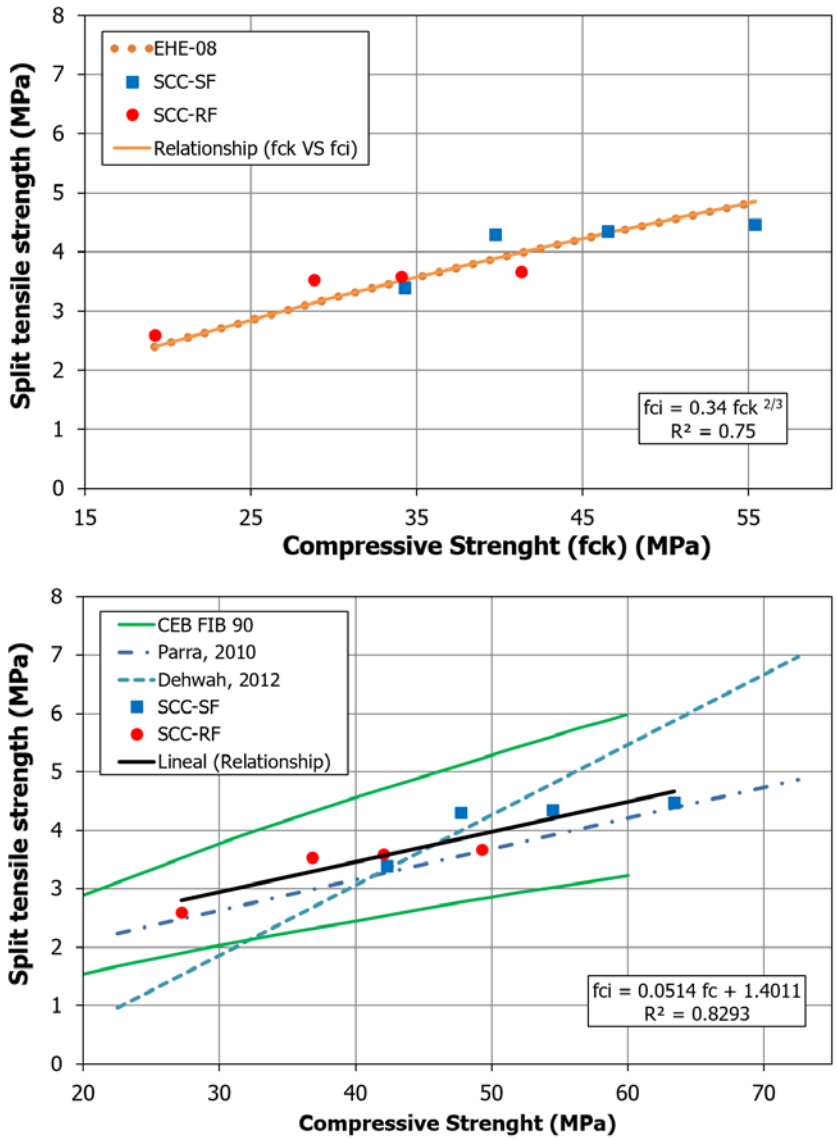

Figure 5.14: Compressive strength versus splitting tensile strength.

Table 5.7
Comparing the experimental results with those estimated using EHE-08 and other references.

Mixtures	Age (days)	Experimental			Estimated by EHE-08			Parra[a]	Correlation ratio			
		f_{ci} (MPa)	$f_{ct,fl}$ (MPa)	E_{cm} (GPa)	f_{ci} (MPa)	$f_{ct,fl}$ (MPa)	E_{cm} (GPa)	f_{ci} (MPa)	$f_{ci(EHE)}$	$f_{ct,fl(EHE)}$	$E_{cm(EHE)}$	$f_{ci(SCC)}$
SCC-SF	7	3.39	6.85		3.52	5.08		2.95	1	1.3		1.2
	28	4.30	8.64	37.5	3.88	6.45	30.8	3.26	1.1	1.2	1.2	1.3
	91	4.35	8.72	41.5	4.31	6.53	32.1	3.62	1	1.2	1.2	1.2
	250	4.47	8.75		4.84	6.70		4.07	0.9	1.2		1.1
SCC-RF	7	2.59	5.86		2.39	3.89		2.01	1.1	1.3		1.3
	28	3.53	7.90	34.2	3.13	5.30	28.3	2.63	1.1	1.3	1.2	1.3
	91	3.59	7.97	36.8	3.50	5.39	29.4	2.94	1	1.3	1.2	1.2
	250	3.66	8.01		3.98	5.50		3.34	0.9	1.3		1.1

[a] (Eq. 5.4)

EHE-08 [21] indicates the tensile strength, f_{ct}, can be calculated from the characteristic compressive strength (compressive strength - 8 MPa), f_{ck} (Eq. 5.2):

$$f_{ct} = 0.3\ f_{ck}^{2/3} \qquad \text{(Eq. 5.2)}$$

and the splitting tensile strength f_{ci} can be calculated from the tensile strength (Eq. 5.3). Parra et al. [54] proposed a modification (Eq. 5.4):

$$f_{ci\ (EHE\text{-}08)} = f_{ct} / 0.9 \qquad \text{(Eq. 3)}$$

$$f_{ci\ (SCC)} = 0.28\ f_{ck}^{2/3} \qquad \text{(Eq. 5.4)}$$

The correlation found in this work is quite close to the correlations proposed by the EHE-08 and by Parra et al. [54]. By contrast, it differs substantially from that proposed by Dehwah [53].

Table 5.7 shows the values for f_{ci} experimentally determined and calculated according to Eqs. 5.3 and 5.4, which are slightly below the experimental data. Therefore, it is concluded that the equation proposed by EHE-08 (Eq. 5.3) adjusts to the values obtained for the SCC in this study. In this case the correlation coefficients are close to 1. The modification proposed by Parra et al. (Eq. 5.4) leads to values slightly lower than the experimental values, with correlation ratios greater than 1, so that the safety margin is higher than that proposed by EHE-08.

5.3.2.5 Flexural strength

The values obtained for flexural strength, 6.85, 8.64, 8.72 and 8.75 MPa for SCC-SF and 5.86, 7.90, 7.97 and 8.01 MPa for SCC-RF after 7, 28, 90 and 250 days respectively, were greater in all cases for SCC-SF than for SCC-RF, as seen in Figure 5.13. Topçu et al. [6] obtained flexural strengths that were slightly higher than ours, due to the incorporation of fly ash along with marble dust. On the contrary, Dehwah [53] obtained results lower than ours. There is a greater difference at 7 days, approximately 14.5%. At other ages the difference in strength between the two mixes is reduced to approximately 8%, not varying significantly with curing time. This behaviour is similar to that observed under compressive strength and splitting tensile

strength. The lower flexural strength in SCC-RF compared to SCC-SF, at a young age, may be due to the size of the particles which are larger in RF (Figure 5.3), which hinders chemical interaction.

Figure 5.15 shows the relationship between flexural strength and compressive strength which can be expressed by Eq. 5.5 with a value of R^2 = 0.6901.

$$f_{fl} = 0.0763\, f_c + 4.3751 \quad \text{(Eq. 5.5)}$$

where f_{fl} is the flexural strength and f_c is the compressive strength. The relationship proposed here differs appreciably from that of Dehwah. [53].

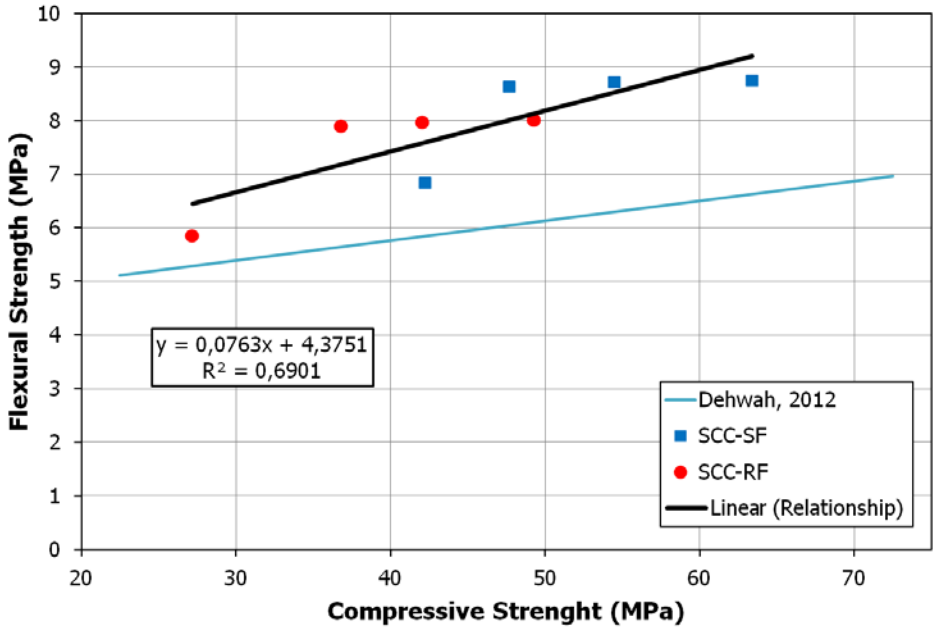

Figure 5.15: Compressive strength versus flexural strength.

EHE-08 [21] establishes that the values of flexural strength, $f_{ct,fl}$, can be calculated from those of splitting tensile strength using Eq. 5.6.

$$f_{ct,fl} = f_{ct} \frac{1+1.5\left(\frac{h}{100}\right)^{0.7}}{1.5\left(\frac{h}{100}\right)^{0.7}} \quad \text{(Eq. 5.6)}$$

where f_{ct} is the tensile strength obtained from the resistance to fracture deriving from splitting tensile strength (Eq. 5.3) and h is the height of the element in mm. The results obtained using Eq. 5.6 are collected in Table 5.7, all of which are lower than the experimental values; consequently, the correlation ratios are in all cases greater than 1, but experimental results are consistent with the validity of application of EHE-08 for SCC.

5.3.2.6 Static modulus of elasticity and Poisson ratio

The modulus of elasticity is an important property that influences the safety, serviceability and service life of concrete. The modulus of elasticity results for both types of concrete are shown in Figure 5.16. There is an increase of this parameter with curing time, SCC-RF having lower values than SSC-SF. This agrees with the compressive strength results abovementioned (Figure 5.13), where there is a slight increase in the trend line slope, between 28 and 250 days. This difference can be attributed to the differences in curing of the SCCs, which affects the density and stiffness in the ITZ. [56]. Parra et al. [54] obtained similar values for SCC-SF at both ages and higher for SCC-RF, which can be related to the different nature of the filler, limestone as opposed to dolomite (RF). By contrast, Felekoglu et al. [57] obtained lower values for similar w/c ratios, which may be attributed to the lower content of coarse aggregates used by these authors (600 kg/m^3 vs. 800 kg/m^3).

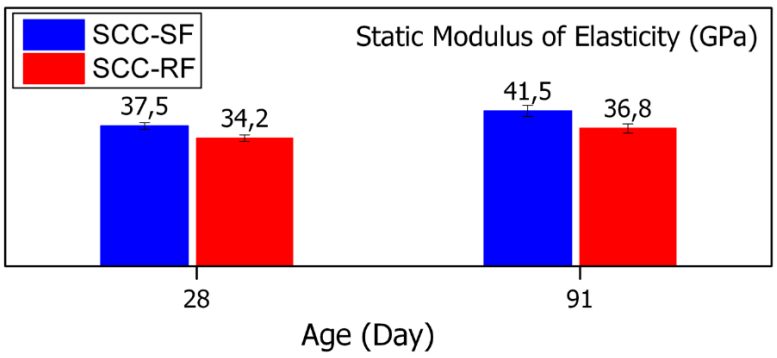

Figure 5.16: Static Modulus of Elasticity of hardened SCCs.

Figure 5.17 shows a lineal adjustment (Eq. 5.7) between modulus of elasticity and compressive strength, with a value of R^2 = 0.9113:

$$E_{cm} = 0.4943\ f_c + 15.626 \qquad \text{(Eq. 5.7)}$$

where f_c is the compressive strength and E_{cm} is the modulus for elasticity. The correlation is within the estimates of the CEB-FIB code.

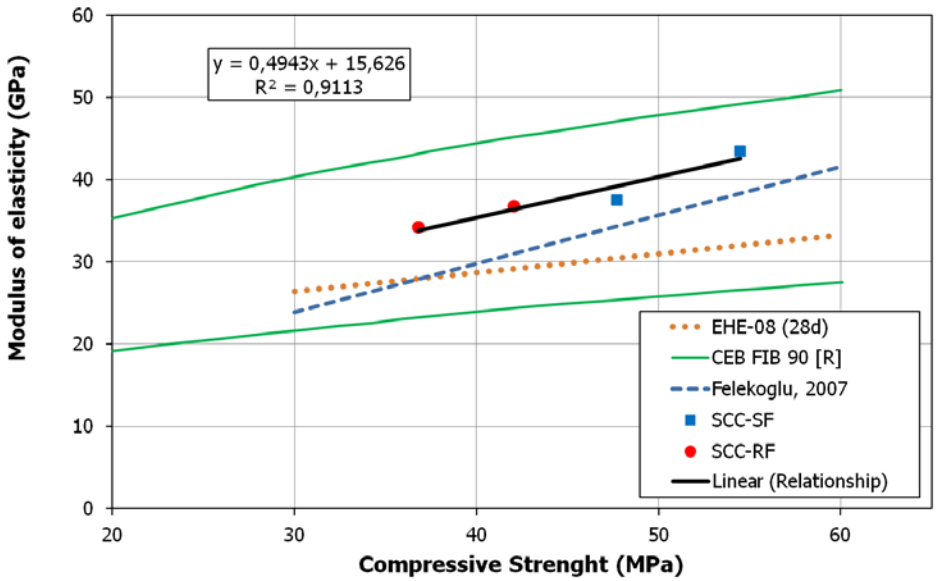

Figure 5.17: Compressive strength versus modulus of elasticity.

EHE-08 [21] determines the modulus of elasticity, E_{cm}, at 28 days, from the average compressive strength of concrete at 28 days (f_{cm}) using Eq. 5.8. It proposes another equation to determine the modulus of elasticity at ages different from 28 days (Eq. 5.9):

$$E_{cm} = \alpha\ 8500\ \sqrt[3]{f_{cm}} \qquad \text{(Eq. 5.8)}$$

$$Ec_m(t) = \alpha\ (f_{cm}(t)^{0.3}/f_{cm})\ E_{cm} \qquad \text{(Eq. 5.9)}$$

where α is the correcting coefficient to take into account the nature of the aggregates (in our case the value is 1, because concrete has been made with aggregates of average characteristics of the quartzite type), $E_{cm}(t)$ the modulus of elasticity at t days, and f_{cm} the average compressive strength, at 28 days. Eq. 5.8 is valid as long

as the stresses, under working conditions, are less than or equal to 0.40 fcm. Eq. 5.9 takes into account that the increase of modulus of elasticity with age is not equal to that of compressive strength.

The correlations proposed by EHE-08 and by Felekoglu et al. [57], although similar to those obtained in our study, lead to values below the experimental ones.

The values obtained from Eq. 5.8 and Eq. 5.9 are shown in Table 5.7 and in all cases they are below those obtained experimentally. There is a correlation ratio of 1.2, which demonstrates the validity of the application of EHE-08 for SCC, initially proposed for OC (Ordinary Concrete).

The coefficient of Poisson values, that provide information on the elastic deformation under normal stresses, were 0.18 and 0.15 for SCC-SF and 0.21 and 0.19 for SCC-RF at 28 and 91 days respectively. These values are close to those specified by the Spanish Code on Structural Concrete (EHE-08), which proposes as reference value 0.2.

5.3.2.7 UPV test

The Ultrasonic Pulse Velocity (UPV) test enables indirectly determining the strength of concrete by relating it to its compacity and density [58]. The values obtained were 4.67, 4.70, 4.91 and 4.93 km/s for SCC-SF and 4.55, 4.60, 4.64 and 4.86 km/s for SCC-RF, measured at 7, 28, 91 and 250 days respectively. There is an increase in the propagation speed as the curing time increases and greater values for SCC-SF than for SCC-RF. This increase is related to gains in compacity and compressive strength.

Figure 5.18 shows a good correlation (R^2 = 0.8634) between propagation speed and compressive strength when curing time increases and can be expressed by Eq. 5.10.

$$UPV = 0.0124\ f_c + 4.171 \qquad \text{(Eq. 5.10)}$$

where UPV is the ultrasonic pulse velocity and fc is the compressive strength. The correlation proposed in this study differs from that proposed by Dehwah [53].

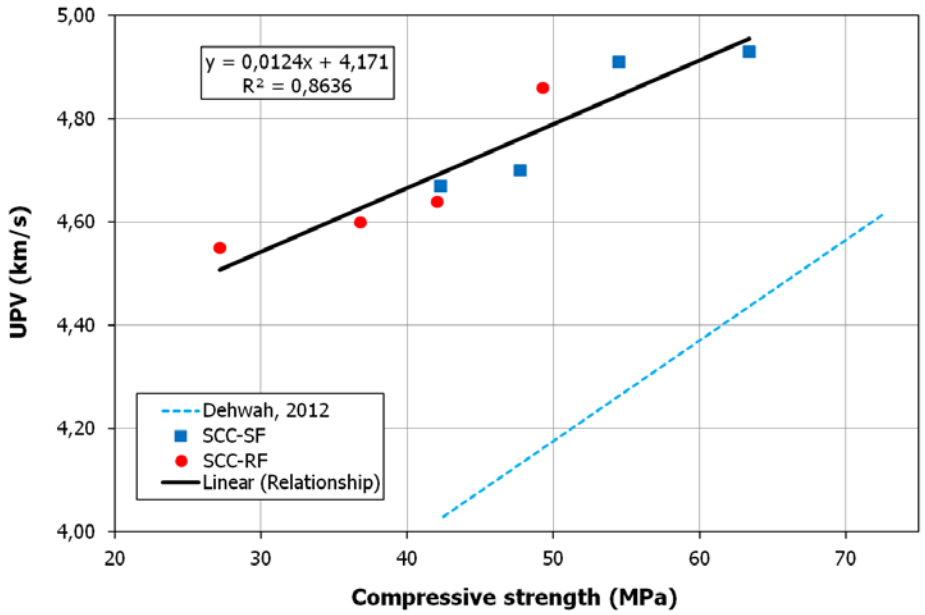

Figure 5.18: Compressive strength versus ultrasonic pulse velocity.

Furthermore, the lower strength of SCC-RF is explained by the reduction effect of the potential binder material and its lower fineness [59, 60]. These results agree with those of other authors who detected a decrease in the UPV with the use of mineral additions with greater particles size [61, 62]. According to the UPV-based criteria proposed by Whitehurst [63], both SCCs can be classified as excellent (>4.5 km/s).

5.3.2.8 Shrinkage

Shrinkage is a complex phenomenon that depends on many factors: temperature and humidity, size of the element, type and content of cement and filler, w/c ratio, size distribution and mineralogical composition of the aggregates, concrete strength, mixing and curing methods, concrete age at the end of curing, and many other factors [64]. A detailed discussion on all those factors is beyond the scope of this paper.

The results of total shrinkage strain, -139, -165, -241 and -343 μ for SCC-SF and -93, -142, -212 and -316 μ for SCC-RF after 7, 14, 28 and 91 days respectively, are shown in Table 5.8. These values are in the lower range those Guneyisi et al. [65]. These authors used a higher amount of binders and fly ash and silica fume as filler (pozzolanic fillers). Consequently, they obtained higher values of shrinkage.

Valcuence et al. [12] obtained higher values of shrinkage using lesser sand content and fly ash as filler. The results obtained in the current paper are close than those obtained by Heirman et al [66] who used limestone powder as filler.

Table 5.8
Total shrinkage.

	Age (days)	SCC-SF	SCC-RF
Total shrinkage strain (μ)	7	-139	-93
	14	-165	-142
	28	-241	-212
	91	-343	-316

Shrinkage was higher for SCC-SF. This can be due to the greater reactivity of SCC-SF relative to SCC-RF. The particle size of SF is lower, around 18 μm, while for RF it is 35 μm (Figure 5.3). The smaller particle size of SF filler in SCC-SF influences the evolution of this property, all the retained water in the porous structure is used to hydrate the cement completely, which agrees with the greater density and mechanical strength of SCC-SF.

Therefore, under normal curing conditions, there is a lower shrinkage in SCC-RF, mainly due to a greater particle size. In short, the SCC produced with recovery filler from plants manufacturing hot-mix asphalt (HMA), SCC-RF, should have better performance than SCC-SF in terms of shrinkage and early appearance of cracks.

5.4 Conclusions

The aim of this paper is the assessment of the feasibility of the fine grain waste, generated in the drying and heating process of aggregates in hot-mix asphalt (HMA) manufacturing plants, as a construction material. This powder is named "recovery filler" (RF).

A comparative study of two types of SCC has been carried out, the first one made with recovery filler (SCC-RF) of dolomitic nature and the second one with commercial siliceous filler (SCC-SF), utilized as reference.

The self-compactability tests show reproducibility. SCC-RF presents values closer to the limit set by EHE-08.

The density of SCC-RF (2.365 T/m^3) in the fresh state is slightly less than that of SCC-SF (2.392 T/m^3), which is related to the lower content of RF filler by volume and higher content of water present in the SCC-RF mixes.

The thermogravimetric study shows that in SCC-SF the higher loss weight occurs in the dehydration zone (0-400 ºC) and in SCC-RF it occurs in the decarbonation area (550-735 ºC). The aging mechanism of the mixes is different. In SCC-SF, portlandite undergoes carbonation processes and pozzolanic reactions and in SCC-RF it only undergoes carbonation processes. This results in a steady increase in the amount of portlandite formed with the setting time for SCC-RF. For SCC-SF, the amount of portlandite formed increases with the setting time in a first stage and then decreases (at 250 days).

The compressive strength, splitting tensile strength, flexural strength, and static modulus of elasticity of SCC produced with RF (SCC-RF) are lower than those of SCC produced with SF (SCC-SF), for all ages. The differences were higher at an early age and are related to a delay in hydration of SCC-RF because the particle size of the RF filler (maximum at 35 µm) is much greater than that of SF (maximum at 18 µm) which hinders it acting as nucleation centre of hydrated calcium silicates.

The splitting tensile strength, flexural strength and static modulus of elasticity values calculated using EHE-08 are lower than those obtained experimentally, i.e. the correlation ratios are in most cases greater than 1. So, the experimental results show the validity of using EHE-08, initially proposed for OC (Ordinary Concrete), in SCC.

There is an increase in ultrasonic pulse velocity relative to curing age and the values for SCC-SF are greater than for SCC-RF, which can be attributed to the increase in compacity and compressive strength.

In the curing conditions of this study there is a lower shrinkage in SCC-RF initially due to the larger size of particles. In short, the SCC produced with recovery filler from

plants manufacturing hot-mix asphalt (SCC-RF) should have better performance than SCC-SF in terms of shrinkage and early appearance of cracks.

One may conclude therefore, that it is possible to obtain an SCC, by replacing (in mass) a natural siliceous filler (SF) with a dolomite waste from plants of hot-mix asphalt (RF) with very slight changes in cement (0.5%) and water (1%) content in order to maintain constant the volume of the mix (1025 L) and obtain compressive strength greater than the minimum levels stipulated by the Spanish Code on Structural Concrete (EHE-08).

5.5 Acknowledgements

This work was partly supported by the Andalusian Regional Government (Research Groups FQM-214 and TEP-227). A. Romero Esquinas also acknowledges funding from MECD (http://www.mecd.gob.es/educacion-mecd/) FPU-13/04030. The authors wish to thank the staff at the Electron Microscopy and Elemental Analysis units of the Central Research Support Service (SCAI) of the University of Cordoba for technical assistance. The authors wish to thank the Fine Chemistry Institute of the University of Córdoba for technical support. The authors wish to thank the Research Plan of the University of Cordoba (2016). The authors wish to thank the Andalusian Innovation Centre for Sustainable Construction (CIAC) the use of the press IBERTEST, model MEH-3000. The authors wish to thank the National Radioactive Waste Company (ENRESA) for Contract of Research 079000146. The authors wish to thank Basf Chemical Company for additive, Glenium 303 SCC, supplied and Portland Valderrivas (Alcalá de Guadaira, Sevilla) for cement, CEM I 42.5 R/SR, supplied. The support of the CERIS-ICIST Research Institute, IST, University of Lisbon, and of FCT (Foundation for Science and Technology) is also acknowledged.

5.6 References

[1] K. Celik, C. Meral, A.P. Gursel, P.K. Mehta, A. Horvath, P.J. Monteiro, Mechanical properties, durability, and life-cycle assessment of self-consolidating concrete mixtures made with blended portland cements containing fly ash and limestone powder, Cement and Concrete Composites 56 (2015) 59-72.

[2] J. Moya, N. Pardo, A. Mercier, Energy efficiency and CO2 emissions: Prospective scenarios for the Cement industry, Publications Office2010.

[3] European Federation of National Associations Representing producers and applicators of specialist building products for Concrete (EFNARC). The European guidelines for self-compacting concrete specification. Production and Use. Hampshire, UK; (2005), www.efnarc.org.

[4] K.E. Alyamaç, R. Ince, A preliminary concrete mix design for SCC with marble powders, Construction and Building Materials 23(3) (2009) 1201-1210.

[5] M. Tennich, A. Kallel, M.B. Ouezdou, Incorporation of fillers from marble and tile wastes in the composition of self-compacting concretes, Construction and building materials 91 (2015) 65-70.

[6] I.B. Topcu, T. Bilir, T. Uygunoğlu, Effect of waste marble dust content as filler on properties of self-compacting concrete, Construction and Building Materials 23(5) (2009) 1947-1953.

[7] M.F. Granata, Pumice powder as filler of self-compacting concrete, Construction and Building Materials 96 (2015) 581-590.

[8] P. Da Silva, J. de Brito, Experimental study of the porosity and microstructure of self-compacting concrete (SCC) with binary and ternary mixes of fly ash and limestone filler, Construction and Building Materials 86 (2015) 101-112.

[9] M.H.W. Ibrahim, N.E.Z. Abidin, N. Jamaluddin, K. Kamaruddin, A.F. Hamzah, Bottom ash–potential use in self-compacting concrete as fine aggregate, (2006).

[10] E.E. Ali, S.H. Al-Tersawy, Recycled glass as a partial replacement for fine aggregate in self compacting concrete, Construction and Building Materials 35 (2012) 785-791.

[11] H. Zhao, W. Sun, X. Wu, B. Gao, The properties of the self-compacting concrete with fly ash and ground granulated blast furnace slag mineral admixtures, Journal of Cleaner Production 95 (2015) 66-74.

[12] M. Valcuende, F. Benito, C. Parra, I. Miñano, Shrinkage of self-compacting concrete made with blast furnace slag as fine aggregate, Construction and Building Materials 76 (2015) 1-9.

[13] M. Mishra, K. Panda, An Experimental Study on Fresh and Hardened Properties of Self Compacting Rubberized Concrete, Indian Journal of Science and Technology 8(29) (2015).

[14] S. Hesami, I.S. Hikouei, S.A.A. Emadi, Mechanical behavior of self-compacting concrete pavements incorporating recycled tire rubber crumb and reinforced with polypropylene fiber, Journal of Cleaner Production 133 (2016) 228-234.

[15] Y. Ghernouti, B. Rabehi, T. Bouziani, H. Ghezraoui, A. Makhloufi, Fresh and hardened properties of self-compacting concrete containing plastic bag waste fibers (WFSCC), Construction and Building Materials 82 (2015) 89-100.

[16] N. Ozerkan, D. Tokgoz, O. Kowita, S. Antony, Assessments of the Microstructural and Mechanical Properties of Hybrid Fibrous Self-Consolidating Concretes using Ingredients of Plastic Wastes, Nature Environment & Pollution Technology (2016).

[17] H. MOHAMMADHOSSEINI, A.A. AWAL, A.H. EHSAN, Influence of palm oil fuel ash on fresh and mechanical properties of self-compacting concrete, Sadhana 40(6) (2015) 1989-1999.

[18] N. Ranjbar, A. Behnia, B. Alsubari, P.M. Birgani, M.Z. Jumaat, Durability and mechanical properties of self-compacting concrete incorporating palm oil fuel ash, Journal of Cleaner Production 112 (2016) 723-730.

[19] EAPA. Asphalt in figures, 2014. European Asphalt Pavement Association (2016).

[20] J. Martin, J.R. Montero, F. Moreno, J.P. Sala, M. Rubio, Feasibility analysis of the reuse of waste filler of bituminous mixtures for the production of self-compacting concrete, Materials & Design 46 (2013) 372-380.

[21] EHE-08. Spanish Structural Concrete Code EHE-08 [Instrucción de Hormigón Estructural EHE-08]. R.D. 1247/2008, Spain (2008).

[22] P. Swarthmore, Joint Committee on Power Diffraction Standard-International Centre for Diffraction Data. (1995).

[23] Asociación Española de Normalización y Certificación, AENOR, Madrid, Spain, (2016).

[24] D.P. Bentz, C.J. Haecker, An argument for using coarse cements in high-performance concretes, Cement and Concrete Research 29(4) (1999) 615-618.

[25] J.M. Pommersheim, Effect of particle size distribution on hydration kinetics, MRS Proceedings, Cambridge Univ Press, 1986, p. 301.

[26] S. Tsivilis, S. Tsimas, A. Benetatou, E. Haniotakis, Study on the contribution of the fineness on cement strength, (1990).

[27] J. Ji, Y. Ge, W. Balsam, J.E. Damuth, J. Chen, Rapid identification of dolomite using a Fourier Transform Infrared Spectrophotometer (FTIR): A fast method

for identifying Heinrich events in IODP Site U1308, Marine Geology 258(1) (2009) 60-68.

[28] T. Vazquez-Moreno, M.T. Blanco-Varela, Tabla de frecuencias y espectros de absorción infrarroja de compuestos relacionados con la química del cemento, Materiales de Construcción 31(182) (1981) 31-48.

[29] J.L. García Calvo, M. Sánchez Moreno, M.C. Alonso Alonso, A. Hidalgo López, J. García Olmo, Study of the Microstructure Evolution of Low-pH Cements Based on Ordinary Portland Cement (OPC) by Mid-and Near-Infrared Spectroscopy, and Their Influence on Corrosion of Steel Reinforcement, Materials 6(6) (2013) 2508-2521.

[30] T. Nguyen, L.J. Janik, M. Raupach, Diffuse reflectance infrared Fourier transform (DRIFT) spectroscopy in soil studies, Soil Research 29(1) (1991) 49-67.

[31] V.C. Farmer, Infrared spectra of minerals, Mineralogical Society (1974).

[32] http://www.master-builders-solutions-basf.es).

[33] G. Azeredo, M. Diniz, Self-compacting concrete obtained by the use of kaolin wastes, Construction and Building Materials 38 (2013) 515-523.

[34] J. Cuenca, J. Rodríguez, M. Martín-Morales, Z. Sánchez-Roldán, M. Zamorano, Effects of olive residue biomass fly ash as filler in self-compacting concrete, Construction and Building Materials 40 (2013) 702-709.

[35] R. Deeb, A. Ghanbari, B.L. Karihaloo, Development of self-compacting high and ultra high performance concretes with and without steel fibres, Cement and concrete composites 34(2) (2012) 185-190.

[36] Contract of Research 079000146, Development of self-compacting concretes for use in the facilities of El Cabril, Empresa Nacional de Residuos Radiactivos (ENRESA). 2012-2014

[37] European Federation of National Associations Representing producers and applicators of specialist building products for Concrete (EFNARC). Specification and guidelines for self-compacting concrete, Hampshire, UK; 2002, www.efnarc.org.

[38] S. Brunauer, P.H. Emmett, E. Teller, Adsorption of gases in multimolecular layers, Journal of the American chemical society 60(2) (1938) 309-319.

[39] American Society of Testing Materials, ASTM International, West Conshohocken, USA, (2016).

[40] N. Nagamoto, K. Ozawa, Mixture properties of self-compacting, high-performance concrete, Special Publication 172 (1999) 623-636.

[41] K. Khayat, Workability, testing, and performance of self-consolidating concrete, Materials Journal 96(3) (1999) 346-353.

[42] R.M.S. Ferreira, "Self-compacting concrete: design methodology", Master dissertation in Civil Engineering (Construction Materials), (2001), Minho University, Guimarães, Portugal.

[43] D. Ho, A. Sheinn, C. Ng, C. Tam, The use of quarry dust for SCC applications, Cement and Concrete Research 32(4) (2002) 505-511.

[44] B. Felekoglu, Utilisation of high volumes of limestone quarry wastes in concrete industry (self-compacting concrete case), Resources, Conservation and Recycling 51(4) (2007) 770-791.

[45] A.W. Saak, Characterization and modeling of the rheology of cement paste: with applications toward self-flowing materials, 2000.

[46] X. Zhang, F. Glasser, K. Scrivener, Reaction kinetics of dolomite and portlandite, Cement and Concrete Research 66 (2014) 11-18.

[47] G. Ye, X. Liu, G. De Schutter, A.-M. Poppe, L. Taerwe, Influence of limestone powder used as filler in SCC on hydration and microstructure of cement pastes, Cement and Concrete Composites 29(2) (2007) 94-102.

[48] S. Barbhuiya, Effects of fly ash and dolomite powder on the properties of self-compacting concrete, Construction and Building Materials 25(8) (2011) 3301-3305.

[49] J. Gibbs, W. Zhu, Strength of hardened self-compacting concrete, Proceedings of First international RILEM Symposium on Self-Compacting Concrete (PRO 7), Stockholm, Suede, 1999, pp. 199-209.

[50] Fernández Rodríguez J.M., "Introducción a los Cementos", Servicio de Publicaciones Universidad de Córdoba (2004), ISBN 84-7801-731-3.

[51] F. Puertas, T. Vázquez, Early hydration cement Effect of admixtures superplasticizers, Materiales de construcción 51(262) (2001) 53-61.

[52] R. Siddique, P. Aggarwal, Y. Aggarwal, Influence of water/powder ratio on strength properties of self-compacting concrete containing coal fly ash and bottom ash, Construction and Building Materials 29 (2012) 73-81.

[53] H. Dehwah, Mechanical properties of self-compacting concrete incorporating quarry dust powder, silica fume or fly ash, Construction and building materials 26(1) (2012) 547-551.

[54] C. Parra, M. Valcuende, F. Gomez, Splitting tensile strength and modulus of elasticity of self-compacting concrete, Construction and Building materials 25(1) (2011) 201-207.

[55] P. Domone, A review of the hardened mechanical properties of self-compacting concrete, Cement and Concrete Composites 29(1) (2007) 1-12.

[56] W. Zhu, P.J. Bartos, Microstructure and properties of interfacial transition zone in SCC, Proceedings of First International Symposium on Design Performance and use of Self Consolidating Concrete, RILEM Publications SARL, Changsha, 2005, pp. 319-27.

[57] B. Felekoğlu, S. Türkel, B. Baradan, Effect of water/cement ratio on the fresh and hardened properties of self-compacting concrete, Building and Environment 42(4) (2007) 1795-1802.

[58] G. Trtnik, F. Kavčič, G. Turk, Prediction of concrete strength using ultrasonic pulse velocity and artificial neural networks, Ultrasonics 49(1) (2009) 53-60.

[59] M. Heikal, H. El-Didamony, M. Morsy, Limestone-filled pozzolanic cement, Cement and Concrete Research 30(11) (2000) 1827-1834.

[60] M. Szybilski, W. Nocuń-Wczelik, The Effect of Dolomite Additive on Cement Hydration, Procedia Engineering 108 (2015) 193-198.

[61] M. Şahmaran, H.A. Christianto, İ.Ö. Yaman, The effect of chemical admixtures and mineral additives on the properties of self-compacting mortars, Cement and concrete composites 28(5) (2006) 432-440.

[62] M. Uysal, K. Yilmaz, Effect of mineral admixtures on properties of self-compacting concrete, Cement and Concrete Composites 33(7) (2011) 771-776.

[63] E.A. Whitehurst, Soniscope tests concrete structures, Journal Proceedings, 1951, pp. 433-444.

[64] A.P.M. Šahinagić-Isović, M. Šahinagić-Isović, G. Markovski, M. Ćećez, Shrinkage strain of concrete-causes and types, Građevinar 64(09.) (2012) 727-734.

[65] E. Güneyisi, M. Gesoğlu, E. Özbay, Strength and drying shrinkage properties of self-compacting concretes incorporating multi-system blended mineral admixtures, Construction and Building Materials 24(10) (2010) 1878-1887.

[66] G. Heirman, L. Vandewalle, D. Van Gemert, V. Boel, K. Audenaert, G. De Schutter, B. Desmet, J. Vantomme, Time-dependent deformations of limestone powder type self-compacting concrete, Engineering Structures 30(10) (2008) 2945-2956.

Capítulo 6

Durability of self-compacting concrete made with recovery filler from hot-mix asphalt plants

"A.R. Esquinas, J.I. Álvarez, J.R. Jiménez, J.M. Fernández, J. de Brito, Durability of self-compacting concrete made with recovery filler from hot-mix asphalt plants, Construction and Building Materials, 161 (2018) 407–419. doi:10.1016/ J.CONBUILDMAT.2017.11.142."

Abstract

In construction, there is a need to respond to environmental challenges and implement the Circular Economy as a strategy for the sustainable growth of the sector.

To eliminate the lack of confidence in the application of the waste from this sector, it is necessary to carry out research in order to achieve an effective and integral management, as well as the reuse and recycling of these materials.

In this work, a detailed study of Self-Compacting Concrete (SCC) was carried out, using as filler a waste from the drying process of the aggregate used in the manufacture of hot-mix asphalt. The results showed that it is possible to obtain a

high-performance SCC in terms of durability by replacing a commercial siliceous filler (SF) with this dolomitic residual powder (RF), with high performance against the attack of aggressive agents (chloride, sulphate and carbonate ions) and shrinkage.

In this study the analysis of the physical parameters of the materials (density, open porosity and pore size distribution as obtained from mercury intrusion porosimetry) and water absorption (by immersion and capillarity) was fundamental. The joint analysis of all the studied parameters allowed obtaining exhaustive results about the durability of the mixes and its interrelation with the properties of the constituents.

Key words: Self-compacting concrete; durability; waste; hot-mix asphalt plants

Highlights:

- A durability-related comparative study of two SCCs was carried out.
- The porous structure of SCC-RF is less fine than that of SCC-SF.
- Both SCCs could be used in aggressive environments in terms of water absorption.
- The mixes have a good performance regarding chloride and sulphate ions penetration.
- The penetration depth of CO2 is related with the porosity and the curing mechanism.
- SCC-RF showed better features than SCC-SF in long-terms shrinkage.

6.1 Introduction

Currently there is a great global need for promoting the integrated productivity of all economic sectors in order to accomplish the optimisation of natural resources, as well as the minimisation and valorisation of waste materials, thus responding to environmental challenges. This is the basis of a circular economy, a concept that arose in 1981, when Stahel & Reday [1] designed a circular economic-productive system in which the comprehensive efficiency of productive processes was the strategy for sustainable industrial growth, an idea that began to gain strength in current world politics. In the particular case of the European Union, it is being carried out by means of the Plan of Action for the Implementation of the Circular Economy

of the European Parliamentary Commission (COM(2017)33) [2], where global actions and commitments, as well as priority sectors, are presented and among which the construction industry plays a major role due to the large amount of waste generated therein. Within this sector, concrete is of particular importance, as it is the most used construction material worldwide (4 tonnes per person) and the one that consumes more natural resources [3, 4].

Innovation in the construction sector, and in particular in the concrete industry, is fundamental for sustainability to be part of the productive system. Arguably the most relevant innovation occurred in the 1980's, when Okumara designed a concrete, called self-compacting concrete (SCC), capable of flowing by just its own weight and compacting without the need of vibration, filling complex areas with a high density of reinforcement bars, thus achieving a high level of homogenisation and better surface finish. Compared to the current technology (ordinary concrete), these characteristics resulted in advantages, such as time and money savings, allowing complex forms in structural design, better surface finishes, fewer work hazards and less noise pollution [5].

Research is the most potent means to accomplish real and integrated management of construction and demolition waste throughout the industry, due to the fact that reusing and recycling this waste is not being fully implemented, the main obstacle being there is a lack of trust in such materials. The 2008/98/CE framework directive establishes the year 2020 as a time-limit for waste recovery in this sector to reach 70%.

Several lines of research have started working towards this goal, developing construction materials that incorporate waste from different industrial processes [6-10]. In the field of SCC in particular, there is a strong line of research focused on the use of fine grain waste (powder) as a substitute for resources such as cement or fine sand, which are indispensable to achieve the potential advantages of SCC. As accumulated knowledge about the mechanical behaviour and durability of these new materials increases, it will be possible to attain an even greater reliance on them compared to those in current use. Tennich et al. [11] obtained SCC made of industrial and construction waste (marble and tile waste) with greater resistance than ordinary

concrete regarding sulphate attack. Sua-Iam & Makul [12] observed the great potential of incinerated sugarcane filter cake for use in SCC, by getting good results in workability and good mechanical performance for substitutions of 10-20% cement, although the strength was lower than that of the reference mixes (made of cement only). Felekoglu [13] and Alyamaç et al. [14] obtained good results in SCC, excellent surface finishes and high mechanical strength by using fine grain mineral waste, such as fine sand and/or filler. Singh & Siddique [15] carried out a study of SCC durability using iron slag as a substitute for fine sand (at 10%, 25% and 40%) improving aspects such as water absorption, permeability to chloride ion and density of the SCC microstructure. Valcuende et al. [16] replaced sand with blast furnace slag in SCC mixes and observed an increase in the mechanical strength due to the waste's reactivity, resulting in greater shrinkage, as well as finer porous structure. Uysal et al. [17, 18] carried out an evaluation of the effectiveness of several waste materials used as mineral additions in SCC production, concluding that limestone filler could be replaced by wastes such as basalt powder, marble powder, fly ash or blast furnace slag. Kapoor et al. [19] improved the permeability and resistance to chloride penetration of SCC made with recycled sand by means of the incorporation of mineral additions such as silica fume or metakaolin. Alsubari et al. [20] came to the conclusion that the use of treated palm oil fuel ash improved the SCC properties, in terms of self-compactability and mechanical behaviour, shrinkage and resistance to chemical attack in acidic environments.

In this study, fine grain waste filler recovered from hot-mix asphalt plants (HMA) was used as a construction material. This powder is produced during the drying and heating of sands used in the manufacture of HMA. The waste (recovery filler, RF) is retained in pipe filters and separated from the gases generated in the drying process (combustion and water gases). Part of this waste is stored in silos for later use in the manufacturing of HMA, limited to an application of 3-4%. The remainder used to be taken to dumps or quarries, which is no longer legally viable. According to the Council of Europe Decision 2003/33/EC, in certain situations this waste cannot be classified as inert, due to it being in direct contact with burner fuel. The generation of this waste is estimated at 4% in weight of HMA production (over 700 million annual tonnes), and in Spain the production of asphalt mixes is over 16 million tonnes (in 2015) [21].

This waste could be reused in applications where fine grain materials are necessary, as in the case of SCC, which require large volumes of them. This would optimise natural resources, save energy, reduce material costs and the amount of waste to be managed.

The use of this waste as filler in SCC has been partially studied by Martin et al. [22] and Esquinas et al. [23], although not its behaviour in terms of durability. This aspect is fundamental in order to resolve the uncertainties regarding its long-term viability, which would enable this industrial sub-product (RF) to be valued and therefore minimise its environmental impact and contribute to making more environmental-friendly concrete.

For this purpose, an analysis of the viability of RF as a filler in SCC has been carried out, including a comparative study of the durability of two types of SCC, one using RF and the other, used as reference, a commercial silicate filler (SF). Firstly, the self-compactibility properties of both SCCs were defined, and then the microstructural properties and their influence on durability were analysed. The work was completed with a study of long-term shrinkage.

6.2 Experimental methodology

6.2.1 Materials

The aggregates used, gravel 4/16, coarse sand 0/4 and fine sand 0/2 (G, S1 and S2 respectively), are of siliceous nature, coming from the crushing plant of company Áridos Gallardo S.L. (Badajoz, Spain). The fine sand accused the presence of quartz as well as orthoclase and albite. A physico-chemical characterisation was carried out by Esquinas et al. [23]. These sands are apt for manufacturing concrete according to EHE-08 [23].

Two types of filler were used; a commercial one (SF), from crushing fine sands supplied by Minas Carmina (Gerona, Spain); the other (RF) from waste powder from asphalt mixture sands supplied by PAMASA (Málaga, Spain). Figure 6.1 shows that

silicate (33-1161) [24] is the only phase present in SF and dolomite (36-0426) [24] in RF, which agrees with the thermogravimetric analysis and data for X-ray dispersive energy [23]. The pore size distribution was obtained from the nitrogen adsorption-desorption isotherms (Figure 6.2), showing pores between 3 and 110 nm for both fillers, calculated from the desorption branch according to the BJH method. The volume of pores shown by SF is insignificant compared to that of RF, as seen in the distribution of pore size and the microphotographs of electronic microscopy of transmission included in Figure 6.2. The RF specimen shows two maximums in the pore diameter, located at 3.5 nm and 7 nm respectively, meaning it is a mesoporous material but with small-sized mesopores.

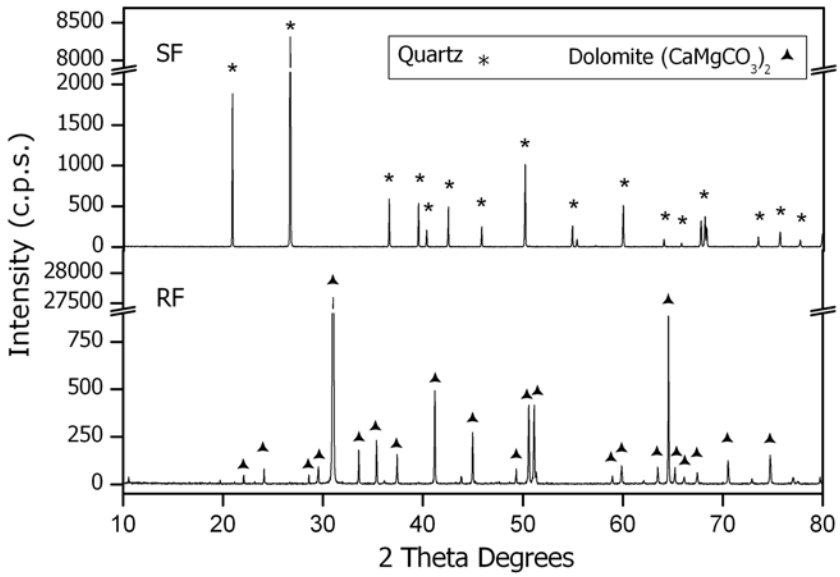

Figure 6.1: PXRD patterns of the SF and RF fillers.

The RF particles have a BET (Brunauer-Emmett-Teller) surface 300 times larger than that of SF (76.04 vs. 0.25) [23], in agreement with a greater adsorption of N_2 in the mesoporous region (Figure 6.2). The particle size distribution obtained applying the standard UNE-EN 933-1 [25] complies with EHE-08 [26] since 100% of both fillers pass through the 2 mm and 0.25 mm sieves, 100% of SF and 99.94% of RF pass through the 0.125 mm sieve and, finally, 74.33% of the commercial filler and 70.35% of the waste filler pass through the 0.063 mm sieve. These results agree with the grain size distribution obtained by means of laser diffraction, using ethanol as dispersant (Figure 6.3), which shows that SF has a narrower distribution than RF

(0.2-100 µm vs. 0.1-200 µm). In SF the maximum is centred around 20 µm and in RF around 40 µm. In the case of SF, 71.3% of particles are between 3 µm and 32 µm, an optimum size for the process of hydration [27-29], which decreases to 49.9% in RF.

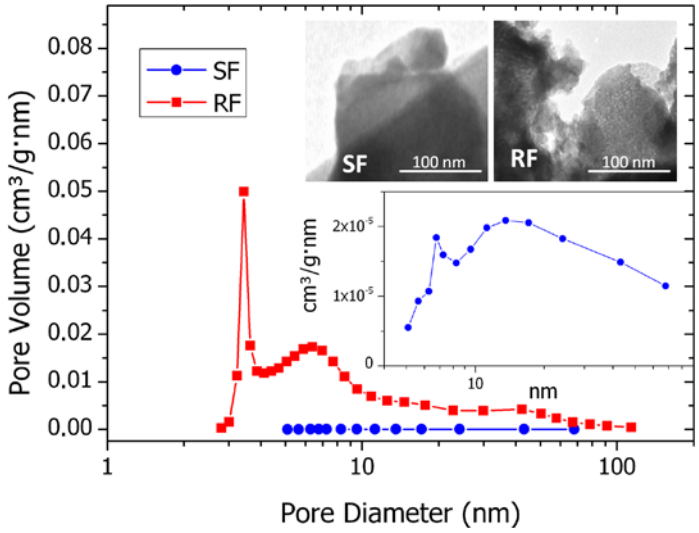

Figure 6.2: Pore size distribution and TEM micrographs of the SF and RF fillers.

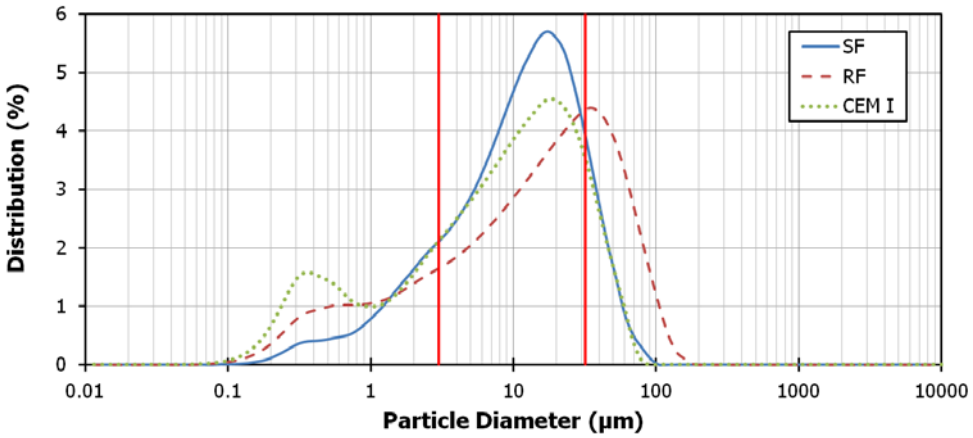

Figure 6.3: Grain-size distribution of the SF and RF fillers as measured by laser diffraction.

The cement used was CEM I 42.5 R/SR (UNE 80303-1 and UNE-EN 197-1) [25]. A physico-chemical characterisation is made in the study of Esquinas et al. [23]. The distribution of particle size of cement (Figure 6.3) shows that the percentage of the majority of particles lies between 3 µm and 32 µm.

A good quality superplasticiser (SP), high-range water reducer, was used, specific for self-compacting concrete and based on polycarboxylated ethers, labelled Glenium 303 SCC from BASF Chemical Company [30].

6.2.2 Concrete mixes and composition tests

With the aim of carrying on with the exhaustive study of the effect of RF as filler on self-compacting concrete and since its mechanical properties have already been studied [23], an analysis was made of its behaviour regarding their durability when in contact with aggressive agents. Two types of mixes were designed according to the composition of Esquinas et al. [23], using SF (SCC-SF) and RF (SCC-RF) fillers, respectively (Table 6.1). For both fillers their reproducibility was analysed, for which the study of the self-compactability properties was repeated according to EHE-08, by analysing the filler capacity (with and without obstruction), the resistance to segregation and the passing capacity in bottlenecks and reinforcement bars, via self-compactability tests (UNE-EN 12350-8, UNE-EN 12350-12, UNE-EN 12350-9 and UNE-EN 12350-10) [25].

The specific requirements for the design of both mixes (SCC-SF and SCC-RF) were: around 800 kg/m^3 of gravel, minimum cement content of 400 kg/m^3, exposure type IIIc, characteristic compressive strength of 40 MPa, maximum w/c ratio of 0.44 and the same amounts of admixture (1.8%) relative to total sum of cement plus filler. They were classified as HA-40/AC/16/IIIc according to EHE-08. The contents adjustment was done by volume (1025 L).

The SCC-SF mix was considered the reference concrete for the study, complying with the recommendations of the European Federation of National Associations representing producers and appliers of specialized building products for concrete (EFNARC) [5, 23, 31]. Some small adjustments were made to the amount of cement and water added in order to obtain SCC-RF.

Table 6.1
Concrete mix proportions and EFNARC composition parameters.

Mixes	**SCC-SF**				**SCC-RF**			
	Dry weight		*Volume*		Dry weight		*Volume*	
Constituent	kg/m^3	%	L/m^3	*%*	kg/m^3	%	L/m^3	*%*
Gravel 4/16 (G)	793.88	32.78	*305.34*	*29.82*	793.88	32.71	*305.34*	*29.82*
Sand 0/4 (S1)	646.08	26.68	*246.59*	*24.08*	646.08	26.62	*246.59*	*24.08*
Sand 0/2 (S2)	276.03	11.40	*106.17*	*10.37*	276.03	11.37	*106.17*	*10.37*
Filler	100.01	4.13	*38.47*	*3.76*	100.01	4.12	*34.76*	*3.39*
Cement	410.00	16.93	*132.26*	*12.92*	412.28	16.99	*132.99*	*12.99*
Superplasticizer	9.18	0.38	*8.87*	*0.87*	9.22	0.38	*8.91*	*0.87*
Water$_{ef}$	180.41	7.45	*180.41*	*17.58*	183.38	7.56	*183.38*	*17.91*
(W/C) $_{total}$	0.472				0.477			
(W/C) $_{ef}$	0.440				0.445			

6.2.3 Test methods

Different techniques were used for the characterisation of the raw materials and curing elements. Particle sizes were measured in a Mastersizer S analyser (Malvern Instruments) using ethanol as dispersant. The samples were analysed by X-ray diffraction patterns (XRD) using a Bruker D8 Discover A25 instrument with CuKα radiation. All diffraction patterns were obtained by scanning the goniometer from 10° to 80° (2θ) at a rate of 0.05° min^{-1}. N_2 isotherms were determined using a Micromeritics ASAP 2010 analyser, the specimens having been previously degassed at 100 ºC under vacuum for 2 h. The surface area was calculated applying the BET method in the range of equilibrium relative pressure 0.05 ≤ P/Po ≤ 0.20 [32]. Microstructural characterisation of the materials was carried out using JEOL 1400 TEM and JEOL 2010 TEM equipment. The electron microprobe technique was carried out in a scanning electron microscope JEOL JSM-6300 using an acceleration of 20 kV and a work distance of 15 mm. The X-ray detector was an ATW2-6699 Oxford Instruments model.

The methodology followed to determine the SCCs' compactability and the analysis of fresh-state density was the same as that used by Esquinas et al. [23].

The bulk density (UNE-EN 12390-7 and UNE 83980) [25] was measured in 150 x 150 x 150 mm specimens cured in water for 28 days, using two test methods for volume calculation. In the first one, it was determined by water displacement and in the second by means of measuring the real size of the specimen. Furthermore, the apparent or skeletal density (UNE 83980) [25] was measured by the ratio between the specimen mass and the corresponding volume of solid material and pores inside the specimen inaccessible to water. The open porosity or porosity accessible to water (UNE 83980) [25] was determined as the ratio between the volume of pores accessible to water and the apparent volume of the specimen. This last property was also determined following the methodology proposed by RILEM Recommendation [33] in specimens of similar characteristics.

The values for mercury intrusion porosimetry (MIP) were obtained using a Micromeritics AutoPore IV 9500 with a pressure range between 0.0015 and 207 MPa. This test was done on representative samples of 1 cm^3, extracted from the central area of cylindrical specimens of 150 mm in diameter and 300 mm in height at 91 days, cured in water. These cylindrical specimens were previously dried in oven at 100 ºC until constant mass before cutting.

The water absorption capacity of hardened concrete was measured by means of two procedures: in the first one, the water absorption was determined by immersion (UNE 83980) [25] in 150 mm cubic specimens, cured beforehand in water for 28 days. These gave two values: one corresponding to immersion until constant mass (without saturation) and the other under vacuum before immersion until constant mass (with saturation). In the second procedure, the water absorption was determined by capillarity (UNE 83982) [25] in 28 days old 100 x 100 x 200 mm specimens, cured in water, which were oven-dried prior to the tests at 60 ºC (according to the standard) or at 100 ºC (not standard) until constant mass. The latter test method enables the determination of resistance to penetration, the absorption coefficient and the effective porosity, which is the interconnected porosity and that connected to the exterior.

Permeability was assessed by testing the depth of penetration of water under pressure (UNE 12390-8) [25], carried out in cylindrical specimens of 150 mm in

diameter and 300 mm in height, cured in water for 28 days. The analysis of concrete permeability is a necessary, but not sufficient, condition to make an adequate evaluation under exposure to aggressive agent attacks.

Chloride ion migration into concrete may be due to several factors. On the one hand, there are chlorides incorporated in the concrete raw materials and, on the other, chlorides may penetrate into concrete due to exposure to environments with a high concentration of this aggressive agent, as a result of a combination of several transport mechanisms, such as capillary absorption, permeability, diffusion and/or migration. For high-quality concrete, without cracks, the most likely predominant transport mechanism is diffusion. For concrete of inferior mechanical performance, with cracks, the probable predominant transport mechanism is permeability [34].

Total chloride content is the sum of free chloride in the liquid of the pores and chloride joined both chemically and physically to the cement matrix. The penetration of chloride ion through the pores in cement results in a chemical attack that takes place because of the reaction of this ion dissolved in water with concrete. This attack produces Friedel salt ($Ca_2Al(OH)_6(Cl,OH)\cdot 2H_2O$), which is expansive. When a threshold value of ion chlorides is reached, corrosion of reinforced concrete takes place.

In this study two test procedures were used to analyse SCC behaviour in aggressive environments that were rich in chlorides. The choice of the experimental test is of significant importance since the information obtained is different.

The most commonly used method is the “Rapid chloride ion penetration test by electrical conductance” (ASTM C1202) [35], owing to its speed and simplicity of analysis of the results obtained. It correlates the total electrical charge that passes through the specimen for a given time with the concrete’s resistance to chloride ion penetration. This procedure was carried out in specimens of 100 mm in diameter and 50 mm in height taken from cylindrical specimens of the same diameter and 200 mm in height, cured for 28 days in water. The method is unable to determine with precision the amount of chloride that penetrates concrete, as well as its spatial distribution, therefore requiring the use of another procedure test: “Determining the

penetration of chloride ion into concrete by ponding" (ASTM C 1543) [35], which enables the study with great precision of the resistance of concrete to chloride ion penetration in quasi-real conditions. Firstly, the chloride ion concentration curve is obtained regarding the depth of penetration in cylindrical specimens of 100 mm in diameter and 200 mm in height previously cured in water for 91 days and subsequently submerged for another 91 days in a dissolution of NaCl to 3%, from which samples are extracted every 5 ± 1 mm until reaching a depth of 30 ± 5 mm according to ASTM C1543 [35] and UNE 112010 [25]. According to ASTM C1556 [35], using equation (6.1) that corresponds to the solution to the Fick's 2nd law, one can determine the coefficient of transport and the theoretical superficial concentration:

$$C(x,t) = Cs - (Cs - Ci) \cdot \operatorname{erf}\left(\frac{x}{\sqrt{4 \cdot De \cdot t}}\right) \qquad (6.2)$$

where C(x,t), is the percentage of chloride concentration at a depth of x meters within concrete at time t in seconds, Cs the percentage of superficial chloride content, erf the error function and De the effective coefficient of chloride transport in m^2/s.

The resistance to CO_2 penetration in concrete was measured by means of an accelerated carbonation test (LNEC E 391 [36] and UNE 112011 [25]) inside a climatic chamber (60% relative humidity at 23 ºC) with 5% of CO_2, in specimens with 100 mm diameter and 50 mm in height obtained by wet-cutting cylindrical specimens of the same diameter and 200 mm in height, cured for 91 days in water. The carbonation depth was measured after 7, 28, 91 and 182 days of exposure. The carbonation coefficient, which is inversely proportional to the concrete resistance to carbonation, can be calculated from Fick's 1st law of diffusion, $x = K\,(t)^{1/2}$, where x is the depth of carbonation (mm), t the exposure time (years) and K the carbonation coefficient ($mm/year^{0.5}$).

Sulphate penetration was determined by means of a procedure based on the standards of chemical analysis of cement (UNE-EN 196-2) [25] and of chloride attack in concrete: ASTM C1543-02 [35] and UNE 112010 [25]. The first step was the preparation of 100 mm cubic specimens cured for 91 days in water, covered by a 1 mm-thick layer of waterproof epoxy resin Sikaguard-62, except for one of the

faces. In the second step, once the resin was dry, two slices 10 mm thick were wet-cut, from the face without resin. The outside part was discarded and the other was kept in curing conditions as a SCC reference (not exposed to the aggressive environment). In the third step the rest of the specimen was submerged with the face without epoxy at the top for 91 days in a solution of Na_2SO_4 in distilled water with a concentration of 8.26 g/L (65% higher than the maximum concentration used in EHE-08 for aggressive environments), which was kept constant during this period. In the fourth step, after exposure time, the specimens were dried and dry samples were taken using a column drill. Six samples were extracted, each 5 ± 1 mm apart until reaching a depth of 30 ± 5 mm. The fifth and final step was the determination of sulphate ion concentrations (UNE-EN 196-2) [25]. These results enabled the determination of the profile of sulphate ion penetration into the SCCs.

The study of total shrinkage (ASTM C157/C157M-08 (2014) e1.) [35] and of the loss of mass during the shrinkage test in the long-term (over 700 days) was carried out in 100 x 100 x 500 mm specimens, which were kept in a curing chamber at constant room temperature (temperature of 20 ºC and relative humidity of 50%).

All the tests were triplicated, in specimens made from the same concrete mix, yielding average values and standard deviations.

6.3 Results and discussion

6.3.1 Properties of SCC in the fresh-state

6.3.1.1 Self-compactability

The results of the mixes under study (Table 6.2) comply with the self compactability requirements [26]. Figure 6.4 shows the slump flow values compared to the V-funnel time of the mixes, as used by Esquinas et al. [23], to analyse the workability using the concept of workability boxes [37]. In addition, the average value of the SCC-SF and SCC-RF mixes is provided. The results show the reproducibility of the mixes, at different times and with different operators.

Table 6.2
Results of the self-compactability tests of the two types of SCC.

Mixtures	**Retakes**	**Slump flow test**		**J-Ring test**		**V-funnel test**	**L-box test**
		T_{50} (s)	d_f (mm)	T_{j50} (s)	$d_f - d_{jf}$	T_v (s)	C_{bL}
SSC-SF	Average (SD) [a]	2.08 (0.15)	759.38 (5.30)	2.84 (0.28)	22.50 (6.45)	6.70 (0.43)	0.85 (0.05)
Class [26]	*AC-V2*	*AC-E3*	*AC-RB2*		*AC-V2*	*AC-RB2*	
SSC-RF	Average (SD) [a]	2.36 (0.11)	681.25 (5.45)	3.19 (0.13)	16.38 (1.44)	9.43 (0.81)	0.83 (0.06)
Class [26]	*AC-V2*	*AC-E2*	*AC-RB2*		*AC-V2*	*AC-RB2*	

[a] Standard deviation

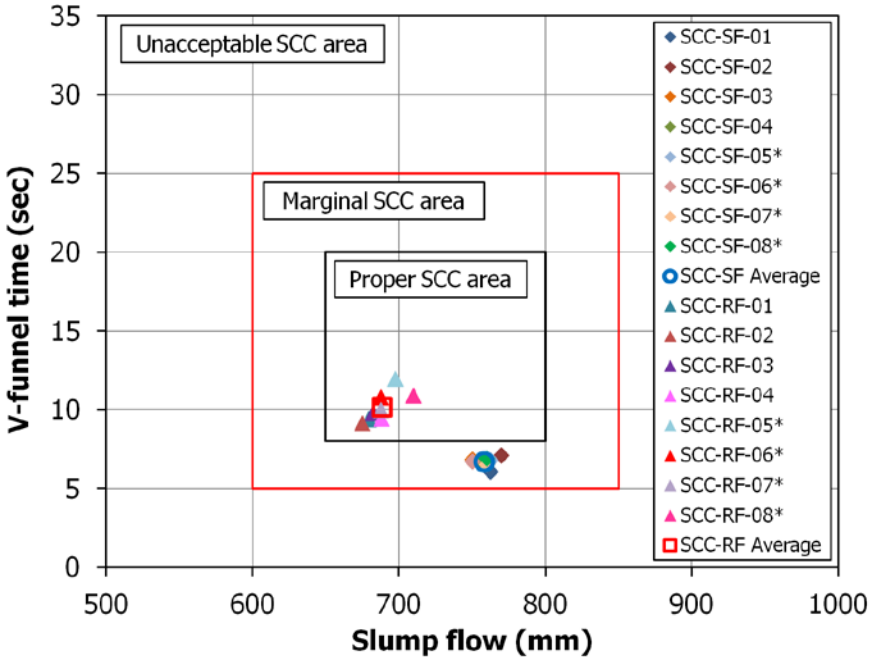

Figure 6.4: Workability boxes of several self-compacting mixes.

The SCC-SF mixes are in the "Marginal SCC-SF area" box (Figure 6.4). Segregation was not observed, although in [37] a slight segregation is reported. Furthermore, the SCC-RF mixes are in the "Proper SCC area" (Figure 6.4), that is to say, they were regarded as adequate and acceptable SCCs. These results concur with the aspect of both mixes in the different tests, meaning a good distribution of coarse aggregates was observed, i.e. they were present at the edges in the flow table test and without segregation or bleeding.

The SCC-RF specimen showed self-compactability values nearer the limit given by EHE-08 (Table 6.2) [26]. This behaviour may be attributed to the different degrees of fineness of particles used in the fillers and the surface porosity (Figures 6.2 and 6.3). The greater BET surface [32] of RF and greater pore content increased the mixing water adsorption, thus producing a lower amount of free water to lubricate the particles and therefore resulting in a viscosity increase of the SCC-RF mix.

This study shows that it is possible to obtain SCC similar to those obtained by Martín et al. [22], using a greater quantity of gravel (800 kg/m^3 vs. 739 kg/m^3) and a lower

content of superplasticizer (1.8% vs. 2.6%). The results were also similar to those obtained by Topçu et al. [38] and Ho et al. [39], who used residual fillers from the mining industry.

6.3.1.2 Density

The fresh density of SCC-RF was 2.374 kg/dm^3 and that of SCC-SF was 2.405 kg/dm^3. These results agree with the residual porous structure (Figure 6.2) as well as with the lower RF filler content in volume, together with greater water content in the SCC-RF mix. The decrease observed in the fresh-state density values of the SCC-RF mix was similar to that found by other authors [22, 23, 38].

6.3.2 Properties of SSC in the hardened-state

6.3.2.1 Physical properties

6.3.2.1.1 Apparent density, evolution during drying and dry density

The bulk density (ρ_{ap}) (measured at 28 days) in SSC-RF and SCC-SF was 2.236 kg/dm^3 and 2.260 kg/dm^3, respectively. The slight difference (1%) may be due to the different W/C ratios of SCC-RF and SCC-SF (Table 6.3). The apparent (skeletal) density (ρ_{sk}) was 2.503 kg/dm^3 and 2.517 kg/dm^3 for SCC-RF and SCC-SF, respectively (0.6% difference). Martin et al. [22] also observed a decrease in the density of SSC produced with residual filler relative to SCC with commercial filler. The greater decrease in bulk density than in apparent (skeletal) density may be due to the fact that in SSC-RF there is a greater open pore content, which agrees with the porous structure of SCC-RF and its greater particle size (Figures 6.2 and 6.3).

A linear behaviour was observed in the bulk density (ρ_{ap}) evolution of SCC-SF (Equation 6.2) and SCC-RF (Equation 6.3) relative to their dry mass loss (m) (Figure 6.5 left):

$$\rho_{ap} = 0.0245\ m - 0.0534 \qquad (6.2)$$

$$\rho_{ap} = 0.0229\ m - 0.0734 \qquad (6.3)$$

Table 6.3
Physical and water absorption properties of the hardened SCCs.

	Unit	Standard/Test	SCC-SF (SD)	SCC-RF (SD)
Bulk density (ρ_{ap})	(T/m³)	UNE 83980	2.260 (0)	2.236 (0)
Apparent (skeletal) density (ρ_{sk})	(T/m³)	UNE 83980	2.517 (0)	2.503 (0)
Open porosity	(%)	UNE 83980	11.4 (0.22)	11.9 (0.32)
Threshold diameter	(µm)	MIP	0.15	0.22
Median pore diameter	(nm)	MIP	40	90
Porosity (MIP)	(%)	MIP	8.3	10.5
Abs. by immersion at 24 h	(%)	UNE 83980	4.14 (0.02)	4.38 (0.04)
Capillary absorption at 24 h	(g/cm²)	UNE 83982	0.2855 (0)	0.2833 (0)
		UNE 83982 (1)	0.5780 (0.01)	0.4710 (0.02)
Capillary absorption coefficient (K)	(g/cm² min$^{1/2}$)	UNE 83982	0.00641 (0)	0.005725 (0)
		UNE 83982 (1)	0.011627 (0)	0.009518 (0)
Resistance to penetration (m)	(min/cm²)	UNE 83982	6.25 (0.08)	9 (0.09)
		UNE 83982 (1)	16 (0.11)	42.25 (0.31)
Effective porosity (ξ)	(%)	UNE 83982	1.55 (0)	1.7 (0)
		UNE 83982 (1)	4.6 (0)	6.2 (0)
Sorptivity (S)	(cm / min$^{1/2}$)	UNE 83982(2)	0.0041	0.0040
		UNE 83982 (1) (2)	0.012	0.0124

(1) Oven dry at 100 ºC.
(2) Using Hall's model.

Both mixes suffered a similar mass loss during the drying stage and showed the same volumetric stability as the regression lines had the same gradient. The slightly lower slope that was observed in SCC-RF may be due to a greater porosity that may hinder the elimination of water in the drying stage.

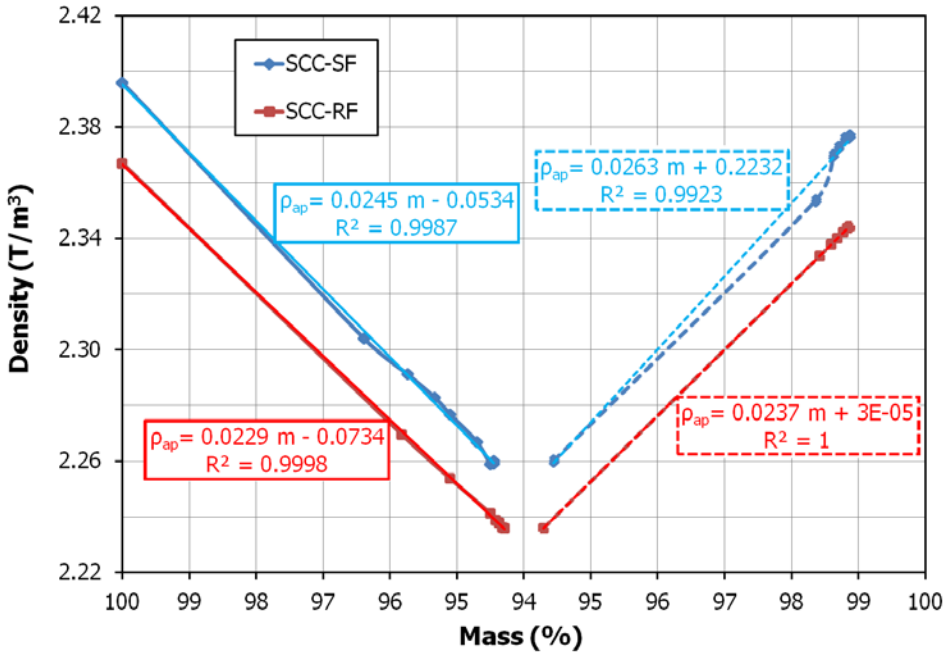

Figure 6.5: Evolution of the density relative to the variation of mass.

6.3.2.1.2 Open porosity or accessible porosity for water

The values for open porosity determined according to the standard UNE 83980 [25] and the RILEM Recommendation CPC 11.3 [36] were practically identical: 11.95% and 11.40% for SCC-RF and SCC-SF, respectively (Table 6.3). The incorporation of RF resulted in an increase in porosity in SCC (4%) relative to SCC-SF and consequently a decrease in density. These differences are due to the characteristics of the fillers used. The poor packing of RF particles and the slight greater W/C ratio in SCC-RF resulted in an increase in porosity.

These results concur with the conclusions obtained by other researchers. Martín et al. [22] observed an increase in porosity in the mix with residual filler, obtaining greater values than those in our study for SCC-RF, which may be attributed to the lower content of cement used by Martin et al. [22] in their mixes. Assié et al. [40] studied the variation of porosity with respect to the W/C ratio of the corresponding mixes of three types of SCC and obtained results within the same range as in this study. Valcuende et al. [41] studied the influence of the W/C ratio and the type of

cement on SCC's porosity, concluding that SCC with lower W/C ratio and cement of greater strength is less porous and has a finer porous structure.

6.3.2.1.3 Pore size distribution

Figure 6.6 top shows the accumulative values of Hg volume in the intrusion and extrusion cycle with respect to the pore diameter, clearly defining the total porosity of both mixes, revealing greater porosity in SCC-RF: 10.5%, as opposed to 8.3% for SCC-SF. Figure 6.6 bottom represents the volume difference of mercury intrusion in function of the pore diameter, showing that the mixes had a similar pattern in terms of pore size. The curve shows three maximums of mercury intrusion. The first one is found in the 100 µm range, which may be due to the trapped air in the mix (pores greater than 100 µm) [42], another around 40 nm (medium capillary pores) and, lastly, one around 6 nm (small gel pores) [43, 44].

In the zone above 70.0 µm, the volume of mercury intrusion in SSC-RF is far greater than that in SCC-SF. In the pore range of 50.0 nm and 10.0 µm (denominated large capillary pores), the volume of mercury intrusion is slightly larger in SSC-RF. These pore sizes affect the permeability of the materials [44]. For the range of pores between 2.5 nm and 10.00 nm (denominated small gel pores), there is a greater intrusion in SCC-SF specimen. In the case of SCC-SF, only in the small gel pore zone the volume of pores is greater, due to the distribution of finer grain and ideal SF (SiO_2) that allows the reaction of SiO_2 with portlandite, $Ca(OH)_2$, to form CSH and consequently it has a different hardening mechanism from that SCC-RF [23]. This leads to the larger pores being filled (filler effect), providing additional nucleation surfaces of the hydrated products, generating smaller crystals and consequently producing a greater percentage of smaller pores. Therefore, SCC-SF will show denser areas interface arid-paste and this range of pores will affect properties such as the shrinkage of the material [41, 44].

Figure 6.6 bottom shows that both mixes have the same maximum concentration in size of pores around 40 nm. The maximum pore diameter in which mercury intrusion increases significantly and continuously is named the threshold diameter. SCC-SF has a threshold diameter of 0.15 µm and SCC-RF 0.22 µm (Table 6.3). This indicates a

finer porous structure of SCC-SF, which agrees with the volume of mercury intrusion in the different pore sizes: in the large capillary size area (50 nm - 10 µm) in the SCC-RF specimen, the volume is 0.159 mL/g against 0.109 mL/g in SCC-SF. In the medium capillary size area (10-50 nm), there is a volume of 0.157 mL/g in SCC-RF and 0.146 in SCC-SF. Lastly, for the small gel pores (2.5-10 nm), the volume is 0.033 mL/g in SCC-RF and 0.042 mL/g in SCC-SF. Taking into account the results obtained in this test, one can conclude that SCC-RF has a coarser porous structure than SCC-SF.

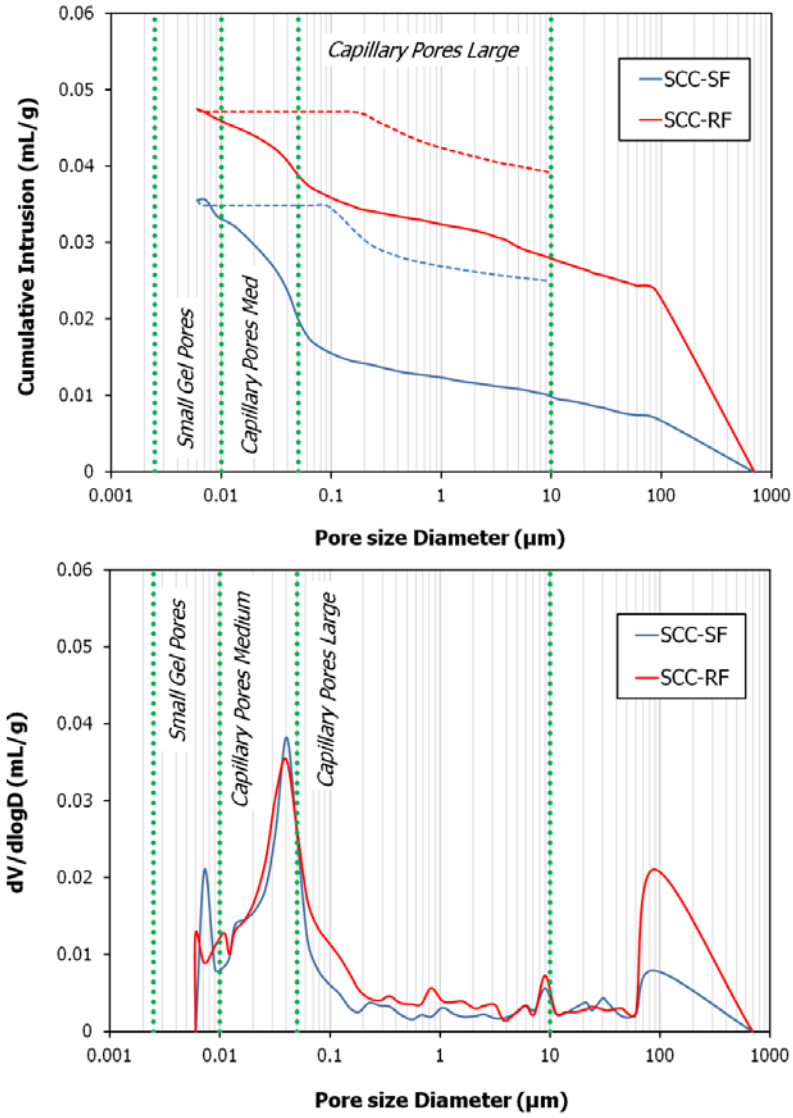

Figure 6.6: Cumulative pore volume and log differential intrusion of the mixes.

The medium pore size in SCC-SF is less than in SCC-RF (40 nm vs. 90 nm). Both mixes showed an average pore size diameter below the threshold diameter, which may indicate that they have a dense microstructure, so that after having reached the relative threshold diameter pressure, few pores remained to be filled with Hg [45].

The results from this study are similar to those obtained by Assié at al. [40], who carried out a study of the porous structure in SCC manufactured with limestone filler, although lower than those obtained by Valcuende et al. [41] who made an analysis of the porous structure of different SCCs, possibly due to the greater percentage of filler used by these authors.

6.3.2.2 Water absorption properties

6.3.2.2.1 Water absorption by immersion and with vacuum

The absorption of water by immersion is a parameter directly related to the accessible pore volume. Figure 6.7 shows, in a time function, the evolution of the mass loss during the drying process, which is similar in both mixes, 6%, although slightly larger in SCC-RF, which agrees with the greater accessible porosity of this mix. It also shows the absorption of water by immersion in a time function, which becomes stable around 5% for both mixes, though slightly larger for SSC-RF. In both mixes, there is a failure to absorb all the water lost during the drying process, i.e. approximately 15% of the total water loss mass in both mixes is not reabsorbed. This behaviour may be attributed to the incomplete rehydration of the small pores (medium capillary pores and small gel pores) [44], inaccessible for water absorption under atmospheric pressure.

The absorption of water by immersion at 24 h and 48 h was 4.14% and 4.42% respectively for SCC-SF and 4.38% and 4.56% respectively for SCC-RF (Table 6.3). The maximum values reached (until constant mass) were 4.75% and 4.86% in SCC-SF and SCC-RF respectively. This agrees with the porous structure of both mixes. These results coincide with those from other researchers such as De Schutter & Audenaert [46], who carried out a detailed study on the absorption of water under immersion in different SCC mixes. Moreover, if one takes into account the absorption

of water by immersion and vacuum (UNE 83980) [25], the average values measured over 24 h and 48 h are greater than the previous ones. In SCC-SF it was 4.9% and 5.1% respectively, and in SCC-RF 5.3% and 5.4% respectively. As expected, the rehydration under vacuum was greater.

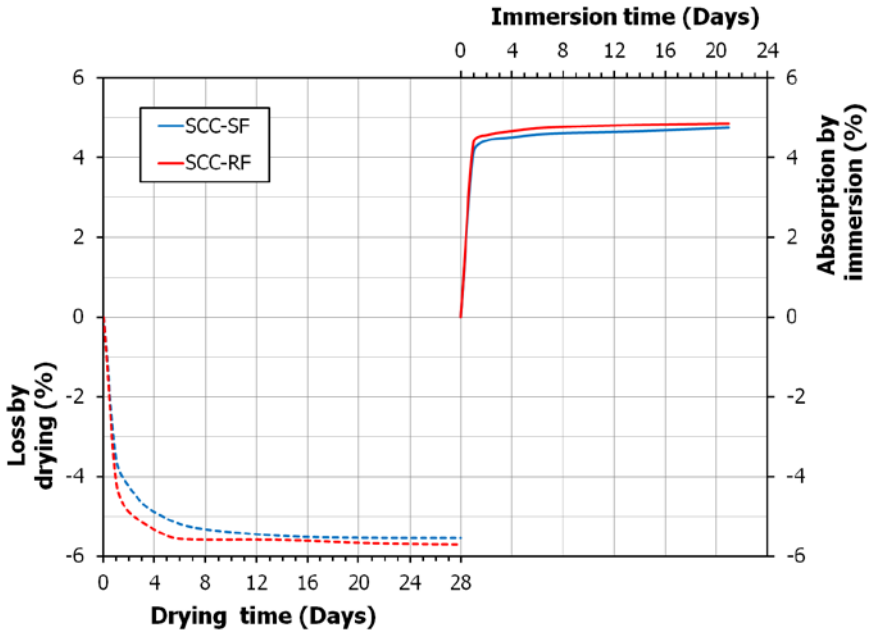

Figure 6.7: Evolution of the mass loss by drying (100 ºC) and absorption by immersion.

Regarding the total mass of water lost during the drying stage, the reabsorbed water under immersion over 48 h was 79.85% for SCC-RF and 79.65% for SCC-SF. If the immersion is done under vacuum, the water absorption over 48 h is 94.6% for SCC-RF and 91.9% for SCC-SF. This may be due to the greater volume of available small gel pores in SCC-SF after the drying process, not accessible to water in the immersion process.

The evolution of bulk density (ρ_{ap}) during the process of water absorption by immersion was studied. A linear behaviour was observed in apparent density relative to the increase in mass (m) of both SCCs (Figure 6.5), which is shown in Equations (6.4) and (6.5) relative to SCC-SF and SCC-RF respectively:

$$\rho_{ap} = 0.0263\ m + 0.2232 \qquad (6.4)$$

$$\rho_{ap} = 0.0237\ m + 0.00003 \qquad (6.5)$$

The density does not reach the starting value, due to the incomplete rehydration of the pores, as mentioned earlier. Furthermore, one can observe a similar variation in the apparent density in the absorption process of both specimens, based on the values of the slope.

6.3.2.2.2 Water absorption by capillarity

The capillarity of hardened cement depends on the inter-connection of the existing pores inside the material. According to Jurin's law [47], the capillary movement increases with the reduction of capillary diameter. According to Fagerlund [48], capillary absorption is defined as a two-state process: initially, ($0 < \sqrt{t} < \sqrt{t_n}$), where filling occurs by absorption of water through capillary pores, and then ($\sqrt{t} \geq \sqrt{t_n}$), which corresponds to water saturation in which a process of diffusion and dissolution of existing air is produced in the porous structure, t_n being the time necessary to reach saturation.

Figure 6.8 shows the average values for capillary obtained from specimens dried at 60 ºC to constant mass (test conditions under the standard UNE 83982) and at 100 ºC to constant mass, for SCC-SF and SCC-RF specimens. The absorption data for capillary presents a good adjustment to second degree polynomial equations (Equations 6.6-6.9) since R^2 varies between 0.9496 and 0.9988:

$$W = -0.000009\,t + 0.0040\,\sqrt{t} + 0.0955 \quad \text{(SCC-SF dried at 60 ºC)} \quad (6.6)$$

$$W = -0.000008\,t + 0.0041\,\sqrt{t} + 0.0937 \quad \text{(SCC-RF dried at 60 ºC)} \quad (6.7)$$

$$W = -0.00002\,t + 0.012\,\sqrt{t} + 0.1041 \quad \text{(SCC-SF dried at 100 ºC)} \quad (6.8)$$

$$W = -0.00002\,t + 0.0124\,\sqrt{t} + 0.0226 \quad \text{(SCC-RF dried at 100 ºC)} \quad (6.9)$$

According to the example proposed by Hall [49], the definition of capillary absorption (W) is given by Equation 6.10:

$$W = A + S\sqrt{t} - C\,t \quad (6.10)$$

where t is time, S is sorptivity or the capillary absorption rate, A and C are constants. The values of capillary absorption and sorptivity for both mixes are shown in Table 6.3.

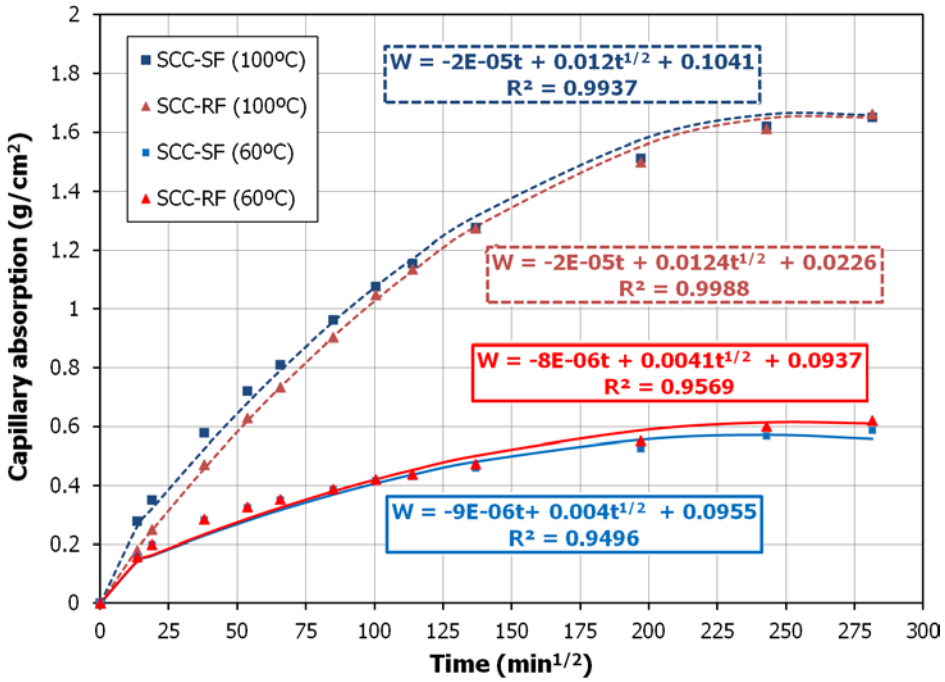

Figure 6.8: Capillary water absorption of the mixes.

The greater capillary absorption and sorptivity for the mixes dried at 100 ºC may be due to the pore diameter deformation in the small capillaries when subjected to temperatures of around 100 ºC [50, 51].

Besides sorptivity, another parameter that can be determined in the capillary absorption test is the effective porosity (the inter-connected and connected porosity with the exterior), which has a decisive influence on the interchange of humidity with the environment and therefore the transport mechanisms. The Ibero-American document RED DURAR in the framework CYTED [52] establishes the value limits for these parameters: 10% for effective porosity and 0.039 cm/min$^{1/2}$ for sorptivity, in structures exposed to highly aggressive environments. Table 6.3 shows the effective porosity values, calculated according to UNE 83982: 1.55% in SCC-SF and 1.7% in SCC-RF, when drying the samples at 60 ºC, and 4.6% in SCC-SF and 6.2% in SCC-RF, when drying the samples at 100 ºC. The sorptivity values are also shown,

according to the Hall model [49], 0.004 cm/min$^{1/2}$ for SCC-SF and 0.0041 cm/min$^{1/2}$ for SCC-RF, for samples dried at 60 ºC and 100 ºC respectively. All the mixes in our work were within the limits previously mentioned, and can therefore be used in aggressive environments with adequate durability.

The experimental results obtained for capillary absorption at 24 h, for specimens dried at 60 ºC, are practically the same for both mixes. These values are similar to those registered by Assié et al. [40] in mixes of SCC manufactured with limestone filler and a W/C ratio of 0.42 (0.282 g/cm^2) and those by da Silva & de Brito [45] in mixes with fly ash and/or limestone filler.

However, for samples dried at 100 ºC the capillary absorption over 24 h is greater in SCC-SF. This is due to the greater content of small gel pores available in this mix that may be water-free, after the process of heating to 100 ºC until constant mass, with no noticeable change when the drying process is undertaken at 60 ºC. This agrees with the porosimetry of mercury data previously mentioned (Table 6.3) because the smaller medium pore radius is more prone to absorption, according to Jurin's law [47].

6.3.2.3 Durability

6.3.2.3.1 Permeability and penetration of water under pressure

The water penetration under pressure allows evaluating the ease with which a fluid moves through the porous structure of a material, under constant pressure applied to the liquid.

Table 6.4 shows the results of maximum penetration observed in the mixes: 2.01 mm for SCC-SF and 4.8 mm for SCC-RF. These results enable considering that these mixes are impermeable in aggressive environments, according to the maximum limits (30 mm) defined by Neville [53].

The small difference observed in permeability in the SCC-SF and SCC-RF mixes is related to the porous structure of the material, specifically with a greater volume of

capillary pores (large and medium) (Figure 6.6) of SCC-RF. These results also agree with those of the tests of absorption by immersion and capillarity of the mixes.

Table 6.4
Durability properties of the hardened SCCs.

	Unit	Standard/Test	SCC-SF (SD)	SCC-RF (SD)
Permeability	(mm)	UNE 12390	2.01	4.8
Permeability coefficient	(10^{-14} m/s)	Valenta Ec.	0.11	0.57
Chloride ion penetrability	-	ASTM C 1202	Low	Low
Effective Cl^- transportation coefficient (D_e)	(10^{-12} m^2/s)	ASTM C 1556	8.3	9.3
Carbonation depth (7 days)	(mm)	LNEC E 391/UNE112011	1.05 (0.4)	2.53 (0.5)
Carbonation depth (28 days)	(mm)	LNEC E 391/UNE112011	2.93 (1.0)	4.77 (0.9)
Carbonation depth (91 days)	(mm)	LNEC E 391/UNE112011	7.92 (0.9)	12.19 (1.8)
Carbonation depth (182 days)	(mm)	LNEC E 391/UNE112011	11.99 (2.6)	15.67 (1.1)
Carbonation coefficient (K_C)	(mm/$year^{1/2}$)	Fick's first law	15.86	22.25
Effective SO_3 transportation coefficient (D_e)	(10^{-12} m^2/s)	ASTM C 1556	8.18	13.1

When the liquid flow is uniaxial, the depth of water penetration allows determining the coefficient of permeability. The permeability coefficients obtained (Table 6.4) are lower, 10-14 m/s in both cases, thus demonstrating the compactness of the mixes. Uysal et al. [18] studied the permeability of SCCs with different natural siliceous powders and limestone as filler, observing lower values of permeability when using siliceous as filler. Da Silva & de Brito [45] observed a greater permeability in the mixes with limestone relative to those with fly ash (natural siliceous). The penetration values were slightly higher for the mixes used by these authors than those obtained in this study, which may be due to the greater W/C ratio and lower quantity of coarse aggregate used.

6.3.2.3.2 Chloride ion penetration

6.3.2.3.2.1 *Rapid chloride ion penetration test by electrical conductance*

This method analyses the chloride ion behaviour present in the dissolution by the action of an applied electric field, causing migration through the cement toward the positive pole. Due to the natural matrix of concrete, consisting of a porous structure and in a water state rich in ions, this material will act electrically as a conductor.

Figure 6.9 shows the evolution of the electrical charge (Coulomb) registered in terms of time. The mixes revealed a similar electrical behaviour, although for SCC-RF the electrical charge was slightly greater than for SCC-SF, which indicates a greater migration of ions in the specimen, even though both mixes (Table 6.4) are within the range set out by ASTM C 1202 as low penetrability of chloride ions.

The values are within the range set out by Tang & Zhu [54], who carried out a literature review on the resistance to chloride ion penetration observed by various authors in SCC mixes, concluding that for the rapid chloride permeability test the values for conductivity ranged between 800 and 1600 Coulombs after 28 days, much lower than 4000 Coulombs for conventional concrete mixes. Uysal et al. [18], who did a study on the durability of SCCs using different types of filler (limestone powder and basalt powder) with filler percentages similar to those used in our work, found a low penetrability of chloride ion.

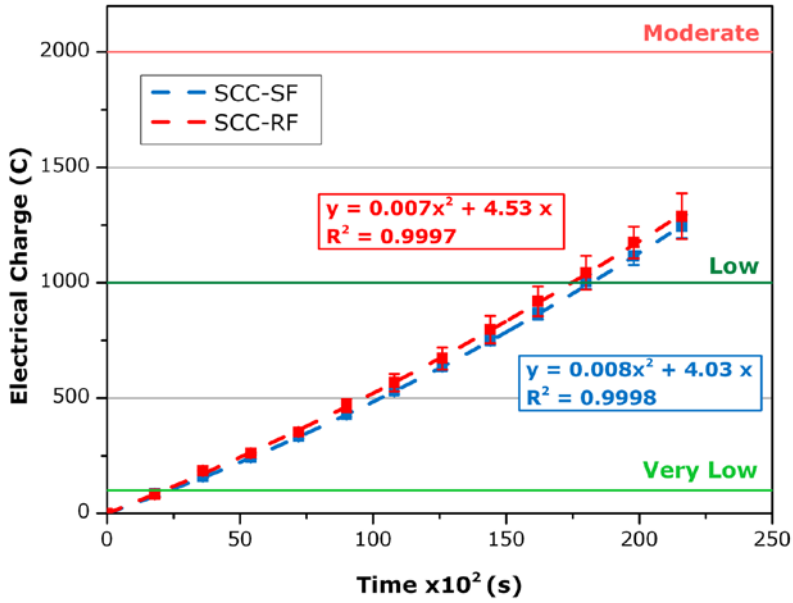

Figure 6.9: Rapid chloride ion penetration test by electrical conductance of the mixes.

6.3.2.3.2.2 *Penetration of chloride ion into concrete determined by ponding*

The determination of chloride ion concentration in function of depth allows defining the intrinsic durability of each mix. These results give information on the movement of chloride ions in dissolution, from the surface of concrete to its core. The speed of flow will depend on the concentration, applied pressure and tortuosity of the porous network.

Figure 6.10 outlines the chloride ion concentration with respect to the depth of penetration for both mixes. A similar evolution is seen for both mixes, although SCC-SF showed slightly lower values than SCC-RF for each specimen depth. These results were adjusted by minimum square roots in Equation (6.1) proposed by the standard ATSM C 1556 [35], obtaining Equations (6.11) and (6.12), with R^2 values higher than 0.9.

$$C(x,t) = 0.49 - (0.49 - 0.02) \cdot \operatorname{erf}\left(\frac{x}{\sqrt{4 \cdot 8.3 \cdot 10^{-12} \cdot 7.86 \cdot 10^{6}}}\right) \quad (6.11)$$

$$C(x,t) = 0.52 - (0.52 - 0.02) \cdot \operatorname{erf}\left(\frac{x}{\sqrt{4 \cdot 9.3 \cdot 10^{-12} \cdot 7.86 \cdot 10^{6}}}\right) \quad (6.12)$$

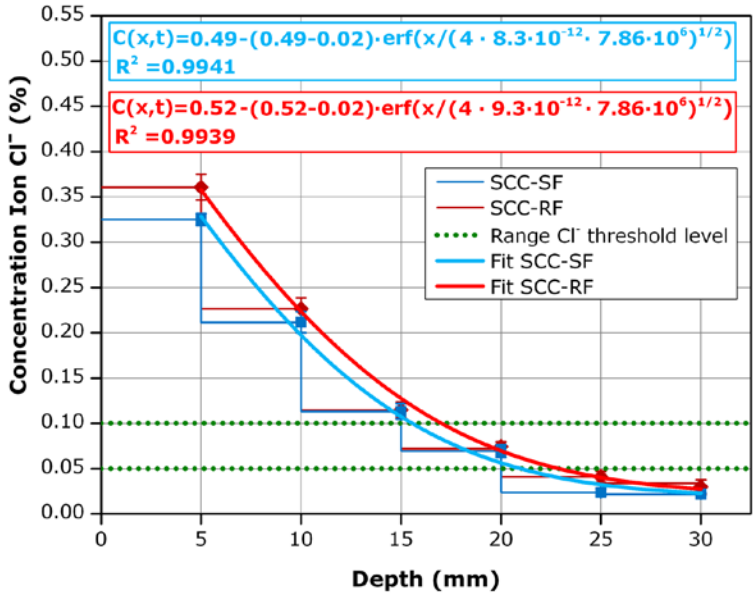

Figure 6.10: Ion Cl^- concentration profile of the mixes.

The adjustments for minimum square roots enabled the calculation of the effective transport coefficients of chloride ion in the two mixes (Table 6.4), resulting in 9.3 x 10^{-12} m^2/s and 8.3 x 10^{-12} m^2/s for SCC-RF and SCC-SF respectively, after 91 days of exposure. The minimum values necessary for theoretical superficial concentration were also obtained, 0.52% and 0.49% for SCC-RF and SCC-SF respectively, in order to outline the profile of diffusion as shown in Figure 6.10. These results concur with the greater number of pores (Figure 6.6) of the SCC-RF specimen.

Figure 6.10 represents the range of typical threshold levels of chloride concentration that may cause steel corrosion in concrete according to Glass & Buenfeld [55]. Thus, if the concentration of Cl- (%) is lower than 0.05%, no risk of corrosion in reinforced concrete is expected and, if it is greater than 0.1%, there is such a risk.

Since the chloride content in the mixes presented in this study is lower than 0.05 for depths greater than 22 mm, reinforced concrete will not be affected if the reinforcement cover is greater than this value. In addition, taking into account durability in aggressive environments [26], the minimum cover required by EHE -08 for the type of SCC defined (HA-40/AC/16/IIIc) [23, 26] is 45 mm, i.e. the safety margin for these mixes is over 20 mm.

The penetration profiles obtained agree with the results of Bermejo [56] for mixes with CEM I 42.5R/SR cement and fly ash and limestone as filler. The penetration for SCC-RF is similar to that of Bermejo for SCC using limestone as filler and for SCC-SF it is slightly greater than that using fly ash as filler, which may be due to the greater reactivity of fly ash relative to SF. Furthermore, Ryan & O'Connor [57] obtained similar effective coefficients of chloride ion movement (10^{-12} m^2/s), although lower than those in our study, using a salt fog chamber. The larger coefficients of SCC-SF and SCC-RF could be due to the constant action of chloride ion in the immersion process relative to the interaction of chloride in the wetting-drying cycles used by the authors.

6.3.2.3.3 Carbonation depth

Carbonation is produced when atmospheric CO_2 reacts with the portlandite generated in the curing process of the mix, forming calcium carbonate in the presence of water. This reaction decreases the pH of the material leading to the loss of passivity of the reinforcement, leaving it exposed to potential corrosion. The factors that the carbonation process depend on are the porous structure, humidity, type of cement, admixtures and permeability.

Table 6.4 shows the depth of carbonation relative to the exposure time in a CO_2 chamber for both mixes. SCC-RF shows penetration values greater than SCC-SF. The difference in the values of carbonation depth is maximum for short exposure periods. SCC-RF's carbonation depth is 140% greater than that of SCC-SF after 7 days of exposure (Table 6.4). This difference decreases with time, reaching a minimum after 182 days, when SCC-RF shows a carbonation depth 30% greater than that of SCC-SF (Table 6.4).

Carbonation produced in material can also be evaluated from the carbonation coefficient. Figure 6.11 shows the carbonation depth (C_d) compared with the square root of time (years). In both mixes the CO_2 penetration is defined by Equations 6.9 (SCC-SF) and 6.10 (SCC-RF), which show a good adjustment (R^2 higher than 0.96).

$$C_d = 15.86 \sqrt{t} \qquad (6.9)$$

$$C_d = 22.25 \sqrt{t} \qquad (6.10)$$

The carbonation coefficient for SCC-SF and SCC-RF is 15.86 mm/year$^{1/2}$ and 22.25 mm/year$^{1/2}$ respectively.

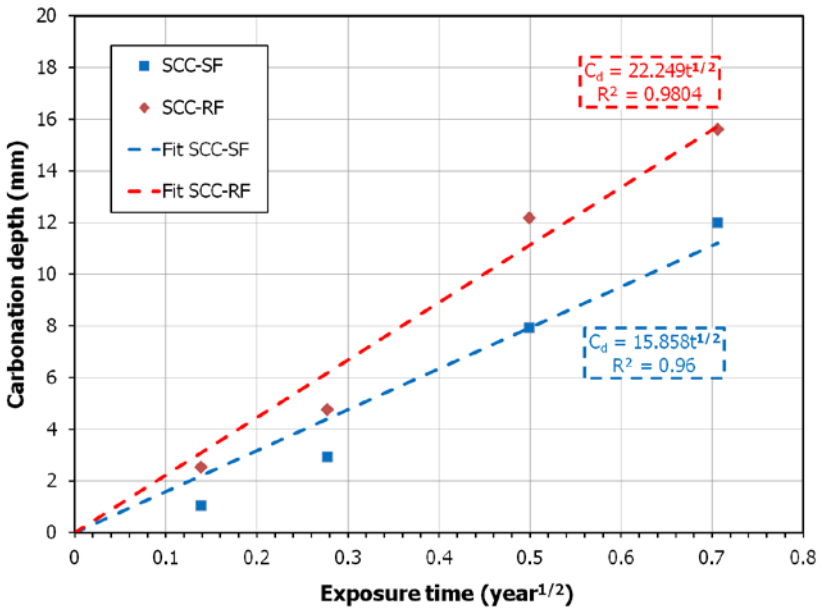

Figure 6.11: Depth of carbonation as a function of $\sqrt{t}$ of the mixes.

These results can be looked at from the point of view of the porosity of the material and the reactions to curing. The SCC-RF mix shows a larger amount of portlandite susceptible to being carbonated compared to SCC-SF [23], due to the fact that the $Ca(OH)_2$ generated in the curing reactions in this mix reacts with SF. Moreover, the greater volume of capillary pores, as well as the larger average pore size of SCC-RF, result in a higher diffusion speed of CO_2 in the material.

Regarding corrosion in reinforced concrete by carbonation for the defined environment, HA-40/AC/16/IIIc, according to EHE-08, the results show a slightly higher degree of safety than those obtained for chloride ion penetration, since the maximum penetration is less than 16 mm. Therefore, the safety margin for these mixes is greater than 25 mm [26].

These results concur with those of Martín et al. [22], who carried out a study of the resistance to carbonation in SCC made with waste filler as replacement of commercial filler, observing that SCC with waste material showed greater carbonation. The depth of carbonation was similar to that of our study, although slightly less, possibly because of the different curing age of the specimens when exposed to a carbonation environment, 7 days as opposed to 91 days (in our study). Likewise, da Silva & de Brito [58] obtained greater penetration for mixes with limestone filler compared to those with fly ash.

6.3.2.3.4 Sulphate ion penetration

Sulphate ion reacts with different components of cement or products of hydration causing the formation of calcium sulphates and/or hydrated sulphoaluminates, of greater volume. This is a very aggressive attack since it may result in disintegration of the material. The factors that affect sulphate attack are: humidity, microstructure, type of cement and speed of ion sulphate penetration, and chemical composition of the sulphate.

Figure 6.12 shows the different behaviour of SCC-SF and SCC-RF in terms of penetration of SO_3. SCC-SF shows lower values than SCC-RF for each specimen depth. The results were adjusted by squared minimums to Fick's 2nd law, obtaining values of R^2 de 0.95 for SCC-SF (Equation 6.13) and 0.99 for SCC-RF (Equation 6.14).

$$C(x,t) = 0.47 - (0.47 - 0.01) \cdot \operatorname{erf}\left(\frac{x}{\sqrt{4 \cdot 8.18 \cdot 10^{-12} \cdot 7.86 \cdot 10^{6}}}\right) \qquad (6.13)$$

$$C(x,t) = 0.43 - (0.43 - 0.02) \cdot \operatorname{erf}\left(\frac{x}{\sqrt{4 \cdot 1.31 \cdot 10^{-11} \cdot 7.86 \cdot 10^{6}}}\right) \qquad (6.14)$$

SCC-SF shows a lower diffusion coefficient than SCC-RF (8.18 x 10^{-12} m^2/s vs 1.31 x 10^{-11} m^2/s respectively). This concurs with the low permeability, which in turn is related to the smaller pore size and lower diffusion of ion SO_3. The greater microstructural density of SCC-SF results in the SO_3 reaching lower penetration depths in this material. The application of Fick's 2nd law indicates that the surface theoretical concentration (Cs), which adjusts to the fast drop in the diffusion of sulphates for the SCC-SF mix, would be greater than that of SCC-RF. After exposure

to the aggressive environment both mixes show no sign of wear-and-tear or deterioration.

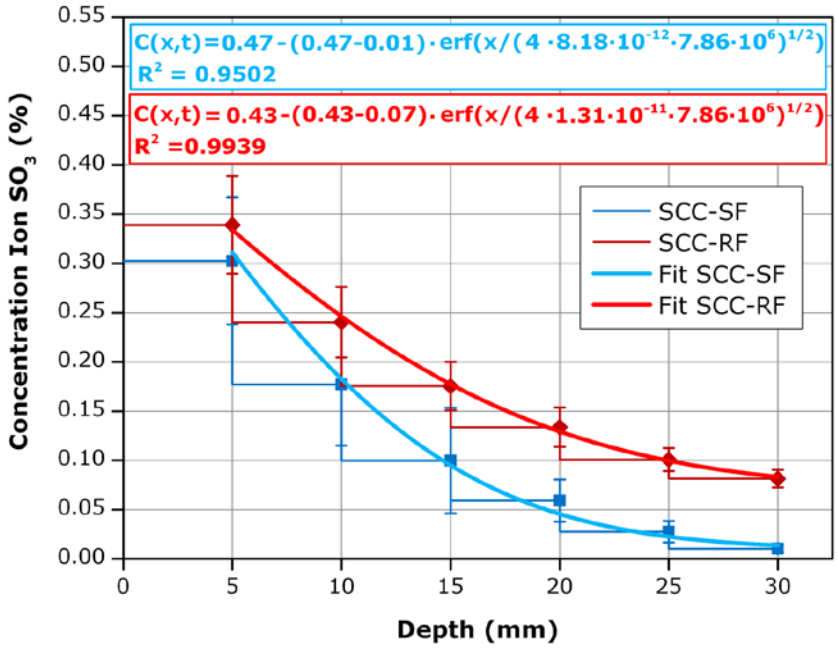

Figure 6.12: Ion SO_3 concentration profile of the mixes.

This behaviour is related to the content of portlandite ($Ca(OH)_2$) generated in the curing process, which is greater in SCC-RF and the CSH and micro-silica (SiO_2) content in SCC-SF [23]. It is also due to the presence of thaumasite ($CaCO_3 \cdot CaSO_4 \cdot CaSiO_3 \cdot 15H_2O$) in the SCC-SF mix and ettringite in SCC-RF, which is related to the afore-mentioned phases (portlandite, CSH & micro-silica). Figures 6.13 and 6.14 show that the SO_3 attack in both cases gives rise to the formation of thaumasite, since at 5 mm depth, where sulphate concentration is maximum (Figure 6.12), the peak at 9.92 Å (represented by the letter T in Figures 6.13 and 6.14) shows the maximum intensity. Likewise, an increase in portlandite content is observed at this depth, produced in the process of the formation of thaumasite starting from the CSH and SO_3 [54]. Moreover, in the SCC-RF specimen at a depth of 5 mm there is a decrease in ettringite content from the specimen at the start, which may also be due to the formation of thaumasite [54].

These results are similar to those of Bassuoni & Nehdi [59], who carried out a study of resistance to SO_3 attack in SCC made with fly ash, silica fume, limestone filler and a sulphoresistant cement. Uysal & Sumer [17] also observed that mixes with granulated blast furnace slag or fly ash showed fewer alterations in their mechanical behaviour than mixes with marble or limestone powders in relation to sulphate attack, mainly due to the reactivity of $Ca(OH)_2$ with SO_3. All of this agrees with De Schutter & Audenaert [54], who concluded that the use of pozzolanic particles (e.g. silica fume, fly ash, slag) would generate denser porous structures, with smaller capillary pores, thus avoiding sulphate attack to a large extent.

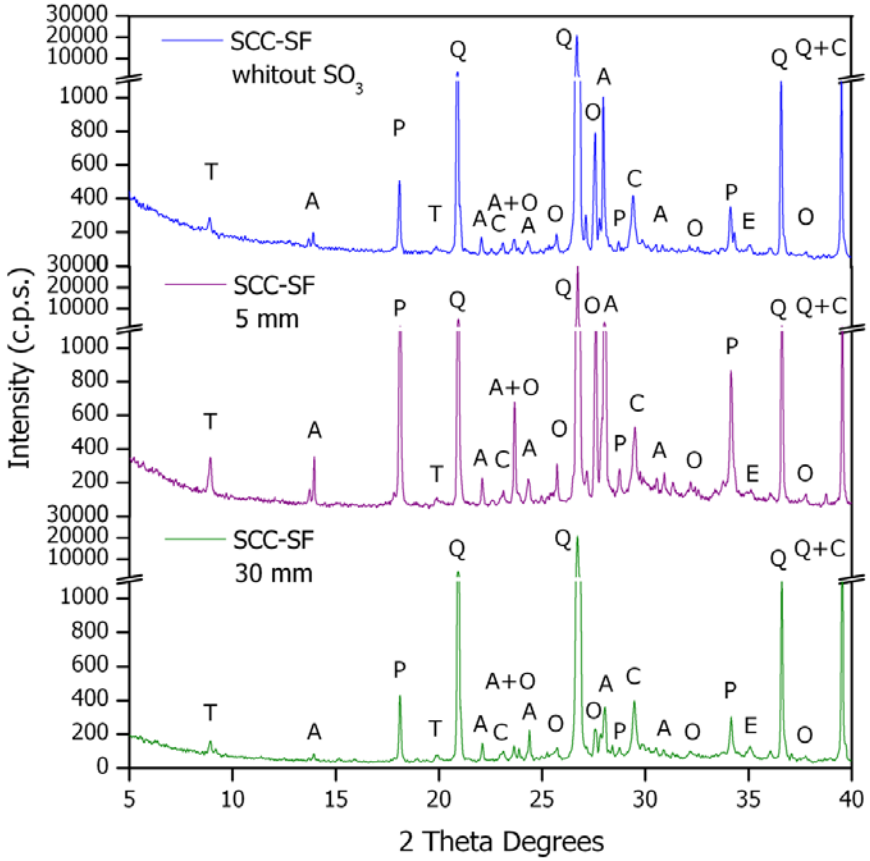

Figure 6.13: PXRD patterns of SCC-SF before and after exposure to SO_3.

(E = Ettringite, T = Thaumasite, P = Portlandite, Q = quartz, C = calcite, A = albite and O = orthoclase)

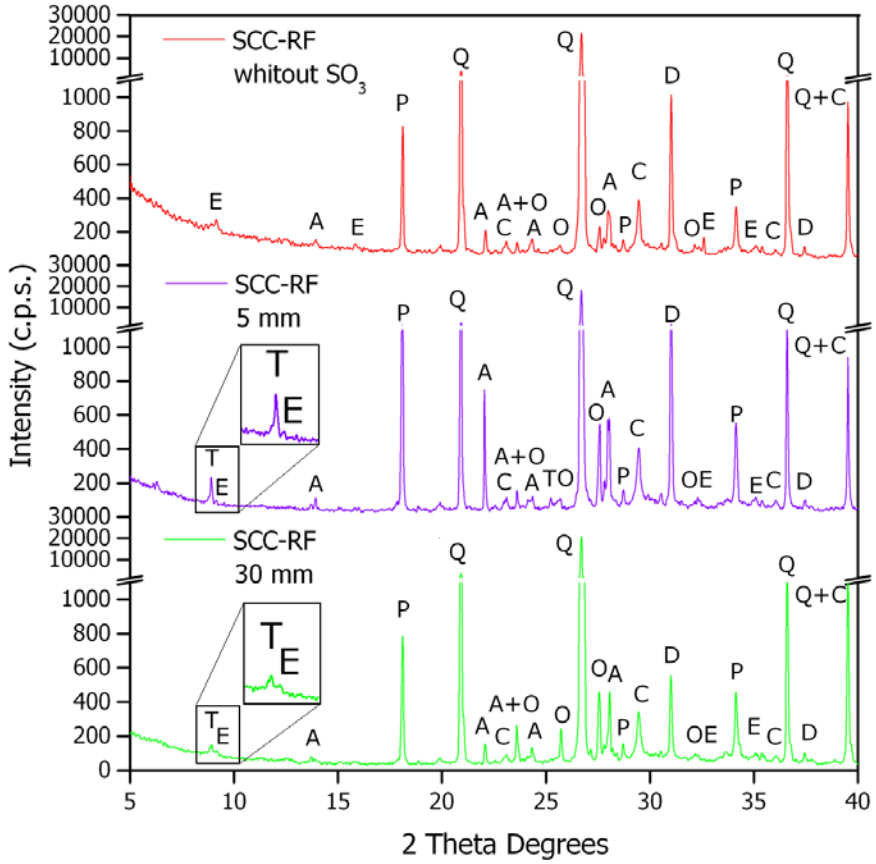

Figure 6.14: PXRD patterns of SCC-RF before and after exposure to SO_3.

(E = Ettringite, T = Thaumasite, P = Portlandite, Q = quartz, D = dolomite, C = calcite, A = albite and O = orthoclase)

6.3.2.3.5 Long-term shrinkage

Shrinkage is a phenomenon that causes dimensional variation in material, which makes it one of the most significant aspects of concrete durability. Besides temperature, humidity, physico-chemical characteristics, among others, time is one of the most basic factors in the study of this parameter due to the fact that deformation depends on it. This is why long-term analysis is of the utmost importance to define its durability.

Figure 6.15 top shows the shrinkage results for the two specimens that stabilize for both mixes after 500 days, under the curing conditions defined in section 2.3 Test

methods. SCC-SF has greater shrinkage (6% approximately) than that of SCC-RF. 90% of the total shrinkage in SCC-SF is reached after 257 days and 269 days for SCC-RF. The development of the deformation is faster in the SCC-SF mix, due to the fact that the physico-chemical characteristics of SF filler favour pozzolanic activity as opposed to RF. Moreover, the finer porous structure present in SCC-SF (Figure 6.6), once the capillary water has been eliminated, results in a greater interaction force between the capillary walls than that of SCC-RF [60] and consequently favours shrinkage in SCC-SF.

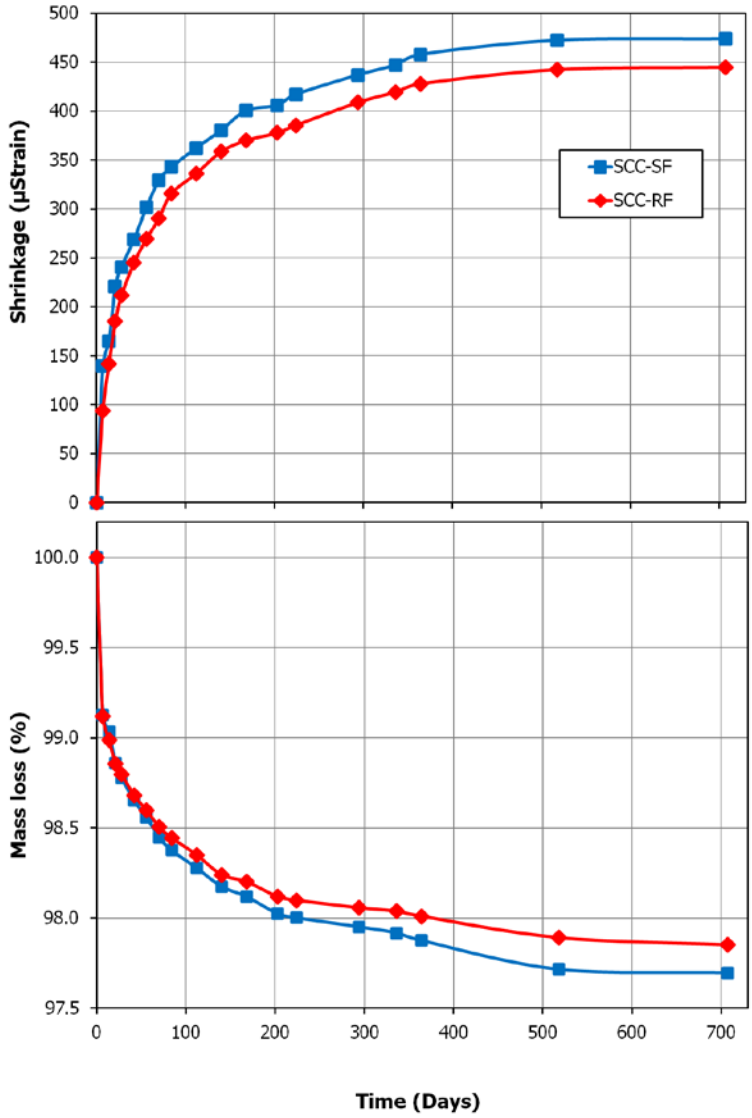

Figure 6.15: Total shrinkage and mass loss of the mixes.

Furthermore, in the SCC-RF mix, RF particles will contain more adsorbed water than SF owing to its greater specific surface (Figure 6.2), which agrees with the greater loss of water by drying at 100 ºC of the SCC-RF sample compared to SCC-SF (Figure 6.7). This gives rise to the slower decrease in humidity in the mix [61]. As a consequence, the necessary time to reach 90% of total shrinkage will be greater in SCC-RF.

In summary, if one takes into account the shrinkage due to pozzolanic activity and drying, to which one must add the effect of the afore-mentioned porous structure, it can be concluded that shrinkage is greater in SCC-SF, which agrees with the greater water content in SCC-SF, determined by means of thermo-gravimetrical analysis [23].

The loss of weight produced during the shrinkage process is slightly greater for SCC-SF (Figure 6.15 bottom), which agrees with the greater water content of hydration [23].

The results of our study agree with those of Valcuende et al. [16], who analysed shrinkage in SCC made with blast furnace slag and fly ash, using several replacement ratios of natural sand with slag, finding an increase in shrinkage when increasing the substitution ratio of natural sand, due to the greater content of reactive chemical species and the finer porous structure of the mixes with blast furnace slag. Shrinkage is less in our study since a smaller amount of reactive materials was used. Likewise, Gesoglu et al. [62] observed that mixes with a large amount of silica fume as mineral admixture showed greater shrinkage that could be lessened if the mix included other fillers. The shrinkage values observed were greater than in our study, where a larger amount of coarse sand and less fine sand were used. Moreover, the SF used is less reactive than silica fume due to its smaller particle size. Da Silva & de Brito [63] observed that, for high replacement ratios of cement with limestone filler or fly ash, shrinkage was greater when using fly ash. Heirman et al. [64] observed similar shrinkage to that of our study using limestone filler, although slightly greater owing to greater paste content. Lastly, Poppe & De Schutter [65] carried out a long-term shrinkage study (1400 days) in SCC made with CEM I and limestone filler, obtaining a similar stabilisation time to that registered in SCC-SF and SCC-RF and shrinkage values similar to those presented in our study.

6.4 Conclusions

A study was carried out on the durability of two types of SCC, one with dolomitic recovery filler (SCC-RF), and the other with commercial siliceous filler (SCC-SF) as a reference, analysing the microstructural properties of both mixes.

The mixes comply with the self-compactability requirements set by EHE-08, as well as showing high reproducibility, tested by different times and different appliers. The fresh-state density of SCC-SF (2.405 kg/dm^3) is slightly greater than that of SCC-RF (2.374 kg/dm^3) due mainly to the different physico-chemical of the fillers.

In the mixes, there is a greater difference between the dry bulk density (1%) than in the apparent dry density (0.6%), influenced by a greater open porosity in SCC-RF, which is 4% greater than in SCC-SF, 11.9% vs. 11.4% respectively. These results agree with the greater porosity of SCC-RF observed in the porosimetry by mercury intrusion, since the volume of intrusion is greater in SCC-RF for pores over 70 µm and between 50.0 nm and 10.0 µm (large capillary pores). In contrast, for the 2.5-10.0 nm range (small gel pores) it is greater in the SCC-SF sample, which demonstrates the less fine porous structure of SCC-RF even though the shape of the curve of distribution of pore size and the maximum pore concentration (around 40 nm) is similar in both mixes.

The absorption of water by immersion is slightly greater in SCC-RF, which is related to its greater porosity. Both mixes showed lower values of absorption by water capillarity than the limits set by the Ibero-American document RED DURAR in the framework CYTED, in terms of effective porosity (<10%) and sorptivity (<0.039 cm/min$^{1/2}$), so that they could be used in aggressive environments with adequate durability.

The results for water penetration under pressure enabled considering that both mixes have high compactability and are impermeable, since they never showed penetration over 30 mm (limit set in the literature as maximum penetration to be considered impermeable).

Chloride ion penetration in both SCC-SF and SCC-RF show the same migratory behaviour of ions within the mix when an electric field is applied, being classified as concrete of low chloride ion penetration according to ASTM C 1202. In relation to the concentration of chloride ion in function of depth, the mixes show a similar behaviour regarding the risk of steel corrosion, since they show a safety margin of more than 20 mm.

The penetration depth of CO_2 in SCC-RF is 30% greater than in SCC-SF, due mainly to two factors: the greater porosity of SCC-RF and the different curing mechanism of this mix relative to SCC-SF.

Regarding the penetration of ion SO_3, there is a different behaviour of the mixes. SCC-SF shows lower values than SCC-RF for each specimen depth. The greater microstructural density of SCC-SF results in the SO_3 reaching lower penetration depths in this material. After the exposure time to aggressive environments neither mix shows any sign of wearing out or deterioration.

Shrinkage in both mixes stabilises after 500 days, under the curing conditions used in this study. SCC-SF has greater shrinkage (≈6%) than SCC-RF. 90% of the total shrinkage of SCC-SF and SCC-RF is reached after 257 and 269 days respectively, since the physico-chemical characteristics of the SF filler, the finer porous structure of SCC-SF, as well as the greater water content, favour shrinkage of that mix. In short, the SCC mix made with recovery filler from plants manufacturing hot mix asphalt SCC-RF should have better features than SCC-SF in terms of shrinkage.

It can therefore be concluded that it is possible to obtain good quality SCC relative to durability by replacing commercial siliceous filler (SF) with dolomitic recovery filler, sourced from hot-mix asphalt plants (RF), with good performance in terms of aggressive agent attack, according to the levels set by the Spanish Code for Structural Concrete.

6.5 Acknowledgements

This work was partly supported by the Andalusian Regional Government (Research Groups FQM-391 and TEP-227). A. Romero Esquinas also acknowledges funding from MECD-Spain (http://www.mecd.gob.es/educacion-mecd/) FPU-13/04030. The authors wish to thank the Research Plan of the University of Cordoba (2016), Spanish Ministry of Economy and Competitiveness (Project MAT2015-70728-P), the staff at the Electron Microscopy and Elemental Analysis units of the Central Research Support Service (SCAI) of University of Cordoba for technical assistance, the Fine Chemistry Institute of the University of Córdoba for technical support, the Andalusian Innovation Centre for Sustainable Construction (CIAC) for the use of the press IBERTEST, model MEH-3000, BASF Chemical Company for supplying the admixture, and Portland Valderrivas (Alcalá de Guadaira, Seville) for the cement supplied, and the National Radioactive Waste Company (ENRESA) for the aggregates supplied. The support of the CERIS-ICIST Research Institute, IST, University of Lisbon, and of FCT (Foundation for Science and Technology) is also acknowledged.

6.6 References

[1] W.R. Stahel, G. Reday-Mulvey, Jobs for tomorrow: the potential for substituting manpower for energy, Vantage Press, New York (1981).

[2] European Commission, Report from the commission to the European parliament, the council, the European Economic and Social Committee and the Committee of the Regions on the Implementation of the Circular Economy Action Plan, (2017).

[3] K. Celik, C. Meral, A.P. Gursel, P.K. Mehta, A. Horvath, P.J. Monteiro, Mechanical properties, durability, and life-cycle assessment of self-consolidating concrete mixtures made with blended portland cements containing fly ash and limestone powder, Cement and Concrete Composites 56 (2015) 59-72.

[4] J. Moya, N. Pardo, A. Mercier, Energy efficiency and CO2 emissions: Prospective scenarios for the Cement industry, Publications Office2010.

[5] European Federation of National Associations Representing producers and applicators of specialist building products for Concrete (EFNARC). The European

guidelines for self-compacting concrete specification. Production and Use. Hampshire, UK; (2005), www.efnarc.org.

[6] M.G. Beltrán, F. Agrela, A. Barbudo, J. Ayuso, A. Ramírez, Mechanical and durability properties of concretes manufactured with biomass bottom ash and recycled coarse aggregates, Construction and Building Materials 72 (2014) 231-238.

[7] M. Cabrera, A.P. Galvin, F. Agrela, M.D. Carvajal, J. Ayuso, Characterisation and technical feasibility of using biomass bottom ash for civil infrastructures, Construction and Building Materials 58 (2014) 234-244.

[8] E. Ledesma, J. Jiménez, J. Ayuso, J. Fernández, J. de Brito, Experimental study of the mechanical stabilization of electric arc furnace dust using fluid cement mortars, Journal of hazardous materials 326 (2017) 26-35.

[9] A. López-Uceda, J. Ayuso, J.R. Jiménez, F. Agrela, A. Barbudo, J. De Brito, Upscaling the use of mixed recycled aggregates in non-structural low cement concrete, Materials 9(2) (2016) 91.

[10] N. Saikia, J. de Brito, Use of plastic waste as aggregate in cement mortar and concrete preparation: A review, Construction and Building Materials 34 (2012) 385-401.

[11] M. Tennich, M.B. Ouezdou, A. Kallel, Behavior of self-compacting concrete made with marble and tile wastes exposed to external sulfate attack, Construction and Building Materials 135 (2017) 335-342.

[12] G. Sua-Iam, N. Makul, Effect of incinerated sugarcane filter cake on the properties of self-compacting concrete, Construction and Building Materials 130 (2017) 32-40.

[13] B. Felekoglu, Utilisation of high volumes of limestone quarry wastes in concrete industry (self-compacting concrete case), Resources, Conservation and Recycling 51(4) (2007) 770-791.

[14] K.E. Alyamaç, R. Ince, A preliminary concrete mix design for SCC with marble powders, Construction and Building Materials 23(3) (2009) 1201-1210.

[15] G. Singh, R. Siddique, Effect of iron slag as partial replacement of fine aggregates on the durability characteristics of self-compacting concrete, Construction and Building Materials 128 (2016) 88-95.

[16] M. Valcuende, F. Benito, C. Parra, I. Miñano, Shrinkage of self-compacting concrete made with blast furnace slag as fine aggregate, Construction and Building Materials 76 (2015) 1-9.

[17] M. Uysal, M. Sumer, Performance of self-compacting concrete containing different mineral admixtures, Construction and Building materials 25(11) (2011) 4112-4120.

[18] M. Uysal, K. Yilmaz, M. Ipek, The effect of mineral admixtures on mechanical properties, chloride ion permeability and impermeability of self-compacting concrete, Construction and Building Materials 27(1) (2012) 263-270.

[19] K. Kapoor, S. Singh, B. Singh, Durability of self-compacting concrete made with Recycled Concrete Aggregates and mineral admixtures, Construction and Building Materials 128 (2016) 67-76.

[20] B. Alsubari, P. Shafigh, M.Z. Jumaat, Utilization of high-volume treated palm oil fuel ash to produce sustainable self-compacting concrete, Journal of Cleaner Production 137 (2016) 982-996.

[21] EAPA. Asphalt in figures, 2015. European Asphalt Pavement Association (2017).

[22] J. Martin, J.R. Montero, F. Moreno, J.P. Sala, M. Rubio, Feasibility analysis of the reuse of waste filler of bituminous mixtures for the production of self-compacting concrete, Materials & Design 46 (2013) 372-380.

[23] A.R. Esquinas, C. Ramos, J. Jiménez, J. Fernández, J. de Brito, Mechanical behaviour of self-compacting concrete made with recovery filler from hot-mix asphalt plants, Construction and Building Materials 131 (2017) 114-128.

[24] P. Swarthmore, Joint Committee on Power Diffraction Standard-International Centre for Diffraction Data. (1995).

[25] Asociación Española de Normalización y Certificación, AENOR, Madrid, Spain, (2017).

[26] EHE-08. Spanish Structural Concrete Code EHE-08 [Instrucción de Hormigón Estructural EHE-08]. R.D. 1247/2008, Spain (2008).

[27] D.P. Bentz, C.J. Haecker, An argument for using coarse cements in high-performance concretes, Cement and Concrete Research 29(4) (1999) 615-618.

[28] J.M. Pommersheim, Effect of particle size distribution on hydration kinetics, MRS Proceedings, Cambridge Univ Press, 1986, 301 p.

[29] S. Tsivilis, S. Tsimas, A. Benetatou, E. Haniotakis, Study on the contribution of the fineness on cement strength, (1990).

[30] http://www.master-builders-solutions-basf.es.

[31] European Federation of National Associations Representing producers and applicators of specialist building products for Concrete (EFNARC). Specification and guidelines for self-compacting concrete, Hampshire, UK; 2002, www.efnarc.org.

[32] S. Brunauer, P.H. Emmett, E. Teller, Adsorption of gases in multimolecular layers, Journal of the American chemical society 60(2) (1938) 309-319.

[33] RILEM CP11.3. Absorption of water by immersion under vacuum, Mater Structres Test (1984) 17(101): 391-94.

[34] E. Poulsen, Chloride profiles - Analysis and interpretation of observations, AEC Laboratory, Vedbæk, Denmark (1995).

[35] American Society of Testing Materials, ASTM International, West Conshohocken, USA, (2017).

[36] LNEC E-391, Concrete determination of carbonation resistance. National Laboratory of Civil Engineering (LNEC), Lisbon, Portugal; 1993.

[37] A.W. Saak, Characterization and modeling of the rheology of cement paste: with applications toward self-flowing materials, 2000.

[38] I.B. Topçu, T. Bilir, T. Uygunoğlu, Effect of waste marble dust content as filler on properties of self-compacting concrete, Construction and Building Materials 23(5) (2009) 1947-1953.

[39] D. Ho, A. Sheinn, C. Ng, C. Tam, The use of quarry dust for SCC applications, Cement and Concrete Research 32(4) (2002) 505-511.

[40] S. Assié, G. Escadeillas, V. Waller, Estimates of self-compacting concrete 'potential'durability, Construction and Building Materials 21(10) (2007) 1909-1917.

[41] M. Valcuende, C. Parra, Natural carbonation of self-compacting concretes, Construction and Building Materials 24(5) (2010) 848-853.

[42] D. Silva, V. John, J. Ribeiro, H. Roman, Pore size distribution of hydrated cement pastes modified with polymers, Cement and Concrete Research 31(8) (2001) 1177-1184.

[43] L. Cui, J.H. Cahyadi, Permeability and pore structure of OPC paste, Cement and Concrete Research 31(2) (2001) 277-282.

[44] Mehta PK, Monteiro PJM. Concrete structure, properties and materials. New Jersey: Prentice Hall, 1993:548.

[45] P. Da Silva, J. De Brito, Experimental study of the porosity and microstructure of self-compacting concrete (SCC) with binary and ternary mixes of fly ash and limestone filler, Construction and Building Materials 86 (2015) 101-112.

[46] G. De Schutter, K. Audenaert, Evaluation of water absorption of concrete as a measure for resistance against carbonation and chloride migration, Materials and Structures 37(9) (2004) 591-596.

[47] J. Jurin, An account of some experiments shown before the Royal Society; with an enquiry into the cause of the ascent and suspension of water in capillary tubes. Philosophical Transactions 30(351-363) (1717) 739-747.

[48] G. Fagerlund, On the capillarity of concrete. Nord Concr Res (1982);1:6.1–6.20.

[49] C. Hall, Water sorptivity of mortars and concretes: a review, Magazine of concrete research 41(147) (1989) 51-61.

[50] J. Howland, A. Martin, Estudio de la absorción capilar y la sorptividad de hormigones con áridos calizos cubanos, Materiales de construcción 63(312) (2013) 515-527.

[51] S.A. Bernal, R.M. de Gutiérrez, A.L. Pedraza, J.L. Provis, E.D. Rodriguez, S. Delvasto, Effect of binder content on the performance of alkali-activated slag concretes, Cement and Concrete Research 41(1) (2011) 1-8.

[52] O. Trocónis-Rincón, A. Romero-Carruyo, C. Andrade, P. Helene, I. Díaz, Manual for inspection, evaluation and diagnosis of corrosion in reinforced concrete structures (in Spanish), DURAR Report, CyTED, Maracaibo, Venezuela, (1997), 208 p.

[53] A.M. Neville, Properties of concrete. 4th ed. Harlow, London: Longman Group Limited; 1995.

[54] G. De Schutter, K. Audenaert, Report 38: Durability of self-compacting concrete - State-of-the-art report, Technical Committee 205-DSC, RILEM publications 2007.

[55] G. Glass, N. Buenfeld, The presentation of the chloride threshold level for corrosion of steel in concrete, Corrosion science 39(5) (1997) 1001-1013.

[56] E.B. Bermejo Núñez, Dosificación, propiedades y durabilidad en hormigón autocompactante para edificación [Ph.D. Thesis]. Universidad Politécnica de Madrid; 2009.

[57] P.C. Ryan, A. O'Connor, Comparing the durability of self-compacting concretes and conventionally vibrated concretes in chloride rich environments, Construction and Building Materials 120 (2016) 504-513.

[58] P.R. da Silva, J. de Brito, Durability performance of self-compacting concrete (SCC) with binary and ternary mixes of fly ash and limestone filler, Materials and structures 49(7) (2016) 2749-2766.

[59] M. Bassuoni, M. Nehdi, Durability of self-consolidating concrete to sulfate attack under combined cyclic environments and flexural loading, Cement and Concrete Research 39(3) (2009) 206-226.

[60] M. Valcuende, E. Marco, C. Parra, P. Serna, Influence of limestone filler and viscosity-modifying admixture on the shrinkage of self-compacting concrete, Cement and Concrete Research 42(4) (2012) 583-592.

[61] S. Zhutovsky, K. Kovler, A. Bentur, Influence of cement paste matrix properties on the autogenous curing of high-performance concrete, Cement and Concrete Composites 26(5) (2004) 499-507.

[62] M. Gesoğlu, E. Güneyisi, E. Özbay, Properties of self-compacting concretes made with binary, ternary, and quaternary cementitious blends of fly ash, blast furnace slag, and silica fume, Construction and Building Materials 23(5) (2009) 1847-1854.

[63] P. Silva, J. de Brito, Experimental study of the mechanical properties and shrinkage of self-compacting concrete with binary and ternary mixes of fly ash and limestone filler, European Journal of Environmental and Civil Engineering 21(4) (2017) 430-453.

[64] G. Heirman, L. Vandewalle, D. Van Gemert, V. Boel, K. Audenaert, G. De Schutter, B. Desmet, J. Vantomme, Time-dependent deformations of limestone powder type self-compacting concrete, Engineering Structures 30(10) (2008) 2945-2956.

[65] A.M. Poppe, G. De Schutter, Creep and shrinkage of self-compacting concrete, First International Symposium on Design, Performance and Use of Self-Consolidating Concrete, China, 2005, pp. 329-336.

Capítulo 7

Mechanical behaviour of self-compacting concrete made with non-conforming fly ash from coal-fired power plants

"A.R. Esquinas, E.F. Ledesma, R. Otero, J.R. Jiménez, J.M. Fernández, Mechanical behaviour of self-compacting concrete made with non-conforming fly ash from coal-fired power plants, Construction and Building Materials, 182 (2018) 385–398. doi:10.1016/J.CONBUILDMAT.2018.06.094."

Abstract

Currently, global sustainability depends on achieving integrated productivity in all economic sectors, making it possible to respond to the environmental challenges facing humanity at present. With the dual objective of optimization of natural non-renewable resources and waste recovery, this study has carried out an evaluation of the fly ash of a coal-fired power plant that does not meet the criteria of conformity as a filler in concrete. One may conclude that it is possible to obtain a self-compacting concrete (SCC) by replacing (in volume) a natural siliceous filler (SF) with non-conforming fly ash (NCFA) from coal-fired power plants to obtain a superior mechanical behaviour than the minimum levels stipulated by the Spanish Code on

Structural Concrete and/or Eurocode 2. The SCC manufactured with NCFA partially presented good performance in terms of self-compactability, mechanical behaviour, and shrinkage. To achieve these results, a comparative study of three mixes of SCC was carried out. In the first (SCC-1), a commercial SF (SCC reference) was used; in the second a mix, 1: 1 in volume, SF and NCFA (SCC-12) was used; and in the third, only NCFA was used (SCC-2). The mechanisms for setting the mixes have been identified. Pozzolanic and mild carbonation reactions were present in the SCC-1 mix. In SCC-12, both pozzolanic and carbonation reactions were observed. In the SCC-2 mix, only carbonation processes were observed. The mechanical behaviour of the SCC-1 and SCC-12 mixes is better than that of SCC-2. The incorporation of NCFA as a filler in SCCs resulted in better shrinkage performance at an early age, and therefore, less cracking.

Key words: Self-compacting concrete; non-conforming fly ash; siliceous filler; setting reactions; mechanical behaviour; ultrasonic pulse velocity; shrinkage.

Highlights:

- A comparative study of three types of SCC was carried out.
- The mixes comply with the self-compacting requirements.
- The aging mechanisms of the SCC mixes (SCC-1, SCC-12, and SCC-RF) were different.
- Pozzolanic reactions occurred during the curing of SCC-1.
- Shrinkage in the NCFA mix was lower because of the larger particle size.
- Non-conforming fly ash from coal-fired power plants is adequate to produce SCC.

7.1 Introduction

Innovation and research are the key to the implementation of a circular economy in the construction sector, which is fundamental for the sustainability of the current world. Along these lines, the European Union (EU) has indicated the actions and compromises in all economic sectors to achieve the optimization of natural resources, as well as the minimization and valorisation of waste, managing to respond to

environmental challenges [1]. In the construction sector, the concrete industry stands out, since concrete is the most widely used construction material [2, 3].

Self-compacting concrete (SCC) was developed in Japan by Professor Okamura in the mid-1980s [4]. The main feature of this type of concrete is the ability to flow and completely fill the entire volume of the formwork by the action of its own weight [5]. This allows for the execution of complex and densely reinforced structures [6, 7]. SCC needs to incorporate a high content of fines (cement, filler, and/or fine aggregates) and chemical additives in its dosage. This particularity means that the SCC can be considered as not very environmentally friendly. Nowadays, a solution would be to use materials of a residual nature as a substitute for the conventional raw materials used in the manufacture of the SCC. This would allow the minimization and valorization of this waste, as well as the optimization of the natural resources used.

Sharma and Khan [8] used copper slag with different percentages of fine aggregate substitution. The results of their research showed the improvement of the self-compactability properties with the increase in the percentage of substitution. Subasi et al. [9] used waste ceramic powder as a filler, and this had a positive effect on the viscosity of the mixes, although the strength suffered a slight reduction. Gesoglu et al. [10] incorporated plastic waste powder in the SCC in different percentages of cement replacement. Esquinas et al. [11, 12] developed SCC, incorporating a dolomitic waste powder from the drying of the aggregates of the hot bituminous mixes as a substitute for the commercial filler of siliceous nature, and they reported good mechanical behaviour and durability.

By-products generated during combustion in different industrial processes have been evaluated for application as raw materials in the SCC by different researchers. Gill and Siddique [13] used rice-husk ash as a substitute for fine aggregates. Ranjbar et al. [14] observed the great potential of palm oil fuel ash as a substitute for cement in SCC. The application of the ashes in SCC, resulting from the combustion of agricultural residues in biomass-fired power plants as a filler was investigated by Cuenca et al. [15].

The most studied by-product from combustion processes has been the fly ash (FA) from coal-fired power plants that meets the criteria of compliance specified by the standards EN 450-1, EN 450-2, EN 14227-4, and ASTM C 618 [16, 17] (conforming fly ash), and is characterized by its pozzolanic nature [18-21].

The global production of FA is estimated at 750 million tons/year, of which 100 million tons/year are generated in Europe [22, 23]. When the FA does not comply with the required fineness, i.e., when the mass retained on the 0.045-mm sieve is greater than 40%, the FA is considered as non-conforming fly ash (NCFA). In addition, we must consider the fact that this by-product represents between 30% and 40% of the total production of FA and it is destined to landfill, significantly impacting the environment [24].

This is a very serious environmental problem since coal will continue to be the most-used fuel for decades, according to the estimates of the International Energy Agency [25]. The FA resulting from the combustion of coal, in accordance with Directive 2008/98/EC of the European Union (European Waste Framework Directive), is considered as waste and must be recovered to achieve the end-of-waste (EoW) status before it may be used again [26].

In the present work, the use of NCFA has been evaluated as a filler in SCC. A comparative study of three SCCs mixes was carried out; in the first mix, a commercial siliceous filler (SF) was used as a reference; in the second a mix, 1:1 in volume, of SF and NCFA was used; and in the third, only NCFA was used. The amount of filler used in volume is similar in all cases. To determine the behaviour of the three SCCs, a fresh-state study was carried out first, and self-compatibility properties were studied, such as fluidity, blocking resistance, and resistance to segregation. Subsequently, a deep analysis of hardened SCCs was carried out, including their mechanical behaviour in the long term and their correlation with the different chemical reactions that occur during setting time. Finally, a short-term shrinkage study is also included to allow a response to the mechanical requirements demanded for the use of this waste.

7.2 Experimental methodology

7.2.1 Materials

The aggregates used were gravel 4/16 (G), coarse sand 0/4 (S1), and fine sand 0/2 (S2), which come from the crushing plant owned by Charamuzca Movimiento de Tierras, Áridos, and Hormigones SL (Córdoba, Spain). Their grading curves are shown in Figure 7.1. The physical–chemical characterization is shown in Table 7.1. The aggregates are suitable for the manufacture of concrete, according to the Spanish Instruction for Structural Concrete (EHE-08) [27]. In the X-ray diffractogram (Figure 7.2), it was observed that the main phase was quartz (33-1161) [28]; in addition, the presence of calcite (05-0586) [28], orthoclase (31-0966) [28], albite (41-1480) [28], and clinochlore (16-0362) [28] was observed.

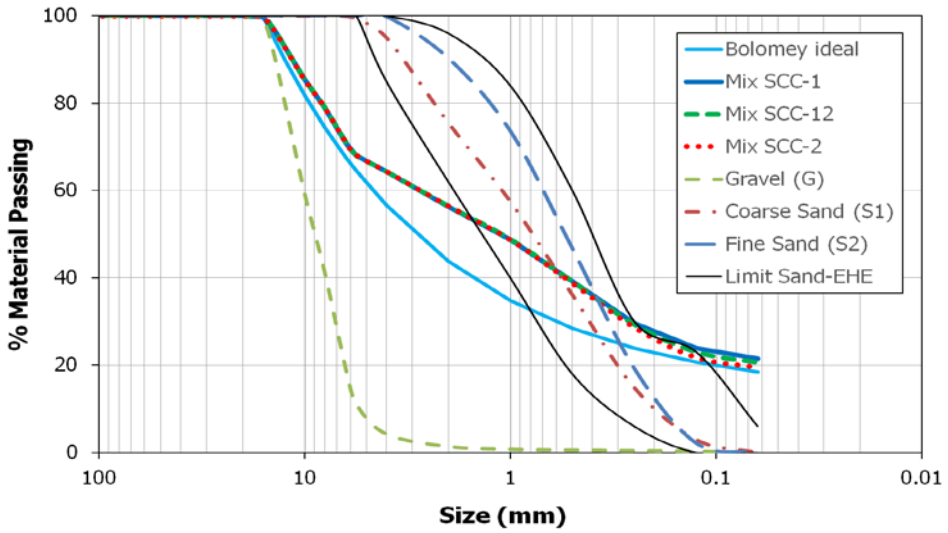

Figure 7.1: Particle size distribution for gravel, coarse and fine sands, mixes SCC-1, SCC-12 and SCC-2.

The commercial filler is of siliceous nature and comes from the Mines Carmina of the company Lorda and Roig S.A. (Gerona, Spain). The NCFA comes from the Puente Nuevo coal-fired power station (Córdoba, Spain) of Viesgo electric company. The SF is in accordance with the requirements set by the EHE-08, and the NCFA presents a size distribution somewhat greater than the one specified by the instruction UNE-EN

933-1 [16]). In addition, an analysis of the grain size distribution was carried out by laser diffraction, using ethanol as the dispersant (Figure 7.3).

Table 7.1
Characterisation of aggregates.

Characteristic	**Standard**	**G**	**S1**	**S2**	**Limit set by EHE-08**
Size (mm)	UNE-EN 933-1	4/16	0/4	0/2	<25
Fines content (%) [a]	UNE-EN 933-1	0.2	1	1	<8
Index slabs (%)	UNE-EN 933-3	10.3	-	-	< 35
Crushed and broken surfaces (%)	UNE-EN 933-5	86	-	-	Not limited
Los Angeles coefficient	UNE-EN 1097-2	18	-	-	≤ 40
Dry sample density ρ_{rd} (g/cm^3)	UNE-EN 1097-6	2.62	2.63	2.66	Not limited
Water absorption (%)	UNE-EN 1097-6	0.73	0.49	0.33	≤ 5
Friability coefficient (%)	UNE 83115	-	17.3	18	< 40 [b]
Surface cleaning (%)	UNE 146130	0.05	-	-	Not limited
Water soluble chlorides (% Cl)	UNE-EN 1744-1	6×10^{-4}	6×10^{-4}	1.4×10^{-3}	≤ 0.03
Acid soluble sulphates (% SO_3)	UNE-EN 1744-1	9×10^{-3}	2×10^{-2}	4×10^{-3}	≤ 0.8
Water soluble sulphates (% SO_3)	UNE-EN 1744-1	2×10^{-2}	7×10^{-3}	2×10^{-2}	≤ 0.8
Sulphur content (%)	UNE-EN 1744-1	ND [c]	ND	ND	≤ 1
Organic matter content (%)	UNE-EN 1744-1	0.05	0.13	0.12	≤ 1 [d] - ≤ 0.5 [e]

[a] Finer than 0.063 mm; [b] Recommendation; [c] ND: No Detected; [d] Coarse aggregates; [e] Fine aggregates

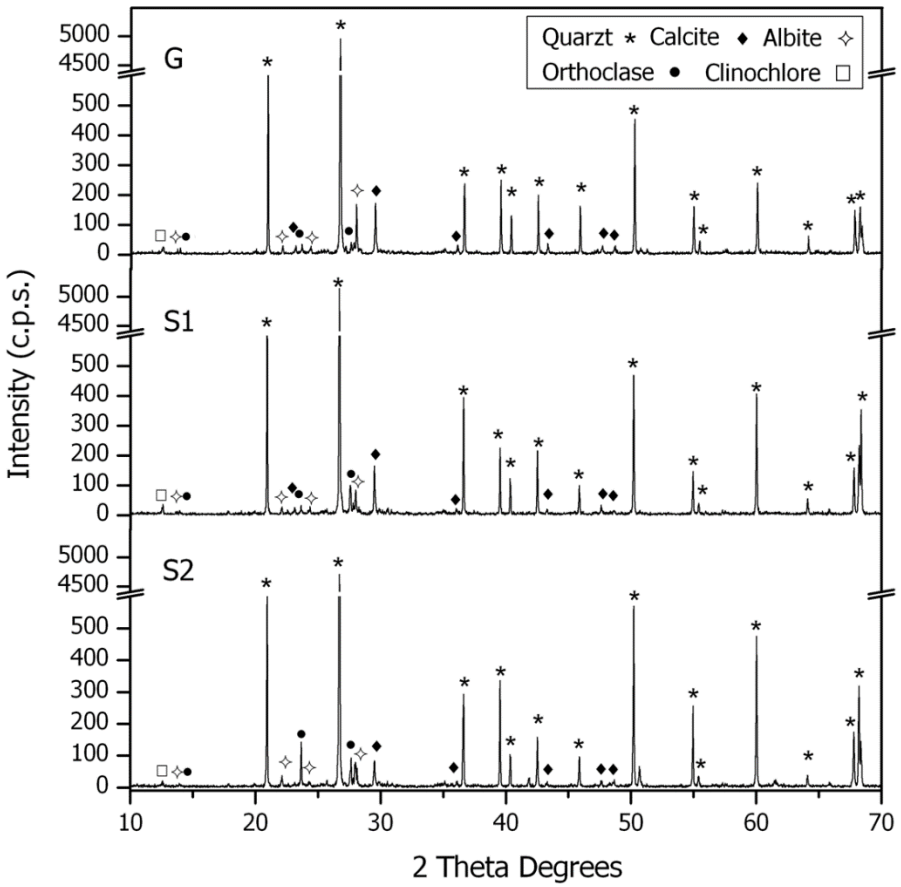

Figure 7.2: PXRD patterns for gravel (G), coarse (S1) and fine (S2) sands.

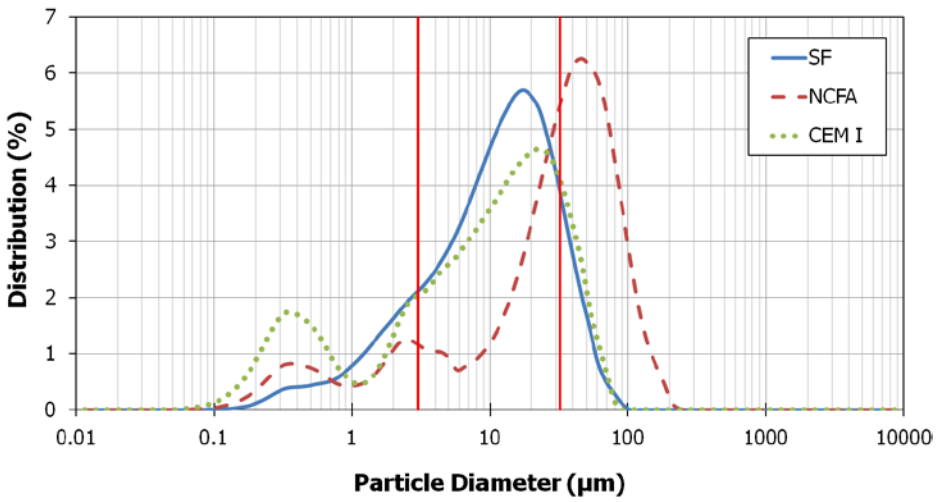

Figure 7.3: Grain-size distribution of SF, NCFA and CEM I by laser diffraction.

The NCFA has a wider distribution than the SF (0.1–240 μm vs 0.1–100 μm). The highest percentage of particles is around 20 μm for the SF and around 45 μm for the NCFA. The SF has the highest percentage of particles between 3 and 32 μm (74.78%). In the NCFA, the percentage of particles found between 3–32 μm is 39.64% (Table 7.2). These results are significant, since above 32 μm (8.09% for the SF vs 45.01% for the NCFA), the particles are too large to fully hydrate, and below 3 μm (17.13% for the SF vs 15.35% for the NCFA), make only a small contribution to the mechanical strength and simultaneously demand more water [29-31]. Moreover, this large number of particles whose size exceeds 45 μm prevents their use as a mineral addition for concrete production, in accordance with UNE-EN 450-1:2003 [16], and hence the name "non-conforming fly ash".

The X-ray diffraction (XRD) patterns (Figure 7.4) revealed that quartz is the only phase of SF present (33-1161) [28], which has a high crystallinity. In the NCFA, besides quartz (33-1161) [28], the presence of mullite (15-0776) [28], dolomite (36-0426) [28], and maghemite (γ-Fe_2O_3) (25-1402) [28] were observed, along with a non-negligible percentage of amorphous phase. The thermogravimetric analysis of the fillers (Figure 7.5) shows the purity of the SF filler, since no thermal effect is observed. In the case of NCFA, two exothermic peaks are observed, which corresponds to a small weight loss (1.2%) between 500 and 700 °C, indicating the decomposition of dolomite.

The Brunauer–Emmett–Teller (BET) surface of both samples (SF and NCFA) was very small, at 2.90 m^2/g and 1.80 m^2/g, respectively (Table 7.2). The pore size distribution, obtained from the adsorption–desorption isotherms of nitrogen, is shown Figure 7.6. Both fillers show a range of pore diameter between 2.5–37 nm, according to the DFT method. The distribution of pore volume is comparable in both materials, although for the NCFA, the range in which the highest quantity of pore volume is centred was slightly lower than SF (2.5–6 nm vs. 2.5–9 nm). Both samples have mesopores of small size, below 10 nm, and the maximum of the pore volume distribution is around 3.2 nm, which is very close to the micropore area (<2 nm).

Table 7.2
Characterisation of filler, cement and aggregates.

Characteristic	Standard	SF	NCFA	Cement	G	S1	S2
SiO_2 %	-	100	28.50	13.30	65.98	52.95	59.85
Al_2O_3 %	-	-	54.90	6.60	13.10	17.33	15.30
Fe_2O_3 %	-	-	14.90	16.60	9.18	15.62	13.10
SO_3 %	-	-	-	5.00	-	-	-
CaO %	-	-	0.60	56.30	5.02	5.01	4.95
MgO %	-	-	0.60	0.70	0.48	0.44	0.40
Na_2O%	-	-	-	-	1.64	2.63	1.80
K_2O%	-	-	-	-	4.59		
Other	-	-	0.50	1.50	-	-	-
Particle size > 32 µm (%)	-	8.09	45.01	9.81	-	-	-
Particle size 3 - 32 µm (%)	-	74.78	39.64	63.81	-	-	-
Particle size < 3 µm (%)	-	17.13	15.35	26.38	-	-	-
BET surface area (m^2/g)	-	2.90	1.80	0.67	-	-	-
Particle density (g/cm^3)	UNE 80103	2.60	1.86	3.10	-	-	-
Bulk density (g/cm^3)	UNE-EN 1097-3	0.69	1.04	-	-	-	-

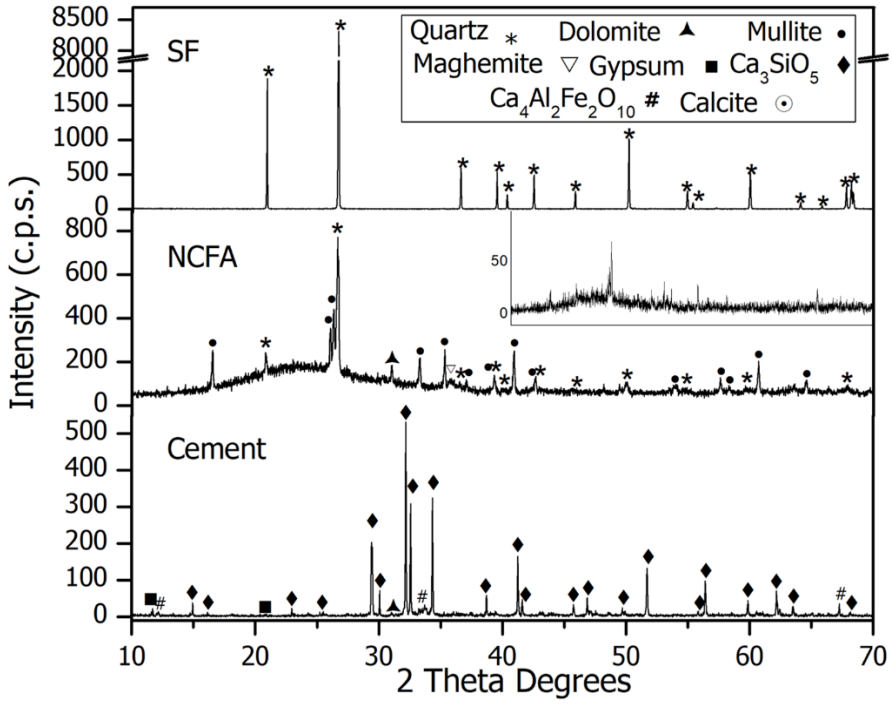

Figure 7.4: PXRD patterns for SF, NCFA and cement.

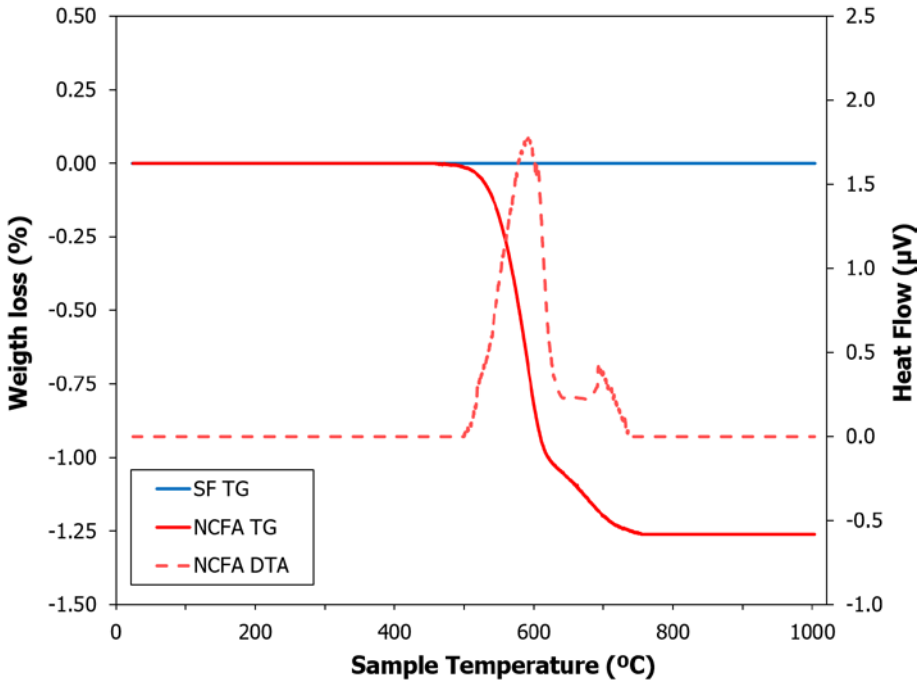

Figure 7.5: TG (solid lines) and DTA (dotted line) curves for the SF and NCFA fillers.

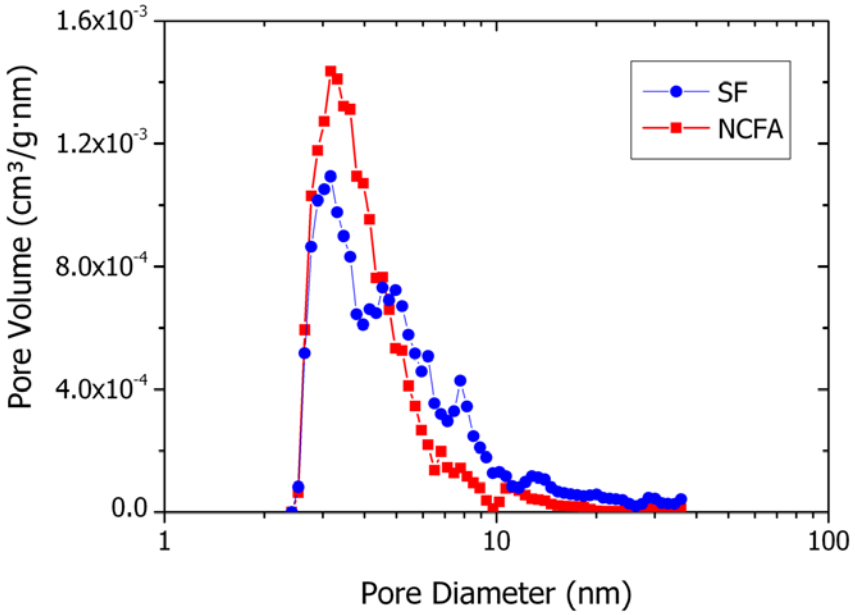

Figure 7.6: Pore size distribution for the SF and NCFA fillers.

The cement used was type CEM I 42,5 R/SR (UNE 80303-1 and UNE-EN 197-1) [16]. Figure 7.3 shows the particle size distribution, which, as in the SF, has the highest percentage of particles between 3 and 32 μm (63.81%) (Table 7.2), and this is important for the hydration process, as mentioned previously. The chemical composition, expressed in the form of oxides, determined by energy-dispersive X-ray analysis (EDX), is shown in Table 7.2. The majority oxide was calcium oxide (CaO), highlighting that the content of aluminium oxide (Al_2O_3) was very low. The X-ray diffractogram (Figure 7.4) showed that the majority mineral phase was tricalcium silicate, Ca_3SiO_5 (42-0551) [28], and a small proportion of gypsum, $CaSO_4 \cdot H_2O$ (33-0311) [28] and calcium ferroaluminate, $Ca_4Al_2Fe_2O_{10}$, (11-0124) [28], were detected.

An additive, superplasticizer/water reducer with high performance, was used, specific for SCC (sp), Glenium 303 SCC BASF Chemical Company, and the objective was to manufacture SCC with a low water/cement ratio (W/C).

7.2.2 Concrete mixes and composition tests

Three mixes (SCC-1, SCC-2, and SCC-12) were designed according the composition of Esquinas et al. [12], with a quantity of gravel of approximately 800 kg/m^3, and a minimum amount of cement of 400 kg/m^3. For all mixes, the specific design requirements were marked: exposure class IIIc, characteristic strength of 40 MPa, cement content 400 kg/m^3, maximum ratio W/C = 0.44, and the same amounts of additive (1.8% cement + filler) and cement. The adjustment of the dosage was made in volume (1025 L) [32].

To study the effect of the NCFA, as a filler, on the properties of SCC, three types of mixes were designed: SCC-1, SCC-2, and SCC-12, with commercial filler, with NCFA, and with a 1:1 mix (by volume) of both materials. For all mixes, we proceeded to the study the self-compactability according to the requirements of the EHE-08 [27].

The SCC-1 mix, whose composition in dry weight and volume is shown in Table 7.3, was considered as reference concrete. The three dosages met the recommendations of the European Federation of National Associations Representing Producers and Applicators of Special Building Products for Concrete (EFNARC) (Table 7.3) [6, 7].

To realize SCCs with NCFA (SCC-2 and SCC-12), maintaining the same filler volume as the reference dosage (SCC-1) and with a similar granular skeleton, small adjustments of the total content of aggregates and water were made, as well as of the relation 0/2 sand with respect to the filler (Table 7.3). It can be observed that the percentage of the different materials in the mixes were similar.

7.2.3 Test methods

The raw materials, as well as the hardened SCC, were characterized using different techniques. Particle sizes were measured in a Mastersizer S analyser (Malvern Instruments), using ethanol as the dispersant. The samples were analysed through XRD patterns by using a Bruker D8 Discover A25 instrument with CuKα radiation. SF and cement diffraction patterns were obtained by scanning the goniometer from 10° to 70° (2θ), at a rate of 0.05° min^{-1}. For NCFA, the rate was 0.006° min^{-1}

(additionally, for comparison, the spot inside a XRD pattern for NCFA, at a rate of 0.05° min^{-1}, was made).

Table 7.3
Concrete mix proportions and dosing tests.

Mixes	**SCC-1**				**SCC-12**				**SCC- 2**			
	Dry weight		*Volume*		Dry weight		*Volume*		Dry weight		*Volume*	
Constituent	Kg/m^3	%	*Liters*	*%*	Kg/m^3	%	*Liters*	*%*	Kg/m^3	%	*Liters*	*%*
Gravel 4/16 (G)	807.65	33.05	*309.80*	*30.26*	797.81	32.97	*306.03*	*29.89*	789.07	32.79	*302.67*	*29.56*
Sand 0/4 (S1)	657.28	26.90	*250. 59*	*24.47*	649.28	26.83	*247.53*	*24.17*	642.16	26.69	*244.82*	*23.91*
Sand 0/2 (S2)	280.82	11.49	*106.33*	*10.38*	284.37	11.75	*107.68*	*10.52*	300.82	12.50	*111.91*	*11.12*
Filler (SF)	101.75	4.16	*39.13*	*3.82*	51.96	2.15	*19.99*	*1.95*	0.00	0.00	*0.00*	*0.00*
Filler (NCFA)	0.00	0.00	*0.00*	*0.00*	41.57	1.72	*22.30*	*2.18*	72.94	3.03	39.13	3.82
Cement	410.00	16.78	*132.26*	*12.92*	410.00	16.94	*132.26*	*12.92*	410.00	17.04	*132.26*	*12.92*
Superplasticizer	9.21	0.38	*8.90*	*0.87*	9.06	0.37	*8.76*	*0.86*	8.69	0.36	*8.40*	*0.82*
Water	176.93	7.24	*176.93*	*17.28*	179.40	7.40	*179.40*	*17.52*	182.75	7.59	*182.75*	*17.8*
(W/C) $_{total}$	0.432				0.437				0.446			
(W/C) $_{ef}$	0.422				0.428				0.436			

	Typical range[a]	SCC-1	SCC-12	SCC-2
Coarse aggregate (kg/m^3)	750-1000	807.65	797.81	789.07
Fine aggregate (sand) (%)	48-55[b]	53.5	53.7	54.2
Fines (kg/m^3) / [L/m^3]	380-600[d]	544.52 / [183.87]	519.98 / [177.95]	486.46 / [168.13]
Water (litres/m^3)	150-210	176.93	179.40	182.75
Paste (litres/m^3)	300-380	360.80	357.35	350.89
Water/fines [c]	0.85-1.10	0.96	1.01	1.09

[a] EFNARC dosage parameters [7] [b] Volume total weight of aggregate in balanced quintiles. % of sand S1and S2 relative to the whole of the aggregates.
[c] by volume. [d] kg/m^3

The thermogravimetric analysis was carried out in a Setaram Setsys Evolution 16/18 apparatus, at a heating rate of 5 °C/min. Specimens (150 × 150 × 150 mm) were kept in an oven at 100 °C. Then, a little portion (a cube of 10 × 10 × 10 mm) was taken from the centre of the specimen for performing the thermic analysis (DTA-TGA). The tangent method was used to identify the temperature range of chemical species decomposition [33]. N_2 isotherms were determined on an Autosorb iQ (Quantachrome), and samples were degassed at 100 °C under vacuum for 2 h prior to this. The surface was calculated by applying the BET method in the range of relative equilibrium pressure $0.05 \leq P/Po \leq 0.20$ [34].

Microstructural characterization of the materials was carried out using an electron microprobe technique implemented on a JEOL JSM-7800F scanning electron microscope, using an acceleration voltage of 15 kV and a working distance of 10 mm. The X-ray detector was an X-MaxN150 from Oxford Instruments.

The self-compactability of mixes were studied according to the requirements of EHE-08. The compressive strength (UNE-EN 12390-3) [16] and the splitting tensile strength (UNE-EN 12390-6) [16] were measured in cylindrical specimens of 300 mm × 150 mm, and flexural strength (UNE-EN 12390-5) [16] was measured in prismatic specimens of 100 × 100 × 400 mm, for the ages 7, 28, 91, 182, and 250 days, cured in water, in accordance with UNE 12390-2 [16]. The secant modulus of elasticity in compression (UNE-EN 12390-13) [16] was studied at ages of 7, 28, 91, 182, and 250 days in cylindrical specimens of 300 mm × 150 mm. For this group of tests, an IBERTEST model MEH-3000 press with a maximum capacity of 3000 kN was used.

The ultrasonic pulse velocity (UPV) (UNE-EN 12504-4) [16] was evaluated at the ages of 7, 28, 91, 182, and 250 days for concrete, using an ultrasonic flow meter from Matest, model C369N. Related to this parameter, the density values (fresh, wet, and dry) (UNE-EN 12390-7 and UNE-EN12350-6) [16] in 150 × 150 × 150 mm specimens cured in water were determined. A total shrinkage study (ASTMC157 / C157M-08e1) [17] during the time of the retraction test, at a young age (up to 91 days), was performed on specimens with dimensions of 100 × 100 × 500 mm. For this test, the specimens were kept in a curing chamber under constant environmental conditions, at a temperature of 20 °C and a relative humidity of 50%. All tests were triplicated,

in specimens made from the same SCC mix, showing average values and standard deviations.

7.3 Results and discussion

7.3.1 Properties of SSC in fresh state

7.3.1.1 Self-compactability

Table 7.4 shows the self-compactability parameters of the three mixes, which agree with the parameters specified by the EHE-08 [27]. Figure 7.7 shows the workability of the mixes based on d_f and Tv [35]. (Four repetitions were made for each mix, and the averages were represented by a solid square, a solid triangle, and a solid circle, respectively). Note that all mixes are within the area in which the SCC would have good self-compactability. For the specific case of SCC-1 (mix with SF), the mix is located in the region known as "Marginal SCC area," an area in which there could be a slight segregation, according to the author, although this aspect was not observed in none of the mixes of the present work, since a good distribution of the coarse aggregate was observed, and there are no signs of segregation and bleeding, which is in accordance with the proximity to the area called "Proper SCC area." SCC-2 (mix with NCFA) and SCC-12 (mix 1:1 of SF and NCFA) remain inside the "Proper SCC area" box, that is, they are considered as appropriate and acceptable SCCs. Additionally, the reproducibility of the mixes in all the repetitions could be observed.

The differentiated behaviour of the mixes SCC-1 and SCC-2 in terms of the workability may be mainly due to the greater particle size presented by NCFA (Figure 7.3), which results in a lower content of fines and volume of the paste (Table 7.3), causing a greater difficulty to flow, compared to the results obtained in the reference mix (SCC-1). This behaviour is in accordance with the greater amount of water (182.75 L/m^3 vs 176.93 L/m^3) necessary to achieve the self-compactability of the SCC-2 mix. A reduction in d_f equal to -7% and an increase in Tv equal to 56% was observed. These percentages are reduced in the SCC-12 mix, around -4% for df and 41% for Tv, compared to the SCC-2 mix; the SCC-12 mix presents a greater fluidity when incorporating 50% in volume of the commercial filler. This may be due to the

improvement of the particle size distribution of the filler when a 1:1 mix of both materials is incorporated, which may result in a better packing factor of the finer particles, and therefore, an improvement in self-compactability properties. This result is in agreement with the fine material and paste content, which is intermediate compared to the other mixes (SCC-1 and SCC-2).

Table 7.4
Results of the self-compactability tests for the two types of SCC.

Mixtures	**Retakes**	[b]**Slump flow test**		[b]**J-Ring test**		[b]**V-funnel test**	[b]**L-box test**
		(UNE-EN 12350-8)		(UNE-EN 12350-12)		(UNE-EN 12350-9)	(UNE-EN 12350-10)
		T_{50} (s)	d_f (mm)	T_{j50} (s)	$d_f - d_{jf}$	T_v (s)	C_{bL}
SSC-1	Average (SD) [a]	2.34 (0.2)	725.13 (6.1)	3.06 (0.6)	38 (2.5)	7.13 (0.4)	0.92 (0.02)
Class [27]	*AC-V2*	*AC-E2*	*AC-RB2*		*AC-V2*	*AC-RB2*	
SSC-12	Average (SD) [a]	4.35 (0.1)	699 (4.53)	5.56 (0.4)	25 (3.2)	10.07 (0.4)	0.82 (0.01)
Class [27]	*AC-V1*	*AC-E2*	*AC-RB2*		*AC-V1*	*AC-RB2*	
SSC-2	Average (SD) [a]	2.69 (0.3)	676.75 (4.3)	3.67 (0.4)	24 (5.3)	11.10 (0.5)	0.84 (0.04)
Class [27]	*AC-V1*	*AC-E2*	*AC-RB2*		*AC-V1*	*AC-RB2*	

[a] Standard deviation; [b]Admissible values [27]: 550 mm ≤ d_f ≤ 850 mm; T_{50} ≤ 8s; d_{jf}≥ d_f - 50 mm; 4 s ≤ Tv ≤ 20 s; 0.75 ≤ C_{bl} ≤ 1

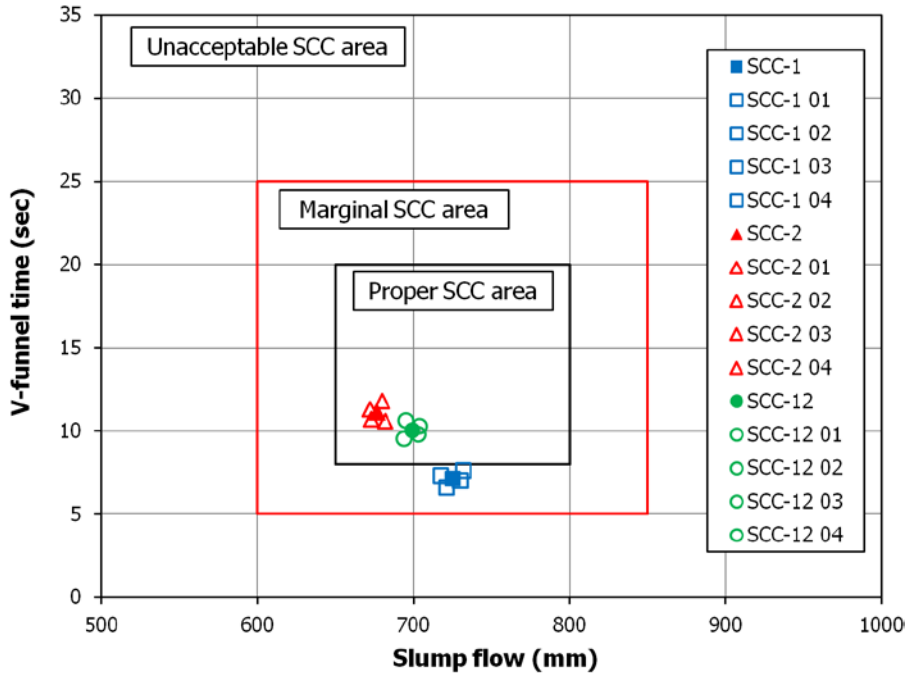

Figure 7.7: Workability boxes for several self-compacting mixes.

These results show that it is possible to obtain SCC within the parameters specified by the EHE-08, using the NCFA residue as the filler, and starting from a dosage in which the natural SF is replaced by NCFA, from 50% to 100% in volume.

These results are in agreement with those obtained by Esquinas et al. [11, 12], who observed a similar behaviour when the SF was replaced by a dolomitic residual powder. This residue had a larger particle size than the SF, of the same order as that observed in the NCFA sample. The self-compactability, as in the present work, is closer to the limits given by the EHE-08, and hence the SCC can be considered as adequate and acceptable, with regard to workability. Silva and de Brito [36] obtained good self-compactability results in dosages that used as a filler a mix of limestone filler and fly ash, in volumetric proportions of 2:1 and 1:2. On the other hand, when in the mixes, conforming fly ash is introduced for use in concrete, the behaviour differs from that observed in this work, since there is an improvement in self-compactability (in terms of filling and passing ability) compared to the reference SCC, as can be seen in the work carried out by Suaiam et al. [20]; this could be due mainly to a fine particle size distribution (<45 μm) that characterizes this material.

7.3.1.2 Density of SCC in fresh state

The fresh density values recorded for SCC-1, SCC-12, and SCC-2 were 2.441 kg/dm^3, 2.421 kg/dm^3, and 2.397 kg/dm^3, respectively. The higher density of SCC-1 relative to the other mixes may be due to the finer and more continuous particle size distribution of the SF compared to the NCFA (Figure 7.3). On the other hand, the higher content of fines presents in the SCC-1 mix (Table 7.3) would be in accordance with the results obtained, since it would yield a higher packing density. These results are in agreement with the densities obtained by other researchers [11, 12, 37].

7.3.2 Properties of SSC in hardened state

7.3.2.1 Physical-chemical characterization of hardened SCC

By means of the thermal analysis, TGA-DTA (Figure 7.8) (only one heat flow curve has been included because the information, for the propose of this paper, was the same), the different processes during the curing of the SCCs were identified.

Three zones can be differentiated: in the first zone, from room temperature to 400 ºC, corresponding to the loss of free water physically adsorbed (until 100 ºC, negligible in the samples studied in this work, since they have been kept in an oven at 100 ºC until constant weight), the loss of interlaminar water, the loss of structural water due to the dehydration processes of hydrated silicates and calcium aluminates, and the water present in the pores. The second zone, between 400 ºC and 550 ºC, corresponds to the dehydroxylation of the portlandite. The third zone, between 550 ºC and 750 ºC, is due to the decomposition of carbonates, initial or formed in the setting process. Finally, from 750 °C, there is a loss corresponding to the elimination of OH residues.

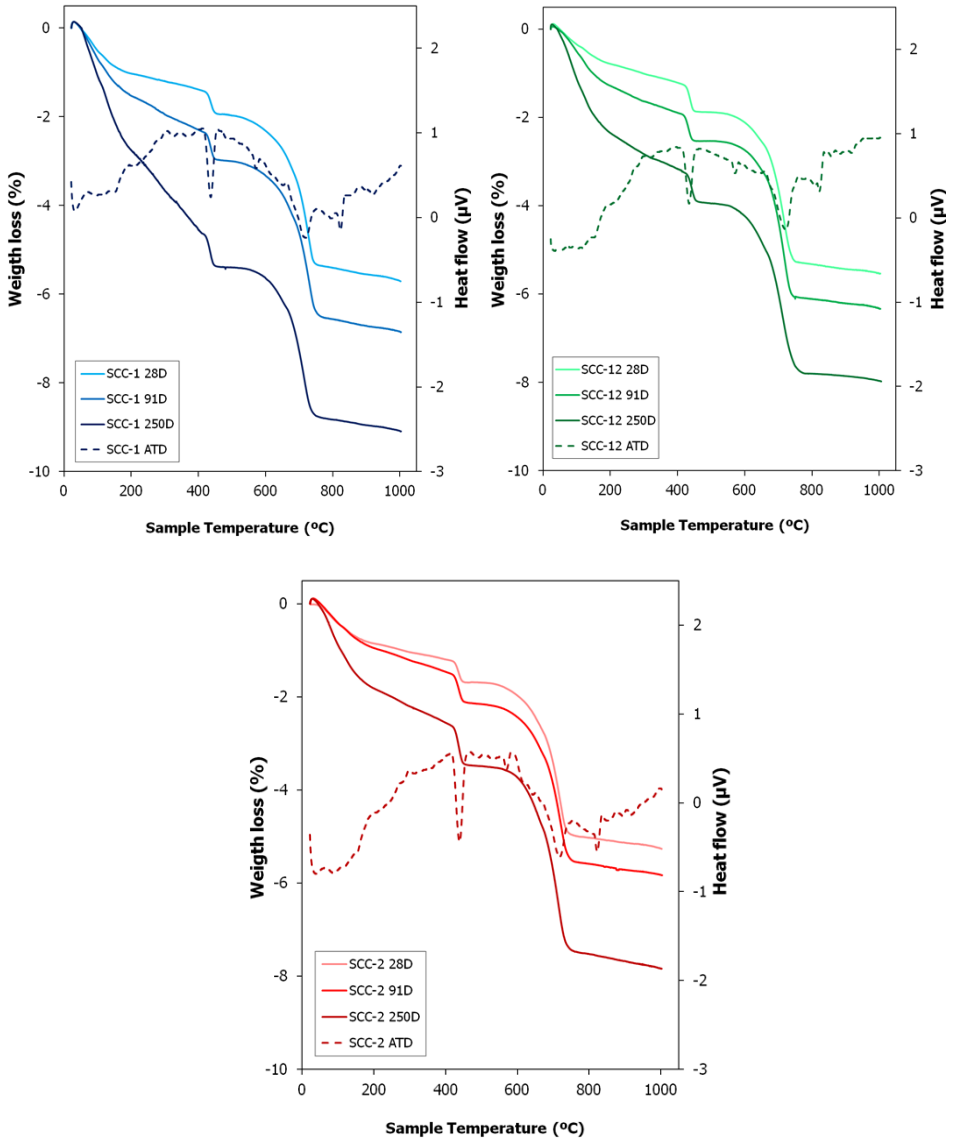

Figure 7.8: TGA (solid lines) and TDA (dotted lines) for several hardened SCCs.

SCC-1 presented a greater degree of hydration with the curing time. The degree of hydration at 250 days was 4.54%, 3.16%, and 2.55% for SCC-1, SCC-12, and SCC-2, respectively (Table 7.5). In the column "H_2O_{Total}" of Table 7.5, it is observed that there is an increase in the water content with curing time in all the mixes. A greater water content is observed at 250 days in the samples of SSC-1 and SCC-12 compared to the SCC-2 mix. This can be attributed to the pozzolanic reaction of the SF with $Ca(OH)_2$ to form CSH, which is in accordance with the lower increase in the total

$Ca(OH)_2$ content that occurs in the SCC-1 mix, followed by SCC-12, compared to SCC-2 for the same curing time.

Table 7.5
Results obtained in the test of thermal analysis (TG/TD) for each SCC studied.

Mixtures	Age (days)	Δ mass (%)				Chemical species (kg/m³)				
		0-400ºC	400-550ºC	550-750ºC	750-800ºC	H_2O_{Total}	$Ca(OH)_2$	$CaCO_3$	$CaCO_3$[a]	$Ca(OH)_{2\ Total}$
SCC-1	28	-1.3828	-0.6951	-3.2415	-0.0881	33.8	69.9	21.1	159.0	85.5
	91	-2.2919	-0.8090	-3.2848	-0.1718	56.0	81.3	23.5	159.0	98.7
	250	-4.5444	-0.8407	-3.2981	-0.0884	111.0	84.5	24.3	159.0	102.5
SCC-12	28	-1.2132	-0.7121	-3.3400	-0.0584	29.4	71.0	25.0	159.0	89.5
	91	-1.8944	-0.6784	-3.5102	-0.0300	45.9	67.6	34.0	159.0	93.1
	250	-3.1612	-0.8999	-3.6453	-0.1642	76.6	89.7	42.0	159.0	120.7
SCC-2	28	-1.1867	-0.5581	-3.2068	-0.0697	28.6	55.2	16.5	159.0	67.4
	91	-1.4592	-0.7625	-3.2762	-0.0868	35.1	75.5	20.3	159.0	90.5
	250	-2.5542	-0.9789	-3.9001	-0.0890	61.5	96.9	54.0	159.0	137.2

[a] Amount $CaCO_3$ present on aggregates.

The amount of $Ca(OH)_2$, which corresponds to the hydration process of the calcium silicates, was determined by the weight loss recorded between 400 ºC and 550 ºC. This amount increases with the time of setting in all the SCCs, since the amount of cement present in the mixes is the same.

The carbonate content was higher in the SCC-2 mix, as observed in the weight loss between 550 °C and 750 °C (Figure 7.8 and Table 7.5), followed by the SCC-12 and SCC-1 mixes. The first column of "$CaCO_3$" in Table 7.5 represents the content of $CaCO_3$ that has been formed by carbonation of $Ca(OH)_2$, and has been calculated from the weight loss between 550 ºC and 750 ºC, from which is subtracted the content of $CaCO_3$ initially present in the aggregates of the mixes (second column of "$CaCO_3^{(a)}$" of Table 7.5), estimated at 6.6% (159 kg/m^3) of the mix. The carbonation of the mixes grows slightly with the setting time, although for the SCC-12 and SCC-2 samples at 250 days, this increase is more important (Table 7.5). Therefore, in the total content of portlandite, the amounts of carbonate formed from $Ca(OH)_2$ should be taken into account and are shown in the "$Ca(OH)_{2\ Total}$" column of Table 7.5.

A correlation was established between the values of the columns "$Ca(OH)_{2\ Total}$" and "H_2O_{Total}" of Table 7.5 (without taking into account the values for 250 days of curing of the mixes SCC-1 and SCC-12, as previously mentioned, regarding the presence of pozzolanity). We used the equation ($y = 0.5236\ x - 8.0445$; $R2=0.71$) to obtain the theoretical portlandite ($Ca(OH)_2$) quantity for the SCC-1 and SCC-12 mixes after 250 days, without taking into account the pozzolanic reaction. The values obtained were 227.5 kg/m^3 and 161.7 kg/m^3, respectively, and are superior to the experimental values $Ca(OH)_{2\ Total}$ (Table 7.5). For the SCC-2 mix, the theoretical total amount of $Ca(OH)_2$ obtained according to the aforementioned correlation was 132.8 kg/m^3, which is very similar to the experimental quantity $Ca(OH)_{2\ Total}$.

The XRD patterns are shown in Figures 7.9 and 7.10. In Figure 7.9, the evolution of the phases presents in the mixes SCC-1 and SCC-2 during short-term curing (up to 91 days) was analysed. Figure 7.10 shows the phases present in the three mixes (SCC-1, SCC-12, and SCC-2) during long-term curing (250 days). The main phases observed in a short curing age were quartz (33-1161), portlandite (04-0733), and

calcite (05-0586), and to a lesser extent ettringite (41-1451), albite (09-0466), orthoclase (31-0966), Ca_2SiO_4 (31-0297), and illite (02-0056) [28].

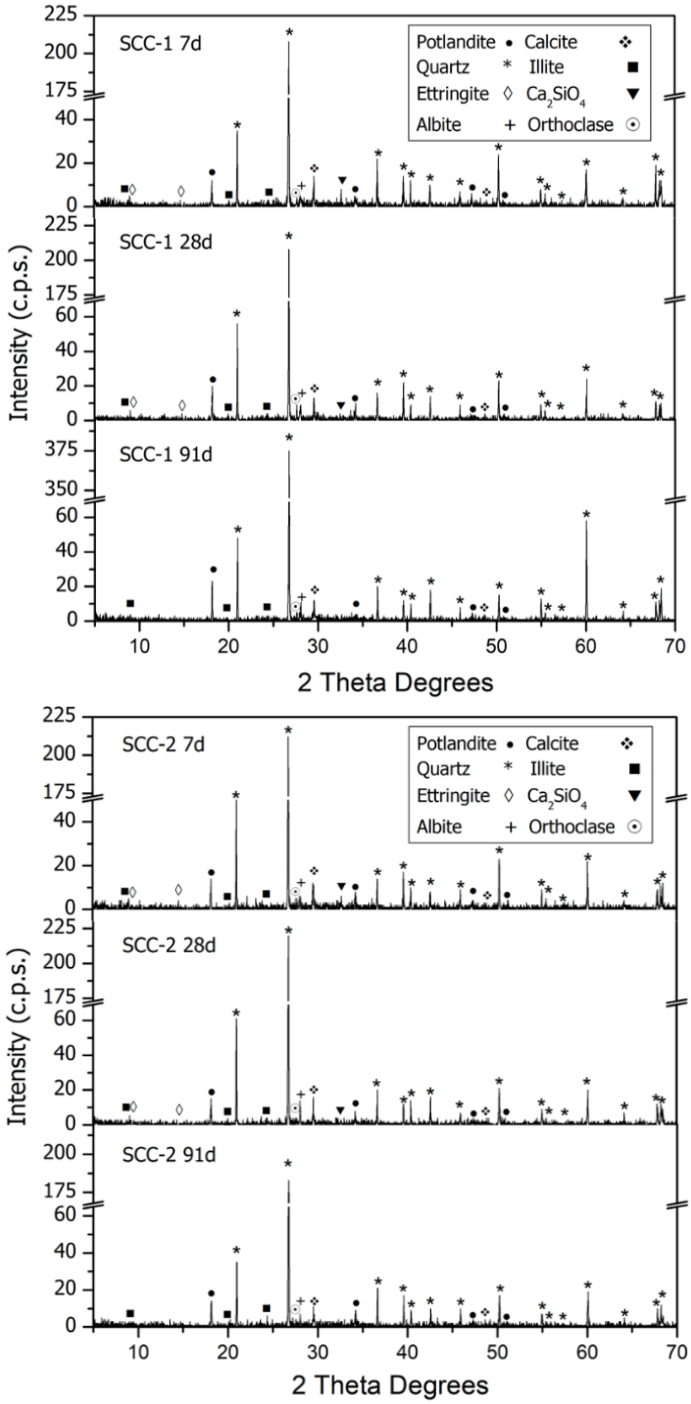

Figure 7.9: PXRD patterns for hardened SCC-1 and SCC-2 in the short term.

At high curing times (250 days) (Figure 7.10), there is a decrease in the peaks corresponding to portlandite with respect to the peaks corresponding to quartz for the SCC-1 sample due to the pozzolanic reaction that occurs between the portlandite and the SF. On the other hand, in the SCC-12 and SCC-2 mixes, an increase of the content of portlandite with respect to the content of quartz is observed.

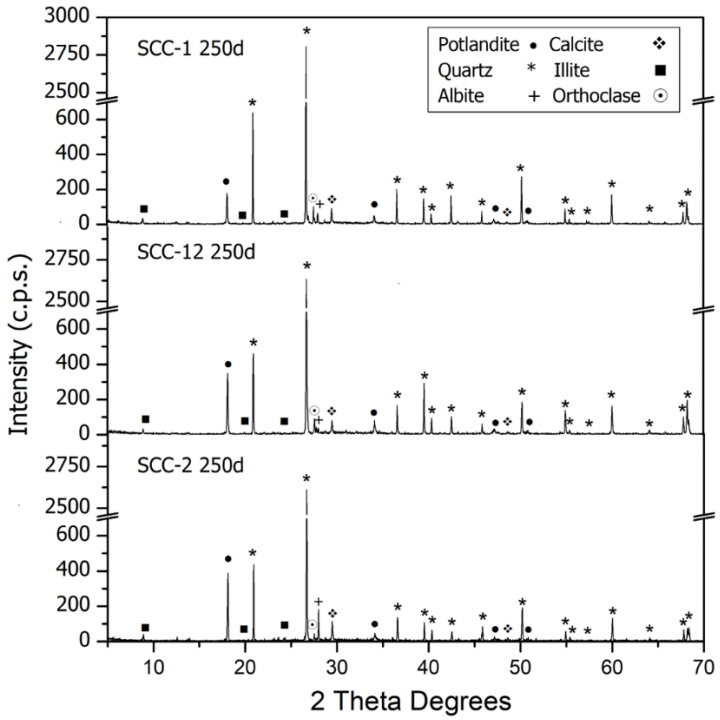

Figure 7.10: PXRD patterns for hardened SCC-1, SCC-12 and SCC-2 at 250 days.

This is in accordance with the greater weight loss suffered by SCC-1 between 0 and 400 ºC (dehydration zone), and in SCC-2, the greatest weight loss occurs in the decarbonation zone (550-750 ºC). It can be concluded that the setting mechanism of both concretes (SCC-1 and SCC-2) is different, depending on the nature of the filler added. In the case of the SCC-12 mix, the behaviour is intermediate. In short, pozzolanic and slight carbonation reactions occur in the SCC-1 mix. In SCC-12, both pozzolanic and carbonation reactions are observed, whereas in the SCC-2 mix, only carbonation processes are observed.

In summary, it can be concluded that in the SCC-1 and SCC-12 mixes, there would be a pozzolanic reaction, which is more intense in the SCC-1 mix, where only SF was

used as the filler. On the other hand, when only NCFA was used as the filler, this reaction was not observed, and hence, the total content of $Ca(OH)_2$ was higher. This is in accordance with the greater percentage of particles of size greater than 32 μm presented by the NCFA, as mentioned in the section Materials and Methods.

7.3.2.2 Density of SCC

The three mixes have similar wet density values (measured at 28 days), although the mixes that incorporate NCFA have slightly lower values: 2.418 kg/dm^3 (SCC-12) and 2.398 kg/dm^3 (SCC-2), compared to 2.438 kg/dm^3 of the reference mix (SCC-1). This is in accordance with the dosages of the three mixes (Table 7.3), in which the presence of NCFA causes a decrease in the wet density of the mix with this waste.

The dry density values (after the drying process at 105 ºC to constant mass) follow the same pattern as that observed for wet density: 2.329 kg/dm^3, 2.323 kg/dm^3, and 2.284 kg/dm^3 for SCC-1, SCC-12, and SCC-2 mixes, respectively. If a comparative analysis of both densities is carried out, it can be concluded that the loss of free water in the drying process was approximately 4.5% in the three mixes. This behaviour is influenced by the effective water content present in the mixes: 17.28%, 17.52%, and 17.85% for SCC-1, SCC-12, and SCC-2 mixes, respectively, and will in turn have an influence on the mechanical behaviour of the SCCs.

These results are in agreement with those obtained by other authors such as Esquinas et al. [12], who observed a decrease in density when replacing a commercial SF with a fine granulometry residue of dolomitic nature and of larger particle size in the mix. Barbhiya [38] observed a lower density in mixes that incorporated FA compared to mixes using a commercial dolomitic filler, with a microfiller effect caused by the fine grain of dolomite powder.

Additionally, the higher density of the SCC-1 mix is favourably influenced by the pozzolanic reactions that fill the gaps of the granular skeleton, compared to the SCC-2 mix.

7.3.2.3 Compressive strength

The compressive strength of SCC-2, which uses NCFA as the filler, is lower than that of SCC-1 (used as a reference). The partial use of this by-product together with the commercial SF (SCC-12 mix) caused an increase in the compressive strength compared to the mix with 100% of the by-product (SCC-2) (Figure 7.11).

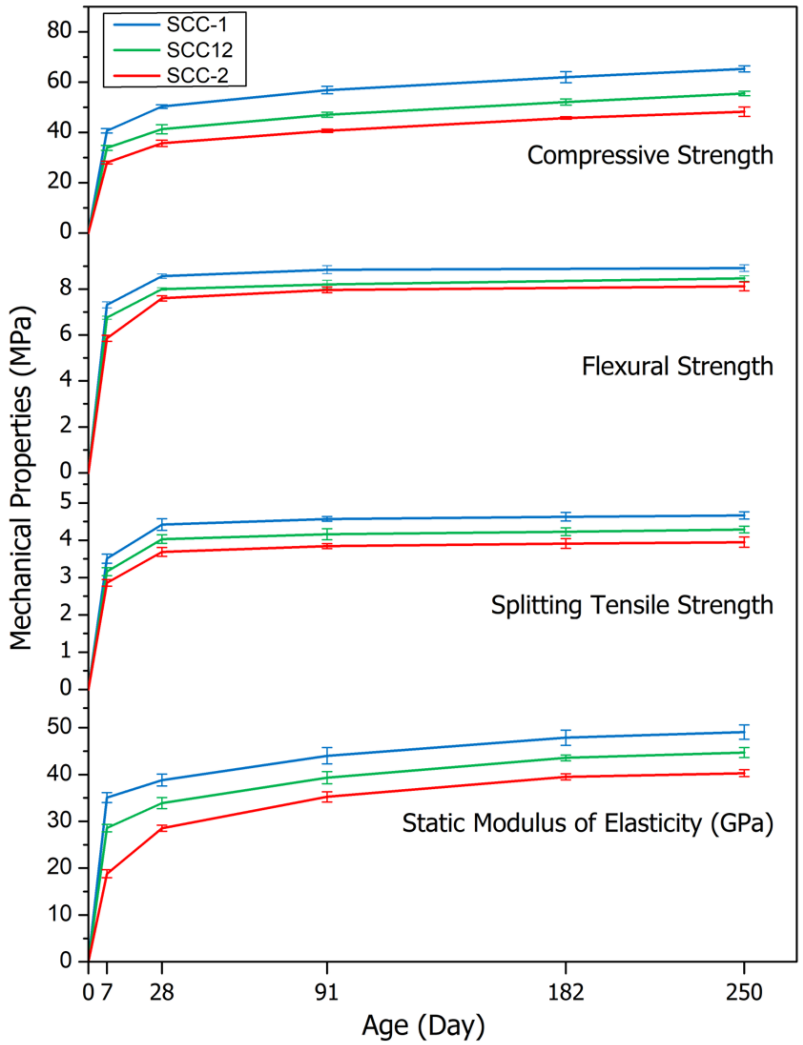

Figure 7.11: Mechanical properties of hardened SCCs.

The compressive strength values for the SCC-1 mix at 7, 28, 91, 182, and 250 days were 40.67, 50.30, 56.87, 61.99, and 65.32 MPa, respectively. For the SCC-12 mix, the results obtained were 33.83, 41.27, 47.01, 52.05, and 55.64 MPa, respectively.

For the SCC-2 mix, the values were 28.02, 35.67, 40.66, 45.69, and 48.77 MPa. At early ages of curing (7 days), there is a greater difference in the compressive strength compared to the SCC-1 mix; 16.8% and 31% for SCC-12 and SCC-2, respectively. The delay in hydration observed in these mixes may be due to the greater particle size distribution of the NCFA, (45% of the particles are greater than 32 μm versus 12% in the SF) (Figure 7.3), which would make the complete hydration of the particles, and consequently, the mechanical development, difficult.

From the age of curing of 28 days, in the SCC-2 mix, there is a slower compressive strength increase than in the SCC-1 mix, since the slope of the trend lines is 5.7% and 6.8%, respectively. The SCC-12 mix presents an intermediate evolution to these values (6.5%). The only factor that differentiates these dosages is the type of filler used, and therefore, this is responsible for the difference in mechanical behaviour. In short, the greater compressive strength of SCC-1 may be due to the particle size distribution of the SF used (71% of the particles have sizes between 3 and 32 μm, Figure 7.3) [39-41]. This evolution is in agreement with the experimental data obtained with the thermogravimetric and DRX analyses of the mixes (Table 7.5 and Figures 7.9 and 7.10), which show a decrease in the content of portlandite in the SCC-1 and SCC-12 mixes, compared to the SCC-2 mix (without SF), as already mentioned in the section on characterization of the hardened mixes.

This behaviour is in agreement with the results obtained by Esquinas et al. [12], who observed a decrease in the compressive strength of the SCC that incorporated a dolomitic waste compared to the SCC with a commercial silicon filler. These by-products caused a delay in the hydration of the SCC due to a greater particle size distribution, as is the case of the NCFA. On the other hand, Dadsetan and Bai [19] carried out a study on the mechanical behaviour of SCC with different types of fillers, observing that the mixes with fly ash had a lower compressive strength compared to mixes with metakaolin and ground granulated blast-furnace slag, mainly due to the high pozzolanic activity of these two additions, similar to the evolution observed in the present work. Finally, Silva and Brito [42] observed an increase in the compressive strength of SCC with conforming FA regarding an addition of a limestone filler, owing to a thicker particle size distribution and absence of pozzolanity.

The results obtained show that it is possible to use NCFA from coal-fired power plants as the filler and achieve compressive strengths above the minimum levels stipulated by the Spanish Structural Concrete Code [27] for a HAC-30. If a mix (1:1) of NCFA + commercial SF is added to SCC, strength higher than 40 MPa can be obtained after 28 days, with a 15% reduction in compressive strength compared to the reference mix.

7.3.2.4 Splitting tensile strength

The results of splitting tensile strength of the different mixes at 7, 28, 91, 182, and 250 days are shown in Figure 7.11. For SCC-1, the splitting tensile strength values obtained were 3.51, 4.42, 4.57, 4.63, and 4.67 MPa, respectively. For SCC-12, they were 3.16, 4.03, 4.16, 4.23, and 4.29 MPa, respectively. The results of the SCC-2 mix were 2.86, 3.68, 3.84, 3.91, and 3.95 MPa, respectively. In the three mixes, an evolution similar to the compressive strength is observed. The strength reached at long-term curing suffers a reduction of approximately 15% when 100% substitution of SF is carried out by NCFA, and of 7% approximately when the substitution is 50% (SCC-12). Both in the SCC-2 and SCC-12 mixes, at an early age, there is a slightly greater difference in resistance compared to the reference mix (SCC-1), which may be due, on the one hand, to the larger particle size of the NCFA, which would hinder the hydration processes, as already mentioned, and on the other hand, to the effect of the physical–chemical nature of the filler [43].

This behaviour is in agreement with the results obtained by other authors. Esquinas et al. [12] observed a decrease of approximately 18% in the splitting tensile strength of SCC when the commercial SF was completely replaced by a dolomitic waste. Dehwah [44] obtained superior splitting tensile strengths in SCC that incorporated silica fume compared to mixes using FA, due to a higher packing density and reactivity. On the other hand, Liu [45] obtained splitting tensile strengths similar to those achieved in this work, with SCC that used different amounts of fly ash as a substitute for cement.

Splitting tensile strength can be defined as a function of compressive strength. Figure 7.12 (top) shows the splitting tensile strengths of all mixes and for all ages, against

compressive strength. All of them are within the limits recommended by the CEB-FIB code (Euro-International Committee of Béton - International Federation for Structural Concrete). The correlation between both parameters has been represented and expressed mathematically by Eq. 7.1, with R^2 equal to 0.85.

$$f_{ci} = 0.31 \cdot f_c^{2/3} \qquad \text{(Eq. 7.1)}$$

where f_{ci} is the splitting tensile strength and f_c is the compressive strength.

The splitting tensile strength f_{ci} can be calculated according to the EHE-08 [27] and Eurocode 2 [46] from the tensile strength, f_{ct}, which can be found from the characteristic compressive strength, f_{ck} (Eq. 7.2) and taking into account Eq. 7.3:

$$f_{ct} = 0.3 \cdot f_{ck}^{2/3} \qquad \text{(Eq. 7.2)}$$

$$f_{ci\,(EHE\text{-}08)} = f_{ct} / 0.9 \qquad \text{(Eq. 7.3)}$$

resulting in Eq. 7.4:

$$f_{ci\,(EHE\text{-}08)} = 0.33 \cdot f_{ck}^{2/3} \qquad \text{(Eq. 7.4)}$$

If the concept of characteristic compressive strength (f_{ck}) defined by EHE-08 [27] and Eurocode [46] is used, Eq. 7.1 would be transformed into Eq. 7.5 (R^2 = 0.80).

$$f_{ci} = 0.35 \cdot f_{ck}^{2/3} \qquad \text{(Eq. 7.5)}$$

Parra et al. [47] proposed Eq. 7.6 for its application to the SCC.

$$f_{ci\,(SCC)} = 0.28 \cdot f_c^{2/3} \qquad \text{(Eq. 7.6)}$$

It can be seen that the correlation found in this work, Eq. 7.1, (Figure 12 top) is close to the correlation proposed by Parra et al. (Eq. 7.6) and very similar to that proposed by Lui [45]. On the contrary, it differs considerably from the correlation proposed by Dehwah [44], with respect to the whole range of resistances. On the other hand, if the characteristic compressive strength (f_{ck}) is taken into account, the correlation,

Eq. 7.5, (Figure 7.12 bottom) is very similar to the one proposed in the EHE-08 and the Eurocode 2 (Eq. 7.4).

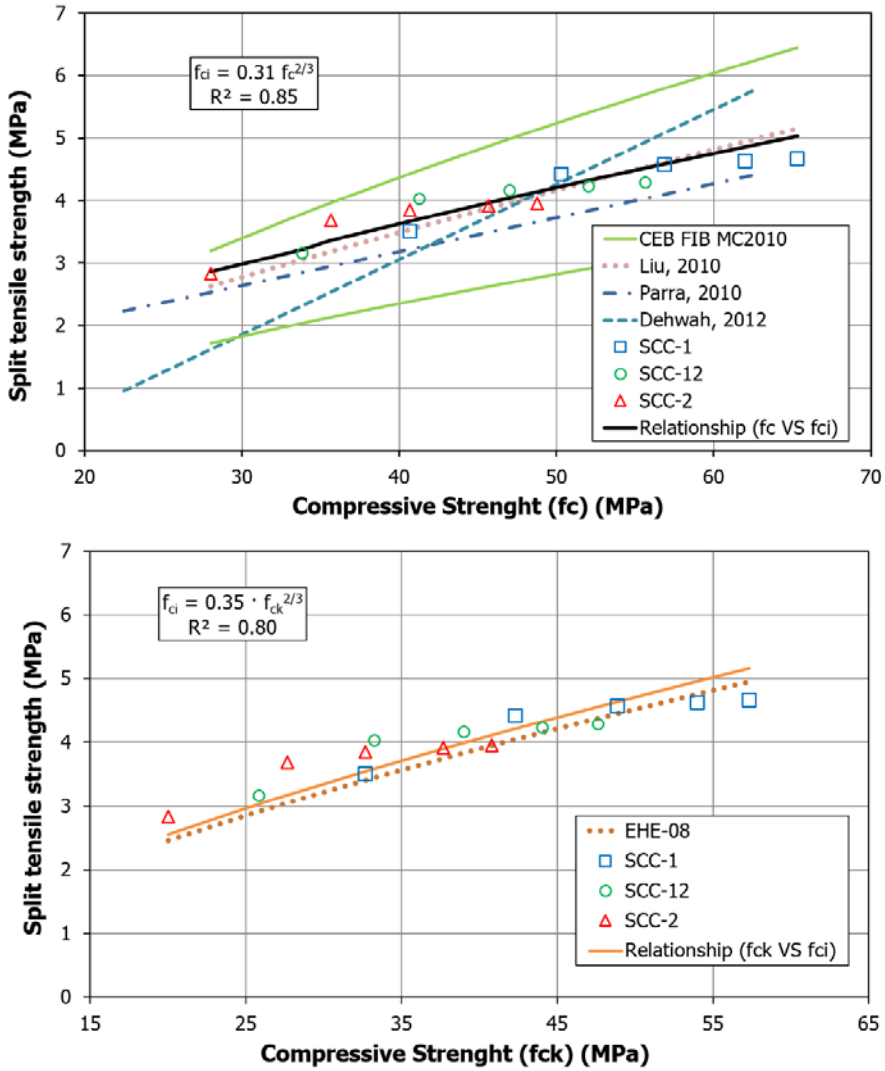

Figure 7.12: Compressive strength (f_c) versus splitting tensile strength (top) and compressive strength (f_{ck}) versus splitting tensile strength (bottom).

Table 7.6 lists the experimental and estimated f_{ci} values according to the EHE-08 and the Eurocode 2 (Eq. 7.4), and the expression proposed by Parra et al. (Eq. 7.6). The calculated values are slightly lower than those obtained experimentally, as shown in Figure 7.12. The correlation coefficients between the experimental values and those estimated by both equations are also included. The average of the correlation coefficients between the experimental values and those obtained when applying the

equation proposed by the EHE-08 and the Eurocode 2 (Eq. 7.4) was 1.06, and for the equation proposed by Parra et al. (Eq. 7.6), it was 1.1.

Table 7.6
Comparing the experimental results with those estimated using EHE-08 and other references.

Mixtures	Age (days)	Experimental			Estimated by EHE-08			Parra[a]	Correlation ratio			
		f_{cl} (MPa)	$f_{ct,fl}$ (MPa)	E_{cm} (GPa)	f_{cl} (MPa)	$f_{ct,fl}$ (MPa)	E_{cm} (GPa)	f_{cl} (MPa)	$f_{cl(EHE)}$	$f_{ct,fl(EHE)}$	$E_{cm(EHE)}$	$f_{cl(SCC)}$
SCC-1	7	3.51	7.32	35.1	3.41	5.27	-	2.86	1	1.3	-	1.1
	28	4.42	8.57	38.8	4.05	6.63	31.4	3.40	1.1	1.2	1.2	1.1
	91	4.57	8.85	44.0	4.46	6.86	32.6	3.74	1	1.2	1.3	1.1
	182	4.63	-	47.9	4.76	-	33.4	4.00	1	-	1.3	1.1
	250	4.67	8.91	49.0	4.96	7.00	33.9	4.16	0.9	1.2	1.3	1
SCC-12	7	3.16	6.76	28.6	2.91	4.74	-	2.45	1.1	1.3	-	1.1
	28	4.03	8.01	33.9	3.45	6.05	29.4	2.90	1.1	1.2	1.1	1.2
	91	4.16	8.20	39.3	3.83	6.24	30.5	3.22	1.1	1.3	1.2	1.1
	182	4.23	-	43.6	4.16	-	31.5	3.49	1	-	1.3	1.1
	250	4.29	8.47	44.7	4.38	6.43	32.1	3.68	1	1.2	1.3	1.1
SCC-12	7	2.86	5.86	18.8	2.46	4.24	-	2.06	1.1	1.3		1.1
	28	3.68	7.60	28.6	3.05	5.53	28.0	2.56	1.2	1.3	1	1.2
	91	3.84	7.97	35.2	3.41	5.77	29.1	2.86	1	1.3	1.2	1.1
	182	3.95	-	39.5	3.75	-	30.1	3.15	1	-	1.2	1.1
	250	3.66	8.12	40.3	3.95	5.93	30.7	3.32	1	1.3	1.2	1.1

[a] (Eq. 7.6)

Therefore, for the dosages used in this work, the equations proposed by the EHE-08 and the Eurocode 2, and by Parra et al. would be valid. The equation of Parra et al. would allow prediction of the behaviour against the splitting tensile strength in concretes that incorporate this type of waste with a slightly higher safety margin.

7.3.2.5 Flexural strength

The flexural strength of the mixes presents a similar behaviour to that of the mechanical properties analysed previously (Figure 7.11). For the different ages of curing (7, 28, 91, and 250 days), the flexural strength values obtained were 7.32, 8.57, 8.85, and 8.91 MPa, respectively, for the SCC-1 mix; 6.76, 8.01, 8.20, and 8.47 MPa, respectively, for the mix SCC-12; and 5.86, 7.60, 7.97, and 8.12 MPa, respectively, for the SCC-2 mix. As can be observed, during short-term curing (7 days), there is a difference between the mixes SCC-12 and SCC-2 with respect to the reference (SCC-1) of 8% and 20%, respectively. This difference is minimized with age; it was observed that for SCC-12 and SCC-2, with respect to the reference (SCC-1), the difference was 5% and 9%, respectively. As for the compressive and splitting tensile strengths, these results are clearly influenced by the characteristics of the fillers used, as discussed above, and the reactions associated with them.

Other researchers have obtained a behaviour similar to that obtained in this work. Esquinas et al. [12] observed that the flexural strength of SCC manufactured with residual filler decreased compared to that of an SCC manufactured with a commercial filler with a finer particle size distribution. On the other hand, Dehwah [44] obtained values of flexural strengths at 28 days for an SCC with FA that were lower than that for an SCC with a mix of limestone filler and silica fume, due to the greater effectiveness of the limestone filler to fill the micropores of the SCC.

The correlation between the experimental values of flexural strength and compressive strength is shown in Figure 7.13. This relationship is expressed by Eq. 7.7, where R^2 is equal to 0.81.

$$f_{fl} = 0.0750 \cdot f_c + 4.494 \qquad \text{(Eq. 7)}$$

where f_{fl} is the flexural strength and f_c is the compressive strength. As can be seen, the correlation proposed in this work differs from that proposed by Dehwah [44].

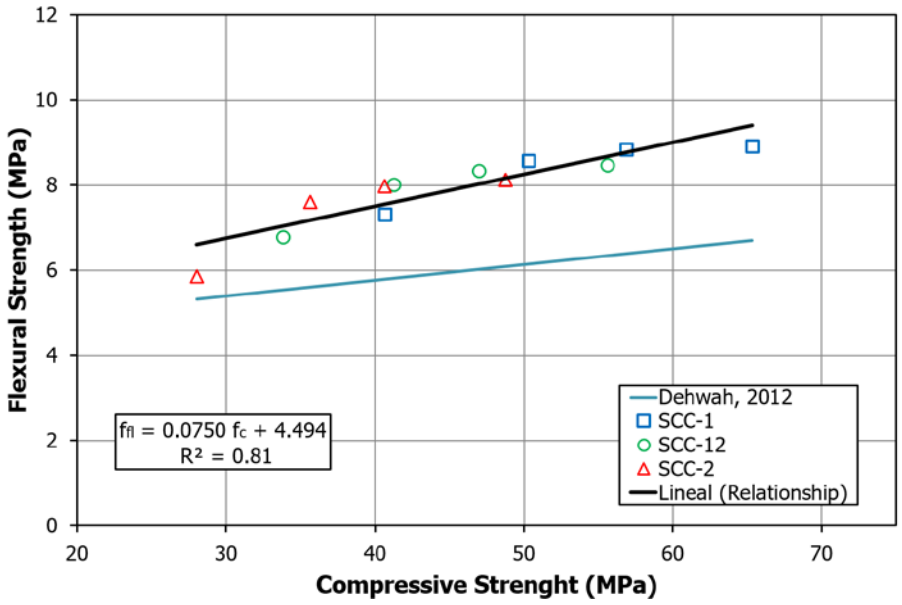

Figure 7.13: Compressive strength versus flexural strength.

The flexural strength, $f_{ct,fl}$, [27] could be calculated from the tensile values (f_{ct}) by using Eq. 7.8:

$$f_{ct,fl} = f_{ct}\frac{1+1.5\left(\frac{h}{100}\right)^{0.7}}{1.5\left(\frac{h}{100}\right)^{0.7}} \qquad \text{(Eq. 7.8)}$$

where f_{ct} is the tensile strength obtained from the experimental values of splitting tensile strength by applying Eq. 7.3, and h is the edge of the element in mm. In Table 7.6, the flexural strength results, $f_{ct,fl}$, obtained by applying Eq. 7.8 are collected. It is observed that the experimental values are higher than the estimated values. For all ages, the correlation coefficients are greater than 1 (Table 7.6). Consequently, the application of the EHE-08 is clearly applicable to the SCC studied in this work, since the lower values of flexural strength estimated with respect to the experimental ones guarantee the safety of the SCC with this type of waste against bending moments.

7.3.2.6 Static elastic modulus

The results of the modulus of elasticity obtained in the three combinations for the different ages of curing (7, 28, 91, 182, and 250 days) are shown in Figure 7.11. The values obtained were 35.1, 38.8, 44.0, 47.9, and 49.1 GPa, respectively, for SCC-1; 28.6, 33.9, 39.3, 43.6, and 44.7 GPa, respectively, for SCC-12; and 18.8, 28.6, 35.2, 39.5, and 40.3 GPa, respectively, for SCC-2. Like the other parameters that define the mechanical behaviour of the SCC, the incorporation of this waste causes a decrease in the values of the modulus of elasticity. The differences in the values of this parameter in SCC-12 and SCC-2, with respect to SCC-1, are reduced with the setting time (8.7% in SCC-12 and 17.7% in SCC-2 at 250 curing days). This behaviour can be due to the delay in hydration and to the differences in the setting of the mixes that incorporate NCFA, as previously mentioned.

This behaviour is in agreement with other authors, such as Esquinas et al. [12], who observed the decrease of the static modulus of elasticity in SCC when replacing the commercial SF with dolomitic waste. The authors related it to a thicker particle size distribution of the by-product that originated a more porous structure [11], as well as to the pozzolanic characteristics of the SF. In the present work, NCFA presents a larger particle size distribution, which will hinder the development of pozzolanic reactions and will lead to lower values of the modulus of elasticity. On the other hand, Silva and Brito [42] observed an increase in the values of this parameter in mixes with FA compared to those that incorporated limestone filler due to the joint action of the smaller particle size of the FA and its pozzolanic capacity.

Figure 7.14 shows the relationship between the experimental values of the modulus of elasticity and the compressive strength for ages greater than 28 days expressed by Eq. 7.9, where R^2 is equal to 0.94:

$$E_{cm} = 1.79 \cdot f_c^{0.8} \qquad \text{(Eq. 7.9)}$$

where f_c is the compressive strength and E_{cm} is the modulus of elasticity. The correlation is within the estimates of the CEB-FIB code.

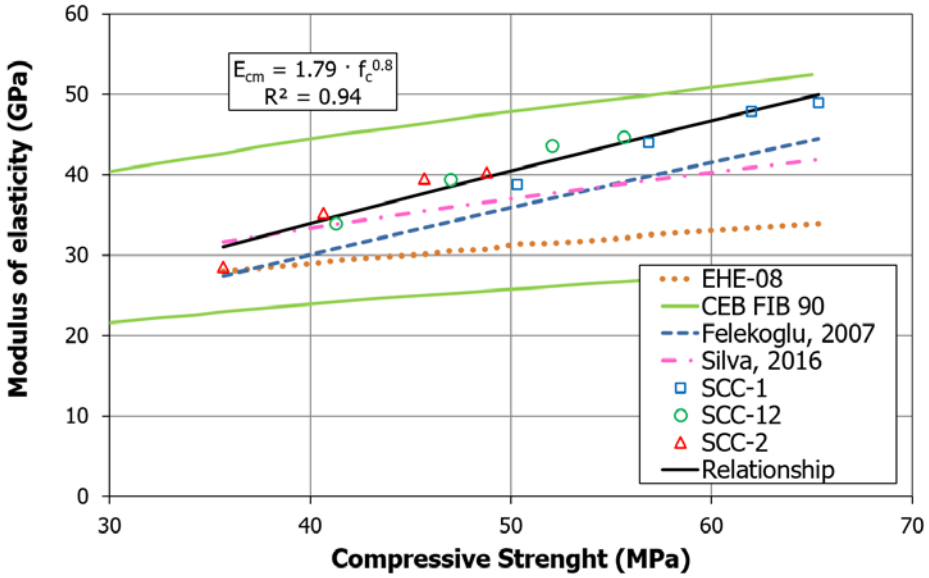

Figure 7.14: Compressive strength versus modulus of elasticity.

The modulus of elasticity, E_{cm}, at 28 days, can be calculated from the average compressive strength of concrete at 28 days (f_{cm}) using Eq. 7.10 proposed by the EHE-08 [27].

$$E_{cm} = \alpha \cdot 8500 \sqrt[3]{f_{cm}} \qquad \text{(Eq. 7.10)}$$

Eq. 7.10 is valid as long as the stresses, under service conditions, do not exceed the value of 0.40 f_{cm}. For the modulus of elasticity at different ages to 28 days, the EHE-08 and the Eurocode 2 propose Eq. 7.11, since the growth of the module with age is different from that experienced by compressive strength.

$$E_{cm}(t) = (f_{cm}(t) / f_{c,m})^{0.3} \cdot E_{cm} \qquad \text{(Eq. 7.11)}$$

where α is the correction coefficient as a function of the nature of the aggregates (in this article, the value of α is 1, because they are concretes manufactured with aggregates of medium characteristics of quartzite type), $E_{cm}(t)$ is the modulus of elasticity at t days, E_{cm} is the modulus of elasticity at 28 days, $f_{cm}(t)$ is the average

compressive strength at t days, and f_{cm} is the average compressive strength at 28 days.

Figure 7.14 includes the correlations established by other authors such as the EHE-08, Silva and Brito [42], and Felekoglu et al. [48], to compare with the data obtained in this work. The equation proposed by Felekoglu et al. has a similar slope, although the values are slightly lower for the same compressive strength, which could be due to the lower content of coarse aggregate (600 kg/m^3 vs 800 kg/m_3) and the inert addition (limestone filler) used by these authors.

Table 7.6 presents the modulus elasticity values estimated by the expressions proposed by the EHE-08 (Eqs. 7.10 and 7.11). It is observed that the estimated values are lower than the experimental values. The correlation factor is close to 1.2, demonstrating the validity of the Spanish instruction EHE-08 for SCCs.

In summary, all the mixes that incorporate NCFA as a filler reach values of modulus of elasticity higher than 40 GPa for long age of curing, fulfilling the requirements specified by the EHE-08, with respect to the elastic deformations under normal tensions.

7.3.2.7 UPV test

This non-destructive test allows indirect determination of the strength presented by the SCC. The UPV depends on the compactness and density of the mixes [49]. The UPV values obtained were 4.76, 4.92, 4.95, 5.01, and 5.07 km/s in SCC-1; 4.67, 4.88, 4.84, 4.96, and 5.02 km/s in SCC-12; and 4.60, 4.77, 4.82, 4.87, and 4.95 km/s in SCC-2, for 7, 28, 91, 182, and 250 days, respectively. The UPV increases with the age of curing in the three mixes, highlighting the values obtained in SCC-1 compared to SCC-12 and SCC-2. This increase in the velocity of propagation coincides with the higher values of compressive strength.

Figure 7.15 shows a good correlation (R^2 = 0.89) between the velocity of propagation and the compressive strength and can be expressed by Eq. 7.12:

$$UPV = 0.0119 \cdot f_c + 4.3211 \qquad \text{(Eq. 7.12)}$$

where UPV is the ultrasonic pulse velocity and f_c is the compressive strength. The correlation proposed by Dehwah [44] differs markedly from the experimental results of this work. On the contrary, the correlation proposed by Liu [45] is considerably close.

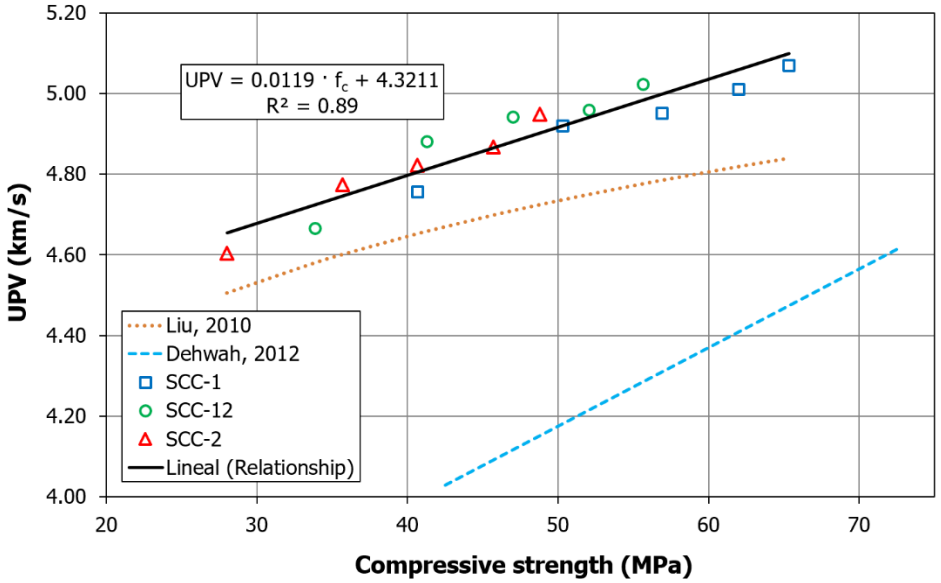

Figure 7.15: Compressive strength versus ultrasonic pulse velocity.

The decrease in UPV observed with decreasing compactness and density of the mixes is similar to that reported by other authors for SCCs using different wastes [12, 45, 50]. Liu [45] used fly ash as a filler and obtained UPV values of the same order as those recorded in this work.

Finally, all the mixes can be considered excellent according to the classification carried out by Whitehurst [51], since they present values higher than 4.5 km/s.

7.3.2.8 Shrinkage

The shrinkage values obtained in the different SCCs were -111, -162, -226, and -322 μstrain in SCC-1; -100, -155, -216, and -312 μstrain in SCC-12; and -83, -131, -185, and -291 μstrain in SCC-2; at 7, 14, 28, and 91 days, respectively (Table 7.7).

Therefore, the mix with the highest shrinkage is the SCC-1 mix followed by the SCC-12 and SCC-2 mixes. This behaviour can be due to the greater chemical and autogenous shrinkage that SCC-1 presents due to the more intense pozzolanic reactions generated by the SF with respect to the other fillers NCFA + SF (SCC-12) or NCFA (SCC-2). This dimensional variation will be produced both by the development of the initial hydration reactions and by the forces of attraction that occur in the walls of the capillaries when the water retained in the porous structure is used (self-desiccation) to generate the reactions of hydration [52-53].

Table 7.7
Total shrinkage.

	Age (days)	SCC-1	SCC-12	SCC-2
Total shrinkage strain (μ)	7	-111	-100	-83
	14	-162	-155	-131
	28	-226	-216	-185
	91	-322	-312	-291

This is in agreement with the results obtained by Esquinas et al. [12], who observed a decrease in the shrinkage in the mixes that incorporated a dolomitic residual powder with a larger size distribution than the SF used in the reference mix, in which a greater shrinkage was observed, and was attributed to the greater reactivity of the SF. In this same sense, Guneyisi et al. [54] observed higher values of shrinkage in the mixes that incorporated silica fume compared to those that incorporated FA due to their larger particle size.

It can be concluded that the SCCs that incorporate NCFA as a filler, SCC-12 and SCC-2, perform better than SCC-1, in relation to shrinkage at an early age, which would result in less cracking by the initial deformation due to these phenomena.

7.4 Conclusions

A comparative study of three SCC mixes was carried out to evaluate an NCFA-like filler in SCC; in the first mix (SCC-1), a commercial SF was used as a reference; in the second (SCC-12) a mix, 1:1 in volume, of SF and NCFA was used; and in the third (SCC-2), only NCFA was used.

The self-compactability tests show reproducibility. All mixes accomplish with the parameters stipulated by the EHE-08.

The densities of SCC-12 (2.421 kg/dm^3) and SCC-2 (2.397 kg/dm^3) in the fresh state are slightly less than that of SCC-1 (2.441 kg/dm^3), and this is related to the finer and continuous particle size distribution of the SF with respect to the NCFA.

The thermogravimetric study shows that in SCC-1, the higher weight loss occurs in the dehydration zone (0–400 ºC); in SCC-2, it occurs in the decarbonation area (550–750 ºC). It can be concluded that the setting mechanism of both concretes (SCC-1 and SCC-2) is different, depending on the nature of filler added. In the case of the SCC-12 mix, the behaviour is intermediate. In short, pozzolanic and mild carbonation reactions occur in the SCC-1 mix. In the SCC-12 mix, both pozzolanic and carbonation reactions are observed. In the SCC-2 mix, only carbonation processes are observed.

The three mixes have similar wet density values (measured at 28 days), although slightly lower for the mixes that incorporate NCFA: 2.418 kg/dm^3 (SCC-12) and 2.398 kg/dm^3 (SCC-2) compared to the mix of references 2.438 kg/dm^3 (SCC-1). The dry densities follow the same pattern as that observed in the case of wet densities: 2.329 kg/dm^3, 2.323 kg/dm^3, and 2.284 kg/dm^3 for SCC-1, SCC-12, and SCC-2 mixes, respectively.

The compressive strength, splitting tensile strength, flexural strength, and static modulus of elasticity of SCCs produced with NCFA (SCC-12 and SCC-2) are lower than those of the SCC produced with SF (SCC-1), for all ages. The differences were higher at an early age.

The delay in hydration observed in these mixes may be due to the greater particle size distribution of the NCFA, (45% of the particles are greater than 32 μm versus 12% in the SF), making the incomplete hydration of the particles and therefore the mechanical development difficult.

The splitting tensile strength, flexural strength, and static modulus of elasticity values calculated using the EHE-08 and/or the Eurocode 2 are lower than those obtained

experimentally, i.e., the correlation ratios are in most cases greater than 1. Hence, the experimental results show the validity of using the EHE-08 and/or the Eurocode 2, initially proposed for ordinary concrete (OC), in SCC.

There is an increase in the UPV relative to the curing age and the values for all mixes, and this can be attributed to the increase in compacity and compressive strength. The mixes can be considered excellent since they present UPV values higher than 4.5 km/s.

The incorporation of NCFA as a filler in SCCs, SCC-12, and SCC-2 resulted in their better performance than SCC-1 in relation to shrinkage at an early age, which would result in less cracking by the initial deformation due to these phenomena.

One may conclude therefore, that it is possible to obtain an SCC, by replacing (in volume) a natural SF with NCFA from coal-fired power plants to achieve a mechanical behaviour greater than the minimum levels stipulated by the Spanish Code on Structural Concrete (EHE-08).

7.5 Acknowledgements

This work was partly supported by the Andalusian Regional Government (Research Groups FQM-391 and TEP-227). A. Romero Esquinas also acknowledges funding from MECD-Spain (http://www.mecd.gob.es/educacion-mecd/) FPU-13/04030. The authors wish to thank the Research Plan of the University of Córdoba (2016), the staff at the Electron Microscopy and Elemental Analysis units of the Central Research Support Service (SCAI) of University of Córdoba for their technical assistance, the Fine Chemistry Institute of the University of Córdoba for their technical support, BASF Chemical Company for supplying the admixture, and Portland Valderrivas (Alcalá de Guadaira, Seville) for the supplied cement. The authors wish to thank the Andalusian Innovation Centre for Sustainable Construction (CIAC) for the use of the press IBERTEST, model MEH-3000. The authors wish to thank the National Radioactive Waste Company (ENRESA) for Contract of Research 079000146. Finally, the authors wish to thank the Puente Nuevo Coal-fired Power Plant of company Viesgo for the supplied NCFA waste.

7.6 References

[1] European Commission, Report from the commission to the European parliament, the council, the European Economic and Social Committee and the Committee of the Regions on the Implementation of the Circular Economy Action Plan, (2017).

[2] K. Celik, C. Meral, A.P. Gursel, P.K. Mehta, A. Horvath, P.J. Monteiro, Mechanical properties, durability, and life-cycle assessment of self-consolidating concrete mixtures made with blended portland cements containing fly ash and limestone powder, Cement and Concrete Composites 56 (2015) 59-72.

[3] J. Moya, N. Pardo, A. Mercier, Energy efficiency and CO2 emissions: Prospective scenarios for the Cement industry, Publications Office2010.

[4] H. Okamura, Self-compacting high-performance concrete, Concrete international 19(7) (1997) 50-54.

[5] Asociación Cientifico Técnica del Hormigón Estructural (ACHE). M-13: Hormigón Autocompactante. Diseño y Aplicación; 2008.

[6] European Federation of National Associations Representing producers and applicators of specialist building products for Concrete (EFNARC). Specification and guidelines for self-compacting concrete, Hampshire, UK; 2002, www.efnarc.org.

[7] European Federation of National Associations Representing producers and applicators of specialist building products for Concrete (EFNARC). The European guidelines for self-compacting concrete specification. Production and Use. Hampshire, UK; (2005), www.efnarc.org.

[8] R. Sharma, R.A. Khan, Durability assessment of self compacting concrete incorporating copper slag as fine aggregates, Construction and Building Materials 155 (2017) 617-629.

[9] S. Subaşı, H. Öztürk, M. Emiroğlu, Utilizing of waste ceramic powders as filler material in self-consolidating concrete, Construction and Building Materials 149 (2017) 567-574.

[10] M. Gesoglu, E. Güneyisi, O. Hansu, S. Etli, M. Alhassan, Mechanical and fracture characteristics of self-compacting concretes containing different percentage of plastic waste powder, Construction and Building Materials 140 (2017) 562-569.

[11] A. Esquinas, J. Álvarez, J. Jiménez, J. Fernández, J. de Brito, Durability of self-compacting concrete made with recovery filler from hot-mix asphalt plants, Construction and Building Materials 161 (2018) 407-419.

[12] A.R. Esquinas, C. Ramos, J. Jiménez, J. Fernández, J. de Brito, Mechanical behaviour of self-compacting concrete made with recovery filler from hot-mix asphalt plants, Construction and Building Materials 131 (2017) 114-128.

[13] A.S. Gill, R. Siddique, Strength and micro-structural properties of self-compacting concrete containing metakaolin and rice husk ash, Construction and Building Materials 157 (2017) 51-64.

[14] N. Ranjbar, A. Behnia, B. Alsubari, P.M. Birgani, M.Z. Jumaat, Durability and mechanical properties of self-compacting concrete incorporating palm oil fuel ash, Journal of Cleaner Production 112 (2016) 723-730.

[15] J. Cuenca, J. Rodríguez, M. Martín-Morales, Z. Sánchez-Roldán, M. Zamorano, Effects of olive residue biomass fly ash as filler in self-compacting concrete, Construction and Building Materials 40 (2013) 702-709.

[16] Asociación Española de Normalización y Certificación, AENOR, Madrid, Spain, (2018).

[17] American Society of Testing Materials, ASTM International, West Conshohocken, USA, (2018).

[18] P. Da Silva, J. De Brito, Experimental study of the porosity and microstructure of self-compacting concrete (SCC) with binary and ternary mixes of fly ash and limestone filler, Construction and Building Materials 86 (2015) 101-112.

[19] S. Dadsetan, J. Bai, Mechanical and microstructural properties of self-compacting concrete blended with metakaolin, ground granulated blast-furnace slag and fly ash, Construction and Building Materials 146 (2017) 658-667.

[20] G. Sua-iam, N. Makul, Incorporation of high-volume fly ash waste and high-volume recycled alumina waste in the production of self-consolidating concrete, Journal of Cleaner Production 159 (2017) 194-206.

[21] K. Celik, M.D. Jackson, M. Mancio, C. Meral, A.-H. Emwas, P.K. Mehta, P.J.M. Monteiro, High-volume natural volcanic pozzolan and limestone powder as partial replacements for portland cement in self-compacting and sustainable concrete, Cement and concrete composites 45 (2014) 136-147.

[22] A. Niyogi, Characterization of fly ash fractions to trace the extent of pollution, 2017 World of Coal Ash (WOCA) Conference in Lexington (2017), http://wwwflyash.info.

[23] European Coal Combustion Products Association (ECOBA). Available online: http://www.ecoba.com/ecobaccpprod.html.

[24] A.I. Torres-Gómez, E.F. Ledesma, R. Otero, J.M. Fernández, J.R. Jiménez, J. de Brito, Combined Effects of Non-Conforming Fly Ash and Recycled Masonry Aggregates on Mortar Properties, Materials 9(9) (2016) 729.

[25] International Energy Outlook 2017, U.S. Energy Information Administration, EIA (2017). http://wwweia.gov/ieo.

[26] Directive 2008/98/EC of the European Parliament and of the Council of 10 November 2008 onWaste. Official Journal of the European Union. 2008.

[27] EHE-08. Spanish Structural Concrete Code EHE-08 [Instrucción de Hormigón Estructural EHE-08]. R.D. 1247/2008, Spain (2008).

[28] P. Swarthmore, Joint Committee on Power Diffraction Standard-International Centre for Diffraction Data. (1995).

[29] J.M. Pommersheim, Effect of particle size distribution on hydration kinetics, MRS Proceedings, Cambridge Univ Press, 1986, p. 301.

[30] S. Tsivilis, S. Tsimas, A. Benetatou, E. Haniotakis, Study on the contribution of the fineness on cement strength, (1990).

[31] D.P. Bentz, E.J. Garboczi, C.J. Haecker, O.M. Jensen, Effects of cement particle size distribution on performance properties of Portland cement-based materials, Cement and Concrete Research 29(10) (1999) 1663-1671.

[32] M. Fernández Cánovas, Hormigón, Ed. Colegio de Ingenieros de Caminos, Canales y Puertos (2007).

[33] V. Kocaba, Development and evaluation of methods to follow microstructural development of cementitious systems including slags, in, EPFL, 2009.

[34] S. Brunauer, P.H. Emmett, E. Teller, Adsorption of gases in multimolecular layers, Journal of the American chemical society 60(2) (1938) 309-319.

[35] A.W. Saak, Characterization and modeling of the rheology of cement paste: with applications toward self-flowing materials, 2000.

[36] P.R.d. Silva, J.d. Brito, Fresh-state properties of self-compacting mortar and concrete with combined use of limestone filler and fly ash, Materials Research 18(5) (2015) 1097-1108.

[37] I.B. Topcu, T. Bilir, T. Uygunoğlu, Effect of waste marble dust content as filler on properties of self-compacting concrete, Construction and Building Materials 23(5) (2009) 1947-1953.

[38] S. Barbhuiya, Effects of fly ash and dolomite powder on the properties of self-compacting concrete, Construction and Building Materials 25(8) (2011) 3301-3305.

[39] J. Gibbs, W. Zhu, Strength of hardened self-compacting concrete, Proceedings of First international RILEM Symposium on Self-Compacting Concrete (PRO 7), Stockholm, Suede, 1999, pp. 199-209.

[40] F. Puertas, T. Vázquez, Early hydration cement Effect of admixtures superplasticizers, Materiales de construcción 51(262) (2001) 53-61.

[41] Fernández Rodríguez J.M., "Introducción a los Cementos", Servicio de Publicaciones Universidad de Córdoba (2004), ISBN 84-7801-731-3.

[42] P. Silva, J. de Brito, Experimental study of the mechanical properties and shrinkage of self-compacting concrete with binary and ternary mixes of fly ash and limestone filler, European Journal of Environmental and Civil Engineering 21(4) (2017) 430-453.

[43] P. Domone, A review of the hardened mechanical properties of self-compacting concrete, Cement and Concrete Composites 29(1) (2007) 1-12.

[44] H. Dehwah, Mechanical properties of self-compacting concrete incorporating quarry dust powder, silica fume or fly ash, Construction and building materials 26(1) (2012) 547-551.

[45] M. Liu, Self-compacting concrete with different levels of pulverized fuel ash, Construction and Building Materials 24(7) (2010) 1245-1252.

[46] European Committe for Standarization, UNE-EN 1992. Eurocode 2. Design of concrete structures. Part 1-1. General Rules and Rules for Building, Madrid, 2013.

[47] C. Parra, M. Valcuende, F. Gomez, Splitting tensile strength and modulus of elasticity of self-compacting concrete, Construction and Building materials 25(1) (2011) 201-207.

[48] B. Felekoğlu, S. Türkel, B. Baradan, Effect of water/cement ratio on the fresh and hardened properties of self-compacting concrete, Building and Environment 42(4) (2007) 1795-1802.

[49] G. Trtnik, F. Kavčič, G. Turk, Prediction of concrete strength using ultrasonic pulse velocity and artificial neural networks, Ultrasonics 49(1) (2009) 53-60.

[50] M. Uysal, K. Yilmaz, Effect of mineral admixtures on properties of self-compacting concrete, Cement and Concrete Composites 33(7) (2011) 771-776.

[51] E.A. Whitehurst, Soniscope tests concrete structures, Journal Proceedings, 1951, pp. 433-444.

[52] A.P.M. Šahinagić-Isović, M. Šahinagić-Isović, G. Markovski, M. Ćećez, Shrinkage strain of concrete-causes and types, Građevinar 64(09.) (2012) 727-734.

[53] M. Valcuende, F. Benito, C. Parra, I. Miñano, Shrinkage of self-compacting concrete made with blast furnace slag as fine aggregate, Construction and Building Materials 76 (2015) 1-9.

[54] E. Güneyisi, M. Gesoğlu, E. Özbay, Strength and drying shrinkage properties of self-compacting concretes incorporating multi-system blended mineral admixtures, Construction and Building Materials 24(10) (2010) 1878-1887.

Capítulo 8

Durability of self-compacting concrete made from non-conforming fly ash from coal-fired power plants

"A.R. Esquinas, J.I. Álvarez, J.R. Jiménez, J.M. Fernández, Durability of self-compacting concrete made from non-conforming fly ash from coal-fired power plants, Construction and Building Materials, 189 (2018) 993–1006. doi:10.1016/J.CONBUILDMAT.2018.09.056."

Abstract

The search for answers to the environmental challenges is one of the obligations of the current society. Therefore, the optimisation of natural resources and the minimisation and revaluation of waste should be present in any activity. These purposes should be included in both the construction and energy sectors owing to the large amount of resources consumed and of pollutants and waste generated by them. The present work carries out a feasibility study of the use of fly ash from coal-fired power plants as a filler for self-compacting concrete (SCC). This kind of fly ash does not meet the compliance criteria determined by the regulations, and thus, it is non-conforming fly ash (NCFA). The dual objective of this work is the optimisation of

a natural non-renewable resource and the recovery of waste, which should achieve the qualification of end of waste before being used as a by-product. For this purpose, a comparative study of three mixes is performed, namely, SCC-1 with commercial siliceous filler (SF) (SCC reference), SCC-12 with a mix 1:1 by volume of SF and NCFA, and SCC-2 with NCFA. All the mixes showed good self-compactability. The analysis of the relevant parameters, i.e., apparent and dry density, open porosity, mercury intrusion porosimetry, absorption of water by immersion, and capillarity, has been significant to know in depth the durability of the mixes. The results show that it is possible to obtain a SCC with high performance with respect to durability, attack of aggressive agents, and shrinkage by replacing the SF of siliceous nature with NCFA.

Key words: Self-compacting concrete; durability; non-conforming fly ash; siliceous filler; aggressive agents.

Highlights:

- A durability-related comparative study of three SCCs was carried out.
- The porous structure of SCC-2 is less fine than that of SCC-1.
- SCCs could be used in aggressive environments in terms of water absorption.
- The mixes have good performance regarding chloride and sulphate ions penetration.
- The penetration depth of CO_2 is related to the porosity and curing mechanism.
- SCC–NCFA showed better features than SCC–SF regarding long-term shrinkage.

8.1 Introduction

One of the construction materials that consume more natural resources is concrete. Owing to its good structural properties, simple manufacture, and low cost, concrete is the most used material, ahead of others such as wood, steel, plastic, and aluminium [1]. For this reason, since its appearance, the concrete industry has been evolving towards technologies that are more efficient. An evolution of the normally vibrated concrete was the self-compacting concrete (SCC) [2]. It was intended to find a concrete whose performance and quality did not depend on the labour force in the

execution process. This special concrete allows the reduction of execution deadlines, the manufacture of complex structures, better surface finishes, reduction of labour, saving in costs, improvement in job security, and reduction in noise and vibrations [3]. The SCC incorporates a high content of fines and chemical additives in its dosage. For this reason, the SCC can be considered as unfriendly to the environment.

Nowadays, a potential alternative to the use of these conventional materials of fine granulometry is the use of residual powders of industrial and/or mining origin. This would allow an optimisation of the used resources, along with the recovery of waste and reduction of its emission to the environment. However, the use of residual materials always involves an uncertainty in their quality from the points of view of mechanical strength and durability. In order to achieve high reliability in all types of environments, the durability properties of these alternative materials must be evaluated against carbonation processes, degradation by attacks of chlorides, sulphates, etc., and the attack mechanisms that govern their processes of deterioration should be identified. To achieve a complete knowledge, it is necessary to carry out a study of the hydration processes, microstructure of the material, and transport mechanisms to the interior of the cement matrix. Therefore, an in-depth investigation of these materials will allow us to continue with innovation in the construction sector.

Sideris et al. [4] investigated the potential use of ladle furnace slag, the main by-product of the secondary steel-production process, as an alternative filler for SCC production because it showed latent pozzolanic and hydraulic properties. They concluded that this residue could be used as a filler because it had a positive effect on the self-compactability, compressive strength, and durability of the mixes. Another residue used in SCC has been copper slag. Sharma et al. [5] observed an improvement in self-compactability and good mechanical and durability performance of the SCC with a high substitution percentage (60%) of fine aggregate. Esquinas et al. [6,7] carried out an analysis of SCCs incorporating a dolomitic waste powder. The setting mechanisms and the microstructure of the mixes were analysed and correlated with their mechanical and durability behaviours, demonstrating the good performance of the SCCs. Tennich et al. [8] investigated the use of marble and tile waste as a replacement of the conventional mineral admixtures in SCC. The results

showed that the use of these residues gave rise to high resistance of the SCC to attack by sulphates, higher than that of the normally vibrated concrete.

Other residues that come from the combustion processes of various industries (ashes) have appropriate physical and chemical characteristics for their use as mineral admixtures in SCCs. Prior to their use, it is necessary to know their behaviour and evaluate their applicability. Kannan [9] studied the effect of rice husk ash on the mechanical and durability properties of SCCs. This author observed a good behaviour in the fresh and hardened states of the mixes that incorporated up to 15% of this residue. The use of palm oil fuel ash in SCC has been investigated by authors such as Ranjbar et al. [10]. The effect of this residue improved the results of the mixes with respect to the attack of chemical agents (chlorides and sulphates), water absorption, and shrinkage. Sua-Iam and Makul [11] carried out an analysis of SCCs incorporating incinerated sugarcane filter cake, which is considered as the largest waste of the sugar industry. These authors concluded that it is possible to produce SCCs using this by-product with acceptable workability and hardened properties. The results obtained by Cuenca et al. [12] clearly indicated that biomass ash could be used in high-quality self-compacting concrete.

Currently, worldwide, one of the most important residues is the fly ash from coal-fired power plants [13]. This waste could be used in the construction sector as long as it complies with the conformity criteria established by the regulations (EN 450-1, EN 450-2, EN 14227-4, and ASTM C 618) [14,15], and it is called conforming fly ash. This by-product is characterised by its pozzolanic and cementitious properties. In the SCCs, this by-product has been extensively studied, being the object of numerous works [16–30].

When this residue does not comply with the required fineness, it is considered as non-conforming fly ash (NCFA) [31], which represents between 30% and 40% of the total production of fly ash and, unlike the conforming fly ash, it has had non-existent or poor applicability [32]. The world production of NCFA is estimated in 250 million ton per year [31,33]. The European Union Directive-2008/98/EC considers fly ash as a waste that must be recovered [34].

The purpose of this work is to carry out an evaluation of the use of NCFA as a filler in SCC from the point of view of durability, which has not been studied yet. A comparative analysis of three mixes has been carried out; in the first SCC, a commercial siliceous filler (SF) was used as reference; in the second one, a mix 1:1 by volume of SF and NCFA was utilised; and in the third one, only NCFA was used. The amount of filler used by volume was similar in all the cases. To determine the behaviour of the three SCCs, a fresh-state study was carried out in the first place, where the self-compactability properties were addressed. Subsequently, the microstructural and physical properties of absorption were analysed. Finally, a study of the durability of these materials was carried out, which was completed with the analysis of their long-term shrinkage.

As a result, it will be possible to reach similar reliability, if not higher, than that of conventional materials. This is an essential aspect to solve the uncertainties in relation to their stability over time. Therefore, this study will be useful for the valorisation of the industrial by-product NCFA, and consequently, the minimisation of its environmental impact, which will undoubtedly contribute to the conversion of concrete into a material friendlier to the environment.

8.2 Experimental methodology

8.2.1 Materials

The aggregates used were gravel 4/16, coarse sand 0/4, and fine sand 0/2 (hereinafter G, S1, and S2, respectively). A characterisation of the aggregates was carried out by Esquinas et al. [31] and it was determined that the aggregates are suitable according to the EHE-08 guideline [35].

As mineral admixtures were employed, on the one hand, SF and, on the other hand, NCFA [31]. In Figure 8.1 it is observed that quartz (33-1161) [36] is the only mineralogical phase of the SF. In NCFA, besides quartz (33-1161) [36], mullite (15-0776) [36], dolomite (36-0426) [36], and maghemite (γ-Fe2O3) (25-1402) [36] are observed. This is in accordance with their respective DTA-TG and energy dispersive X-ray (EDX) analysis (Figure 8.2 and Table 8.1).

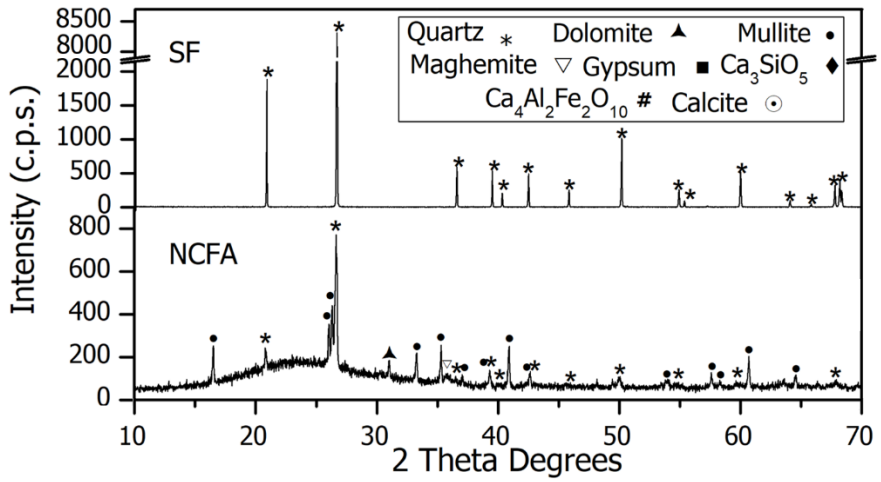

Figure 8.1: PXRD patterns for SF and NCFA.

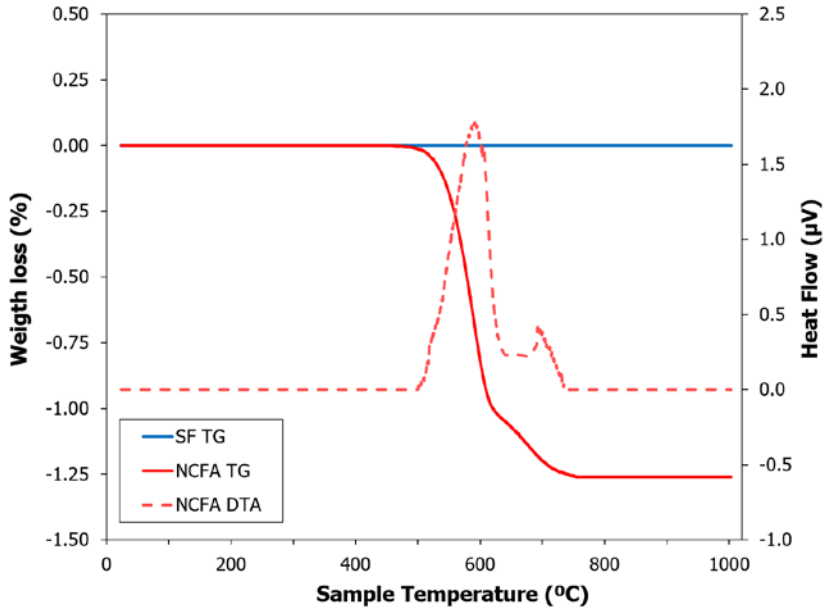

Figure 8.2: TG (solid lines) and DTA (dotted line) curves for the SF and NCFA fillers.

The granulometric distribution of the fillers, in accordance with the standard UNE-EN 933-1 [15], showed that through the 2 mm sieve passes 100% of both materials; through the 0.25 mm sieve pass 100% and 92.4% of SF and NCFA, respectively; through the 0.125 mm sieve pass 100% and 59.6% of SF and NCFA, respectively; and through the 0.063 mm sieve pass 74.33% and 27.5% of SF and NCFA, respectively. NCFA presents a granulometric distribution slightly greater than the one

that establishes the norm (70% goes through the sieve 0.063 mm, 85% goes through the sieve 0.125 mm, and 100% goes through the sieve 2 mm) [35]. In addition, an analysis of the grain size distribution was carried out by laser diffraction using ethanol as a dispersant (Figure 8.3 and Table 8.1).

Table 8.1
Characterisation of filler and cement.

Characteristic	Standard	SF	NCFA	Cement
SiO_2 %	-	100	28.50	13.30
Al_2O_3 %	-	-	54.90	6.60
Fe_2O_3 %	-	-	14.90	16.60
SO_3 %	-	-	-	5.00
CaO %	-	-	0.60	56.30
MgO %	-	-	0.60	0.70
Na_2O%	-	-	-	-
Other	-	-	0.50	1.50
BET surface area (m^2/g)	-	2.90	1.80	0.67
Particle density (g/cm^3)	UNE 80103	2.60	1.86	3.10
Bulk density (g/cm^3)	UNE-EN 1097-3	0.69	1.04	-

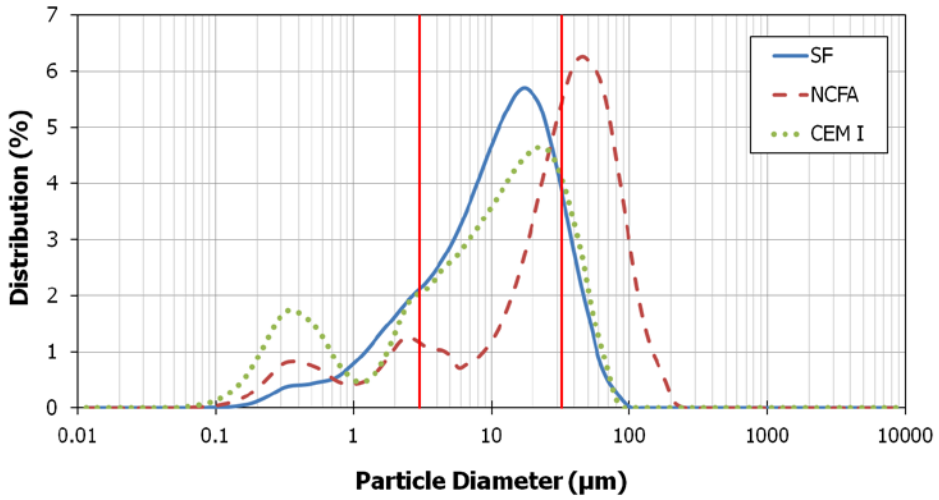

Figure 8.3: Grain-size distribution of SF, NCFA and CEM I as measured by laser diffraction.

It was observed that NCFA has a wider distribution than SF (0.1–240 µm vs. 0.1–100 µm), and a majority in percentage of the NCFA particles are around 45 µm, compared to 20 µm of the SF. Regarding the range of optimal sizes (3–32 µm) for

the hydration process of the particles [37–39], SF presents a percentage of 74.78%, compared to 39.64% in NCFA. This material has a higher percentage of particles of sizes greater than 32 μm (45.01%), which are too large to hydrate completely. The porosity of the filler was defined by the nitrogen adsorption–desorption isotherms (Figure 8.4). Both samples are characterised by a low Brunauer–Emmett–Teller (BET) surface (2.90 m^2/g for SF and 1.80 m^2/g for NCFA) (Table 8.1), which is in accordance with their respective grain size distributions (Figure 8.3), and the larger the particle size is, the smaller the surface area. Regarding the pore size distribution, determined according to the density functional theory (DFT) method, a range of pore diameter between 2.5–37 nm was observed. Additionally, the morphology of the particles of both fillers is shown by transmission electron microscopy (Figure 8.4).

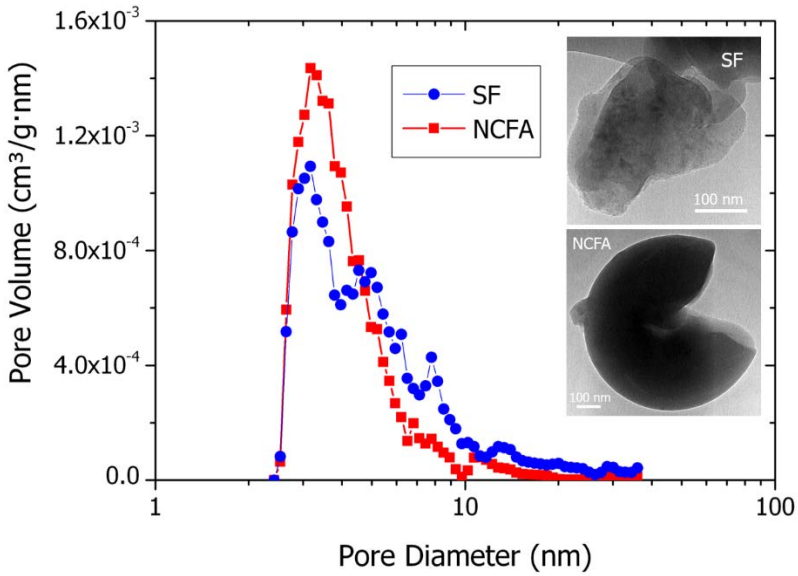

Figure 8.4: Pore size distribution for the SF and NCFA fillers.

The cement used was of type CEM I 42.5 R/SR (UNE 80303-1 and UNE-EN 197-1) [15]. The physico-chemical composition was analysed previously by Esquinas et al. [31]. The grain size distribution of the cement (Figure 8.3) shows that the larger particle percentage, 59.96%, is between 3 and 32 μm (Table 8.1).

As an additive, it was used a high-performance superplasticiser/water reducer specific for self-compacting concrete, Glenium 303 SCC of Basf Chemical Company (based on polycarboxylic ether polymers).

8.2.2 Concrete mixes and composition tests

To carry out an exhaustive analysis of the use of NCFA as a filler in SCC, it is necessary to carry out a study of the durability of these materials against aggressive agents. Three mixes were defined (Table 8.2) according to the dosage of Esquinas et al. [31]. In all the mixes, the study of the parameters in fresh state was carried out in order to check their reproducibility, according to the EHE-08 guideline [6,35].

The specific requirements determined for the dosages were approximately 800 kg/m^3 of gravel, 400 kg/m^3 as a minimum of cement, the same amounts of additive (1.8% of cement + filler) and cement, maximum W/C ratio of 0.44, characteristic resistance of 40 MPa, and exposure class IIIc. According to EHE-08, it was classified as HA-40/AC/16/IIIc. The adjustment of the dosage was made by volume (1025 L) [40].

The SCC-1 mix was considered the reference concrete in this study. All the mixes [31] complied with the recommendations of the EFNARC [3,41]. Small adjustments in the total amount of aggregates and water, and in the ratio of sand 0/2 with respect to the filler, were made to obtain the SCC-12 and SCC-2 mixes. In these mixes, the filler volume and granular skeleton were kept constant at the reference SCC. In Table 8.2, it can be seen that the percentages of the different materials of the mixes were similar.

8.2.3 Test methods

The materials were characterised by different techniques. The grain sizes were measured in a Mastersizer S analyser (Malvern Instruments) using ethanol as dispersant. The samples were analysed by X-ray diffraction analysis (XRD) using a Bruker D8 Discover A25 instrument with CuKα radiation. All diffraction patterns were obtained by scanning the goniometer from 10° to 70° (2θ) at a rate of 0.05° min^{-1}. For NCFA, the rate was 0.006° min^{-1}.

Table 8.2
Concrete mix proportions and dosing tests.

Mixes	**SCC-1**				**SCC-12**				**SCC- 2**			
	Dry weight		*Volume*		Dry weight		*Volume*		Dry weight		*Volume*	
Constituent	kg/m^3	%	*dm^3*	*%*	kg/m^3	%	*dm^3*	*%*	kg/m^3	%	*dm^3*	*%*
Gravel 4/16 (G)	807.65	33.05	*309.80*	*30.26*	797.81	32.97	*306.03*	*29.89*	789.07	32.79	*302.67*	*29.56*
Sand 0/4 (S1)	657.28	26.90	*250. 59*	*24.47*	649.28	26.83	*247.53*	*24.17*	642.16	26.69	*244.82*	*23.91*
Sand 0/2 (S2)	280.82	11.49	*106.33*	*10.38*	284.37	11.75	*107.68*	*10.52*	300.82	12.50	*111.91*	*11.12*
Filler (SF)	101.75	4.16	*39.13*	*3.82*	51.96	2.15	*19.99*	*1.95*	0.00	0.00	*0.00*	*0.00*
Filler (NCFA)	0.00	0.00	*0.00*	*0.00*	41.57	1.72	*22.30*	*2.18*	72.94	3.03	39.13	3.82
Cement	410.00	16.78	*132.26*	*12.92*	410.00	16.94	*132.26*	*12.92*	410.00	17.04	*132.26*	*12.92*
Superplasticizer	9.21	0.38	*8.90*	*0.87*	9.06	0.37	*8.76*	*0.86*	8.69	0.36	*8.40*	*0.82*
Water	176.93	7.24	*176.93*	*17.28*	179.40	7.40	*179.40*	*17.52*	182.75	7.59	*182.75*	*17.85*
(W/C) $_{total}$	0.431				0.437				0.446			
(W/C) $_{ef}$	0.422				0.428				0.436			

The N_2 isotherms were determined on an Autosorb iQ (Quantachrome), and the samples were previously degassed at 100 °C under vacuum for 2 h, as a strict degassing of the sample is required for determination of the content of micropores or small mesopores. The surface was calculated by applying the BET method in the range of relative equilibrium pressure $0.05 \leq P/Po \leq 0.20$ [42]. The pore size distribution was calculated using the density functional theory (DFT) method. The microstructural characterisation of the materials was carried out using an electron microprobe technique, which was implemented on a JEOL JSM-7800F scanning electron microscope using an acceleration voltage of 15 kV and a working distance of 10 mm. The X-ray detector was an X-MaxN150 from Oxford Instruments. The surface morphology of some samples was obtained using a scanning electron microscope JEOL JSM 7800F, applying an acceleration voltage of 5 kV.

The self-compactability of the SCCs and the analysis of the density in fresh state was determined following the same methodology as the one used by Esquinas et al. [6,7,31,43].

Physical properties of hardened SCCs: the bulk density and skeletal density (UNE-EN 12390-7 and UNE 83980) [15], the open porosity (UNE 83980) [15], the mercury intrusion porosimetry (MIP) values; and water adsorption properties of hardened SCCs: the immersion water absorption (UNE 83980) [15], water absorption by capillarity (UNE 83982) [15], were determined according to Esquinas et al. [7].

The durability properties of hardened SCCs: the depth of penetration of water under pressure (UNE 12390-8) [15], the rapid chloride ion penetration test by electrical conductance method (ASTM C1202) [14], the penetration of chloride ion into concrete by ponding (ASTM C 1543) [14], the resistance to CO_2 penetration in concrete (LNEC E 391 [44] y UNE 112011 [15]), the penetration of sulphate ion into concrete by ponding (UNE-EN 196-2) [15], and the total shrinkage (ASTM C157/C157M-08(2014)e1.) [14] were determined according to Esquinas et al. [7].

All the tests were triplicated, in specimens made from the same concrete mix, yielding average values and standard deviations.

8.3 Results and discussion

8.3.1 Properties of SCC in fresh state

8.3.1.1 Self-compactability

The self-compactability parameters recorded in the fresh state of the mixes (Table 8.3) agree with the EHE-08 guideline [35].

Table 8.3
Results of the self-compactability tests for the two types of SCC.

Mixtures	**Retakes**	**Slump flow test**		**J-Ring test**		**V-funnel test**	**L-box test**
		T_{50} (s)	d_f (mm)	T_{j50} (s)	$d_f - d_{jf}$	T_v (s)	C_{0L}
SSC-1	Average (SD) [a]	2.72 (0.2)	730 (5.1)	3.23 (0.7)	28 (6.5)	7.42 (0.3)	0.89 (0.02)
Class [36]	*AC-V2*	*AC-E2*	*AC-RB2*		*AC-V2*	*AC-RB2*	
SSC-12	Average (SD) [a]	3.85 (0.7)	699 (4.2)	4.56 (0.7)	23 (8.3)	9.5 (0.4)	0.84 (0.03)
Class [36]	*AC-V1*	*AC-E2*	*AC-RB2*		*AC-V1*	*AC-RB2*	
SSC-2	Average (SD) [a]	3.07 (0.2)	676 (4.6)	4.03 (0.5)	22 (4.8)	10.9 (0.4)	0.83 (0.04)
Class [36]	*AC-V1*	*AC-E2*	*AC-RB2*		*AC-V1*	*AC-RB2*	

[a] Standard deviation

Figure 8.5 shows the values of slump flow (d_f) versus V-funnel time (Tv), based on which the workability of the mixes can be defined using the concept of workability boxes [45], regarding its self-compactability. In this figure, the repetitions of each mix are collected, and the measured values are obtained. As can be seen, the mixes are within the area where the SCCs would have an acceptable self-compactability. The mix with SF (SCC-1) is located in the boundary of the regions called 'proper SCC area' and 'marginal SCC area', according to Saak [45], and in this last region a slight segregation may appear. This was not observed in any mix, which would be in accordance with the proximity to the area called 'proper SCC area'. Besides, both the mix with NCFA (SCC-2) and that made with a combination 1:1 by volume of both fillers (SCC-12) were within the area defined as 'proper SCC area', which is characterised by good self-compactability. The results show the reproducibility of the repetitions of the mixes.

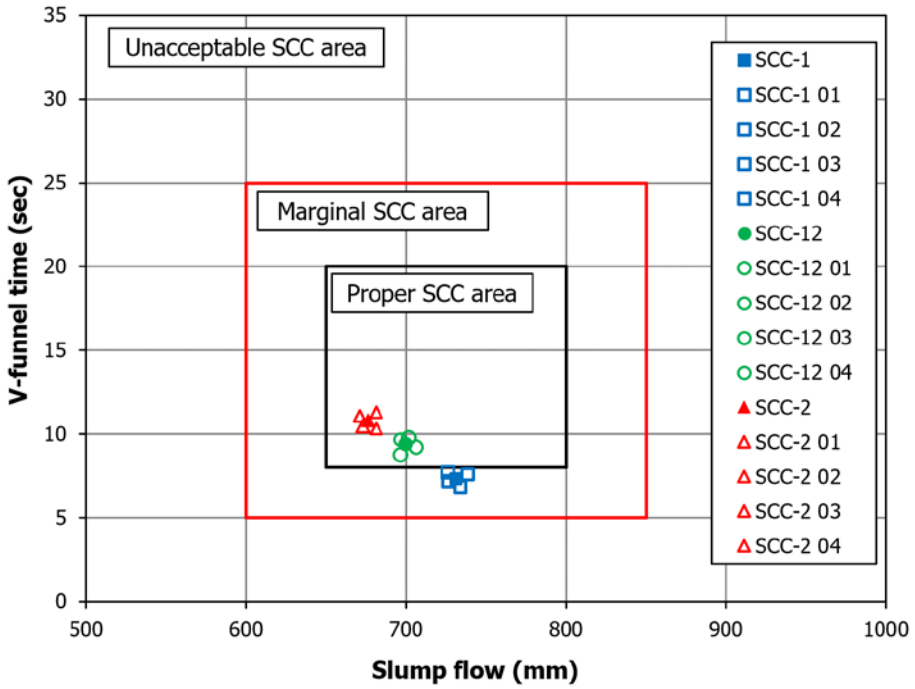

Figure 8.5: Workability boxes for several self-compacting mixes.

The differences in self-compactability observed in the mixes may be due to the distribution of the coarser grain sizes presented by the NCFA (Figure 8.3), which may hinder the movement of the mix (SCC-2) by its own weight because the quantity of fines [31] is smaller compared to the reference dosage (SCC-1). This observed

behaviour justifies the amount of water necessary to obtain self-compactability in SCC-2 (182.75 dm^3/m^3 versus 176.93 dm^3/m^3 for SCC-2 and SCC-1, respectively) (Table 8.2). This leads to a reduction of −7% in the slump flow (d_f) and a 47% increase in the V-funnel time (Tv) of SCC-2 compared to SCC-1. In SCC-12, these percentages present intermediate values to the previous ones (−4% and 28% for d_f and Tv, respectively) with respect to SCC-1, and thus, an increase in the fluidity is observed when using a combination of both fillers with respect to SCC-2. This could be attributed, on the one hand, to the increase in the amount of fines and paste in SCC-12 (Table 8.2) [31] and, on the other hand, to the finer grain size distribution of the filler used (i.e., the 1:1 mix by volume of both materials). This finer granulometry of SCC-12 with respect to SCC-2 would result in a better packaging factor, which would also result in an improvement in self-compactability. It can be concluded that it is possible to obtain SCC using the NCFA waste as filler, and with dosages where the natural siliceous filler, SF, was replaced by 50% and 100% of NCFA by volume.

This behaviour is in agreement with that indicated by Esquinas et al. [6,7], who observed that the use of a residual filler with a grain size distribution thicker than the SF caused a self-compacting closer to the limits of EHE-08. However, as in the present work, these authors observed a self-compactability that could be defined as acceptable SCC in relation to the workability box. It is worth noting the different behaviour of the NCFA and fly ash regarding the self-compactability of the mixes. As observed by different researchers [17,24], unlike what is observed in the present work, the incorporation of fly ash produces an improvement in self-compactability with respect to the reference SCC without this admixture. This behaviour could be mainly associated with the fine grain size distribution (<45 μm) that characterises the fly ash of conforming characteristics with respect to the residue (NCFA) used in this work.

8.3.1.2 Density of SCC in fresh state

The density in the mixes was of 2.444 kg/dm^3, 2.427 kg/dm^3, and 2.402 kg/dm^3 for SCC-1, SCC-12, and SCC-2, respectively. It is observed that SCC-1 has the highest density, which may be due to the finer and continuous grain size distribution of SF with respect to that of NCFA (Figure 8.3). The higher volume of fines in SCC-1

(Table 8.2) [31] would be in accordance with the results obtained, because the packaging factor would be higher. These results are in agreement with other researchers [6,7,46].

8.3.2 Properties of SSC in the hardened state

8.3.2.1 Physical properties of hardened SCCs

8.3.2.1.1 Bulk density and evolution during drying and skeletal density

Figure 8.6 (left side) shows the evolution of the density of the samples cured at 28 days with respect to the mass loss (m) produced during the drying of the mixes until constant mass.

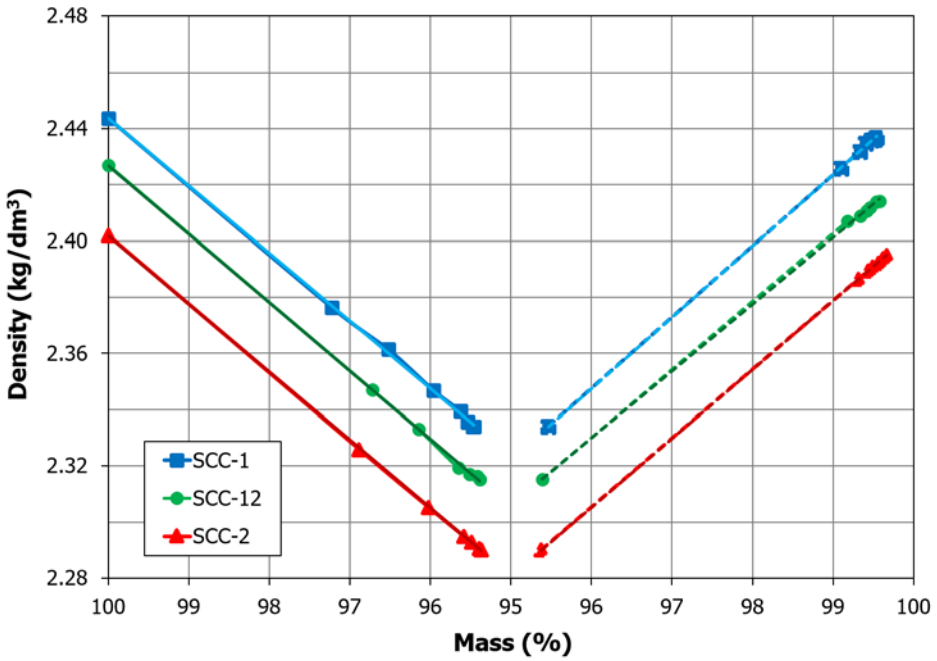

Figure 8.6: Evolution of the density relative to the variation of mass.

The last data of each mixture corresponds to the bulk density (ρ_{ap}). A linear behaviour is observed, which can be expressed by the following Eqs. (8.1), (8.2), and (8.3) for SCC-1, SCC-12, and SCC-2, respectively:

$$\rho_{ap} = 0.0241\ m - 0.0354 \qquad (R^2 = 0.9995) \qquad (8.1)$$

$$\rho_{ap} = 0.0243\ m - 0.0072 \qquad (R^2 = 0.9995) \qquad (8.2)$$

$$\rho_{ap} = 0.0242\ m - 0.0175 \qquad (R^2 = 0.9999) \qquad (8.3)$$

All the mixes show similar evolution during drying, which is in accordance with an analogous evolution of the volume and which corresponds to slopes of the same order for Eqs. (8.1), (8.2), and (8.3).

The bulk densities of SCC-1, SCC-12, and SCC-2 were collected in Table 8.4. Regarding the reference mix (SCC-1), a decrease of 1% in SCC-12 and of 2% in SCC-2 was observed. This could be due to the modification of the type of filler used in the different mixes (Figures 8.3 and 8.4), and to the variation in water content to obtain the appropriate self-compacting parameters (Table 8.2). Regarding skeletal density (Table 8.4), a decrease was observed, with respect to SCC-1, of 0.6% for SCC-12 and of 1.1% for SCC-2. A smaller difference is observed in the skeletal density values than in the bulk density, owing to the definition of both densities, which causes that the differences be damped for the skeletal density. This is because in the bulk density, the influence of the accessible pores (that are empty) is suppressed only in the value of mass (dry mass), whereas in the skeletal density, the influence of this porosity is eliminated in the values of both mass and volume.

Other authors [7,47] also observed a decrease in the density of the mixes made with a residual filler with a coarser grain size distribution than the SF used as a reference in the SCC. Besides, Kristiawan et al. [23] observed an increase in the density of the mixes that incorporated fly ash owing to the pozzolanic reactions, which caused a finer porosity of the SCCs.

Table 8.4
Physical and water absorption properties hardened SCCs.

	Unit	Standar/Test	SCC-1 (SD)	SCC-12 (SD)	SCC-2 (SD)
Bulk density (ρ_{ap})	(kg/dm³)	UNE 83980	2.346 (0)	2.322 (0)	2.300 (0)
Skeletal density (ρ_{sk})	(kg/dm³)	UNE 83980	2.623 (0)	2.607 (0)	2.594 (0)
Open porosity	(%)	UNE 83980	10.7 (0)	10.9 (0.1)	11.3 (0.2)
Threshold diameter	(µm)	MIP	0.13	0.19	0.21
Median Pore Diameter	(nm)	MIP	44	50	70
Porosity (MIP)	(%)	MIP	9.3	11.1	11.4
Abs. by inmersion at 24h	(%)	UNE 83980	3.81 (0.03)	3.97 (0.02)	4.08 (0.02)
Abs. by inmersion at 48h	(%)	UNE 83980	4.05 (0.02)	4.14 (0.01)	4.21 (0.01)
Capillary Absorption at 24 h	(g/cm²)	UNE 83982	0.1900 (0.01)	0.2167 (0.01)	0.2400 (0.01)
		UNE 83982 (1)	0.4400 (0.01)	0.5600 (0.01)	0.7100 (0.01)
Capillary Abs. Coef. (K)	(g/cm² · min$^{1/2}$)	UNE 83982	0.0043 (0)	0.0044 (0)	0.0046 (0)
		UNE 83982 (1)	0.0085 (0)	0.0104 (0)	0.0109 (0)
Resistance to penetration (m)	(min/cm²)	UNE 83982	11 (0.05)	16 (0.12)	19 (0. 30)
		UNE 83982 (1)	16 (0.16)	19 (0.21)	25 (0.11)
Effective Porosity (ξ)	(%)	UNE 83982	1.40 (0.01)	1.74 (0.01)	1.98 (0.01)
		UNE 83982 (1)	3.30 (0)	4.47 (0)	5.37 (0)
Sorptivity (S)	(cm/min$^{1/2}$)	UNE 83982(2)	0.00462	0.00516	0.00588
		UNE 83982 (1) (2)	0.01005	0.01340	0.01387

(1) Oven dry at 100ºC.
(2) Using Hall's model.

8.3.2.1.2 Open porosity or accessible porosity for water

The percentage of pores accessible to water in the hardened mixes calculated from the skeletal and bulk densities is presented in Table 8.4. It is observed that as the content of NCFA increases, an increase in accessible porosity occurs. This increase can be quantified as 2.7% for SCC-12 and 6.4% for SCC-2 with respect to SCC-1. As previously mentioned, this increase in porosity may be due, on the one hand, to the thicker grain size distribution of the NCFA that causes poorer packaging and, on the other hand, to the higher W/C ratio of the SCCs with NCFA.

These results are in agreement with those observed by other researchers [7,47] who used fillers with a coarser grain size distribution. In contrast, Kristiawan et al. [23] found the opposite effect when they incorporated fly ash, justifying this phenomenon in that its pozzolanic effect caused a decrease in accessible porosity. Additionally, researchers such as Sfikas et al. [48], who incorporated silica fume, or Badogiannis et al. [49], who incorporated metakaolin, observed a decrease in the open porosity of the mixes. Other authors [50–52] analysed the influence of the W/C ratio on the porosity of the SCC, concluding that the mixes that had a lower W/C ratio had lower porosity.

8.3.2.1.3 Pore size distribution

The cumulative values of Hg volume in the intrusion–extrusion cycle with respect to the pore diameter of the three mixes are shown in Figure 8.7, top. It is observed that SCC-2 has a higher porosity, followed by SCC-12, and SCC-1 (Table 8.4). These results are congruent with the open porosity test discussed above. Figure 8.7, bottom, considers the volume differential of mercury intrusion with respect to the pore diameter. A similar pattern of porous distribution was observed in the three mixes, highlighting a majority of content of pores in three zones, namely, approximately 90–100 μm (occluded air), 40 nm (medium capillary pores), and between 6 and 8 nm (small gel pores) [53–55]. Moreover, all mixes have the same maximum pore concentration around a pore size of 40 nm, approximately.

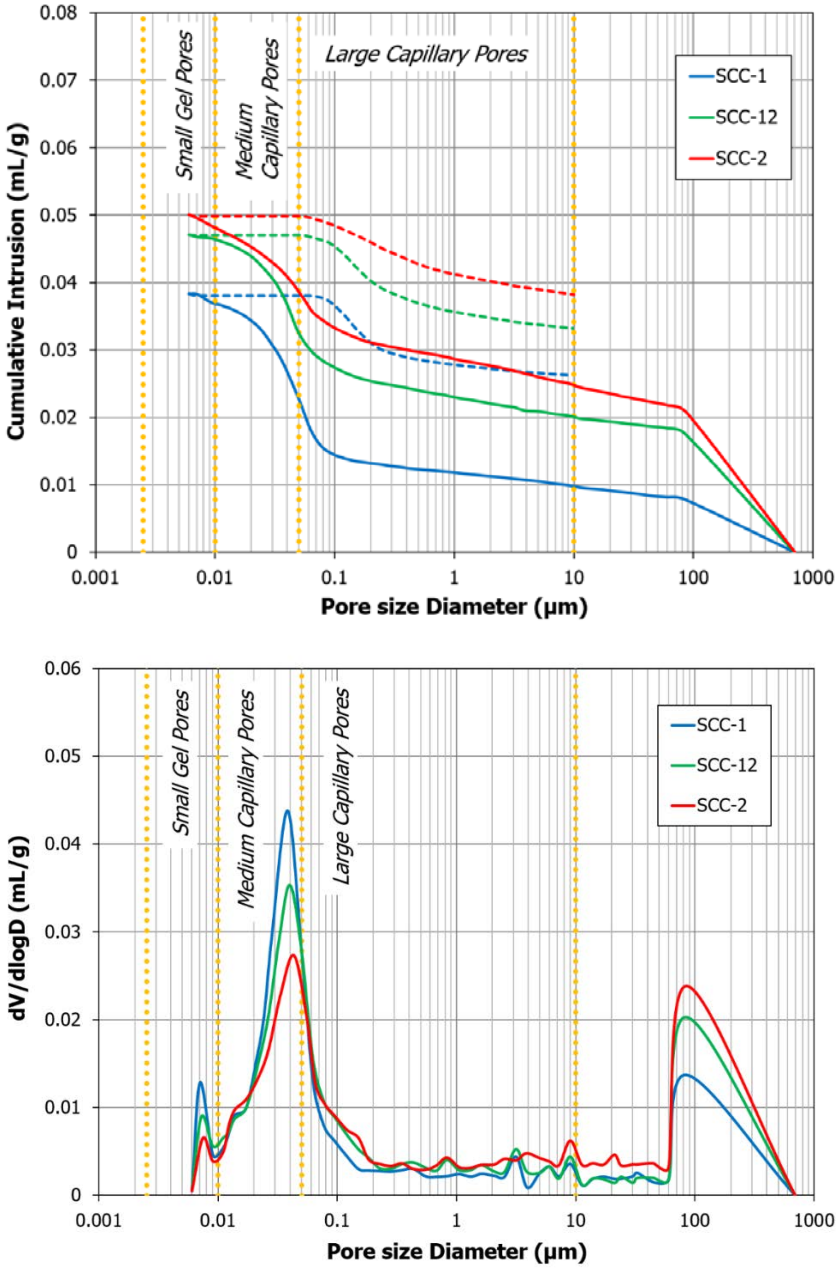

Figure 8.7: Cumulative pore volume and log differential intrusion of the mixes. (Dotted line) extrusion and (solid line) instrusion.

The volume of intrusion in the area above 60–70 µm was 0.031 mL/g, 0.036 mL/g, and 0.056 mL/g for the mixes SCC-1, SCC-12, and SCC-2, respectively. In the area of large capillary pores (50 nm–10 µm), the volumes for samples SCC-1, SCC-12, and

SCC-2 were 0.083 mL/g, 0.110 mL/g, and 0.139 mL/g, respectively. In the zone of medium capillary pores (10 nm–50 nm), the volumes of the SCC-1, SCC-12, and SCC-2 samples were 0.169 mL/g, 0.160 mL/g, and 0.113 mL/, respectively. The pore volume in these areas will make it possible to justify the permeability of the mixes [53]. Finally, in the area of small gel pores (10 nm–2.5 nm) the volumes in samples SCC-1, SCC-12, and SCC-2 were 0.018 mL/g, 0.015 mL/g, y 0.011 mL/g, respectively. Porosity of less than 10 nm will influence the shrinkage of the material [51,53].

A reduction of the large capillary pores, and consequently, a finer pore distribution in the mixture with SF (SCC-1) is observed. This may be related to an optimum grain size distribution, between 3 and 32 μm (Figure 8.3), to react with portlandite, $Ca(OH)_2$, and form hydrated products such as the CSH phases, which will fill the porous structure, forming smaller pores [31]. In addition, it would lead to the development of mixes with a higher structural density, as was evident in the results of the densities previously discussed. The W/C ratio will also influence the porous structure, the lower the W/C ratio the higher the structural density. The SCC-12 mix has an intermediate porosity according to the registered Hg volume.

The minimum pore diameter, where the continuous increase in the volume of Hg in the intrusion (threshold diameter) varies between the different mixes, is 0.13 μm for SCC-1, 0.19 μm for SCC-12, and 0.21 μm for SCC-2 (Table 8.4). This indicates a finer porous structure, which is in accordance with the Hg intrusion volumes in the different zones, as already discussed. The connectivity of the porosity and the continuity of the channels through the hardened SCC will depend on the filler or mineral admixture used and will be relevant to define the transport mechanisms of liquid or gas agents in the mixes. When NCFA is used, there is an increase in the threshold pore size in the mix with respect to the use of SF, and therefore, there is a thicker and more interconnected porous structure. Additionally, the three mixes presented a highly dense microstructure, as the average pore diameter (Table 8.4) is smaller than the threshold diameter in all cases [56].

This is in agreement with Esquinas et al. [7], who observed that the substitution of an SF with a dolomitic waste powder and with a thicker grain size distribution caused a SCC with a less fine porous structure, that is, there was an increase in the large

capillary pores. Da Silva & de Brito [56] performed an analysis of the porous structure of mixes with limestone filler and fly ash, and observed that the mixes with fly ash had finer porosity and higher microstructural density. Likewise, Mohammed et al. [29] observed in mixes with fly ash a higher percentage of microporosity than in mixes using limestone filler; this behaviour was justified by the grain size distribution and the chemical nature of the fly ash. That is, finer mineral admixtures and greater pozzolanic capacity (chemical nature) will result in finer porosity and microstructure of higher density.

Therefore, it can be concluded that the mix with NCFA has a higher percentage of pores larger than 10 μm (air voids and large capillary pores) compared to the mix with SF, which has a larger number of pores smaller than 10 μm (medium capillary pores and small gel pores), giving rise to a finer porous structure. The incorporation of 50% of NCFA into the mix results in an intermediate porosity and microstructural density.

8.3.2.2 Water absorption properties of hardened SCCs.

6.3.2.2.1 Water absorption by immersion and with vacuum

The physical properties above analysed will influence the absorption capacity of SCCs. The evolution of the mass loss during the drying process as a function of time of the samples after 28 days of curing in water is shown in Figure 8.8, bottom left. A similar drying process is observed between the samples, and the loss of mass is stabilised around 5%. The percentage is slightly higher in SCC-2 and SCC-12. This behaviour can be justified by the greater porosity of the mixes observed in both MIP and open porosity, discussed above, which will result in a greater amount of water contained in the porous structure, which can be evaporated. These results are in accordance with the W/C ratio (Table 8.2).

In the same way, these properties will influence the water absorption stage of the mixes (Figure 8.8, top right). It is observed that these mixes present an analogous stabilisation of the mass, around 4%, after the absorption process. However, there is a slight increase in this percentage in the SCC-2 and SCC-12 mixes with respect to

that in SCC-1. It is perceived that the SCCs after the drying process do not recover all the lost water, which represents approximately 12% of the total mass of water evaporated during drying. This fact is related to the incomplete rehydration suffered by the medium capillary pores and small gel pores [53], which are hardly accessible to water at atmospheric pressure (absorption process). It can be seen that SCC-1 presents a slightly higher percentage of water not reabsorbed (12.63%) compared to SCC-12 (11.98%) and SCC-2 (11.05%), which coincides with the larger volume of medium capillary pores–small gel pores of SCC-1 compared to the other mixes.

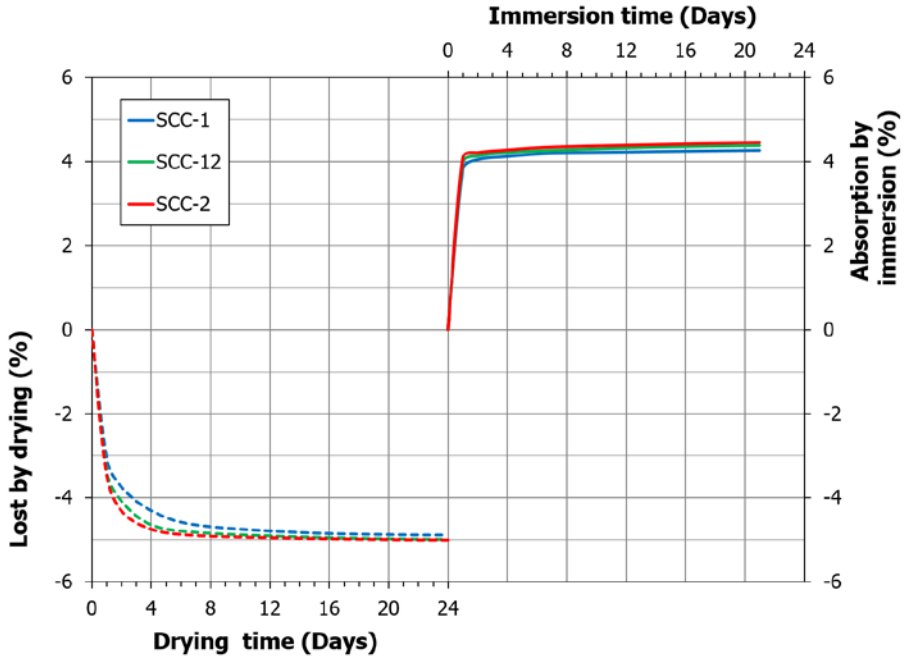

Figure 8.8: Evolution of the mass loss by drying (100 ºC) and absorption by immersion.

From Figure 8.8, we can obtain the parameters for the absorption of water by immersion, at 24 h and 48 h (Table 8.4). The values of maximum absorption of water by immersion to constant mass were of 4.27%, 4.39%, and 4.45% for SCC-1, SCC-12, and SCC-2, respectively.

These results are in agreement with Esquinas et al. [7], who observed an increase in water absorption by immersion in an SCC with a dolomitic residual powder as filler with respect to the SCC with an SF. In addition, after being dried to constant mass, they did not rehydrate completely. In the same way, these results agree with those

obtained by Schutter et al. [57], who made an extensive examination of the absorption of water by immersion with different mixes of SCC.

Considering the water absorption by immersion and vacuum (UNE 83980) [15], we observe an increase in the absorption values (at 48 h) of 4.5% 4.7%, and 4.9% for SCC-1, SCC- 12, and SCC-2, respectively. Thus, the water reabsorbed by vacuum immersion, taking into account the total water evaporated by the drying process (-4.89%, -4.99%, and −5.01% for SCC-1, SCC-12, and SCC-2, respectively), is 92% for SCC-1, 94% for SCC-12, and 97% for SCC-2. This decrease in the differences between the different mixes can be associated with the greater content of medium capillary pores of the SCC-1 and SCC-12 mixes with respect to SCC-2. The percentage of water not reabsorbed is related to the content of small gel pores that these mixes present, as previously commented.

Similarly, to the study of bulk density during the drying process, previously discussed in Section 8.3.2.1.1, an analysis of the evolution of this density during the water absorption process by immersion can be carried out. The observed linear behaviour with respect to the increase in mass (Figure 8.6, right side) is expressed by the following Eqs. (8.4), (8.5), and (8.6) relative to SCC-1, SCC-12, and SCC-2, respectively:

$$\rho_{ap} = 0.0273\ m + 0.243 \qquad (R^2 = 0.9923) \qquad (8.4)$$

$$\rho_{ap} = 0.0238\ m + 0.0494 \qquad (R^2 = 0.9996) \qquad (8.5)$$

$$\rho_{ap} = 0.0245\ m - 0.0425 \qquad (R^2 = 1) \qquad (8.6)$$

A similar variation in bulk density can be observed with respect to the mass of the mixes in the absorption process, according to the slopes of the linear adjustments that define the process.

8.3.2.2.2 Water absorption by capillarity

The porous structure of the SCCs will significantly influence the water absorption by capillarity, in the same way as with the previous parameter. The transport mechanisms and moisture exchange within the SCCs will depend on the pore

interconnection of the mixes. The capillarity absorption is divided into two phases. In the initial phase, the capillary pores are filled by absorption ($0<\sqrt{t}<\sqrt{t_n}$), and then the saturation of the porous structure occurs by diffusion and dissolution of the gas phase in the pores ($\sqrt{t}\geq\sqrt{t_n}$). The variable t_n is defined as the time necessary to reach saturation.

Figure 8.9 shows the capillary absorption of the mixes as a function of time, both for the mixes dried at 60 ºC up to constant mass (in accordance with the UNE 83982 standard) and for the mixes dried at 100 ºC until constant mass. A different behaviour can be observed between both test conditions and, according to some authors [58,59], it can be due to the deformation of the pore diameter of the small capillaries when subjected to a temperature of the order of 100 °C.

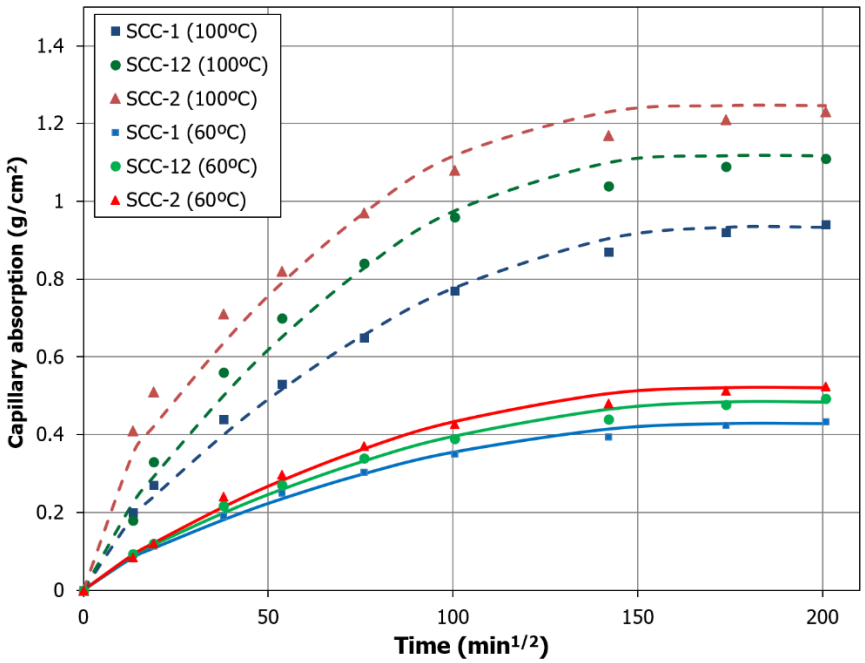

Figure 8.9: Capillary water absorption of the mixes.

If we analyse the absorption by capillarity at 24 h (Table 8.4), we observe that the mixes SCC-2 and SCC-12 have slightly higher values than that of SCC-1. This is in agreement with the greater volume of large capillary pores of SCC-2 with respect to the other mixes, as previously described. Thus, large capillary pores will have a

greater influence on the absorption of water by capillarity than, for example, the medium capillary or small gel pores, which are less abundant in SCC-2.

Hall [60] proposed the model represented by Eq. (8.7) to define the absorption by capillarity (W):

$$W = A + S\sqrt{t} - C\,t \qquad (8.7)$$

where t is time, S is sorptivity or the capillary absorption rate, and A and C are constants.

In all cases, the capillary absorption values can be adjusted to the following equations (Eqs. (8.8) – (8.13)), whose R^2 values are between 0.9593 and 0.9929:

$$W = -0.000013\,t + 0.004\,6\sqrt{t} + 0.0248 \qquad (8.8)$$

R^2=0.9915 (SCC-1 dried at 60 ºC)

$$W = -0.000014\,t + 0.0052\sqrt{t} + 0.0234 \qquad (8.9)$$

R^2=0.9923 (SCC-12 dried at 60 ºC)

$$W = -0.000017\,t + 0.0059\sqrt{t} + 0.0156 \qquad (8.10)$$

R^2=0.9929 (SCC-2 dried at 60 ºC)

$$W = -0.000029\,t + 0.0101\sqrt{t} + 0.0599 \qquad (8.11)$$

R^2=0.9911 (SCC-1 dried at 100 ºC)

$$W = -0.000042\,t + 0.0134\sqrt{t} + 0.0523 \qquad (8.12)$$

R^2=0.9852 (SCC-12 dried at 100 ºC)

$$W = -0.000044\,t + 0.0139\sqrt{t} + 0.1733 \qquad (8.13)$$

R^2=0.9593 (SCC-2 dried at 100 ºC)

The absorption values by capillary action and sorptivity of both mixes are presented in Table 8.4.

The effective porosity has also been determined (Table 8.4) using the capillary absorption value obtained from Eq. (8.7). This parameter provides information regarding the interconnected and connected porosity with the outside, which will have

a significant importance in the exchange of humidity with the environment and in the transportation mechanisms.

The Ibero–American document RED DURAR in the framework CYTED [61] establishes the limits of effective porosity and sorptivity (<10% y <0.039 cm/min$^{1/2}$, respectively) that structures exposed to highly aggressive environments must have. If we take into account these limits, and in accordance with the results of effective porosity (the values obtained vary between 1.4% and 5.37%) and of sorptivity (between 0.00462 cm/min$^{1/2}$ and 0.01387 cm/min$^{1/2}$) (Table 8.4), it can be seen that all the mixes have values lower than the proposed limits. Therefore, the SCCs of this work could be used in aggressive environments with adequate durability.

This is in agreement with Esquinas et al. [7], who used a dolomitic residue as filler of larger grain size than the SF used in the reference SCC. Silva & de Brito [56] observed a decrease in capillary absorption in mixes with fly ash as a mineral admixture compared to limestone filler mixes, owing to a finer microstructure when fly ash was used. In this sense, Jalal et al. [27] and Turk et al. [22] obtained lower capillary water absorption values in mixes that incorporated silica fume, with respect to mixes that used fly ash as mineral admixture, owing to the greater reactivity and finer grain size distribution of the silica fume.

8.3.2.3 Durability

8.3.2.3.1 Permeability and penetration of water under pressure

The maximum recorded penetration was of 1.7 mm, 2.7 mm, and 5.6 mm for SCC-1, SCC-12, and SCC-2 (Table 8.5), respectively. As can be seen, the mixes do not have high penetration, and thus, water does not move easily through the porous structure of the SCC under a differential pressure. The differences are not significant, although these are in agreement with the increase in pore volume greater than 50 nm of SCC-2 with respect to SCC-12 and SCC-1 (Figure 8.7). These results are also in agreement with the previously described absorption by immersion and absorption by capillarity of SCCs.

Table 8.5
Durability properties hardened SCCs.

	Unit	Standar/Test	SCC-1 (SD)	SCC-12 (SD)	SCC-2 (SD)
Permeability	(mm)	UNE 12390	1.7	2.7	5.6
Permeability coefficient	(10^{-14} m/s)	Valenta Ec. [64]	0.07	0.38	1.0
Chloride Ion Penetrability	-	ASTM C 1202	Low	Low	Low-Moderate
Effect. Cl^- Transp. Coeff. (D_e)	(10^{-12} m^2/s)	ASTM C 1556	4.8	5.6	6.2
Carbonation depth (7 days)	(mm)	LNEC E 391/UNE112011	1.78 (0.7)	3.06 (0.6)	5.78 (0.2)
Carbonation depth (28 days)	(mm)	LNEC E 391/UNE112011	3.06 (1.3)	6.00 (0.8)	8.20 (1.1)
Carbonation depth (91 days)	(mm)	LNEC E 391/UNE112011	9.29 (1.6)	11.14 (1.3)	12.70 (1.2)
Carbonation depth (182 days)	(mm)	LNEC E 391/UNE112011	13.11 (1.4)	15.85 (1.0)	18.14 (1.5)
Carbonation coefficient (K_C)	(mm/$year^{1/2}$)	Fick's first law	17.98	22.33	26.34
Effect. SO_3 Transp. Coeff. (D_e)	(10^{-12} m^2/s)	ASTM C 1556	5.00	6.03	6.17

Taking into account that the flow of the liquid is uniaxial, the penetration can approach the coefficient of permeability [62,63]. The coefficients of permeability obtained (Table 8.5) are lower than 10^{-14} m/s in both cases, which shows the high compactness of the SCCs. In addition, and according to Neville [64], these mixes can be considered as waterproof as none of them has a penetration greater than 30 mm.

This is in agreement with that indicated by Esquinas et al. [7], who observed slightly higher penetration values in SCCs that incorporated a dolomitic residual powder as substitute for the siliceous filler used in the reference mix, although both show good performance against the penetration of water under pressure. Da Silva & de Brito [56] observed higher permeability in limestone filler mixes than in mixes using fly ash as filler, owing to their finer porosity that gave rise to a less interconnected porous system, and therefore, greater compactness. In addition, other researchers, such as Gesoglu et al. and Saleh et al. [21,26], observed lower penetration of water under pressure in an SCC that incorporated silica fume compared to an SCC with fly ash, which was due to a greater development of pozzolanic activity of the silica fume compared to that of fly ash.

8.3.2.3.2 Rapid chloride ion penetration test by electrical conductance

The evolution of the electric charge with respect to time for the three mixes is shown in Figure 8.10. This electrical behaviour would be related to the mobility of ions within the material. The reached electric charge was of 1270 C for SCC-1, 1555 C for SCC-12, and 1995 C for SCC-2. Taking into account the ranges established by the ASTM C 1202 standard, all the mixes are within the range considered as low penetrability of the chloride ion (Table 8.5), although the electrical behaviour of SCC-2 is in the limit zone of low penetrability.

The porosity of the mixes will significantly influence the penetration of the chloride ion, as its mobility in the aqueous phase within the material, when subjected to the action of the electric field, will depend on the porous structure, which will behave as a barrier. It is observed that mixes having lower porosity and finer porous structure

(SCC-1 and SCC-12) present lower penetrability with respect to the mix having higher porosity and less fine porous structure (SCC-2).

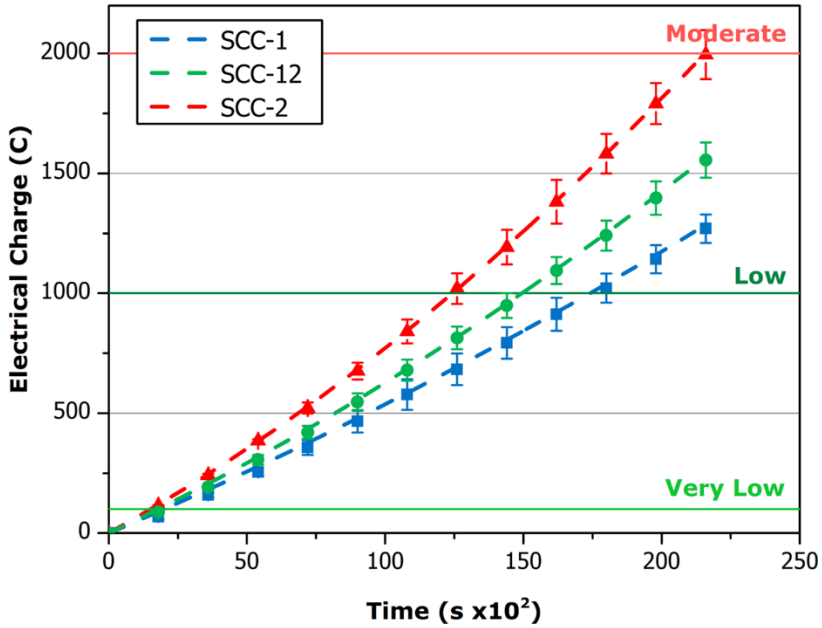

Figure 8.10: Rapid chloride ion penetration test by electrical conductance of the mixes.

The electric charge registered for each mix is within the range indicated by Tang & Zhu [65], which concludes that, with the rapid chloride permeability test, the conductivity values oscillate between 800–1600 C for samples of 28 days of age, which are much lower than the 4000 C of conventional concrete. The penetration of the chloride ion by migration obtained in this work is in agreement with that indicated by Saleh et al. [26], who observed lower penetrability of chlorides in SCC that incorporated silica fume compared to SCC with fly ash, which could be related to the development of finer porous structures of the mixes with silica fume compared to mixes with fly ash. Likewise, Esquinas et al. [7] observed that SCCs with SF presented slightly lower chloride penetration levels than SCCs with residual dolomitic filler, which were characterised by a less fine porous structure.

8.3.2.3.3 Penetration of chloride ion into concrete determined by ponding

Figure 8.11 shows the concentration profile of the chloride ion with respect to the depth of penetration for the three mixes, which allows the definition of the intrinsic durability of each mix. As can be seen, SCC-1 is the mix that presents the lowest chloride ion concentration, followed by SCC-12 and SCC-2. Therefore, in this mix, the entrance of the chloride ion from the surface of the concrete to the interior will be more difficult. In the three mixtures, the same tendency is observed, which was adjusted to the solution to the Fick's 2nd law [31], proposed in the ASTM C 1556 standard [14], obtaining Eqs. (8.14) for SCC-1, (8.15) for SCC- 12, and (8.16) for SCC-2, which have a value of R^2 greater than 0.99.

$$C(x,t) = 0.47 - (0.47 - 0.03) \cdot \operatorname{erf}\left(\frac{x}{\sqrt{4 \cdot 4.8 \cdot 10^{-12} \cdot 7.86 \cdot 10^{6}}}\right) \quad (8.14)$$

$$C(x,t) = 0.55 - (0.55 - 0.03) \cdot \operatorname{erf}\left(\frac{x}{\sqrt{4 \cdot 5.6 \cdot 10^{-12} \cdot 7.86 \cdot 10^{6}}}\right) \quad (8.15)$$

$$C(x,t) = 0.68 - (0.68 - 0.04) \cdot \operatorname{erf}\left(\frac{x}{\sqrt{4 \cdot 6.2 \cdot 10^{-12} \cdot 7.86 \cdot 10^{6}}}\right) \quad (8.16)$$

This adjustment allows the identification of the effective coefficients of transport for the chloride ion (Table 8.5) after 91 days of exposure. The minimum values necessary for the theoretical superficial concentration were also obtained, namely, 0.47% for SCC-1, 0.55% for SCC-12, and 0.68% for SCC-2. These results are in agreement with the pore size distribution (Figure 8.7), where we can observe that SCC-1 has the lowest porosity and finest porous structure, followed by SCC-12 and SCC-2.

Considering the concentration range of the chloride threshold (0.05–0.1%) that would cause corrosion of the steel in concrete [66] (Figure 8.11), the mixes reached a chloride concentration of less than 0.05% at a depth greater than 16 mm for SCC-1, 19 mm for SCC-12, and 23 mm for SCC-2; thus, the reinforcements would not be affected if the cover is higher than these values. Taking into account that, in terms of durability under aggressive environments [35], the minimum cover required by EHE -08 for the type of SCC defined (HA-40/AC/16/IIIc) [35] is 45 mm, the safety margin for the mixes is more than 20 mm.

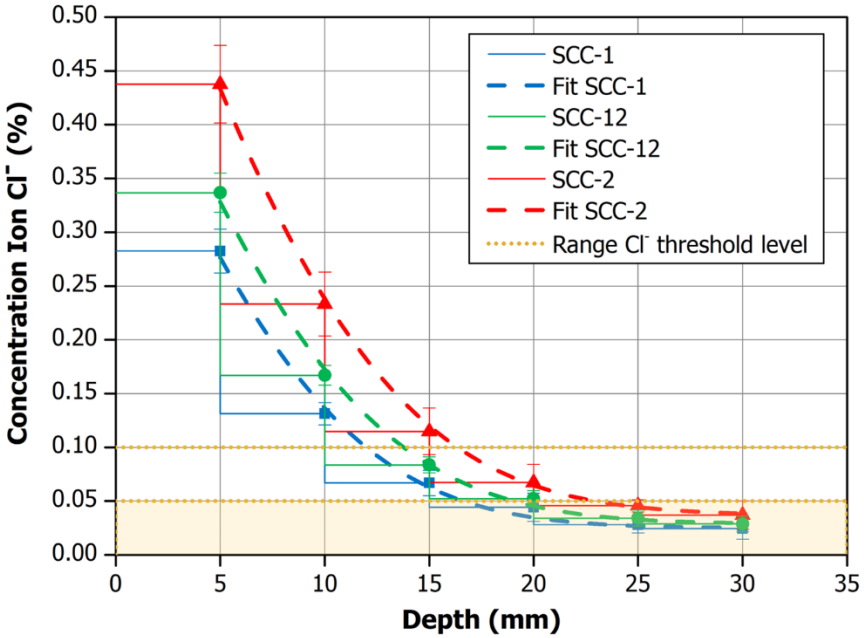

Figure 8.11: Ion Cl^- concentration profile of the mixes.

The penetration of chloride ion presented by the mixes of this work is in agreement with Esquinas et al. [7], who observed a good behaviour regarding the penetration of the chloride ion in an SCC that incorporated residual filler of dolomitic nature as a substitute of the SF. Bermejo-Nuñez [20], in mixes that incorporated fly ash as a mineral admixture, observed percentages of chlorides below the threshold at depths of the order of 10 mm. This differential behaviour could be due to the differences between fly ash and NCFA. In this sense, Sabet et al. [18] observed a reduction in chloride ion penetration in SCCs that used silica fume as a mineral admixture with respect to mixes that incorporated fly ash, which was associated with the greater pozzolanic activity of the silica fume with respect to fly ash.

8.3.2.3.4 Carbonation depth

The carbonation depth of the mixes for 7, 28, 91, and 182 days of exposure is shown in Table 8.5. The lowest penetration values were obtained for SCC-1, followed by SCC-12 and SCC-2. The greater difference between the mixes can be observed at short exposure times (7 days of exposure). This differential can be quantified, with respect to SCC-1, in 225% for SCC-2 and 72% for SCC-12. For prolonged exposure

times (182 exposure days), the differences with respect to SCC-1, as previously discussed, decrease to 38% for SCC-2 and 21% for SCC-12.

The depth of carbonation versus the square root of time (years) is shown in Figure 8.12. The penetration of CO_2 in the mixes can be adjusted according to the following Eqs, (8.17 - 8.19) relative to SCC-1, SCC-12, and SCC-2, respectively, and these expressions have high R^2 values, greater than 0.97:

$$C_d = 17.98\ \sqrt{t} \qquad R^2=0.9807 \qquad (8.17)$$

$$C_d = 22.33\ \sqrt{t} \qquad R^2=0.9997 \qquad (8.18)$$

$$C_d = 26.34\ \sqrt{t} \qquad R^2=0.9695 \qquad (8.19)$$

From this adjustment, the carbonation coefficient of the mixes can be defined, which will depend on the characteristics of the material and the environmental conditions. The coefficients obtained were 17.98 mm/year$^{1/2}$, 22.33 mm/year$^{1/2}$, and 26.34 mm/year$^{1/2}$, for SCC-1, SCC-12, and SCC-2, respectively.

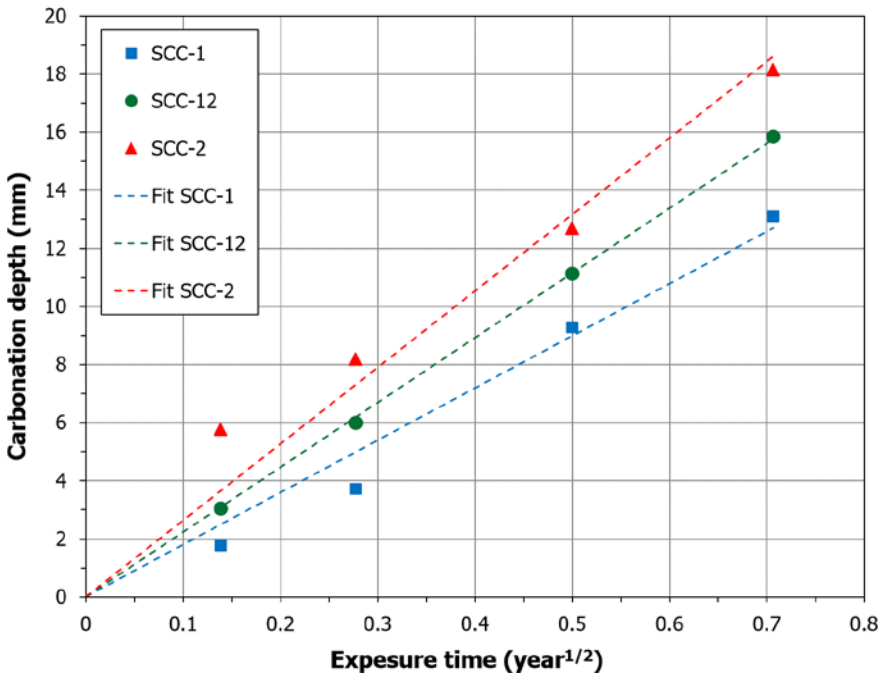

Figure 8.12: Depth of carbonation as a function of $\sqrt{t}$ of the mixes.

The porosity and chemical species generated during setting of the mixes will significantly influence the carbonation process suffered by them. The greater depth observed in SCC-2 is in agreement with the greater amount of portlandite generated during setting [31], which is able to react with CO_2 and form $CaCO_3$. This would be in accordance with the less fine porous structure of SCC-2 with respect to SCC-12 and SCC-1, above discussed, as SCC-2 has a greater porosity, between 1 and 100 μm, and thus, the speed of diffusion of CO_2 within it will be greater and there will be greater interaction with this aggressive agent.

Regarding the cover required by EHE-08 [35] for the defined environment (45 mm) as protection of the reinforcement against corrosion, it is observed that there is a safety margin of approximately 25 mm. Therefore, for the three mixes, the reinforcements will be protected by the cover, in accordance with the maximum penetrations reached in the SCCs and taking into account that the concentration of CO_2 in the atmosphere is 0.04% (125 times lower than the set point of CO_2 concentration of the carbonation chamber).

These results are in agreement with Esquinas et al. [7], who observed an increase in the carbonation of mixes that incorporated residual dolomitic filler with respect to mixes that used SF. Bermejo [20] and da Silva & de Brito [67] obtained greater CO_2 penetration in mixes made with limestone filler compared to those made with fly ash, as this admixture gave rise to finer porosity and higher microstructural density of the mixes. Regarding the admixture, Mohammed et al. [30] observed a lower penetration of CO_2 in SCCs that incorporated silica fume and fly ash with respect to the mixes that incorporated limestone filler, which is associated with the densification of the porous structure and the consumption of portlandite to form CSH, thus avoiding the formation of $CaCO_3$.

8.3.2.3.5 Sulphate ion penetration

The penetration of the SO_3 (SO_4^{2-} from chemical point of view) ion in the SCC-1, SCC-12, and SCC-2 mixes is shown in Figure 8.13. The mix with the lowest penetration is SCC-1, followed by SCC-12 and SCC-2. The concentrations obtained for each sampling depth were adjusted to the solution equation of the second Law of

Fick (Eqs. (8.20-8.22) for SCC-1, SCC-12, and SCC-2, respectively), obtaining R^2 values higher than 0.98.

$$C(x,t) = 0.54 - (0.54 - 0.05) \cdot \text{erf}\left(\frac{x}{\sqrt{4 \cdot 5 \cdot 10^{-12} \cdot 7.86 \cdot 10^{6}}}\right) \quad (8.20)$$

$$C(x,t) = 0.62 - (0.62 - 0.06) \cdot \text{erf}\left(\frac{x}{\sqrt{4 \cdot 6.03 \cdot 10^{-12} \cdot 7.86 \cdot 10^{6}}}\right) \quad (8.21)$$

$$C(x,t) = 0.84 - (0.84 - 0.08) \cdot \text{erf}\left(\frac{x}{\sqrt{4 \cdot 6.17 \cdot 10^{-12} \cdot 7.86 \cdot 10^{6}}}\right) \quad (8.22)$$

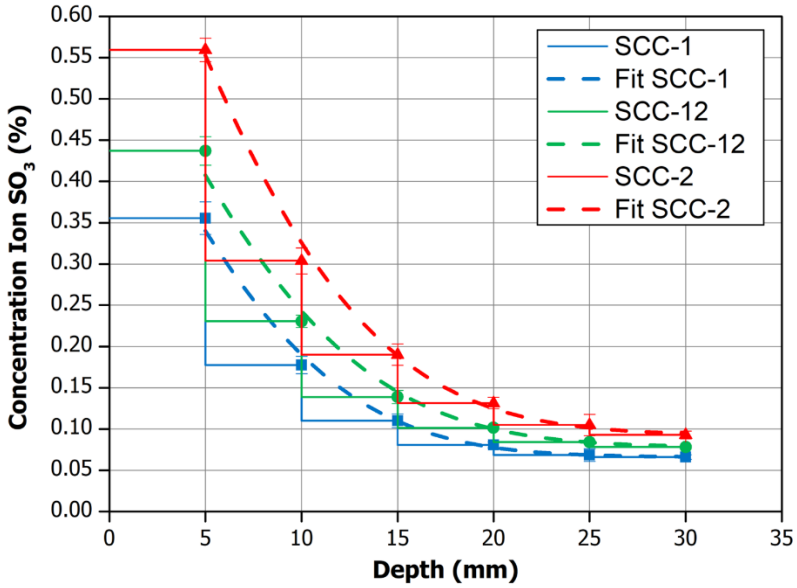

Figure 8.13: Ion SO_3 concentration profile of the mixes.

After 91 days of exposure, the effective SO_3 ion transport coefficients obtained were $5.0 \cdot 10^{-12}$ m^2/s, $6.03 \cdot 10^{-12}$ m^2/s, and $6.17 \cdot 10^{-12}$ m^2/s for SCC-1, SCC-12, and SCC-2, respectively (Table 8.5). In addition, the application of the second Law of Fick indicates that the theoretical surface concentration (Cs) would be higher in SCC-2 (0.84%) with respect to SCC-12 (0.62%) and SCC-1 (0.54%). This is in accordance with the porous structure, and therefore, with the permeability of the mixes, which leads to a more remarkable decrease in the concentration of SO_3 ion in the SCC-1 and SCC-12 mixes with respect to SCC-2, and thus, to lower diffusion and penetration depth of the sulphate. For all the mixes, after the time of exposure, there was no sign of wear or deterioration.

Figures 8.14 and 8.15 show the different chemical species formed during the attack by SO_3 for the SCC-1 and SCC-2 mixes, according to the X-ray diffractograms of samples taken at 5 and 30 mm and of samples of SCC without attack of SO_3, which will be related to the setting mechanisms of the SCCs. Ettringite ($6CaO{\cdot}Al_2O_3{\cdot}3SO_3{\cdot}32H_2O$) was observed in the two mixtures at 5 mm, where the sulphate concentration is maximum (Figure 8.13) compared to the original. For this same depth, the formation of gypsum is observed in SCC-2, which is in accordance with the higher content of portlandite generated during the setting of this mix with respect to SCC-1 [31]. In SCC-1, in addition to ettringite, the presence of thaumasite ($CaCO_3{\cdot}CaSO_4{\cdot}CaSiO_3{\cdot}15H_2O$) can also be observed, which is in accordance with the higher CSH content observed in the setting of SCC-1 [31]. This highlights the increase in portlandite for this depth (5 mm) with respect to the sample without attack, which could be due to the formation process of thaumasite from the CSH and SO_3 [65].

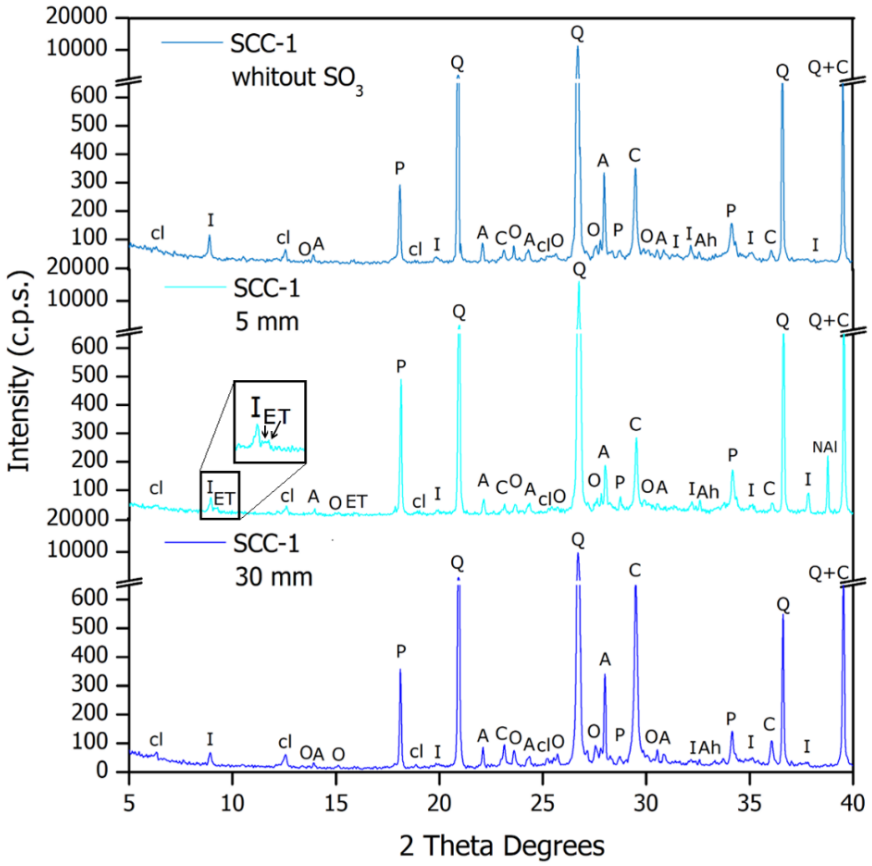

Figure 8.14: PXRD patterns of SCC-1 before and after exposure to SO_3

(E = Ettringite, T = Thaumasite, P = Portlandite, Q = Quartz, C = Calcite, A = Albite, O = Orthoclase, cl=Clinochlore, I = Illite, Ah = Calcium Aluminum Silicate Hydroxide and NAl = Sodium Aluminum Sulfate)

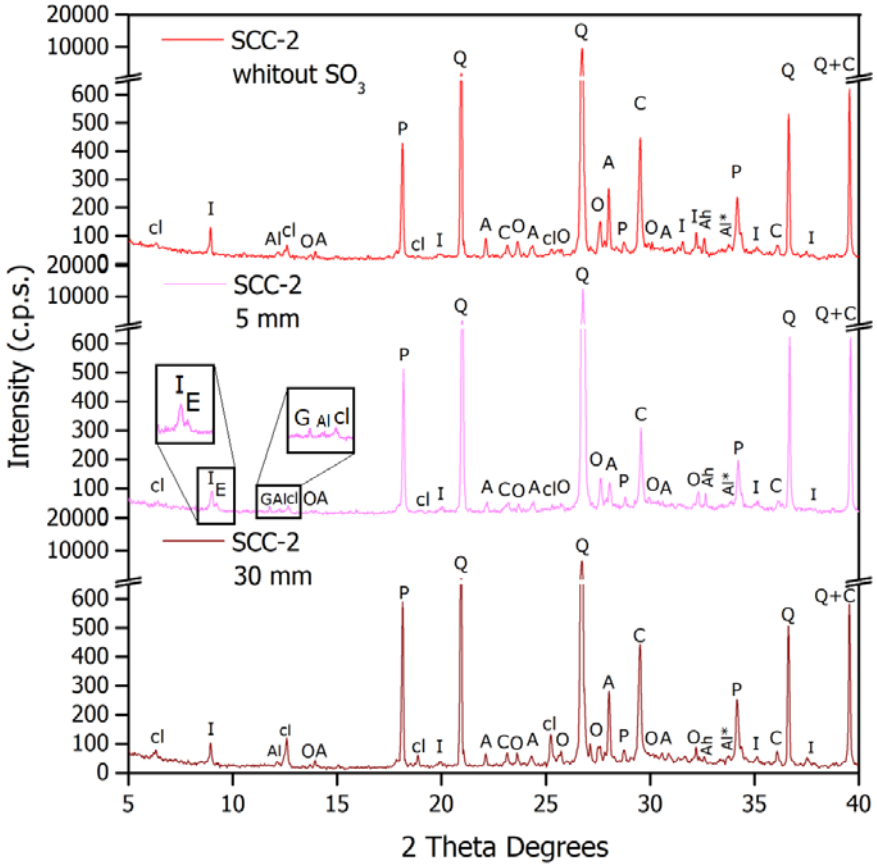

Figure 8.15: PXRD patterns of SCC-2 before and after exposure to SO_3.

(E = Ettringite, P = Portlandite, Q = Quartz, C = Calcite, A = Albite, O = Orthoclase, cl = Clinochlore, I = Illite, Ah = Calcium Aluminum Silicate Hydroxide, G = Gypsum, Al = Calcium Aluminum Oxide) and Al* = Calcium Aluminum Silicate)

This is in agreement with Esquinas et al. [7], who observed lower SO_3 ion penetration in SCCs manufactured with SF compared to SCCs manufactured with residual dolomitic filler, which is mainly due to differences in microstructural density, although both mixtures showed no signs of wear and deterioration after their exposure to sulphates. Bassuoni et al. [68] observed the presence of thaumasite and ettringite in SCCs manufactured with silica fume, slag, and a sulphur-resistant cement after their exposure to an environment rich in SO_3. In this sense, Uysal et al. [19] observed that an SCC with filler of siliceous nature and a distribution of fine grain size (fly ash and granulated blast furnace slag) presented a high performance to attack by sulphates, which could be due to the reactivity of these mineral admixtures during the setting and to the refinement of the porous structure. All this is in agreement with Schutter

et al. [65], who concluded that the use of pozzolanic particles would generate more dense porous structures with a finer porosity, which would avoid to a greater extent the sulphate attack.

8.3.2.3.6 Long-term shrinkage

The shrinkage suffered by long-term mixes (more than 700 days) is shown in Figure 8.16. SCC-1 suffers the highest shrinkage, 5% more than SCC-12 and around 12% more than SCC-2. It can be observed that the evolution of the deformation is greater for SCC-1, which could be due to the physical and chemical characteristics of the SF filler, which favours the pozzolanic activity compared to the NCFA. This is also in accordance with the finer porous structure presented in SCC-1 (Figure 8.7), which will support the interaction forces between the walls of the capillaries once the water is removed from the capillary [69], and consequently, will foster the shrinkage of SCC-1. The smaller shrinkage of SCC-2 may be related to the larger pore size, which is a consequence of the greater grain size distribution of the NCFA filler and the higher W/C ratio of the mix. After about 450 days, stabilisation of the shrinkage of the mixes can be observed.

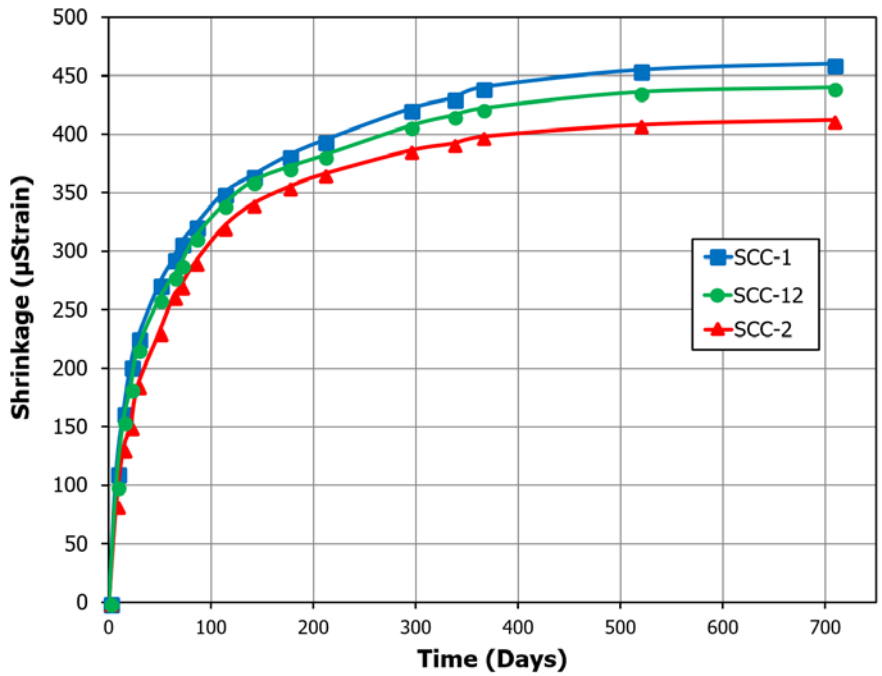

Figure 8.16: Total shrinkage of the mixes.

Consequently, SCC-1 will present greater shrinkage owing to the pozzolanic activity of the SF, the drying process, and the effect of the porous structure. This would be in accordance with the higher hydration water content of SCC-1 determined by thermogravimetry (between 100–400 ºC). SCC-12 has an intermediate behaviour between the other two mixes.

This is in agreement with that indicated by Esquinas et al. [7], who observed greater shrinkage in mixes that incorporated siliceous filler with respect to SCCs that incorporated dolomitic filler and with thicker grain size distribution. In this sense, da Silva & J. de Brito [25] observed a greater shrinkage in SCCs with fly ash versus SCCs with limestone filler, particularly in the mixes that contained a high content of these powders. Gesoglu et al. [21] observed that the mixes that incorporated silica fume presented higher shrinkage compared to the mixes that incorporated fly ash, which is related to the smaller grain size of the silica fume. Shrinkage in the present work is lower because less reactive mineral admixtures were used (siliceous filler vs. silica fume and NCFA vs. fly ash), in addition to using a lower content of coarse aggregate and a higher content of fine aggregate

8.4 Conclusions

In the present work, a study of the durability of three types of SCCs was carried out. The first SCC, the reference mix, was a mix with SF (SCC-1), the second one was a mix with NCFA (SCC-2), and the third one was a mix with a 1:1 combination (by volume) of both materials (SCC-12).

It is observed that all the mixes comply with the self-compacting requirements set by the EHE-08 guideline. The fresh-state density in SCC-1 is slightly higher than those in SCC-12 and SCC-2 owing to the finer and continuous grain size distribution of SF with respect to that of NCFA.

There is a greater difference between the bulk densities of the mixes (≈1–2%) than between their skeletal densities (≈0.6–1%). This is due to the very definition of both densities, which causes that the differences be damped in the skeletal density. Regarding open porosity, it is higher in SCC-2, followed by SCC-12 and SCC-1. These

results correlate with the MIP as the mix with NCFA (SCC-2) has a higher percentage of pores over 10 μm compared to the mix with SF (SCC-1), which has a greater number of pores smaller than 10 μm, resulting in a finer porous structure. The incorporation of 50% of NCFA (SCC-12) into the mix results in an intermediate porosity and microstructural density.

The above stated properties explain the slightly greater absorption of water by immersion in SCC-2. After carrying out the analysis of absorption by capillarity, and in accordance with the limits set by the CYTED's DURAR network, all the mixes could be used in structural elements exposed to highly aggressive environments with adequate durability.

According to the results of water penetration under pressure, it is reasonable to consider that the mixes have high compactness and are waterproof because, in all cases, they have a penetration of more than 30 mm.

In accordance with ASTM C 1202, all the mixes are in the range considered of low penetrability to the chloride ion. In relation to the chloride ion concentration as a function of depth, in all the mixes a concentration lower than 0.05% was reached for depths greater than 23 mm, and thus, the reinforcements would not be affected if the cover is greater than this value. Consequently, the safety margin for the mixes is greater than 20 mm, compared to the required cover (45 mm) by EHE-08.

The carbonation depth of SCC-2 is superior to that of SCC-12 and SCC-1 due, on the one hand, to the greater amount of portlandite generated during setting in SCC-2 and, on the other hand, to its less fine porous structure. The results show a safety margin of approximately 25 mm. Therefore, with the three mixes, the reinforcement will be protected by the cover as the concentration of CO_2 in the atmosphere is 0.04%, 125 times lower than the CO_2 concentration of the carbonation chamber.

Regarding the penetration of SO_3, the mix that registered a lower value was SCC-1 followed by SCC-12 and SCC-2. The finer and denser porous structure in the SCC-1 and SCC-12 mixes will lead to a remarkable decrease in the concentration of SO_3 ion with respect to SCC-2, and therefore, to a lower diffusion and depth of sulphate

penetration. After the exposure time, neither mix shows any sign of wearing or deterioration.

The deformation suffered by the mixes by the action of shrinkage was stabilised at 450 days under the curing conditions used in this work. SCC-1 showed higher shrinkage than that of the SCC-12 and SCC-2 samples, which is due to the pozzolanic activity of the SF, the drying process, and the effect of the porous structure. SCC-12 has an intermediate behaviour between the other two mixes. In short, the SCC manufactured with NCFA from coal-fired power plants is better than SCC-1 in relation to shrinkage.

In summary, it is possible to obtain an SCC with high performance with respect to durability against the attack of aggressive agents and shrinkage by replacing totally or partially the SF with NCFA from coal-fired power plants.

8.5 Acknowledgements

This work was partly supported by the Andalusian Regional Government (Research Groups FQM-391 and TEP-227). A. Romero Esquinas also acknowledges the funding from MECD-Spain (http://www.mecd.gob.es/educacion-mecd/) FPU-13/04030. The authors wish to thank the Research Plan of the University of Cordoba (2016), the Spanish Ministry of Economy and Competitiveness (Project MAT2015-70728-P), the staff at the Electron Microscopy and Elemental Analysis units of the Central Research Support Service (SCAI) of the University of Cordoba for their technical assistance, the Fine Chemistry Institute of the University of Córdoba for their technical support, the BASF Chemical Company for supplying the admixture, and Portland Valderrivas (Alcalá de Guadaira, Seville) for the supplied cement. Finally, the authors wish to thank the Puente Nuevo coal-fired power plant of the Viesgo company for the supplied NCFA waste. The support of the CERIS-ICIST Research Institute, IST, University of Lisbon, and Foundation for Science and Technology (FCT) is also acknowledged.

8.6 References

[1] K. Celik, C. Meral, A. Petek Gursel, P.K. Mehta, A. Horvath, P.J.M. Monteiro, Mechanical properties, durability, and life-cycle assessment of self-consolidating concrete mixtures made with blended portland cements containing fly ash and limestone powder, Cem. Concr. Compos. 56 (2015) 59–72.

[2] H. Okamura, Self-Compacting High Performance Concrete, Concr. Int. 19 (1997) 50–54.

[3] European Federation of National Associations Representing producers and applicators of specialist building products for Concrete (EFNARC). The European guidelines for self-compacting concrete specification. Production and Use. Hampshire, UK; (2005).

[4] K.K. Sideris, C. Tassos, A. Chatzopoulos, P. Manita, Mechanical characteristics and durability of self compacting concretes produced with ladle furnace slag, Constr. Build. Mater. 170 (2018) 660–667.

[5] R. Sharma, R.A. Khan, Durability assessment of self compacting concrete incorporating copper slag as fine aggregates, Constr. Build. Mater. 155 (2017) 617–629.

[6] A.R. Esquinas, C. Ramos, J.R. Jiménez, J.M. Fernández, J. de Brito, Mechanical behaviour of self-compacting concrete made with recovery filler from hot-mix asphalt plants, Constr. Build. Mater. 131 (2017) 114–128.

[7] A.R. Esquinas, J.I.I. Álvarez, J.R.R. Jiménez, J.M.M. Fernández, J. de Brito, Durability of self-compacting concrete made with recovery filler from hot-mix asphalt plants, Constr. Build. Mater. 161 (2018) 407–419.

[8] M. Tennich, M. Ben Ouezdou, A. Kallel, Behavior of self-compacting concrete made with marble and tile wastes exposed to external sulfate attack, Constr. Build. Mater. 135 (2017) 335–342.

[9] V. Kannan, Strength and durability performance of self compacting concrete containing self-combusted rice husk ash and metakaolin, Constr. Build. Mater. 160 (2018) 169–179.

[10] N. Ranjbar, A. Behnia, B. Alsubari, P. Moradi Birgani, M.Z. Jumaat, Durability and mechanical properties of self-compacting concrete incorporating palm oil fuel ash, J. Clean. Prod. 112 (2016) 723–730.

[11] G. Sua-Iam, N. Makul, Effect of incinerated sugarcane filter cake on the properties of self-compacting concrete, Constr. Build. Mater. 130 (2017) 32–40.

[12] J. Cuenca, J. Rodríguez, M. Martín-Morales, Z. Sánchez-Roldán, M. Zamorano, Effects of olive residue biomass fly ash as filler in self-compacting concrete, Constr. Build. Mater. 40 (2013) 702–709.

[13] R.N.L. Cohen, Haim, Coal Residues: The new Golden Treasure, in: World, 2017 World of Coal Ash (WOCA) Conference in Lexington (2017).

[14] American Society of Testing Materials, ASTM International, West Conshohocken, USA, (2018).

[15] Asociación Española de Normalización y Certificación, AENOR, Madrid, Spain, (2018).

[16] S. Dadsetan, J. Bai, Mechanical and microstructural properties of self-compacting concrete blended with metakaolin, ground granulated blast-furnace slag and fly ash, Constr. Build. Mater. 146 (2017) 658–667.

[17] G. Sua-iam, N. Makul, Incorporation of high-volume fly ash waste and high-volume recycled alumina waste in the production of self-consolidating concrete, J. Clean. Prod. 159 (2017) 194–206.

[18] F.A. Sabet, N.A. Libre, M. Shekarchi, Mechanical and durability properties of self consolidating high performance concrete incorporating natural zeolite, silica fume and fly ash, Constr. Build. Mater. 44 (2013) 175–184.

[19] M. Uysal, M. Sumer, Performance of self-compacting concrete containing different mineral admixtures, Constr. Build. Mater. 25 (2011) 4112–4120.

[20] E.B. Bermejo Núñez, Dosificación, propiedades y durabilidad en hormigón autocompactante para edificación [Ph.D. Thesis]. Universidad Politécnica de Madrid; 2009.

[21] M. Gesoğlu, E. Güneyisi, E. Özbay, Properties of self-compacting concretes made with binary, ternary, and quaternary cementitious blends of fly ash, blast furnace slag, and silica fume, Constr. Build. Mater. 23 (2009) 1847–1854.

[22] Turk K, Caliskan S, Yazicioglu S. Capillary water absorption of self-compacting concrete under different curing conditions. Indian J Eng Mater Sci 2007; 14:365–72.

[23] S.A. Kristiawan, Sunarmasto, G.Y. Murti, Porosity of Self-Compacting Concrete (SCC) incorporating high volume fly ash, IOP Conf. Ser. Mater. Sci. Eng. 176 (2017) 012043.

[24] P.R. da Silva, J. de Brito, Fresh-state properties of self-compacting mortar and concrete with combined use of limestone filler and fly ash, Mater. Res. 18 (2015) 1097–1108.

[25] P. Silva, J. de Brito, Experimental study of the mechanical properties and shrinkage of self-compacting concrete with binary and ternary mixes of fly ash and limestone filler, Eur. J. Environ. Civ. Eng. 21 (2017) 430–453.

[26] R. Saleh Ahari, T.K. Erdem, K. Ramyar, Permeability properties of self-consolidating concrete containing various supplementary cementitious materials, Constr. Build. Mater. 79 (2015) 326–336.

[27] M. Jalal, A. Pouladkhan, O.F. Harandi, D. Jafari, Comparative study on effects of Class F fly ash, nano silica and silica fume on properties of high performance self compacting concrete, Constr. Build. Mater. 94 (2015) 90–104.

[28] K. Celik, C. Meral, M. Mancio, P.K. Mehta, P.J.M. Monteiro, A comparative study of self-consolidating concretes incorporating high-volume natural pozzolan or high-volume fly ash, Constr. Build. Mater. 67 (2014) 14–19.

[29] M.K. Mohammed, A.R. Dawson, N.H. Thom, Production, microstructure and hydration of sustainable self-compacting concrete with different types of filler, Constr. Build. Mater. 49 (2013) 84–92.

[30] M.K. Mohammed, A.R. Dawson, N.H. Thom, Carbonation of filler typed self-compacting concrete and its impact on the microstructure by utilization of 100% CO2 accelerating techniques, Constr. Build. Mater. 50 (2014) 508–516.

[31] A.R. Esquinas, E.F. Ledesma, R. Otero, J.R. Jiménez, J.M. Fernández, Mechanical behaviour of self-compacting concrete made with non-conforming fly ash from coal-fired power plants, Constr. Build. Mater. 131 (2018) 114–128.

[32] A. Torres-Gómez, E. Ledesma, R. Otero, J. Fernández, J. Jiménez, J. de Brito, Combined Effects of Non-Conforming Fly Ash and Recycled Masonry Aggregates on Mortar Properties, Materials (Basel). 9 (2016) 729.

[33] A. Niyogi, Characterization of fly ash fractions to trace the extent of pollution, 2017 World of Coal Ash (WOCA) Conference in Lexington (2017).

[34] Directive 2008/98/EC of the European Parliament and of the Council of 10 November 2008 onWaste. Official Journal of the European Union. 2008.

[35] EHE-08. Spanish Structural Concrete Code EHE-08 [Instrucción de Hormigón Estructural EHE-08]. R.D. 1247/2008, Spain (2008).

[36] P. Swarthmore, Joint Committee on Power Diffraction Standard-International Centre for Diffraction Data. (1995).

[37] D.P. Bentz, C.J. Haecker, An argument for using coarse cements in high-performance concretes, Cem. Concr. Res. 29 (1999) 615–618.

[38] S. Tsivilis, S. Tsimas, A. Benetatou, E. Haniotakis, Study on the contribution of the fineness on cement strength, (1990).

[39] J.M. Pommersheim, Effect of particle size distribution on hydration kinetics, MRS Proceedings, Cambridge Univ Press, 1986, p. 301.

[40] M. Fernández Cánovas, Hormigón, Ed. Colegio de Ingenieros de Caminos, Canales y Puertos (2007).

[41] European Federation of National Associations Representing producers and applicators of specialist building products for Concrete (EFNARC). Specification and guidelines for self-compacting concrete, Hampshire, UK; 2002

[42] S. Brunauer, P.H. Emmett, E. Teller, Adsorption of gases in multimolecular layers, J. Am. Chem. Soc. 60 (1938) 309–319.

[43] A.R. Esquinas, D. Motos-Pérez, M.E. Jiménez, C. Ramos, J.R. Jiménez, J.M. Fernández, Mechanical and durability behaviour of self-compacting concretes for application in the manufacture of hazardous waste containers, Constr. Build. Mater. 168 (2018).

[44] LNEC E-391, Concrete determination of carbonation resistance. National Laboratory of Civil Engineering (LNEC), Lisbon, Portugal;, 1993.

[45] A.W. Saak, Characterization and modeling of the rheology of cement paste: With applications toward self-flowing materials, 2000.

[46] I.B. Topcu, T. Bilir, T. Uygunoğlu, Effect of waste marble dust content as filler on properties of self-compacting concrete, Constr. Build. Mater. 23 (2009) 1947–1953.

[47] J. Martín, J.R. Montero, F. Moreno, J.L.P. Sala, M.C. Rubio, Feasibility analysis of the reuse of waste filler of bituminous mixtures for the production of self-compacting concrete, Mater. Des. 46 (2013) 372–380.

[48] I.P. Sfikas, A. Kanellopoulos, K.G. Trezos, M.F. Petrou, Durability of similar self-compacting concrete batches produced in two different EU laboratories, Constr. Build. Mater. 40 (2013) 207–216.

[49] E.G. Badogiannis, I.P. Sfikas, D. V Voukia, K.G. Trezos, S.G. Tsivilis, Durability of metakaolin self-compacting concrete, Constr. Build. Mater. 82 (2015) 133–141.

[50] A. El Mir, S.G. Nehme, Porosity of self-compacting concrete, Procedia Eng. 123 (2015) 145–152.

[51] M. Valcuende, C. Parra, Natural carbonation of self-compacting concretes, Constr. Build. Mater. 24 (2010) 848–853.

[52] S. Assie, G. Escadeillas, V. Waller, Estimates of self-compacting concrete 'potential'durability, Constr. Build. Mater. 21 (2007) 1909–1917.

[53] Mehta PK, Monteiro PJM. Concrete structure, properties and materials. New Jersey: Prentice Hall, 1993:548

[54] D.A. Silva, V.M. John, J.L.D. Ribeiro, H.R. Roman, Pore size distribution of hydrated cement pastes modified with polymers, Cem. Concr. Res. 31 (2001) 1177–1184.

[55] L. Cui, J.H. Cahyadi, Permeability and pore structure of OPC paste, Cem. Concr. Res. 31 (2001) 277–282.

[56] P.R. da Silva, J. de Brito, P.R. Silva, J. De Brito, P.R. da Silva, J. de Brito, P.R. Silva, J. De Brito, P.R. da Silva, J. de Brito, Experimental study of the porosity and microstructure of self-compacting concrete (SCC) with binary and ternary mixes of fly ash and limestone filler, Constr. Build. Mater. 86 (2015) 101–112.

[57] G. De Schutter, K. Audenaert, Evaluation of water absorption of concrete as a measure for resistance against carbonation and chloride migration, Mater. Struct. 37 (2004) 591–596.

[58] S.A. Bernal, R. Mejía de Gutiérrez, A.L. Pedraza, J.L. Provis, E.D. Rodriguez, S. Delvasto, Effect of binder content on the performance of alkali-activated slag concretes, Cem. Concr. Res. 41 (2011) 1–8.

[59] J.J. Howland, A.R. Martín, Study about the capillary absorption and the sorptivity of concretes with Cuban limestone aggregates, Mater. Construcción. 63 (2013) 515–527.

[60] C. Hall, Water sorptivity of mortars and concretes: a review, Mag. Concr. Res. 41 (1989) 51–61.

[61] O. Trocónis-Rincón, A. Romero-Carruyo, C. Andrade, P. Helene, I. Díaz, Manual for inspection, evaluation and diagnosis of corrosion in reinforced concrete structures, DURAR Report, CyTED, Maracaibo, Venezuela, (1997), 208 p.

[62] O. Valenta, The permeability and durability of concrete in aggressive conditions, in: Proc. 10th Int. Congr. Large Dams, Montr., 1970: pp. 103–117.

[63] Z. Li, Advanced concrete technology, John Wiley & Sons, 2011.

[64] A.M. Neville, Properties of concrete. 4th ed. Harlow, London: Longman Group Limited; 1995.

[65] G. De Schutter, K. Audenaert, Report 38: Durability of Self-Compacting Concrete-State-of-the-Art Report of RILEM Technical Committee 205-DSC, RILEM publications, 2007.

[66] G.K. Glass, N.R. Buenfeld, The presentation of the chloride threshold level for corrosion of steel in concrete, Corros. Sci. 39 (1997) 1001–1013.

[67] P.R. Da Silva, J. de Brito, Durability performance of self-compacting concrete (SCC) with binary and ternary mixes of fly ash and limestone filler, Mater. Struct. 49 (2016) 2749–2766.

[68] M.T. Bassuoni, M.L. Nehdi, Durability of self-consolidating concrete to sulfate attack under combined cyclic environments and flexural loading, Cem. Concr. Res. 39 (2009) 206–226.

[69] M. Valcuende, E. Marco, C. Parra, P. Serna, Influence of limestone filler and viscosity-modifying admixture on the shrinkage of self-compacting concrete, Cem. Concr. Res. 42 (2012) 583–592.

Capítulo 9

Conclusiones / conclusions. Futuras líneas de investigación

9.1 Conclusiones

Teniendo en cuenta los objetivos y los resultados alcanzados, las conclusiones por capítulos de esta Tesis Doctoral son expuestos a continuación:

- Capítulo 4: "*Mechanical and durability behaviour of self-compacting concretes for application in the manufacture of hazardous waste containers*".

Se ha llevado a cabo un estudio comparativo de cuatro tipos de HAC, en las cuales se analizó el efecto de la cantidad de árido grueso, fino y filler sobre las propiedades en estado fresco (autocompactabilidad) y en estado endurecido (estructura porosa, comportamiento mecánico y durabilidad).

1. Las mezclas cumplen con los requisitos de autocompactabilidad marcados por la EHE-08, por lo que es posible obtener HAC con dosificaciones donde parámetros, tales como la cantidad de árido grueso, pasta y ratio agua/finos

no están dentro de los valores propuestos por la EFNARC. Los ensayos de autocompactabilidad muestran una alta reproducibilidad.

2. La densidad de las mezclas presenta ligeras diferencias, 2.367 T/m^3 en la mezcla SCC-A, 2.340 T/m^3 en la mezcla SCC-B, 2.376 T/m^3 en la mezcla SCC-C y 2.363 T/m^3 en la mezcla SCC-D. Los factores que tienen una influencia más significativa en la densidad de las mezclas son la presencia de filler y la ratio A/C, ya que las mayores densidades se obtienen en las mezclas con filler y menor A/C (SCC-C y SCC-A).
3. Estos resultados están de acuerdo con la menor porosidad observada en la distribución de tamaño de poro de las mezclas que incorporan filler ya que el volumen de intrusión de mercurio en los poros de diámetro superiores a 70 µm y entre 50.0 nm y 10.0 µm (poros capilares grandes) es superior en SCC-B y SCC-D y por el contrario para el rango entre 10nm – 50nm (poros capilares medianos) y 2.5 y 10.0 nm (poros gel pequeños) es mayor para las muestras SCC-A y SCC-C. Lo que pone de manifiesto la estructura porosa más fina de las mezclas con filler. Por otro lado, las mezclas con menor contenido de árido grueso (SCC-C y SCC-D) presentan una mayor compacidad respecto a las mezclas con un mayor porcentaje árido grueso (SCC-A y SCC-B).
4. El comportamiento mecánico de los HAC sin filler silíceo y con diferentes cantidades de árido grueso (SCC-B y SCC-D), demuestran que es posible conseguir resistencias a compresión superiores a los niveles mínimos estipulados por el Código Español de Hormigón Estructural para un HAC-30. Y por otra parte se pueden obtener resistencias a 28 días en torno a 50 MPa para mezclas que incorporen filler silíceo (SCC-A y SCC-C), incluso con bajo contenido de árido grueso.
5. Los valores de resistencia a tracción indirecta y de resistencia a flexión aplicando la EHE-08 (calculados a partir de la resistencia a compresión) son inferiores a los valores obtenidos experimentalmente. Esto significa que los resultados experimentales son congruentes con la validez de aplicación de la EHE-08 al HAC, propuesta inicialmente para el hormigón convencional.
6. Las mezclas que incorporan filler silíceo (SCC-A y SCC-C) presentan un mejor comportamiento ante la absorción de agua por inmersión respecto a las mezclas que no lo incorporan (SCC-B y SCC-D). En cuanto a la absorción de

agua por capilaridad, las mezclas con filler presentan una menor absorción por capilaridad y sorptividad que las mezclas sin filler. Así mismo, las mezclas que tienen un mayor contenido de árido grueso, SCC-A y SCC-B presentan valores de absorción mayores que las mezclas SCC-C y SCC-D respectivamente. Todas mezclas presentan valores inferiores a los límites establecidos en términos de porosidad efectiva y sorptividad. Por lo que podrían ser usadas en ambientes agresivos con una adecuada durabilidad.

7. Los resultados de penetración de agua bajo presión permiten considerar que todas mezclas tienen una alta compacidad y son impermeables, ya que, en ningún caso, presentan una penetración superior a 30 mm, límite marcado en literatura como penetración máxima para ser consideradas como impermeables.
8. Respecto a la penetración de los iones de Cl^- y SO_3, se observa que la mezcla SCC-C presenta menores valores, seguido de las mezclas SCC-A, SCC-D y SCC-B. La mayor densidad microestructural de las mezclas con filler da lugar a menores profundidades de penetración en este material. Tras el tiempo de exposición al ambiente agresivo las muestras no presentan ningún signo de desgaste o deterioro.
9. La retracción por secado de las mezclas se estabiliza para una edad en torno a 100 días, bajo las condiciones de curado utilizadas en este trabajo. La mezcla SCC-C es la que menor retracción presenta seguido de las mezclas SCC-A, SCC-D y SCC-B. La presencia de filler tiene una influencia más significativa en la retracción que la variación del contenido de árido grueso en la dosificación.
10. Se puede concluir que es posible obtener un HAC de altas prestaciones desde el punto de vista mecánico y de durabilidad, disminuyendo el contenido de árido grueso e incorporando filler silíceo a la dosificación para obtener HAC de altas resistencias. Y para aplicaciones donde no es necesario este requisito mecánico, es posible obtener un HAC con un alto rendimiento frente al ataque de agentes agresivos como Cl^- y SO_3 sin utilizar filler silíceo.

- Capítulo 5: "*Mechanical behaviour of self-compacting concrete made with recovery filler from hot-mix asphalt plants*".

Se evaluó la viabilidad de los residuos de grano fino, generados en el proceso de secado y calentamiento de los áridos empleados en las plantas de fabricación de mezclas bituminosas calientes, como material de construcción. Este polvo es denominado "filler de recuperación" (RF). Se ha llevado a cabo un estudio comparativo de dos tipos de HAC, el primero realizado con filler de recuperación (SCC-RF) de naturaleza dolomítica y el segundo con filler silíceo comercial (SCC-SF), utilizado como referencia.

1. Los ensayos de autocompactabilidad son reproducibles. SCC-RF presenta valores más cercanos al límite establecido por EHE-08.
2. La densidad en estado fresco del SCC-RF (2.365 T/m^3) es ligeramente menor que la del SCC-SF (2.392 T/m^3), lo cual está relacionado con el menor contenido de filler en volumen y mayor contenido de agua presente en las mezclas SCC-RF.
3. El estudio termogravimétrico muestra que el SCC-SF presenta una mayor pérdida de peso en la zona de deshidratación (0-400 ºC) y en el SCC-RF ocurre en el área de descarbonatación (550-735 ºC). Los mecanismos de endurecimiento de las mezclas son diferentes. En el SCC-SF, la portlandita sufre procesos de carbonatación y reacciones puzolánicas y en el SCC-RF solo se producen procesos de carbonatación. Esto da como resultado el aumento de la portlandita formada con el tiempo de fraguado para el SCC-RF. Para el SCC-SF, la cantidad de portlandita formada aumenta con el tiempo de fraguado en una primera etapa y luego disminuye (a los 250 días).
4. La resistencia a compresión, a tracción indirecta, a flexión y el módulo estático de elasticidad del HAC con RF (SCC-RF) son inferiores a los del HAC con SF (SCC-SF) para todas las edades. Las diferencias fueron mayores a una edad temprana y están relacionadas con un retraso en la hidratación de SCC-RF debido al mayor tamaño de partícula del RF (35 µm) respecto al SF (18 µm), lo que dificultará que actúe como centro de nucleación de silicatos de calcio hidratados.

5. Los valores de la resistencia a tracción indirecta, a flexión y del módulo estático de elasticidad calculados mediante EHE-08 son inferiores a los obtenidos experimentalmente, es decir, los coeficientes de correlación son en la mayoría de los casos superiores a 1. Por lo tanto, los resultados experimentales muestran la validez de la EHE-08 para HAC, inicialmente propuesto para el hormigón convencional.
6. Hay un aumento en la velocidad de propagación de ultrasonidos con respecto a la edad de curado y los valores para el SCC-SF son mayores que para el SCC-RF, lo que puede atribuirse al aumento en compacidad y resistencia a la compresión.
7. Bajo las condiciones de curado de este estudio, hay una menor retracción en el SCC-RF inicialmente debido al mayor tamaño de las partículas. En resumen, el HAC con RF debería tener un mejor rendimiento que el SCC-SF en términos de retracción y aparición temprana de grietas.
8. Por lo tanto, se puede concluir que es posible obtener un HAC, reemplazando (en masa) un filler silíceo natural (SF) por un residuo dolomítico procedente de plantas de mezclas bituminosas calientes (RF) con muy pocos cambios en el contenido de cemento (0,5%) y el contenido de agua (1%) para mantener constante el volumen de la mezcla (1025 L) y obtener una resistencia a la compresión superior a los niveles mínimos estipulados por el Código Español de Hormigón Estructural (EHE-08).

- Capítulo 6: "*Durability of self-compacting concrete made with recovery filler from hot-mix asphalt plants*".

Se realizó un estudio de la durabilidad de dos tipos de HAC, uno con filler residual (SCC-RF) de naturaleza dolomítica y otro con filler silíceo comercial (SCC-SF) como referencia, analizando las propiedades microestructurales de ambos hormigones.

1. Las mezclas cumplen los requisitos de autocompactabilidad marcados por la EHE-08, además muestran una alta reproducibilidad, realizadas en tiempos y con operarios distintos. La densidad en estado fresco en el SCC-SF (2.405 kg/dm^3) es ligeramente superior que en el SCC-RF (2.374 kg/dm^3)

debido principalmente a las diferentes características físico-químicas de los filler.

2. Existe en las mezclas una diferencia mayor entre las densidades secas (1%) que entre las densidades aparentes secas (0.6%), influenciado por una mayor porosidad abierta, un 4% superior, del SCC-RF (11.9%) respecto al SCC-SF (11.4%). Estos resultados están de acuerdo con la mayor porosidad de la mezcla SCC-RF observada en la porosimetría por intrusión de mercurio, ya que el volumen de intrusión de mercurio es superior en SCC-RF para poros superiores a 70 µm y entre 50.0 nm y 10.0 µm (poros capilares grandes), por el contrario, para el rango entre 2.5 y 10.0 nm (poros capilares medianos) es mayor para la muestra SCC-SF, lo que pone de manifiesto la estructura porosa menos fina del SCC-RF. Aunque la forma de la curva de distribución de tamaño de poro y la concentración máxima de poros (en torno a 40 nm) es similar en ambas mezclas.
3. La mayor absorción de agua por inmersión es ligeramente superior en el SCC-RF, lo cual está relacionada con su mayor porosidad. En cuanto a la absorción de agua por capilaridad ambas mezclas presentan valores inferiores a los límites marcados por RED DURAR de CYTED, en cuanto a porosidad efectiva (<10%) y sorptividad (<0.039 $cm/min^{1/2}$) por lo que podrían ser usadas en ambientes agresivos con una adecuada durabilidad.
4. Los resultados de penetración de agua bajo presión permiten considerar que ambas mezclas tienen una alta compacidad y son impermeables, ya que, en ningún caso, presentan una penetración superior a 30 mm (límite marcado en literatura como penetración máxima para ser consideradas como impermeables).
5. La penetración de ion cloruro tanto en el SCC-SF como en el SCC-RF presenta el mismo comportamiento migratorio de iones dentro del HAC ante la acción de un campo eléctrico, clasificándose como hormigones de baja penetrabilidad del ion cloruro de acuerdo con la ASTM C 1202. En relación a la concentración del ion cloruro respecto a la profundidad, ambas mezclas muestran un similar comportamiento en cuanto al riesgo de corrosión del acero, ya que presentan un margen de seguridad de más de 20 mm.
6. La penetración del CO_2 en el SCC-RF es un 30% superior al SCC-SF, debido principalmente a dos factores, por un lado, a la mayor porosidad presente

en el SCC-RF y por otro al diferente mecanismo de fraguado de esta mezcla respecto al SCC-SF.

7. Respecto a la penetración del ion SO_3 es observa un diferente comportamiento entre ambas mezclas. El SCC-SF presenta valores inferiores que el SCC-RF para cada profundidad de muestreo. En definitiva, la mayor densidad microestructural del SCC-SF da lugar a que el SO_3 alcance menores profundidades de penetración en este material. Tras el tiempo de exposición al ambiente agresivo ambas muestras no presentan ningún signo de desgaste o deterioro.
8. La retracción en las dos mezclas se estabiliza para una edad superior a 500 días, bajo las condiciones de curado utilizadas en este trabajo. La mezcla SCC-SF tiene una retracción superior (≈6%) a la de la muestra SCC-RF. El 90% de la retracción total en la SCC-SF se alcanza a una edad de 257 días y a 269 días para SCC-RF, ya que las características físico-químico del filler SF, la estructura porosa más fina del SCC-SF, así como el mayor contenido de agua favorecen la retracción de la mezcla. En resumen, el SCC-RF debería tener un mejor rendimiento que el SCC-SF en términos de retracción.
9. Se puede concluir, por tanto, que es posible obtener un HAC de altas prestaciones respecto a la durabilidad sustituyendo un filler comercial de naturaleza silícea (SF) por un polvo residual de naturaleza dolomítica, procedente de plantas de mezclas bituminosas calientes (RF), alcanzando un alto rendimiento frente al ataque de agentes agresivos de acuerdo a los niveles marcados por el Código Español de Hormigón Estructural para un HAC-30.

- Capítulo 7: "*Mechanical behaviour of self-compacting concrete made with non-conforming fly ash from coal-fired power plants*".

Se llevó a cabo un estudio comparativo de tres mezclas de HAC para evaluar cenizas volantes no conformes procedentes de centrales termoeléctricas de carbón (NCFA) como filler; en la primera mezcla (SCC-1), se utilizó un filler comercial (SF) como referencia; en el segundo (SCC-12) se usó una mezcla, 1:1 en volumen, de SF y NCFA; y en el tercero (SCC-2), solo se utilizó NCFA.

1. Los ensayos de autocompactabilidad son reproducibles. Todas las mezclas cumplen con los parámetros estipulados por el EHE-08.
2. Las densidades en estado fresco de SCC-12 (2.421 kg/dm^3) y SCC-2 (2.397 kg/dm^3) son ligeramente menores que las de SCC-1 (2.441 kg/dm^3), y esto está relacionado con la distribución tamaño de partícula más fina y continua del SF con respecto al NCFA.
3. El estudio termogravimétrico muestra que en el SCC-1, la mayor pérdida de peso ocurre en la zona de deshidratación (0-400 ºC); en el SCC-2, ocurre en el área de descarbonatación (550-750 ºC). Se puede concluir que el mecanismo de endurecimiento de ambos hormigones (SCC-1 y SCC-2) es diferente, dependiendo de la naturaleza del filler empleado. En el caso de la mezcla SCC-12, el comportamiento es intermedio. En resumen, en la mezcla SCC-1 se producen reacciones puzolánicas y una débil carbonatación. En la mezcla SCC-12, se observan reacciones puzolánicas y de carbonatación. En la mezcla SCC-2, solo se observan procesos de carbonatación.
4. Las tres mezclas tienen valores de densidad húmeda similares (medidos a los 28 días), aunque ligeramente inferiores para las mezclas que incorporan NCFA: 2.418 kg/dm^3 (SCC-12) y 2.398 kg/dm^3 (SCC-2) en comparación con la mezcla de referencia 2.438 kg/dm^3 (SCC-1). Las densidades secas siguen el mismo patrón que el observado en el caso de las densidades húmedas: 2.329 kg/dm^3, 2.323 kg/dm^3 y 2.284 kg/dm^3 para las mezclas SCC-1, SCC-12 y SCC-2, respectivamente.
5. La resistencia a compresión, a tracción indirecta, a flexión, así como el módulo estático de elasticidad de los HAC fabricados con NCFA (SCC-12 y SCC-2) son inferiores a los del HAC producido con SF (SCC-1) para todas las edades. Las diferencias fueron mayores a una edad temprana.
6. El retraso en la hidratación observado en estas mezclas puede deberse a la mayor distribución del tamaño de partícula del NCFA (45% de las partículas son mayores de 32 μm versus 12% en la SF), lo que da lugar a una hidratación incompleta de las partículas y, por lo tanto, dificulta el desarrollo mecánico.
7. Los valores de resistencia a tracción indirecta, de resistencia a flexión y del módulo estático de elasticidad calculados utilizando el EHE-08 y/o el Eurocódigo 2 son inferiores a los obtenidos experimentalmente, es decir, los

coeficientes de correlación son en la mayoría de los casos superiores a 1. Por lo tanto, los resultados muestran la validez del uso del EHE-08 y/o el Eurocódigo 2, inicialmente propuesto para hormigón convencional.

8. Hay un aumento en la UPV respecto a la edad de curado para todas las mezclas, lo cual puede ser atribuido al aumento en compacidad y resistencia a la compresión. Las mezclas pueden considerarse excelentes ya que presentan valores de UPV superiores a 4.5 km/s.
9. La incorporación de NCFA como filler en HAC, SCC-12 y SCC-2 dio como resultado un mejor rendimiento que SCC-1 en relación con la retracción a una edad temprana, lo que daría como resultado menos agrietamiento por la deformación inicial debido a estos fenómenos.
10. Se puede concluir que es posible obtener un HAC, reemplazando (en volumen) un filler comercial por NCFA de centrales eléctricas de carbón consiguiendo un comportamiento mecánico mayor que los niveles mínimos estipulados por el Código Español del Hormigón Estructural (EHE-08).

- Capítulo 8: "*Durability of self-compacting concrete made from non-conforming fly ash from coal-fired power plants*".

Se realizó un estudio de la durabilidad de tres tipos de HAC: con filler silíceo comercial (SCC-1), usado como mezcla de referencia, con cenizas no conformes procedentes de centrales termoeléctricas de carbón (SCC-2) y con una combinación 1:1 (en volumen) de ambos materiales (SCC-12).

1. Se observa que todas las mezclas cumplen con los requisitos de autocompactabilidad marcados por la EHE-08. La densidad en estado fresco en el SCC-1 es ligeramente superior que en el SCC-12 y el SCC-2 debido a la distribución de tamaño de grano más fina y continua del SF respecto NCFA.
2. Existe una mayor diferencia entre las densidades secas de las mezclas (≈1-2%) que entre las densidades aparentes secas (≈0.6-1%), debido a la propia definición de ambas densidades que provoca que las diferencias se amortigüen en la densidad aparente seca. En cuanto a la porosidad abierta, es mayor para el SCC-2 seguido de SCC-12 y SCC-1. Estos resultados se correlacionan con la porosimetría por intrusión de mercurio, ya que la mezcla

con NCFA (SCC-2) presenta un mayor porcentaje de poros superiores a 10 µm respecto a la mezcla con SF (SCC-1), la cual tiene una mayor cantidad de poros de tamaño inferior a 10 µm, dando lugar a una estructura porosa más fina. La incorporación del NCFA al 50% (SCC-12) en la mezcla origina una porosidad y densidad microestructural intermedia.

3. Las propiedades del párrafo anterior justifican la ligera mayor absorción de agua por inmersión en la mezcla SCC-2. Tras llevar a cabo el análisis de absorción por capilaridad y de acuerdo con los límites marcados por RED DURAR de CYTED, todas las mezclas podrían ser utilizadas en elementos estructurales expuestos a alta agresividad ambiental con una adecuada durabilidad.
4. Los resultados de penetración de agua bajo presión permiten considerar que las mezclas tienen una alta compacidad y son impermeables, ya que, en ningún caso, presentan una penetración superior a 30 mm.
5. Teniendo en cuenta la norma ASTM C 1202, todas las mezclas están en el intervalo considerado como de baja penetrabilidad del ion cloruro. En relación a la concentración del ion cloruro en función de la profundidad, en todas las mezclas alcanzaron una concentración de inferior al 0.05% para profundidades mayores que 23 mm, por lo que las armaduras no se verían afectadas si el recubrimiento es superior a estos valores. Consecuentemente, el margen de seguridad para las mezclas es de más 20 mm, comparado con el recubrimiento mínimo requerido (45 mm) por la EHE-08.
6. La profundidad de carbonatación de SCC-2 es superior a SCC-12 y SCC-1, debido principalmente a dos factores, por un lado, a la mayor cantidad de portlandita generada durante el fraguado en SCC-2 y, por otro lado, a la estructura porosa menos fina. Los resultados muestran un margen de seguridad de aproximadamente 25 mm. Por lo que, para las tres mezclas la armadura quedará protegida por el recubrimiento ya que la concentración de CO_2 en la atmosfera es del 0.04%, 125 veces inferior a la concentración de CO_2 de la cámara de carbonatación.
7. Respecto a la penetración de SO_3, la mezcla que registra un valor inferior fue SCC-1 seguido de SCC-12 y SCC-2. En definitiva, la estructura porosa más fina y densa dará lugar a una disminución destacable de la concentración de ion SO_3 en las mezclas SCC-1 y SCC-12 respecto SCC-2 y por tanto a una

menor difusión y profundidad de penetración del sulfato. Para todas las mezclas, tras el tiempo de exposición al ambiente agresivo, no existió ningún signo de desgaste o deterioro.

8. La deformación que sufren las mezclas por acción de la retracción se estabilizó a los 450 días, bajo las condiciones de curado utilizadas en este trabajo. La mezcla SCC-1 tiene una retracción superior a la de las muestras SCC-12 y SCC-2, debido a la actividad puzolánica del SF, al secado y al efecto de la estructura porosa. La mezcla SCC-12 presenta un comportamiento intermedio entre las otras dos mezclas. En resumen, el SCC-2 tiene un mejor rendimiento que el SCC-1 en términos de retracción.
9. En resumen, es posible obtener un HAC con altas prestaciones respecto a la durabilidad, frente al ataque de agentes agresivos y retracción, sustituyendo total o parcialmente el SF por NCFA.

9.2 Conclusions

Taking into account the objectives and results achieved, the conclusions by chapters of this Doctoral Thesis are explained below:

- Chapter 4: "*Mechanical and durability behaviour of self-compacting concretes for application in the manufacture of hazardous waste containers*".

A comparative study of four types of SCCs was carried out, in which the effects of the amounts of coarse and fine aggregates, and fillers in fresh-state (self-compacting) and hardened-state (porous structure, mechanical behaviour and durability) were analysed.

1. The mixes comply with the self-compacting requirements of EHE-08, showing that it is possible to obtain SCC dosages where parameters such as the amounts of coarse aggregate, paste, and water-fines ratio are not within the values proposed by EFNARC. The self-compactability tests show high reproducibility.
2. Slight differences are presented by the densities of the mixes. The factors that have more significant influences on the density of the mixes are the

presence of fillers and water-cement ratio, because the mixes with fillers and smaller water-cement ratios (SCC-C and SCC-A) exhibited higher densities.

3. These results conform with the lower porosity observed in the pore size distribution of mixes incorporating fillers (SCC-A and SCC-C). The volume of mercury intrusion in pores having diameters greater than 70 μm and 50.0 nm–10.0 μm (large capillary pores) is higher in SCC-B and SCC-D. By contrast, in the ranges of 10–50 nm (medium capillary pores) and 2.5–10.0 nm (small gel pores), the volume of mercury intrusion is higher in SCC-A and SCC-C samples. All these reveal that the structures of mixes with fillers are more fine and porous. On the other hand, the greater compactness of the mixes SCC-C and SCC-D relative to SCC-A and SCC-B agrees with the greater mercury intrusion volume in the zones between medium and large capillary pores.
4. The mechanical behaviour of SCCs without SF and with different amounts of coarse aggregates (SCC-B and SCC-D), shows that it is possible to obtain compressive strengths above the minimum levels stipulated by the Spanish Code of Structural Concrete for a HAC-30. Furthermore, it is possible to obtain strengths of approximately 50 MPa for SCC mixes in 28 days by incorporating SF (SCC-A and SCC-C) even with low coarse aggregate contents.
5. The values of splitting tensile and flexural strengths calculated by applying EHE-08 (calculated from the compressive strength) are lower than the values obtained experimentally. This means that the experimental results are congruent with the validity of EHE- 08—originally proposed for OC—when applied to SCC.
6. The mixes incorporating SF (SCC-A and SCC-C) presented better performance in absorption of water by immersion than mixes that do not (SCC-B and SCC-D). For the absorption of water by capillarity, mixes with fillers presented lower absorption by capillarity and sorptivity than mixes without fillers. Moreover, mixes with higher contents of coarse aggregates, SCC-A and SCC-B, presented higher absorption values than SCC-C and SCC-D mixes, respectively. All mixes had values lower than established limits in terms of effective porosity and sorptivity. Hence, these mixes could be used in aggressive environments along with adequate durability.

7. The results of penetration of water under pressure lead to the conclusion that all mixes have high compactness and are impermeable, because there were no penetrations higher than 30 mm, which is marked in literature as the maximum penetration for cementitious material to be considered impermeable.
8. As to the penetration of Cl^- and SO_3 ions, the SCC-C mix showed lower attacks, followed by the SCC-A, SCC-D and SCC-B mixes, respectively. The higher microstructural densities of the mixes with fillers led to lower penetration depths in those materials. After the exposure to aggressive environments, not one of the mixes showed signs of wearing out or deterioration.
9. Under the curing conditions used in this research, the drying shrinkage of the mixes are stabilised at an age of approximately 100 days. The SCC-C mix presented the lowest shrinkage, followed by the SCC-A, SCC-D, and SCC-B mixes, respectively. The presence of fillers had a more significant influence on shrinkage than the amount of coarse aggregates.
10. It can be concluded that it is possible to obtain high performance SCC in relation to mechanical and durability properties, by reducing the content of coarse aggregates, and incorporating SF in the dosage. Moreover, for applications where high mechanical requirements are not necessary, it is possible to obtain SCCs with high performances against attacks of aggressive agents such Cl^- and SO_3 without using SF.

- Chapter 5: "*Mechanical behaviour of self-compacting concrete made with recovery filler from hot-mix asphalt plants*".

The aim of this chapter is the assessment of the feasibility of the fine grain waste, generated in the drying and heating process of aggregates in hot-mix asphalt (HMA) manufacturing plants, as a construction material. This powder is named "recovery filler" (RF). A comparative study of two types of SCC has been carried out, the first one made with recovery filler (SCC-RF) of dolomitic nature and the second one with commercial siliceous filler (SCC-SF), utilized as reference.

1. The self-compactability tests show reproducibility. SCC-RF presents values closer to the limit set by EHE-08.
2. The density of SCC-RF (2.365 T/m^3) in the fresh state is slightly less than that of SCC-SF (2.392 T/m^3), which is related to the lower content of RF filler by volume and higher content of water present in the SCC-RF mixes.
3. The thermogravimetric study shows that in SCC-SF the higher loss weight occurs in the dehydration zone (0-400 ºC) and in SCC-RF it occurs in the decarbonation area (550-735 ºC). The aging mechanism of the mixes is different. In SCC-SF, portlandite undergoes carbonation processes and pozzolanic reactions and in SCC-RF it only undergoes carbonation processes. This results in a steady increase in the amount of portlandite formed with the setting time for SCC-RF. For SCC-SF, the amount of portlandite formed increases with the setting time in a first stage and then decreases (at 250 days).
4. The compressive strength, splitting tensile strength, flexural strength, and static modulus of elasticity of SCC produced with RF (SCC-RF) are lower than those of SCC produced with SF (SCC-SF), for all ages. The differences were higher at an early age and are related to a delay in hydration of SCC-RF because the particle size of the RF filler (maximum at 35 µm) is much greater than that of SF (maximum at 18 µm) which hinders it acting as nucleation centre of hydrated calcium silicates.
5. The splitting tensile strength, flexural strength and static modulus of elasticity values calculated using EHE-08 are lower than those obtained experimentally, i.e. the correlation ratios are in most cases greater than 1. So, the experimental results show the validity of using EHE-08, initially proposed for OC (Ordinaty Concrete), in SCC.
6. There is an increase in ultrasonic pulse velocity relative to curing age and the values for SCC-SF are greater than for SCC-RF, which can be attributed to the increase in compacity and compressive strength.
7. In the curing conditions of this study there is a lower shrinkage in SCC-RF initially due to the larger size of particles. In short, the SCC produced with recovery filler from plants manufacturing hot-mix asphalt (SCC-RF) should have better performance than SCC-SF in terms of shrinkage and early appearance of cracks.

8. One may conclude therefore, that it is possible to obtain an SCC, by replacing (in mass) a natural siliceous filler (SF) with a dolomite waste from plants of hot-mix asphalt (RF) with very slight changes in cement (0.5%) and water (1%) content in order to maintain constant the volume of the mix (1025 L) and obtain compressive strength greater than the minimum levels stipulated by the Spanish Code on Structural Concrete (EHE-08).

- Chapter 6: " Durability *of self-compacting concrete made with recovery filler from hot-mix asphalt plants*".

A study was carried out on the durability of two types of SCC, one with dolomitic recovery filler (SCC-RF), and the other with commercial siliceous filler (SCC-SF) as a reference, analysing the microstructural properties of both mixes.

1. The mixes comply with the self-compactability requirements set by EHE-08, as well as showing high reproducibility, tested by different times and different appliers. The fresh-state density of SCC-SF (2.405 kg/dm^3) is slightly greater than that of SCC-RF (2.374 kg/dm^3) due mainly to the different physico-chemical of the fillers.
2. In the mixes, there is a greater difference between the dry bulk density (1%) than in the apparent dry density (0.6%), influenced by a greater open porosity in SCC-RF, which is 4% greater than in SCC-SF, 11.9% vs. 11.4% respectively. These results agree with the greater porosity of SCC-RF observed in the porosimetry by mercury intrusion, since the volume of intrusion is greater in SCC-RF for pores over 70 µm and between 50.0 nm and 10.0 µm (large capillary pores). In contrast, for the 2.5-10.0 nm range (small gel pores) it is greater in the SCC-SF sample, which demonstrates the less fine porous structure of SCC-RF even though the shape of the curve of distribution of pore size and the maximum pore concentration (around 40 nm) is similar in both mixes.
3. The absorption of water by immersion is slightly greater in SCC-RF, which is related to its greater porosity. Both mixes showed lower values of absorption by water capillarity than the limits set by the Ibero-American document RED DURAR in the framework CYTED, in terms of effective porosity (<10%) and

sorptivity (<0.039 cm/min$^{1/2}$), so that they could be used in aggressive environments with adequate durability.

4. The results for water penetration under pressure enabled considering that both mixes have high compactability and are impermeable, since they never showed penetration over 30 mm (limit set in the literature as maximum penetration to be considered impermeable).
5. Chloride ion penetration in both SCC-SF and SCC-RF show the same migratory behaviour of ions within the mix when an electric field is applied, being classified as concrete of low chloride ion penetration according to ASTM C 1202. In relation to the concentration of chloride ion in function of depth, the mixes show a similar behaviour regarding the risk of steel corrosion, since they show a safety margin of more than 20 mm.
6. The penetration depth of CO_2 in SCC-RF is 30% greater than in SCC-SF, due mainly to two factors: the greater porosity of SCC-RF and the different curing mechanism of this mix relative to SCC-SF.
7. Regarding the penetration of ion SO_3, there is a different behaviour of the mixes. SCC-SF shows lower values than SCC-RF for each specimen depth. The greater microstructural density of SCC-SF results in the SO_3 reaching lower penetration depths in this material. After the exposure time to aggressive environments neither mix shows any sign of wearing out or deterioration.
8. Shrinkage in both mixes stabilises after 500 days, under the curing conditions used in this study. SCC-SF has greater shrinkage (≈6%) than SCC-RF. 90% of the total shrinkage of SCC-SF and SCC-RF is reached after 257 and 269 days respectively, since the physico-chemical characteristics of the SF filler, the finer porous structure of SCC-SF, as well as the greater water content, favour shrinkage of that mix. In short, the SCC mix made with recovery filler from plants manufacturing hot mix asphalt SCC-RF should have better features than SCC-SF in terms of shrinkage.
9. It can therefore be concluded that it is possible to obtain good quality SCC relative to durability by replacing commercial siliceous filler (SF) with dolomitic recovery filler, sourced from hot-mix asphalt plants (RF), with good performance in terms of aggressive agent attack, according to the levels set by the Spanish Code for Structural Concrete.

- Chapter 7: "*Mechanical behaviour of self-compacting concrete made with non-conforming fly ash from coal-fired power plants*".

A comparative study of three SCC mixes was carried out to evaluate an NCFA-like filler in SCC; in the first mix (SCC-1), a commercial SF was used as a reference; in the second (SCC-12) a mix, 1:1 in volume, of SF and NCFA was used; and in the third (SCC-2), only NCFA was used.

1. The self-compactability tests show reproducibility. All mixes accomplish with the parameters stipulated by the EHE-08.
2. The densities of SCC-12 (2.421 kg/dm^3) and SCC-2 (2.397 kg/dm^3) in the fresh state are slightly less than that of SCC-1 (2.441 kg/dm^3), and this is related to the finer and continuous particle size distribution of the SF with respect to the NCFA.
3. The thermogravimetric study shows that in SCC-1, the higher weight loss occurs in the dehydration zone (0–400 ºC); in SCC-2, it occurs in the decarbonation area (550–750 ºC). It can be concluded that the setting mechanism of both concretes (SCC-1 and SCC-2) is different, depending on the nature of filler added. In the case of the SCC-12 mix, the behaviour is intermediate. In short, pozzolanic and mild carbonation reactions occur in the SCC-1 mix. In the SCC-12 mix, both pozzolanic and carbonation reactions are observed. In the SCC-2 mix, only carbonation processes are observed.
4. The three mixes have similar wet density values (measured at 28 days), although slightly lower for the mixes that incorporate NCFA: 2.418 kg/dm^3 (SCC-12) and 2.398 kg/dm^3 (SCC-2) compared to the mix of references 2.438 kg/dm^3 (SCC-1). The dry densities follow the same pattern as that observed in the case of wet densities: 2.329 kg/dm^3, 2.323 kg/dm^3, and 2.284 kg/dm^3 for SCC-1, SCC-12, and SCC-2 mixes, respectively.
5. The compressive strength, splitting tensile strength, flexural strength, and static modulus of elasticity of SCCs produced with NCFA (SCC-12 and SCC-2) are lower than those of the SCC produced with SF (SCC-1), for all ages. The differences were higher at an early age.
6. The delay in hydration observed in these mixes may be due to the greater particle size distribution of the NCFA, (45% of the particles are greater than

32 μm versus 12% in the SF), making the complete hydration of the particles and therefore the mechanical development difficult.

7. The splitting tensile strength, flexural strength, and static modulus of elasticity values calculated using the EHE-08 and/or the Eurocode 2 are lower than those obtained experimentally, i.e., the correlation ratios are in most cases greater than 1. Hence, the experimental results show the validity of using the EHE-08 and/or the Eurocode 2, initially proposed for ordinary concrete (OC), in SCC.
8. There is an increase in the UPV relative to the curing age and the values for all mixes, and this can be attributed to the increase in compacity and compressive strength. The mixes can be considered excellent since they present UPV values higher than 4.5 km/s.
9. The incorporation of NCFA as a filler in SCCs, SCC-12, and SCC-2 resulted in their better performance than SCC-1 in relation to shrinkage at an early age, which would result in less cracking by the initial deformation due to these phenomena.
10. One may conclude therefore, that it is possible to obtain an SCC, by replacing (in volume) a natural SF with NCFA from coal-fired power plants to achieve a mechanical behaviour greater than the minimum levels stipulated by the Spanish Code on Structural Concrete (EHE-08).

- Chapter 8: "*Durability of self-compacting concrete made from non-conforming fly ash from coal-fired power plants*".

In this chapter, a study of the durability of three types of SCCs was carried out. The first SCC, the reference mix, was a mix with SF (SCC-1), the second one was a mix with NCFA (SCC-2), and the third one was a mix with a 1:1 combination (by volume) of both materials (SCC-12).

1. It is observed that all the mixes comply with the self-compacting requirements set by the EHE-08 guideline. The fresh-state density in SCC-1 is slightly higher than those in SCC-12 and SCC-2 owing to the finer and continuous grain size distribution of SF with respect to that of NCFA.

2. There is a greater difference between the bulk densities of the mixes (≈1–2%) than between their skeletal densities (≈0.6–1%). This is due to the very definition of both densities, which causes that the differences be damped in the skeletal density. Regarding open porosity, it is higher in SCC-2, followed by SCC-12 and SCC-1. These results correlate with the MIP as the mix with NCFA (SCC-2) has a higher percentage of pores over 10 μm compared to the mix with SF (SCC-1), which has a greater number of pores smaller than 10 μm, resulting in a finer porous structure. The incorporation of 50% of NCFA (SCC-12) into the mix results in an intermediate porosity and microstructural density.
3. The above stated properties explain the slightly greater absorption of water by immersion in SCC-2. After carrying out the analysis of absorption by capillarity, and in accordance with the limits set by the CYTED's DURAR network, all the mixes could be used in structural elements exposed to highly aggressive environments with adequate durability.
4. According to the results of water penetration under pressure, it is reasonable to consider that the mixes have high compactness and are waterproof because, in all cases, they have a penetration of more than 30 mm.
5. In accordance with ASTM C 1202, all the mixes are in the range considered of low penetrability to the chloride ion. In relation to the chloride ion concentration as a function of depth, in all the mixes a concentration lower than 0.05% was reached for depths greater than 23 mm, and thus, the reinforcements would not be affected if the cover is greater than this value. Consequently, the safety margin for the mixes is greater than 20 mm, compared to the required cover (45 mm) by EHE-08.
6. The carbonation depth of SCC-2 is superior to that of SCC-12 and SCC-1 due, on the one hand, to the greater amount of portlandite generated during setting in SCC-2 and, on the other hand, to its less fine porous structure. The results show a safety margin of approximately 25 mm. Therefore, with the three mixes, the reinforcement will be protected by the cover as the concentration of CO_2 in the atmosphere is 0.04%, 125 times lower than the CO_2 concentration of the carbonation chamber.
7. Regarding the penetration of SO_3, the mix that registered a lower value was SCC-1 followed by SCC-12 and SCC-2. The finer and denser porous structure

in the SCC-1 and SCC-12 mixes will lead to a remarkable decrease in the concentration of SO_3 ion with respect to SCC-2, and therefore, to a lower diffusion and depth of sulphate penetration. After the exposure time, neither mix shows any sign of wearing or deterioration.

8. The deformation suffered by the mixes by the action of shrinkage was stabilised at 450 days under the curing conditions used in this work. SCC-1 showed higher shrinkage than that of the SCC-12 and SCC-2 samples, which is due to the pozzolanic activity of the SF, the drying process, and the effect of the porous structure. SCC-12 has an intermediate behaviour between the other two mixes. In short, the SCC manufactured with NCFA from coal-fired power plants is better than SCC-1 in relation to shrinkage.
9. In summary, it is possible to obtain an SCC with high performance with respect to durability against the attack of aggressive agents and shrinkage by replacing totally or partially the SF with NCFA from coal-fired power plants.

9.3 Futuras líneas de investigación

Tras la exposición y análisis de los resultados obtenidos en este trabajo sería interesante plantear diferentes estudios que podrían ser abordados en el futuro para ampliar, profundizar y desarrollar el uso de materiales residuales o subproductos de granulometría fina en hormigones autocompactantes y que se exponen a continuación:

- Llevar a cabo un inventario de los residuos de granulometría fina generados en el sector industrial y minero a nivel autonómico y nacional.
- Realizar una profunda caracterización físico-química y microestructural de estos residuos.
- Hacer una catalogación de estos residuos, destacando las diferencias y similitudes con respecto a los filler comerciales existentes.
- Desarrollar un estudio de las propiedades en estado fresco de HAC con estos materiales residuales en sustitución total o parcial de los materiales convencionales. Deberán ser tenidas en cuenta posibles combinaciones de residuos que permitan aminorar o eliminar la falta de cumplimiento con los

requerimientos marcados en la normativa, con el objeto de conseguir un material de características óptimas y con una calidad avalada igual, sino superior, a los materiales convencionales.

- Desarrollar un estudio de las propiedades en estado endurecido de los HAC para identificar sus características a nivel de microestructura, propiedades mecánicas y de durabilidad, con el objeto de conseguir un material de características óptimas y con una calidad avalada igual, sino superior, a los materiales convencionales.
- Todo esto podría culminar en una guía técnica de recomendaciones de uso de residuos de granulometría fina en los HAC, que serviría de apoyo a las empresas generadoras de estos residuos, a las entidades gestoras, a las empresas constructoras y del prefabricado, así como, a la administración pública para su posible inclusión en los pliegos de prescripciones técnicas.

Anexo A

Producción científica derivada directamente de la Tesis Doctoral

A continuación, se enumera la producción científica derivada directamente de la Tesis Doctoral, la cual se resume en 5 publicaciones internacionales y varias comunicaciones en congresos nacionales e internacionales que aportan a dicho trabajo un alto índice de calidad.

- Publicaciones científicas:

1. Título: Mechanical behaviour of self-compacting concrete made with recovery filler from hot-mix asphalt plants.
   Autores: A.R. Esquinas, C. Ramos, J.R. Jiménez, J.M. Fernández, J. de Brito.
   Título de la revista: Construction and Building Materials
   Número de revista: 131 Año: 2017 Páginas: 114-128 ISSN: 0950-0618
   Índice de impacto: 3.485 Citas: 8
   Índice relativo de su categoría: 11/125 Engineering, Civil (1^{er} Cuartil / 1^{er} Decil)

2. Título: Durability of self-compacting concrete made with recovery filler from hot-mix asphalt plants.
   Autores: A.R. Esquinas, J.I. Álvarez, J.R. Jiménez, J.M. Fernández, J. de Brito.
   Título de la revista: Construction and Building Materials
   Número de revista: 161 Año: 2018 Páginas: 407-419 ISSN: 0950-0618
   Índice de impacto: 3.485 Citas: 2
   Índice relativo de su categoría: 11/125 Engineering, Civil (1er Cuartil / 1er Decil)

3. Título: Mechanical and durability behaviour of self-compacting concretes for application in the manufacture of hazardous waste containers.
   Autores: A.R. Esquinas, D. Motos-Pérez, M.E. Jiménez, C. Ramos, J.R. Jiménez, J.M. Fernández.
   Título de la revista: Construction and Building Materials
   Número de revista: 168 Año: 2018 Páginas:442-458 ISSN: 0950-0618
   Índice de impacto: 3.485 Citas: 1
   Índice relativo de su categoría: 11/125 Engineering, Civil (1er Cuartil / 1er Decil)

4. Título: Mechanical behaviour of self-compacting concrete made with non-conforming fly ash from coal-fired power plants.
   Autores: A.R. Esquinas, E.F. Ledesma, R. Otero, J.R. Jiménez, J.M. Fernández.
   Título de la revista: Construction and Building Materials
   Número de revista: 182 Año: 2018 Páginas:385-398 ISSN: 0950-0618
   Índice de impacto: 3.485 Citas: 1
   Índice relativo de su categoría: 11/125 Engineering, Civil (1er Cuartil / 1er Decil)

5. Título: Durability of self-compacting concrete made from non-conforming fly ash from coal-fired power plants.
   Autores: A.R. Esquinas, J.I. Álvarez, J.R. Jiménez, J.M. Fernández.
   Título de la revista: Construction and Building Materials
   Número de revista: 189 Año: 2018 Páginas:993-1006 ISSN: 0950-0618
   Índice de impacto: 3.485 Citas: 0
   Índice relativo de su categoría: 11/125 Engineering, Civil (1er Cuartil / 1er Decil)

- Comunicaciones en congresos:

1. Título: Desarrollo de un hormigón autocompactante para la construcción de contenedores para el Cabril (ENRESA).
   Autores: A.R. Esquinas, C. Ramos, M.E. Jiménez, J. Ayuso, J.R. Jiménez, J.M. Fernández.
   Congreso: V WORKSHOP NANOUCO. Encuentro sobre Nanociencia y Nanotecnología de Investigadores Andaluces.
   Año: 2014
   Entidad Organizadora: Instituto Universitario de Investigación en Química Fina y Nanoquímica (IUIQFN), Universidad de Córdoba.
   Lugar: Córdoba (España)

2. Título: Caracterización del fraguado y propiedades mecánicas de hormigones autocompactantes fabricados con filler residual.
   Autores: A.R. Esquinas, J.R. Jiménez, J.M. Fernández.
   Congreso: V Congreso Científico de Investigadores en Formación de la Universidad de Córdoba.
   Año: 2016
   Entidad Organizadora: Escuela de Doctorado de la Universidad de Córdoba (Vicerrectorado de Estudio de Postgrado y Formación Continua).
   Lugar: Córdoba (España)

3. Título: Self-compacting concrete made with recovery filler from hot-mix asphalt plants: Mechanical properties.
   Autores: A.R. Esquinas, J.M. Fernández, J.R. Jiménez.
   Congreso: Second international conference on concrete sustainability.
   Año: 2016
   Entidad Organizadora: Universidad Politécnica de Madrid, Asociación Científico Técnica del Hormigón Estructural (ACHE), American Concrete Institute (ACI), Asociación Latinoamericana de Control y Calidad, Patología y Recuperación de la Construcción (ALCONPAT Internacional), International Federation For Structural Concrete (FIB-CEB-FIP), Japan Concrete Institute (JCI) y International Union of

Laborratories and Experts in Construction Materials, Systems and Structures (RILEM).
Lugar: Madrid (España)

4. Título: Aplicación de residuos de granulometría fina procedentes de tratamiento de áridos en hormigones autocompactantes.
   Autores: A.R. Esquinas, J.R. Jiménez, J.M. Fernández.
   Congreso: VI WORKSHOP NANOUCO. Encuentro sobre Nanociencia y Nanotecnología de Investigadores Andaluces.
   Año: 2017
   Entidad Organizadora: Instituto Universitario de Investigación en Química Fina y Nanoquímica (IUIQFN), Universidad de Córdoba.
   Lugar: Córdoba (España)

5. Título: HAC con filler de recuperación de las plantas de mezclas bituminosas calientes: durabilidad.
   Autores: A.R. Esquinas, R. Otero, J.R. Jiménez, J.M. Fernández.
   Congreso: VII Congreso Internacional de Estructuras. Congreso de la Asociación Científico-Técnica del Hormigón Estructural.
   Año: 2017
   Entidad Organizadora: Asociación Científico-Técnica del Hormigón Estructural (ACHE).
   Lugar: A Coruña (España)

6. Título: Título de la contribución: Utilización segura de residuos como materia prima para la fabricación de hormigones autocompactantes.
   Autores: A.R. Esquinas, J.R. Jiménez, J.M. Fernández.
   Congreso: VI Congreso Científico de Investigadores en Formación de la Universidad de Córdoba.
   Año: 2018
   Entidad Organizadora: Escuela de Doctorado de la Universidad de Córdoba (Vicerrectorado de Estudio de Postgrado y Formación Continua).
   Lugar: Córdoba (España)

7. Título: Self-compacting concrete made with non-conforming fly ash as filler: mechanical properties and setting characterization.
   Autores: A.R. Esquinas, E.F. Ledesma, J.R. Jiménez, J.M. Fernández.
   Congreso: 3er International Symposium on Inorganic and Environmental Materials (ISIEM 2018).
   Año: 2018
   Entidad Organizadora: Ghent University y Society Inorganic Material of Japan.
   Lugar: Ghent (Bélgica)

Anexo B

Producción científica derivada directamente de la Tesis Doctoral, en fase de publicación

A continuación, se exponen una serie de trabajos que han sido desarrollados durante el periodo de Tesis Doctoral y que se encuentran en fase de publicación. El objetivo de los mismos ha sido llevar a cabo un estudio de viabilidad técnica de aplicación de cenizas procedentes de la Planta de Valorización Energética de Residuos Sólidos Urbanos de la empresa Valorsul, localizada en Lisboa (Portugal) como filler en HAC. Para la consecución de este objetivo se han desarrollado las siguientes tareas:

- Caracterizar todos los materiales convencionales utilizados en la fabricación del HAC (fase mortero). Se realizó un estudio completo de las propiedades físico-químicas y microestructurales de los mismos.

- Caracterizar cenizas procedentes de plantas de valorización energética de residuos sólidos urbanos. Se llevó a cabo un completo estudio de las propiedades físico-químicas y microestructurales del residuo, lo cual permitió evaluar la influencia de este subproducto en el comportamiento del HAC (fase mortero) respecto a filler convencionales.

- Diseñar dosificaciones de HAC (fase mortero) con materiales convencionales y residuos y evaluar sus propiedades en estado fresco. Se realizó el diseño de varias dosificaciones de HAC (fase mortero) y se llevó a cabo un estudio de la influencia de la cantidad de cemento y de residuo, así como de diferentes % de sustitución del filler convencional en las propiedades de autocompactabilidad de las mezclas.

- Analizar y comparar el comportamiento mecánico y durable de las dosificaciones de HAC (fase mortero) diseñadas. Se llevó a cabo un análisis profundo, evaluando el comportamiento mecánico y su correlación con las diferentes reacciones químicas que se producen durante el endurecimiento del HAC (fase mortero). Posteriormente se analizaron las propiedades microestructurales y propiedades físicas de absorción de los HAC. Y, por último, se realizó un estudio de la durabilidad ante las acciones de agentes agresivos que se completó con el análisis de la retracción.

- Evaluar y analizar las propiedades en estado fresco y endurecido (comportamiento mecánico y durable) de las dosificaciones anteriormente diseñadas sustituyendo (al 50% y al 100%) los áridos naturales utilizados por residuos de construcción y demolición (RCD).

Dicho trabajo está en fase de difusión en publicaciones científicas internacionales, donde se exponen y analizan los resultados obtenidos. La estructura de los trabajos científicos es la siguiente:

A) Estudio experimental de HAC (fase mortero) fabricado con cenizas volantes con marcado CE y cenizas de plantas de valorización energética de residuos sólidos urbanos y RCD: propiedades en estado fresco.

Este trabajo analiza el comportamiento en estado fresco y comportamiento mecánico a corta edad (7 días) de dos familias de HAC (fase mortero). La familia 1 con un 70% de cemento y un 30% de adiciones. Esta familia está formada por cuatro dosificaciones con diferentes porcentajes de cenizas volantes con marcado CE y cenizas de plantas de valorización energética de residuos sólidos urbanos (30/0, 20/10, 10/20 y 30/0, respectivamente). La familia 2 con un 40% de

cemento y un 60% de adiciones. Esta familia está formada por cuatro dosificaciones con diferentes porcentajes de cenizas volantes con marcado CE y cenizas de plantas de valorización energética de residuos sólidos urbanos (60/0, 40/20, 20/40 y 0/60, respectivamente). Teniendo en cuenta las propiedades en estado fresco de las 8 dosificaciones se seleccionan 4 (dos mezclas de cada familia) para completar el estudio de las propiedades en estado fresco (densidad fresca y aire ocluido) y en estado endurecido (resistencia a compresión a 28 días y su densidad seca a dicha edad). Por último, se analizan las propiedades en estado fresco de las 4 mezclas seleccionadas sustituyendo el árido natural por RCD.

B) Efecto de las cenizas de plantas de valorización energética de residuos sólidos urbanos en las propiedades mecánicas del HAC (fase mortero).

En este trabajo se lleva a cabo una amplia investigación de las propiedades mecánicas (resistencia a compresión, a flexión, módulo de elasticidad dinámico, coeficiente de Poisson, densidad seca, UPV a los 3, 7, 28 y 91 días) de las dosificaciones seleccionadas anteriormente. Su comportamiento mecánico se correlaciona con los mecanismos de endurecimiento analizados por DRX y ATD-TG. Lo que permite conocer de manera más exhaustiva el comportamiento mecánico de HAC (fase mortero) con este residuo.

C) Efecto de las cenizas de plantas de valorización energética de residuos sólidos urbanos en la durabilidad del HAC (fase mortero).

En este trabajo se analizan las propiedades físicas de las mezclas seleccionadas en la primera fase (pérdida por secado, evolución de la densidad seca y resistividad eléctrica) y la absorción de agua por capilaridad. Se definieron las propiedades microestructurales (estructura porosa) y su influencia en la durabilidad, para lo cual se estudió la profundidad de carbonatación. Estos aspectos son fundamentales para resolver las incertidumbres en el uso de este residuo y permitir su puesta en valor.

D) Comportamiento mecánico y durable del HAC (fase mortero) con cenizas de plantas de valorización energética de residuos sólidos urbanos y RCD.

En primer lugar, en este trabajo se lleva a cabo un análisis de las propiedades mecánicas (resistencia a compresión, a flexión, módulo de elasticidad dinámico, coeficiente de Poisson, densidad seca, UPV a los 3, 7, 28 y 91 días) de las mezclas seleccionadas sustituyendo el árido natural por RCD y su correlación con los mecanismos de endurecimiento analizados por DRX y ATD-TG. Además, se evalúa las propiedades físicas (pérdida por secado, evolución de la densidad seca y resistividad eléctrica) y la absorción de agua por capilaridad. También se definieron las propiedades microestructurales (estructura porosa) y su influencia en la profundidad de carbonatación. Lo que permite conocer de manera más exhaustiva el comportamiento en estado endurecido del HAC (fase mortero) fabricado con este residuo y RCD en sustitución del árido natural. Lo que contribuirá a convertir al HAC en un material más amigable con el medio ambiente.

Anexo C

Otras aportaciones científicas

A continuación, se presentan otras aportaciones científicas vinculadas con el autor, realizadas durante el periodo de Tesis Doctoral.

- Publicaciones científicas:

1. Título: Potential use of modified hydrotalcites as adsorbent of bentazon and metazachlor.
   Autores: A. Pérez, R. Otero, A.R. Esquinas, J.R. Jiménez, J.M. Fernández.
   Título de la revista: Applied Clay Science
   Número de revista: 141 Año: 2017 Páginas: 300-307 ISSN: 0169-1317
   Índice de impacto: 3.641 Citas: 3
   Índice relativo de su categoría: 5/29 Mineralogy (1er Cuartil)

2. Título: Wastes as aggregates, binders or additions in mortars: selecting their role based on characterization.
   Autores: C.B. Farinha, J. de Brito, R. Veiga, J.M. Fernández, J.R. Jiménez, A.R. Esquinas.
   Título de la revista: Materials
   Número de revista: 11 Año: 2018 Páginas: 453-480 ISSN: 1996-1944

Índice de impacto: 2.467 Citas: 0

Índice relativo de su categoría: 111/285 Materials Science, Multidisciplinary (2er Cuartil)

- Comunicaciones en congresos:

8. Título: Morteros industriales realizados con aguas procedentes de EDAR. Autores: D. Motos-Pérez, A.R. Esquinas, J.M. Fernández.
   Congreso: II Congreso Científico de Investigadores Noveles.
   Año: 2018
   Entidad Organizadora: Vicerrectorado de Investigación. Universidad de Córdoba.
   Lugar: Córdoba (España)

9. Título: Effects of biomass fly ash and mixed recycled aggregates on the mechanical properties of masonry mortar
   Autores: A.I. Torres-Gómez, E.F. Ledesma, A.R. Esquinas, A. Lozano, J.R. Jiménez, J.M. Fernández.
   Congreso: 3er International Symposium on Inorganic and Environmental Materials (ISIEM 2018).
   Año: 2018
   Entidad Organizadora: Ghent University y Society Inorganic Material of Japan.
   Lugar: Ghent (Bélgica)

UNIVERSIDAD
DE CÓRDOBA